



**INVESTIGATION OF TENSILE, FLEXURAL,
AND VIBRATION BEHAVIOR OF
LAMINATED HYBRID COMPOSITES**

A Dissertation

Submitted to the Council of the Erbil Technical Engineering
College at Erbil Polytechnic University in Partial
Fulfillment of the Requirements for the Degree of Doctor of
Philosophy (Ph.D.) of Science in Mechanical and Energy
Engineering

By

Ava Ali Kamal Mohammed

B.Sc. in Mechanical Engineering, 1996

M.Sc. in Applied Mechanics, 1999

Supervised by

Asst. Prof. Dr. Gailan Ismail Hassan

Asst. Prof. Dr. Younis Khalid Khdir

Iraq - Kurdistan - Erbil

April 2024

DECLARATION

I declare that the Ph.D. dissertation entitled: **INVESTIGATION OF TENSILE, FLEXURAL, AND VIBRATION BEHAVIOR OF LAMINATED HYBRID COMPOSITES** is my original work, and with this, I certify that unless stated, all work contained within this dissertation is my independent research and has not been submitted for the award of any other degree at any institution, except where due acknowledgment is made in the text.

Signature:

Student Name: Ava Ali Kamal Mohammed

Date: 4 April 2024

LINGUISTIC REVIEW

I confirm that I have reviewed the dissertation titled **INVESTIGATION OF TENSILE, FLEXURAL, AND VIBRATION BEHAVIOR OF LAMINATED HYBRID COMPOSITES** from the English linguistic point of view, and I can confirm that it is free of grammatical and spelling errors.

Signature:

Name of Reviewer: Asst. Prof. Dr. Abdulkhalek M. Kadir

Date: 4 April 2024

SUPERVISOR CERTIFICATE

This dissertation has been written under our supervision and has been submitted for the award of the degree of Ph.D. of Science in Mechanical and Energy Engineering with our approval as supervisors.

Signature

Name: Asst. Prof. Dr. Gailan Ismail Hassan

Date: 4/4/2024

Signature

Name: Asst. Prof. Dr. Younis Khalid Khdir

Date: 4/4/2024

I confirm that all requirements have been fulfilled.

Signature:

Name: Professor Dr. Ahmed Mohammed Adham

Head of the Department of Mechanical and Energy Engineering Techniques

Date: 4/4/2024

I confirm that all requirements have been fulfilled.

Postgraduate Office

Signature:

Name: Mr. Bayad Abdulqader Ahmed

Date:

EXAMINING COMMITTEE CERTIFICATION

We certify that we have read this dissertation: **INVESTIGATION OF TENSILE, FLEXURAL, AND VIBRATION BEHAVIOR OF LAMINATED HYBRID COMPOSITES**, and as an examining committee examined the student (Ava Ali Kamal Mohammed) in its content and what is related to it. We approve that it meets the standards of a dissertation for the degree of Ph.D. in Mechanical and Energy Engineering.

Signature

Name: Prof. Dr. Basim Mohammed Fadhil
Member

Date: 4/4/2024

Signature

Name: Prof. Dr. Sarkawt Rostam Hassan
Member

Date: 4/4/2024

Signature

Name: Prof. Dr. Payman Sahbah Ahmed
Member

Date: 4/4/2024

Signature

Name: Asst. Prof. Dr. Dlair Obaid Ramadan
Member

Date: 4/4/2024

Signature

Name: Prof. Dr. Shawnam Rashied Jalal
Chairman

Date: 4/4/2024

Signature

Name: Asst. Prof. Dr. Gailan I. Hassan
Supervisor

Date: 4/4/2024

Signature

Name: Asst. Prof. Dr. Younis Khalid Khdir
Supervisor

Date: 4/4/2024

Signature

Name: Prof. Dr. Ayad Zaki Saber
Dean of Erbil Technical Engineering College

Date:

Acknowledgment

Before everything, my great gratitude goes to Allah Almighty; who helped me and gave me the strength and patience all the time to complete this work.

I would like to express my sincere and heartfelt gratitude to my supervisors Assistant Professor Dr. Gailan Ismail Hassan and Assistant Professor Dr. Younis Khalid Khdir for their supervision of my PhD research. I am grateful to the head of the Mechanical and Energy department, Professor Dr. Ahmed Mohammed Adham, and the academic staff. I also want to acknowledge and appreciate Dr. Nazhad Ahmed, Dr. Muhammed Tahir Muhammed Saeed, Engineer Emad Oodish, in the Mechanical Engineering department at Salahaddin University and Dr Dara Khalid Khidir and Engineer Rebaz Kawa Omer in the Manufacturing Engineering department at Koya University for completing the experimental part of the research.

Finally, my deep gratitude and sincere appreciation go to my parents, family, and husband. I'm indebted to everything they gave me in which I wouldn't be at this status.

ABSTRACT

Fiber-reinforced polymer composite (FRPC) and fiber metal laminate (FML) sandwich with and without nano Al_2O_3 are the two types of structural laminated materials used in this work.

Their tensile and flexural properties are investigated through experimentation and validated numerically through the application of the finite element method (ANSYS workbench 19.2). The results show that the more carbon plies positioned in the middle of the laminate, the stronger the FRPC's tensile characteristics. The flexural properties of FRPC increase as the carbon layer gets closer to the surface. Adding 2% nano Al_2O_3 increases both the tensile and flexural properties of FRPC. Furthermore, the primary factor influencing the tensile and flexural properties of FML is the bonding between the metal and fiber layers. The maximum practical tensile load of FRPC is 2%-15% higher than FEM, while for FML is half that of FEM. The maximum practical flexural load of FRPC is 5%-6% higher than FEM except for 3 sample configurations, while for FML one is 2%-15% lower than FEM except for 1 sample configuration.

Flexural modulus, natural frequency, and damping ratio are all increased simultaneously by adding two glass plies to the FRPC's outer surface as opposed to just one glass ply for quasi-FRPC. When 2% nano Al_2O_3 was added to the FRPC, compared to the non-nano addition case, the natural frequency slightly decreased and the flexural modulus and damping ratio increased. Practical, analytical, and numerical natural frequencies are identical for FRPC. The FRPC core's fiber orientation and stacking order have no bearing on the free vibration of FML.

For metal, FML, and FRPC, the bending stiffness coefficient d_{mn} primarily determines the maximum deflection resulting from a uniformly distributed load and the fundamental natural frequency. The primary influence

on the d_{mn} value, which results in the material being more resistant to elastic deformation, comes from the D22 element in the bending stiffness matrix and, consequently, the young modulus in the y-direction. In the FML sandwich, the stainless-steel metal skin contributes more than the fiber-reinforced polymer core.

Contents

<i>Subject</i>		<i>Page No.</i>
<i>Abstract</i>		VI
<i>Contents</i>		VIII
<i>List of symbols</i>		XIV
<i>List of Abbreviations and Acronyms</i>		XVI
<i>List of Figures</i>		XVII
<i>List of Tables</i>		XXIV
<i>Chapter One: Introduction</i>		
<i>1.1</i>	<i>Introduction</i>	1
<i>1.2</i>	<i>Composite Materials</i>	1
<i>1.3</i>	<i>Fibrous Composites</i>	4
<i>1.3.1</i>	<i>Fibers</i>	4
<i>1.3.2</i>	<i>Matrix</i>	5
<i>1.4</i>	<i>Laminated Composite</i>	6
<i>1.5</i>	<i>Hybrid Composite</i>	7
<i>1.6</i>	<i>Fiber Metal Laminate</i>	8
<i>1.7</i>	<i>Aim and Objective</i>	10
<i>1.8</i>	<i>Problem Statement</i>	10
<i>1.9</i>	<i>Dissertation Layout</i>	11
<i>Chapter Two: Literature Review</i>		
<i>2.1</i>	<i>Introduction</i>	12
<i>2.2</i>	<i>Mechanical Behavior of Hybrid Laminated Composite</i>	12

2.2.1	<i>Glass: Carbon Fiber Hybrid Composite</i>	13
2.2.2	<i>Inter-ply and Intra-ply Hybrid Composite</i>	14
2.2.3	<i>Impact of Stacking Sequence and Angle of Orientation on the Hybrid Composite</i>	15
2.2.4	<i>Nano Composite</i>	16
2.3	<i>Mechanical Behavior of Fiber Metal Laminate</i>	17
2.3.1	<i>Glass Fiber Composite/Aluminum (Glare)</i>	17
2.3.2	<i>Impact of Nano Addition on the Mechanical Behavior of Glare</i>	18
2.3.3	<i>(Glass Fiber Composite/Stainless Steel Base) Fiber Metal Laminate</i>	19
2.3.4	<i>Carbon Fiber Composite/Aluminum (Caral)</i>	20
2.3.5	<i>(Carbon Fiber Composite/Titanium Base) Fiber Metal Laminate</i>	21
2.3.6	<i>Glass and Carbon Hybrid Fiber Composite/Aluminum</i>	22
2.3.7	<i>Comparison Between Aral, Caral, and Glare</i>	24
2.4	<i>Free Vibration of Fiber Reinforced Polymer Composite</i>	24
2.4.1	<i>Dynamic Behavior of Glass and Carbon Fiber Reinforced Polymer Composite</i>	25
2.4.2	<i>Relationship Between Flexural Modulus, Natural Frequency, and Damping Ratio</i>	25
2.4.3	<i>Mechanical and Damping Characteristics of Glass Fiber Reinforced Composite</i>	26
2.4.4	<i>Impact of Nano-Addition on the Dynamic Properties of Glass fiber Reinforced Composite</i>	26
2.4.5	<i>Relationship Between Mechanical and Dynamic Properties of Fiber Reinforced Polymer Composite</i>	27
2.4.6	<i>Hybrid Composite</i>	29

2.5	<i>Free Vibration of Fiber Metal Laminate</i>	30
2.5.1	<i>Glass Fiber Composite/Aluminum</i>	30
2.5.2	<i>(Glass/Copper Base) Fiber Metal laminate</i>	32
2.5.3	<i>Carbon Fiber Composite/Aluminum (Caral) FML</i>	32
2.5.4	<i>(Glass and Carbon Hybrid Fiber Composite/Aluminum) FMLL</i>	33
2.6	<i>Deflection and Natural Frequency of Metal, FRPC, and FML composite Plates.</i>	34
2.6.1	<i>Isotropic Plate</i>	34
2.6.2	<i>Factors Impacted on the Deflection and Natural Frequency of FRPC Plate</i>	34
2.6.3	<i>Fiber Metal Plate</i>	36
2.7	<i>Summary</i>	37
<i>Chapter Three: Theoretical and Numerical Work</i>		
3.1	<i>Introduction</i>	38
3.2	<i>Classical Lamination Theory</i>	38
3.3	<i>Orthotropic Stress-Strain Relationship</i>	40
3.4	<i>Laminate Under Tensile and Shear Load</i>	42
3.5	<i>Laminate Under Bending Moment</i>	43
3.6	<i>Equation of Motion in Terms of Displacements</i>	44
3.7	<i>Symmetrical Laminate</i>	46
3.8	<i>Cross Laminate</i>	46
3.9	<i>Quasi-Isotropic Laminate</i>	46
3.10	<i>Bending of Simply Supported Rectangular Plate</i>	46
3.11	<i>The Navier Solution for Symmetric Cross Laminate</i>	48

3.12	<i>The Load Coefficient Q_{mn} for Uniform Load $q(x, y)$</i>	49
3.13	<i>The Navier Solution for Symmetric Quasi-Isotropic Laminate</i>	50
3.14	<i>Vibration of Symmetric Cross Simply Supported Plate</i>	51
3.15	<i>Vibration of Symmetric Quasi-Isotropic Simply Supported Plate</i>	52
3.16	<i>Static Deflection and Free Vibration of Isotropic Simply Supported Plate</i>	53
3.17	<i>Bending of Beam</i>	54
3.17.1	<i>Bending of Isotropic Beam</i>	54
3.17.2	<i>Bending of Orthotropic Symmetric Beam</i>	56
3.18	<i>Transverse Free Vibration of Isotropic and Orthotropic Beams</i>	56
3.19	<i>Numerical Work (Finite Element Modeling)</i>	58
3.20	<i>Beam Modeling</i>	59
3.20.1	<i>FRPC Modeling</i>	59
3.20.1.1	<i>Tensile Test Modeling</i>	59
3.20.1.2	<i>Flexural Test Modeling</i>	60
3.20.1.3	<i>Free Vibration Test Modeling</i>	60
3.20.2	<i>FML Modeling</i>	61
3.20.2.1	<i>Tensile Test Modeling</i>	61
3.20.2.2	<i>Flexural Test Modeling</i>	62
3.20.2.3	<i>Free Vibration Test Modeling</i>	62
3.21	<i>Plate Bending Modeling</i>	63
3.21.1	<i>Metal Plate Modeling</i>	63
3.21.1.1	<i>Plate Thickness</i>	63

3.21.1.2	<i>Metal Type</i>	63
3.21.2	<i>FRPC Plate Modeling</i>	64
3.21.2.1	<i>Stacking Sequence and Angle of Orientation</i>	64
3.21.2.2	<i>Nano Al₂O₃ Addition</i>	65
3.21.2.3	<i>Aspect Ratio</i>	65
3.21.2.4	<i>Hybrid Ratio</i>	65
3.21.3	<i>Fiber Metal Laminate Sandwich</i>	67
Chapter Four: Experimental Work		
4.1	<i>Introduction</i>	69
4.2	<i>Materials</i>	69
4.3	<i>Fiber Reinforced Epoxy Laminated Composite Manufacturing</i>	71
4.3.1	<i>Ultrasonic- Dual Mixing Method</i>	71
4.3.2	<i>Vacuum- Assisted Resin Infusion Molding Process</i>	72
4.4	<i>Mechanical Properties Measurement of Unidirectional FRPC</i>	75
4.5	<i>Fiber Metal Laminate SS304/ FRPC/ SS304 Manufacturing</i>	79
4.6	<i>Mechanical Tests</i>	84
4.7	<i>Scanning Electron Microscopy Sample Preparation Technique and Devices</i>	85
4.8	<i>Free Vibration Test</i>	86
Chapter Five: Results and Discussion		
5.1	<i>Introduction</i>	88
5.2	<i>Tensile Behavior of Fiber-Reinforced Polymer Composite</i>	88
5.3	<i>Tensile Behavior of Sandwich SS304/FRPC/SS304 FML</i>	92

5.4	<i>Flexural Behavior of Fiber-Reinforced Polymer Composite</i>	98
5.5	<i>Flexural Behavior of Sandwich SS304/FRPC/SS304 FML</i>	104
5.6	<i>Morphology (Scanning Electron Microscopy) Images</i>	111
5.7	<i>Free vibration Response of Fiber Reinforced Polymer Composite</i>	116
5.8	<i>Free Vibration Response of Sandwich SS304/FRPC/SS304 FML</i>	124
5.9	<i>Factors Affecting the Deflection and Fundamental Natural Frequency of Metal, FRPC, and FML Sandwich Plates.</i>	131
5.9.1	<i>Metal</i>	131
5.9.1.1	<i>Plate Thickness</i>	131
5.9.1.2	<i>Metal Type</i>	132
5.9.2	<i>Fiber Reinforced Polymer Composite</i>	134
5.9.2.1	<i>Stacking Sequence and Angle of Orientation</i>	134
5.9.2.2	<i>Nano Al₂O₃ Addition</i>	136
5.9.2.3	<i>Aspect Ratio</i>	137
5.9.2.4	<i>Hybrid Ratio</i>	140
5.9.3	<i>Fiber Metal Laminate Sandwich</i>	142
<i>Chapter Six: Conclusions and Recommendations</i>		
6.1	<i>Conclusions</i>	151
6.2	<i>Recommendation for Future Work</i>	152
	<i>References</i>	R1

List of Symbols

<i>Symbol</i>	<i>Meaning</i>	<i>Units</i>
$\begin{Bmatrix} \varepsilon_x \\ \varepsilon_y \\ \varepsilon_{xy} \end{Bmatrix}$	<i>Laminate Strains</i>	<i>mm/mm</i>
$\begin{Bmatrix} \varepsilon_x^0 \\ \varepsilon_y^0 \\ \gamma_{xy}^0 \end{Bmatrix}$	<i>Midplane Strains</i>	<i>mm/mm</i>
$\begin{Bmatrix} \kappa_x \\ \kappa_y \\ \kappa_{xy} \end{Bmatrix}$	<i>Flexural Strains</i>	<i>mm/mm</i>
$[\bar{Q}]$	<i>Transformed Reduced Stiffness Matrix</i>	<i>MPa</i>
A_{ij}, B_{ij}, D_{ij}	<i>Extensional, Extensional- Bending Coupling and Bending Stiffness Matrices</i>	<i>Pa.m, Pa.m², Pa.m³</i>
E_x	<i>Effective longitudinal Young Modulus</i>	<i>MPa</i>
ν_{xy}	<i>Major Effective Poisson's Ratio</i>	
E_y	<i>Effective Transverse Young Modulus</i>	<i>MPa</i>
G_{xy}	<i>Effective Shear Modulus</i>	<i>MPa</i>
E_x^f	<i>Effective Flexural Longitudinal Modulus</i>	<i>MPa</i>
E_y^f	<i>Effective Flexural Transverse Modulus</i>	<i>MPa</i>
ν_{xy}^f	<i>Major Effective Flexural Poisson's Ratio</i>	
G_{xy}^f	<i>Effective Flexural Shear Modulus</i>	<i>MPa</i>
h	<i>total laminate thickness</i>	<i>mm</i>
$w_0(x, y)$	<i>Plate Lateral Deflection</i>	<i>mm</i>
$q(x, y)$	<i>Lateral load</i>	<i>N</i>
a, b	<i>plate length and width</i>	<i>mm</i>

d_{mn}	<i>Bending Stiffness Coefficient</i>	<i>Pa/m</i>
W_{mn}	<i>Deflection Coefficient</i>	<i>m</i>
Q_{mn}	<i>Load Coefficient</i>	<i>N</i>
S	<i>Plate Aspect Ratio</i>	
I_0	<i>mass moment of inertia</i>	<i>kg/m²</i>
w_{mn}	<i>Plate Fundamental Natural Frequency</i>	<i>Hz</i>
w_n	<i>Beam Fundamental Natural Frequency</i>	<i>Hz</i>
Al_2O_3	<i>Aluminum Oxide</i>	

List of Abbreviations and Acronyms

<i>Abbreviation</i>	<i>Meaning</i>
FRPC	Fiber Reinforced Polymer Composite
FML	Fiber Metal Laminate
G	Glass Fiber
C	Carbon Fiber
K	Kevlar Fiber
ARAL	Aramid Fiber Composite/Aluminum base FML
GLARE	glass Fiber Composite/Aluminum base FML
CARAL	Carbon Fiber Composite/Aluminum base FML
CTBN	Carboxyl-Terminated Butadiene Acrylonitrile
FRM	Fiber Reinforced Matrix
PEEK	Polyether ether ketone
ACP(Pre)	Ansys Composite Pre-Post
MGS L285	Laminating epoxy resin
H285	Hardener
UDMM	Ultrasonic Dual Mixing Method
VARIM	Vacuum-Assisted Resin Infusion Molding
FEM	Finite Element Method
SEM	Scanning Electron Microscopy
CLPT	Classical Laminate Plate Theory

List of Figures

Figure No.	Subject	Page No.
1.1	<i>Classification of Composite Materials (Kar, 2016)</i>	3
1.2	<i>Types of fibers, (a) Continuous, (b) Discontinuous (Campbell, 2010)</i>	5
1.3	<i>Transversely Isotropic Lamina (Daniel, 2006)</i>	6
1.4	<i>Inter-ply Hybrid laminated composite between glass and carbon fiber (Chawla, 2012)</i>	8
1.5	<i>classification of FML according to layer arrangement (Ding et al., 2021)</i>	8
1.6	<i>Example of Al-base metal /glass fiber reinforcement FML (Ding et al., 2021)</i>	9
3.1	<i>The displacement u and v relative to midplane displacement and slope (Kaw, 2006)</i>	39
3.2	<i>Simply Supported Plate boundary conditions (Reddy 2004)</i>	47
3.3	<i>Q_{mn} for uniform distributed load condition (Reddy, 2004)</i>	49
3.4	<i>The bending of isotropic beam: (a)before bending, (b) after bending (Kaw, 2006).</i>	55
3.5	<i>The first four natural frequencies and their mode shapes for cantilever beam (Rao, 2007)</i>	57
3.6	<i>Finite element modeling of FML beam</i>	58
3.7	<i>Steps of modeling tensile test for FRPC laminates in ANSYS workbench</i>	59
3.8	<i>FRPC tensile sample with tabs</i>	59
3.9	<i>Steps of modeling flexural test for FRPC laminates in ANSYS workbench</i>	60

3.10	<i>Steps of modeling laminates in ANSYS workbench</i>	60
3.11	<i>Steps of modeling tensile test for FML in ANSYS workbench</i>	61
3.12	<i>FML sandwich plies tensile sample</i>	61
3.13	<i>Steps of modeling flexural test for FML laminates in ANSYS workbench</i>	62
3.14	<i>fiber metal laminate modeling in (ANSYS) workbench</i>	62
3.15	<i>Steps of modeling isotropic plate in ANSYS workbench to evaluate deflection and natural frequencies</i>	63
3.16	<i>Steps of modeling orthotropic plate in ANSYS workbench to evaluate deflection and natural frequencies</i>	64
3.17	<i>Schematic sketch of metal/C1 composite/metal FML sandwich</i>	67
3.18	<i>Steps of modeling FML sandwich plates in ANSYS workbench to evaluate deflection and natural frequency</i>	68
4.1	<i>The ingredients utilized to fabricate fiber-reinforced polymer laminate composite and fiber metal laminate sandwich</i>	70
4.2	<i>Aluminium Oxide Nanopowder (Al_2O_3) and epoxy resin suspension mixing process, (a) UDMM, (b) Vacuum chamber degassing process</i>	71
4.3	<i>laminated fiber epoxy composite fabrication:(a) Schematic diagram of VARIM, (b) Practical producing FRP laminate</i>	73
4.4	<i>RADWAG AS 220.R2 Density Measurement Device</i>	76
4.5	<i>strain gauge cleaning and sticking tools;(a) Acidic, (b) glue, (c) 0-90 strain gauge stucked to the sample surface</i>	77

4.6	<i>Poisson's ratio measurement apparatus: (a) Data Collect Logger and its different view, (b) the overall connection</i>	78
4.7	<i>Material analysis OXFORD instrument, X-MET 7500</i>	80
4.8	<i>Pneumatic sandblasting gun: (a) PARKSIDE PISTOLA NEUMATICA, (b) sandblasting sample surface</i>	81
4.9	<i>FML manufacturing: (a) layers sequence arrangement in mold, (b) compression machine</i>	82
4.10	<i>Universal tester and samples of (a) tensile test and (b) Three-point flexural test</i>	85
4.11	<i>Scanning electron microscope (SEM) sequence: (a) Prepared sample, (b) gold spraying coater machine, (c) Zeiss EVO 50 scanning electron microscope.</i>	86
4.12	<i>Free vibration test set up and its parts</i>	87
4.13	<i>Free vibration Test of FML: (a) accelerometer sensor, (b) rubber impact hummer</i>	87
5.1	<i>Tensile stress-strain curves for both symmetrical hybrid cross and quasi-laminated epoxy composite with and without nano-Al_2O_3</i>	89
5.2	<i>Tensile properties for both cross and quasi-laminated epoxy composite with and without nano-Al_2O_3: (a)Ultimate tensile strength, (b) Ultimate tensile strain %, and (c) Tensile toughness</i>	90
5.3	<i>Tensile failure modes for both cross and quasi-laminated epoxy composite with and without nano-Al_2O_3</i>	91
5.4	<i>Practical and FEM maximum tensile load difference of FRPC</i>	92
5.5	<i>Comparison between tensile load-extension of Cross FRPC and FML.</i>	94

5.6	<i>Comparison between tensile load-extension of quasi FRPC and FML</i>	95
5.7	<i>Tensile properties for both FRPC and FML with and without nano-Al₂O₃: (a)maximum tensile load, (b) Displacement at maximum load, and (c) Tensile toughness</i>	96
5.8	<i>Tensile failure modes for both cross and quasi-laminated epoxy composite /stainless steel 304 base with and without nano-Al₂O₃</i>	97
5.9	<i>Practical and FEM maximum tensile load difference of FRPC and FML sandwiches</i>	98
5.10	<i>Flexural stress-strain curves for both symmetrical hybrid cross and quasi-laminated epoxy composite with and without nano-Al₂O₃</i>	99
5.11	<i>Flexural properties for both cross and quasi-laminated epoxy composite with and without nano-Al₂O₃: (a)Ultimate Flexural strength, (b) Ultimate Flexural strain, and (c) Flexural toughness</i>	101
5.12	<i>Flexural failure modes for both cross and quasi-laminated epoxy composite with and without nano-Al₂O₃.</i>	102
5.13	<i>FRPC flexural sample with supports and load</i>	103
5.14	<i>Practical and FEM maximum flexural load difference of FRPC</i>	103
5.15	<i>Comparison between bending load-extension of Cross FRPC and FML</i>	106
5.16	<i>Comparison between bending load-extension of quasi FRPC and FML</i>	107
5.17	<i>Flexural properties for both FRPC and FML with and without nano-Al₂O₃: (a)maximum tensile load, (b) Deflection at maximum load, and (c) Flexural toughness</i>	108

5.18	<i>Flexural failure modes for both cross and quasi-laminated epoxy composite /stainless steel 304 base with and without nano-Al_2O_3</i>	109
5.19	<i>FML flexural sample with supports and load</i>	110
5.20	<i>Practical and FEM maximum flexural load difference of FRPC and FML sandwiches</i>	110
5.21	<i>SEM of Q2 quasi laminate tensile sample: (a) crack propagation, (b) good interfacial adhesion, (c) fiber pull-out, (d) fiber imprints, (e) matrix fragmentation</i>	112
5.22	<i>SEM of Q2WN quasi laminate tensile sample: (a) crack propagation, (b) Fiber pull out, (c) debonding, (d) fiber breakage, (e) matrix fragmentation</i>	113
5.23	<i>SEM of C1 cross-laminate flexural sample: (a) 0° fiber and 90° fiber at the failed region, (b) fiber pull-out, (c) good interfacial adhesion, (d) matrix fragmentation</i>	114
5.24	<i>SEM of C1WN cross-laminate flexural sample: (a) 0° fiber and 90° fiber at the failed region, (b) Delamination, (c) fiber imprints, (d) matrix fragmentation</i>	115
5.25	<i>Frequency responses of laminated epoxy composites with and without nano Al_2O_3: a) C1, b) C1WN, c) C2, d) C2WN, e) Q1, f) Q1WN, g) Q2, and h) Q2WN</i>	120
5.26	<i>Vibration responses of laminated epoxy composites with and without nano Al_2O_3: a) C1, b) C1WN, c) C2, d) C2WN, e) Q1, f) Q1WN, g) Q2, and h) Q2WN</i>	121
5.27	<i>Dynamic Characteristics of FRPC with and without nano Al_2O_3: (a) Natural Frequency, (b) Damping Ratio</i>	122

5.28	<i>Natural frequencies comparison in analytical, practical, and numerical methods</i>	123
5.29	<i>Frequency responses of fiber metal laminate sandwiches with and without nano Al₂O₃: a) SS/C1/SS, b) SS/C1WN/SS, c) SS/C2/SS, d) SS/C2WN/SS, e) SS/Q1/SS, f) SS/Q1WN/SS, g) SS/Q2/SS, and h) SS/Q2WN/SS</i>	126
5.30	<i>Vibration responses of laminated epoxy composites with and without nano Al₂O₃: a) SS/C1/SS, b) SS/C1WN/SS, c) SS/C2/SS, d) SS/C2WN/SS, e) SS/Q1/SS, f) SS/Q1WN/SS, g) SS/Q2/SS, and h) SS/Q2WN/SS</i>	127
5.31	<i>Dynamic Characteristics of FML with and without nano Al₂O₃: (a) Natural Frequency, (b) Damping Ratio</i>	129
5.32	<i>Analytical, practical, and numerical natural frequencies comparison</i>	129
5.33	<i>Effect of stainless steel 304 plate thickness change on the (a) bending stiffness, (b) rotary inertia, (c) maximum deflection, and (d) fundamental natural frequency</i>	131
5.34	<i>Effect of metal type on the (a) bending stiffness, (b) rotary inertia, (c) maximum deflection, and (d) fundamental natural frequency</i>	133
5.35	<i>Effect of stacking sequence and angle of orientation on the (a) bending stiffness coefficient, (b) maximum deflection, and (c) fundamental natural frequency of FRPC plate</i>	135
5.36	<i>Effect of nano Al₂O₃ addition on the (a) bending stiffness coefficient, (b) maximum deflection, and (c) fundamental natural frequency of FRPNC plate</i>	136
5.37	<i>Effect of aspect ratio on (a) the bending stiffness coefficient, (b) the maximum deflection, and, (c) the fundamental natural frequency of C1, C2, Q1, and Q2 fiber-reinforced epoxy composite plates</i>	138

5.38	<i>Effect of hybrid ratio on (a) the bending stiffness coefficient, (b) the maximum deflection, and, (c) the fundamental natural frequency of C1, C1A, C1B, C2, C2A, C2B, Q1, Q1A, Q1B, Q2, Q2A, and Q2B fiber reinforced epoxy composite plates</i>	141
5.39	<i>Effect of metal skin type on the (a) bending stiffness coefficient, (b) rotary inertia, (c) maximum deflection, and (d) fundamental natural frequency of FML plates</i>	144
5.40	<i>Comparison between (a) bending stiffness coefficient, (b) rotary inertia, (c) maximum deflection, and (d) fundamental natural frequency of metal, FRPC, and FML simply supported plates</i>	148

List of Tables

Table		Page No.
2.1	<i>Comparative dynamic behavior of glass and carbon fiber reinforced polymer composite</i>	25
3.1	<i>Mechanical properties of aluminum 606-T6 and Titanium alloy Ti-6AL-4V (Hibbeler, 2012)</i>	63
3.2	<i>C1, C2, Q1, and Q2 fiber reinforced epoxy composite configuration plates</i>	64
3.3	<i>Hybrid ratio and carbon ply position change in C1, C2, Q1, and Q2 FRPC configurations</i>	66
3.4	<i>Fiber metal laminate sandwich plate configuration</i>	68
4.1	<i>Stacking Sequence G: C configuration of hybrid laminated epoxy composites</i>	74
4.2	<i>Mechanical properties of unidirectional glass and carbon fiber with and without nano Al₂O₃</i>	79
4.3	<i>The Chemical composition of 304 stainless steel by using material analysis instrument</i>	80
4.4	<i>The mechanical properties of 304 stainless steel.</i>	80
4.5	<i>Stacking sequence arrangement of sandwich [SS/FRPC/SS] FML</i>	83
5.1	<i>Flexural stiffness matrix, theoretical flexural modulus E_b, and fundamental natural frequency ω_n</i>	117
5.2	<i>The first six natural frequencies and its mode shapes for all laminates</i>	123
5.3	<i>Flexural stiffness matrix, theoretical flexural modulus E_b, and fundamental natural frequency ω_n for all fiber metal laminate sandwich</i>	125
5.4	<i>The first six natural frequencies and its mode shapes</i>	130

5.5	<i>The first six natural frequencies and its mode shapes for all SS/FRPC/SS</i>	145
5.6	<i>The first six natural frequencies and its mode shapes for all AI/FRPC/AI</i>	146
5.7	<i>The first six natural frequencies and its mode shapes for all Ti/FRPC/Ti</i>	147

CHAPTER ONE

INTRODUCTION

1.1 Introduction

In general, materials can be divided into four main groups: metals, ceramics, polymers, and composite. Each group has significant properties and characteristics that distinguish it from the others. Composite materials are formed by combining two or more distinct components, each with its own physical and chemical properties, to produce a material with enhanced characteristics. These composites possess distinctive mechanical and dynamic properties that distinguish them from conventional single-material products.

1.2 Composite Materials

Researches are directed to replace metal with composite material in transportation especially in the aviation industry due to the need to develop mechanical properties by increasing strength and stiffness and decreasing weight and corrosion. On the other hand, the consumption of fuel besides global warming is another reason for this replacement (Barros, Fujiyama, and Leite, 2015). Composite materials consist of two components, the first one is the matrix which is used to fix firmly the second phase “reinforcement” by surrounding it (Barros, Fujiyama, and Leite, 2015). For example, fiber-reinforced polymer composite, where the purpose of the matrix is (Akay, 2015; Barros, Fujiyama, and Leite, 2015):

- Contain the fibers simultaneously in load direction.
- Save and shield the fibers from deterioration and environmental fight.
- Transfer utilized load to the fibers through the interface shear stress.
- Prepare a perfect surface for the composite object.

While the task of reinforcement is (Akay, 2015)

- Increase the strength of the composite.
- Increase the stiffness of the composite.

- Forbid and stop crack propagation, which is initiated in the weakest matrix region.

According to the type of matrix, composite can be classified into (Kaw, 2005)

- Polymer Matrix Composites (PMCs).
- Metal Matrix Composites (MMCs).
- Ceramic Matrix Composites (CMCs).
- Carbon-carbon composites (CCs).

According to the type of reinforcement, composite can be classified (Kar, 2016) as shown in Figure (1.1)

- Fibrous Composites.
- Particulate Composites.

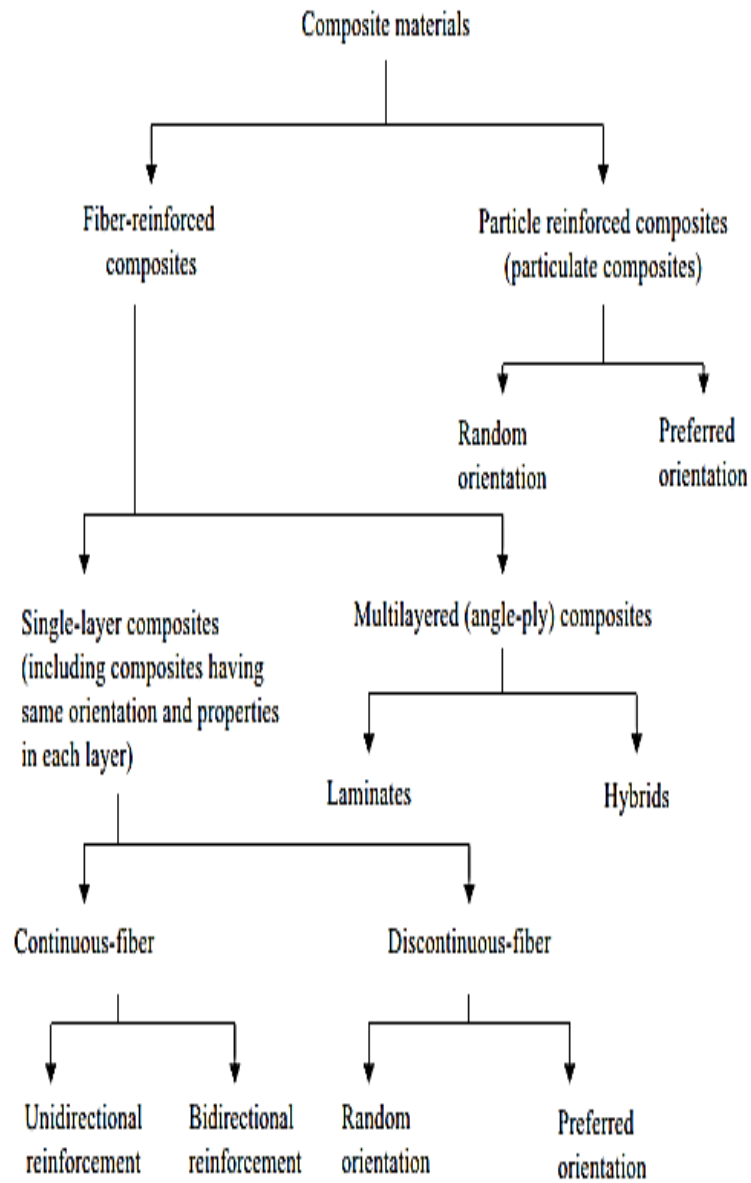


Figure (1.1) Classification of Composite Materials Based on the Type of Reinforcement (Kar, 2016).

1.3 Fibrous Composites

Fiber-reinforced polymer composites (FRPCs) are those types of composite in which man-made fibers like glass, carbon, and aramid fibers, or natural fibers are immersed completely in a polymer matrix with different arrangements according to the required design in specific applications (Rajak *et al.*, 2019). The addition of fibers to polymers makes them suitable for structural application because of their resistance to creep phenomena (Barbero, 2010).

1.3.1 Fibers

Fibers represent the load-carrying capacity of the FRPCs, where the fibers may be continuous or discontinuous as shown in Figure (1.2). FRPC's high strength is retained by the small diameter of their fibers which leads to fewer flaws compared to bulk solid materials (Campbell, 2010).

Many types of synthetic fibers can be used in the fabrication of FRPCs according to the application requirements. Glass and carbon are the most general inorganic fibers that are used in FRPCs. Various types of glass and carbon fibers for different purposes can be gained by regulating the chemical constituents and production process. Glass fibers are the most popular type of fiber used in low-cost industrial usages due to their properties of flexibility, lightweight, and inexpensive. Different strength values and nearly equal stiffness are possessed by glass fibers. Compared to glass fibers, carbon fibers are lighter, stiffer, and stronger, this will lead to reduce the amount of strain in the polymer matrix for a given load, but the cost is the main factor that reduces the use of carbon fiber. Carbon fibers exist with a wide range of stiffness and strength values (Barbero, 2010).

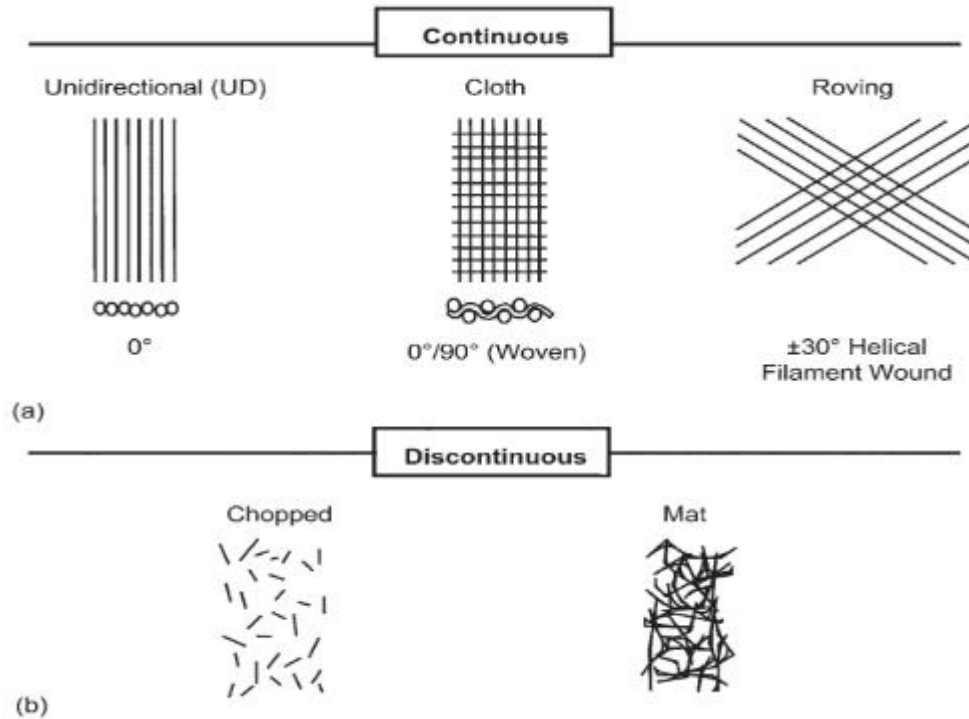


Figure (1.2) Types of fibers, (a) Continuous, (b) Discontinuous (Campbell, 2010).

1.3.2 Matrix

Polymers are the common matrix used in industry compared to metals and ceramics because of the low cost of fabrication and their ability to form more complex shapes. Polymers are petrochemical products, their structure contains chains of monomers (basic units of polymer) connected chemically by covalent carbon bonds through the polymerization technique (Chawla, 2012). There are two types of polymers, the first one is thermoset which is available in resin form, to prepare it, mix it with a hardener according to the instructor ratio to form a solid-state polymer like epoxy. After curing the object cannot be recycled or reproduced. The second type is the thermoplastic available in powder or particle form treated with temperature over melting temperature to be able to produce and fabricate it into the required shapes. The product can be recycled for a limited number of cycles according to the instructor's information like PEEK (Barbero, 2010).

1.4 Laminated Composite

Lamina is a plane containing unidirectional fiber fabric that is oriented to a specific direction in a polymer matrix like epoxy. Each lamina possesses three principal directions, longitudinal (direction 1) with the direction of fibers, transverse (direction 2) normal to direction 1 in-plane, and transverse (direction 3) normal to direction 1 out-plane as shown in Figure (1.3). When one of the principal planes is a plane of isotropy (the properties are the same in every point in plane 23) then the material is converted from orthotropic to transversely isotropic and needs only five Engineering constants to define it which are (C_{11} , C_{12} , C_{22} , C_{23} , and C_{55}) (Daniel, 2006).

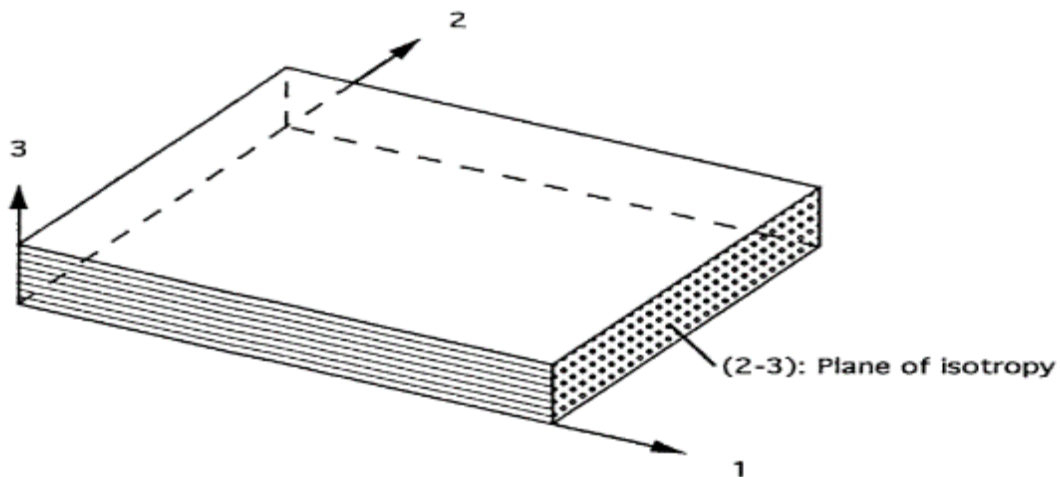


Figure (1.3) Transversely isotropic lamina (Daniel, 2006).

Lamina is the basic building unit of laminated fiber composite, group of lamina with different fiber orientations according to the design required are stacked to each other to create a laminated fiber composite in which the properties of it will depend on the properties of each lamina (Kaw, 2005).

1.5 Hybrid Composite

Combining either two or more reinforcements in one matrix or blending two polymer matrices in the same composite is the idea of hybridization. A hybrid composite is a future successful material that depends on the cooperative effect of the components to produce a new promising structural composite material with advanced mechanical properties compared with the non-hybrid one. Hybrid composite can be classified into five types (Harris, 1999; Kaw, 2005; Thakur, Thakur and Gupta, 2017; Rajak *et al.*, 2019)

- Inter-ply involves two or more types of unidirectional or woven fiber layers stacked together.
- Intra-ply involves two or more types of various fibers in the same lamina.
- Inter-ply-intra-ply involves successive layers of inter-ply and intra-ply lamina.
- Resin hybrid involves two matrices blended in the same laminated fiber composite.
- Nano composite involves the addition of nanoparticle powder to a polymer resin matrix.
- Fiber metal laminate involves alternative layers of metal and fiber layers.

A hybrid of a unidirectional glass fabric layer with a carbon fabric layer in the epoxy matrix is an example of an inter-ply hybrid laminate composite as shown in Figure(1.4) in which the synergetic effect between the two fibers is utilized, where the expensive carbon fiber has higher strength and stiffness with lower strain to failure comparing to the cheap glass fiber then the hybridization will eliminate the disadvantage and highlight the advantage of each fiber in the same matrix (Harris, 1999; Chawla, 2012; Thakur, Thakur and Gupta, 2017).

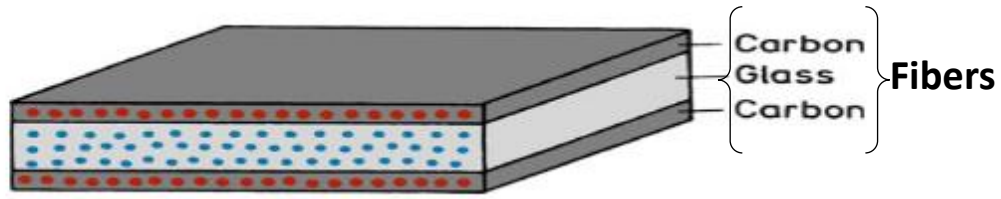


Figure (1.4) Inter-ply Hybrid laminated composite between glass and carbon fiber (Chawla, 2012).

1.6 Fiber Metal Laminate

Both metal and FRPCs have disadvantages that limit the use of them in specific applications. Laminated fiber polymer composite compared to metal has low weight, high strength and stiffness, and high corrosion resistance, but their disadvantages are low impact resistance, high humidity absorption, and low level of operating temperature. Therefore, fiber metal laminate FML is suggested and consists of layers of metal and FRPCs to merge the advantages and eliminate the disadvantages of both and create new FML material (Thakur, Thakur, and Gupta, 2017).

FML is categorized according to the arrangement of ingredient material layers into the asymmetrical, sandwich, and multi-stack configurations as shown in Figure (1.5) (Ding *et al.*, 2021).

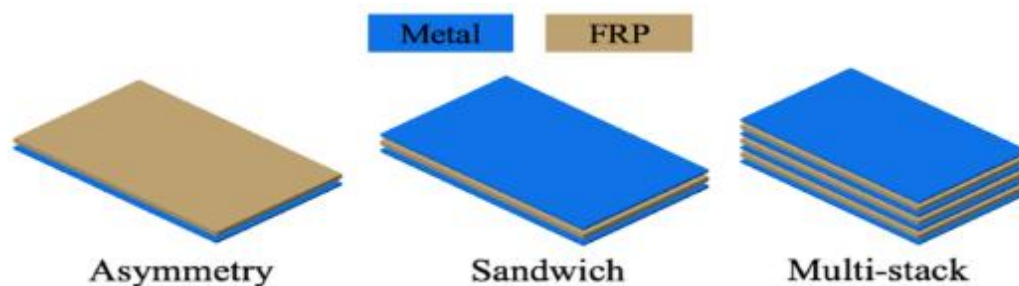


Figure (1.5) classification of FML according to layer arrangement (Ding *et al.*, 2021).

The most popular FMLs are aluminum-based FMLs with epoxy reinforced with carbon, glass, and aramid fibers, which are referred to as CARAL, GLARE, and ARAL, respectively (Logesh *et al.*, 2017) as shown in Figure (1.6) (Ding *et al.*, 2021). The Mechanical behavior of FML is influenced by the following factors (Thakur, Thakur and Gupta, 2017)

- Metal and FRP composite properties.
- Metal composite interface.
- Treatment of metal surface.
- Stacking sequence of plies and fiber angle of orientation.
- Fabrication method.

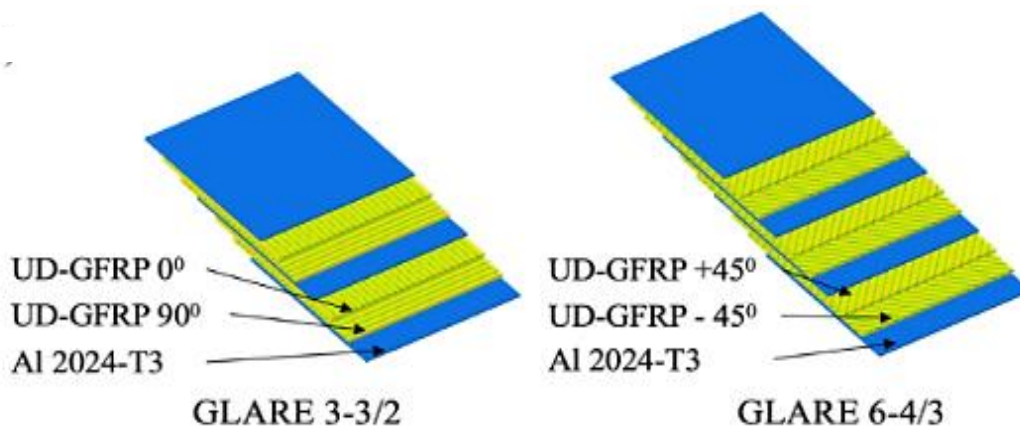


Figure (1.6) Example of Al-base metal /glass fiber reinforcement FML (Ding *et al.*, 2021)

Fabrication of FML is more complicated than metal because it consists of alternative layers of metal and fibers connected by adhesive (Ding *et al.*, 2021). FML products depend primarily on the interface bond between metal and fibers and are empty from faults like voids or delamination (Ding *et al.*, 2021).

1.7 Aim and Objective

In this study, three types of hybridization were used. Firstly, the hybridization of carbon fiber with glass fiber in the same epoxy matrix. Secondly, hybridization of the epoxy matrix with nano Al_2O_3 . Finally, hybridization of fiber core with metal skins to form FML sandwich.

This dissertation will answer the following inquiries:

- How to increase the ductility behavior of FRPC and FML.
- How to increase the dynamic behavior of FRPC and FML.
- How to increase flexural modulus, natural frequency, and damping ratio simultaneously.
- To analyze the factors that affect the maximum deflection due to uniformly distributed load and on the fundamental natural frequency of isotropic, orthotropic, (isotropic /orthotropic/ isotropic) simply supported plate theoretically and numerically by using FEM (ANSYS 19.2).

1.8 Problem Statement

The mechanical and dynamical behavior of fiber-reinforced polymer (FRP) composites is influenced by the type of reinforcement and the presence of additives. This study aims to investigate the effects of incorporating glass/carbon hybrid fibers and nano- Al_2O_3 particles on the performance of FRPC and stainless-steel base fiber metal laminates (FMLs). The goal is to determine how these modifications impact the material's strength, stiffness, energy absorption, and vibration-damping characteristics. The results could provide valuable insights for designing more robust and efficient FML structures for various applications in industries such as aerospace, and automotive.

1.9 Dissertation Layout

The dissertation is divided into six chapters.

The **First Chapter** covers sufficient definitions for both FRPC and FML, the aim and objective of the study, the problem statement, and the dissertation layout.

The **Second Chapter** covers a comprehensive overview of the tensile, flexural, and free vibration behavior for both FRPC and FML. Also, deflection and fundamental natural frequency for metal, FRPC, and FML were covered. During this investigation, a notable research gap has been identified within this field.

Chapter Three Displays the theoretical analysis of the bending of metal, FRPC, and FML plates and beams. Furthermore, the FEM (ANSYS 19.2) modeling of tensile, flexural, and free vibration, of FRPC is displayed. Finally, the FEM (ANSYS 19.2) modeling of metal, FRPC, and FML plate bending is displayed.

In **Chapter Four**, the process of fabrication of eight FRPC (G/C) configurations, and stainless-steel-based FML is presented. Also, the equipment used to determine the mechanical and dynamic properties of materials is presented.

In **Chapter Five**, the tension, flexural, and free vibration behavior of FRPC and FML are shown and discussed. The maximum practical tensile and flexural load as well as fundamental natural frequency are validated numerically. Furthermore, the maximum deflection and fundamental natural frequency of simply supported plates for metal, FRPC, and FML are determined theoretically and validated numerically.

Chapter Six The study's main conclusions are summarized along with suggestions for future work.

CHAPTER TWO LITERATURE REVIEW

2.1 Introduction

In this chapter, a review of the previous research related to the mechanical and dynamic properties of fiber-reinforced polymer composite and fiber metal laminate has been conducted. In addition, adequate reviews have also been done on the factors influenced on the deflection and natural frequency of isotropic, orthotropic, and sandwich FML.

2.2 Mechanical Behavior of Hybrid Laminated Composite

High specific strength (strength to density ratio) and high specific stiffness (modulus to density ratio) connected with lightweight and enhancement in corrosion, wear, and fatigue resistance are the essential reasons to replace the conventional metal by fiber reinforced polymer laminated composite (FRPC) in structural applications like aerospace, automobile, and turbine blades (Daniel, 2006). The most common fibers used in industrial applications are carbon and glass. The use of carbon fiber in structural parts alone is unsuitable, despite its high strength and modulus due to its low strain-to-failure. To overcome the disadvantages of carbon, glass fiber was added to it, where the latter has low strength and modulus, but the strain to failure is high (Ikbal, Wang and Li, 2016). Hybridizing carbon with glass and vice versa is one of the important ways to eliminate the disadvantages of the fibers and to reduce the weight and cost. As a result of the contrastive coefficient of thermal expansions of carbon fiber and glass fiber, the stress-strain curve of CFRP after hybridization moves to higher strain-to-failure because of the formation of residual compressive strain in carbon fiber following the curing process, (Kretsis, 1987; Swolfs, Gorbatiikh and Verpoest, 2014).

2.2.1 Glass: Carbon Fiber Hybrid Composite

It is possible to obtain hybrid composite materials in several ways and then find their mechanical properties related to the previous works. Zhang *et al.*, (2012); Jesthi, *et al.*, (2018 a); Jesthi, *et al.*, (2018 b); Jesthi, *et al.*, (2018 c) investigated the influence of stacking sequence and the hybrid ratio of woven glass and carbon on the mechanical properties (strength & stiffness) of inter-ply hybrid FRP laminated composites. When the glass: carbon (G: C) hybrid ratio is 1:1, the balance mechanical properties were evaluated either by putting the carbon layers at the surface or by putting different layer types alternatively (Zhang *et al.*, 2012). Jesthi, *et al.*, (2018 a); Jesthi, *et al.*, (2018 b); and Jesthi, *et al.*, (2018 c) researchers fabricated ten layers of carbon and glass laminated composites. The [GCGGC]s has tensile and flexural strength more than [CGGCG]s, while [CGGCG]s has higher tensile and flexural modulus by 20% and 36.2%, respectively, as compared to [GCGGC]s (Jesthi, *et al.*, 2018 a). Tensile strength, strains, and flexural extension of [G3C2]s were higher by 11.5%, 23%, and 39% than [C2G3]s, but flexural strength and modulus of [C2G3]s were higher by 23% and 64% than [G3C2]s (Jesthi, *et al.*, 2018 b). The tensile and flexural strength of [G2C2G]s were higher by 10.5% and 2.5%, respectively than that of [CG3C]s, but the tensile strain and flexural extension of [G2C2G]s was 17.5% and 35.8% more than that of [CG3C]s, respectively (Jesthi, *et al.*, 2018c). Two types of unidirectional (UD) glass and carbon fiber were used by Dong and Davies, (2013) to form three hybrid composites (S-2&T700S, S-2&TR30S, and E&TR30S) which are ordered in two stacking sequences of [0G/04C] and [02G/03C], and found that the compression failure is predominated. Therefore, putting glass fiber on the upper side and carbon fiber on the lower side of the laminated composites was better to get the best bending properties as long as the glass volume fraction percentage does not exceed 25%. The catastrophic brittle fracture of CFRP composite can be minimized (Khan *et al.*, 2021) by hybridization of 3k-carbon fabric with E-

glass fabric alternatively in eight layers of laminated composite via increasing the strain to failure (ductility) by 30% in comparison with CFRP composite during flexural test and increasing the flexural strength and modulus by 149% and 144% compared with GFRP composite. Alcludia-Zacarías *et al.*, (2020) demonstrated G: C hybrid ratio equal to 4:2, [GCG]s has the best tensile and bending mechanical properties, where the hybrid effects range from 1.3 to 1.8. On the other hand, the 2:4 G: C hybrid ratio [CGC]s has the best mechanical properties where the hybrid effects range from 1.1 to 2.49. This is due to the presence of carbon between two layers of glass in the first case and vice versa in the second case.

2.2.2 Inter-ply and Intraply Hybrid Composite

Inter-ply (inter-layer) and intra-ply (intra-layer) are two ways to hybridize low-elongation fibers (carbon) with high-elongation fibers (glass). In the first one, the individual layers of fibers are stacked on each other in a different sequence, but in the second type, the combined fibers (yarn-to-yarn) are partnership in the same layer (Swolfs, Gorbatikh and Verpoest, 2014). Many researchers investigated the mechanical properties for both inter-layer and intra-layer laminated composite. Ikbal, Wang, and Li, (2016) studied the bending properties at different hybrid ratios G: C equal to 1:1, 2:1, and 4:1, and found that the hybrid ratio 1:1 gave the highest bending strength and modulus while the hybrid ratio 4:1 gave the highest strain to failure to the laminated composite. Ikbal *et al.*, (2017) used only the hybrid ratio G: C equal to 1:1 and found that the tensile and compression properties for the intra-layer are a little bit more than the inter-layer. The flexural, tensile, and compression properties were researched at various hybrid ratios G: C is equal to 1:1, 2:1, 3:1, 4:1, and various stacking sequences for the same hybrid ratio (Wu *et al.*, 2018; Wu, Wang, and Li, 2018). It can get superior flexural properties by controlling the hybrid ratio and stacking sequence of glass and carbon for both inter-layer and intra-layer (Wu *et al.*, 2018). With increasing glass fiber content, the flexural

modulus decreases, and the strain to failure increases, while the flexural strength depends mainly on the stacking sequence. Increasing carbon content increased the tensile modulus and strength while the strain to failure decreased (Wu, Wang, and Li, 2018). The tensile and compressive modulus for inter-layer and intra-layer are near to each other for the same hybrid ratio and stacking sequence. The ratio of tensile strength to compression strength (R_{TC}) mainly depends on the stacking sequence. When the glass fiber is at the outer surfaces, R_{TC} is minimized and vice versa when the carbon fiber is at the outer surfaces of the laminated composite. Guo *et al.*, (2022) evaluated the interlaminar shear ISS, bending, and tensile strength for uniformly distributed intra-layer G/C hybrid rod composite, which are higher by 10.9%, 60.3%, and 58.69% than interlayer (core-shell) glass/carbon hybrid rod composite.

2.2.3 Impact of Stacking Sequence and Angle of Orientation On the Hybrid Composite

Many researchers studied the effect of stacking sequence and angle of orientation of glass and carbon on the mechanical properties of hybrid composites. Agarwal, *et al.* (2014) discovered that the best tensile strength was achieved with a stacking sequence of GCGCGCG with 32% glass fabric and 18% carbon fabric, and the best flexural strength was achieved with CCGGGCC with 22% glass fabric and 28% carbon fabric. Pujar, *et al.* (2019) demonstrated the mechanical properties of ten layers of glass/carbon and found that the best tensile strength with arrangement [G4C]s at 0° angle of orientation increased by 37.5% compared with pure glass arrangement. The maximum bending strength for fiber arrangement [CG4]s, was at 0° angle of orientation, which is increased by 10.5% compared with pure glass arrangement. Abd Ghani and Mahmud, (2020) used two stacking sequences for both balanced hybrid G/C cross-ply and balanced hybrid G/C quasi-isotropic laminated composites. They concluded that the tensile modulus and strength for the balanced cross-ply [2G₉₀^o/2C₀^o/2G₉₀^o] were equal to 58.2724 GPa and 663.73

MPa, respectively, and were higher than the balanced quasi-isotropic composite. The maximum flexural modulus and strength were evaluated for quasi-isotropic arrangement [$2G_0^0/2G_{90}^0/2C_{\pm 45}^0$] which is equal to 22.675 GPa and 797.77MPa, respectively.

2.2.4 Nano Composite

A perfect adhesion between matrix and fiber is required to modify the load transfer from the matrix to the fiber, in which nano or micro fillers powder is added to the matrix to enhance the load-carrying capacity of the hybrid laminated epoxy composite. The addition of nanofiller to the composite is in the range of (0-2)% to avoid agglomeration in the matrix, which leads to a drop in mechanical properties (Matykiewicz, 2020). The best method for mixing the nanofiller with epoxy resin is using a sonication mixer with a magnetic mixer at the same time by dual mixing process (Halder *et al.*, 2013; Ghosh, Kumar, and Chaudhary, 2015). Adding nano alumina (Al_2O_3) concentration at weight percentages of 1,2, 3, 4, and 5% to the epoxy matrix is to tough short carbon/glass fibers of length 1-7 mm. The optimum dispersions of nano Al_2O_3 equal to 2wt.% improve the impact and flexural properties compared to neat epoxy (Mohanty and Srivastava, 2015). The best concentration of nano SiO_2 to provide balanced mechanical properties is 0.5% according to research by Afrouzian *et al.* (2017) on the tensile, bending, and indentation quasi-static properties and ballistic impact dynamic properties for woven glass laminated composite (12 layers). In Kaybal *et al.*, (2018), carbon fiber laminated reinforced epoxy composite was toughened by different weight percentages of nano Al_2O_3 at 1-5% and found practically that the concentration of 2% nano Al_2O_3 showed the highest tensile strength and strain, equal to 759.4 MPa and 3.73%, respectively, and the highest bending strength and strain, which were equal to 440.6 MPa and 1.32%, respectively. In addition to tension and bending, low-impact tests with velocities ranging from 2, 2.5, and 3 m/s were performed, and found that the addition of 2% of nano Al_2O_3 gave the highest

impact force and less damage area. To improve the mechanical properties of wind turbine blades, it is suggested by Abu-Okail *et al.*, (2021) that a carbon/glass hybrid laminated epoxy composite be toughened by 1.5% nano alumina and 1.5% nanographene.

2.3 Mechanical Behavior of Fiber Metal Laminate (FML)

Fiber metal laminates (FMLs) are hybrid laminate composites that integrate high ductility metal sheets with brittle fiber-reinforced polymer composite to access superior mechanical and dynamic properties.

2.3.1 Glass Fiber Composite/Aluminum (Glare)

Mechanical behavior of glass fiber composite/aluminum (Glare) inspected by many researchers. Hassan *et al.*, (2015) studied the leverage of the number of woven E-glass layers 1, 2, 4, 6, and 8 in Glare. The experimental results demonstrated that tensile strength increased with increasing the number of E-glass layers until 6 layers. The tensile strength for Glare with 6 E-glass layers increased by 58.35% than that one with 1 E-glass layer. On the other hand, flexural strength and modulus for Glare with 8 E-glass layers increased by 69.25% and 64.134% than that of one with 1 glass layer, respectively. Merzuki *et al.*, (2018) verified the experimental tensile performance of Glare by numerical finite element modeling based on a C3D8R element with 8 nodes. Dahshan *et al.*, (2020) found a close convenience between the practical results and numerical analysis model for the stress-strain curves of Al/G/G/Al/G/G/Al. The tensile behavior started elastically in a linear manner until interlaminar shear stress was generated at interfaces due to the yielding of aluminum sheets. Fiber breakage and matrix cracking of woven glass/epoxy occurred before the maximum tensile strength was 319 MPa and the maximum tensile strain was 2.7 %. Eventually, delamination between glass fiber and aluminum sheet accompanied by a steep dropping in the stress-strain curve. The bending behavior started elastically in a linear manner. The upper aluminum sheet buckled and deboned (interlaminar shear stress) between it and the next glass

layers accompanied by fiber breakage and matrix cracking. Consequently, abrupt load decline due to the failure of the last glass fibers and aluminum sheet by tensile stress. The maximum bending stress is 596 MPa and the maximum bending strain is 2 %. Ammar *et al.*, (2019) examined three configuration stacking sequences, 2/1, 3/2, and 4/3 aluminum-based FML tensile properties. Whenever the aluminum layer thickness increased and the number of stacked layers decreased, the tensile properties increased. Consequently, layup 2/1 has higher tensile strength and modulus which are equal to 123.8 MPa and 54.65 GPa, respectively. Annamalai *et al.*, (2021) emphasized the results of Ammar *et al.*, (2019) for the stacking sequence 3/4 (Al/G/G/Al/G/G/Al) and 5/4 (Al/G/Al/G/Al/G/Al/G/Al). The first one has the almost best mechanical properties. The bending modulus and deflection are inversely varying. So, the flexural modulus of 5/4 Glare increased by 12% compared to the 3/4 one.

2.3.2 Impact of Nano Addition on the Mechanical Behavior of Glare

Many researchers have conducted studies on the impact of incorporating nanoparticles on the mechanical properties of Glare fiber metal laminates. Megahed *et al.*, (2019) found out giant improvement in tensile strength, tensile modulus, tensile toughness, flexural strength, and flexural modulus via adding 1% nano SiO₂ pursued by nano Al₂O₃, Al, and Cu compared to neat Glare. Furthermore, the interlaminar shear strength that is responsible for the interfacial bonding between metal layers and composite outer surfaces and between composite layers itself perfected with the addition of 1% nano Al₂O₃ tailed by 1% nano SiO₂, Al, Cu in comparison with neat Glare. On the contrary, these properties deteriorated via adding 1% of NC (nano clay) and TiO₂ compared with neat Glare. Keshavarz, Aghamohammadi, and Eslami-Farsani, (2020) detect the bending performance of Glare consisting of 10 glass fiber layers sandwiched between two Al 6061 aluminum sheets without and with (0.25, 0.5 & 1% wt.) nanoplatelets graphene under several naval situations. The

superior bending strength and modulus for 0.25% GPN Glare which is 2.26 and 1.56 times more than 0% GPN Glare. The four conditions immersed in 3.5% wt. NaCl water mixture for distinct time intervals (7, 14 & 28 days). With increasing the immersed time interval, the bending properties generally dropped. The minimal water absorption for Glare with 0.25% wt. GPN compared with the other conditions. For these reasons, Keshavarz and his group preferred 0.25% wt. GPN for maritime implementations. To increase mechanical properties of 3/2 quasi-isotropic Glare [Al/(G0/G90/G45/G-45)s/Al/(G0/G90/G45/G-45)s/Al], 1% wt. of halloysite nanotubes added to it (El-baky and Attia, 2022). The tensile strength, tensile modulus, tensile strain, bending strength, bending modulus, and bending failure of 1% NHT Glare increased by 26.3%, 22.4%, 7.83%, 33.5%, 28%, and 23.3% in comparison with neat Glare.

2.3.3 (Glass Fiber Composite/ Stainless Steel Base) Fiber Metal Laminate

Khalili, Mittal, and Kalibar, (2005) introduced stainless steel metal to glass fiber reinforced composite to form stainless steel base fiber metal laminate. They prepared four stacking sequences of 3/2 FML by utilizing two types of metal stainless steel as well as aluminum with woven glass fabric, the first one is [SS/G/Al/G/SS], the second one is [Al/G/SS/G/Al], the third one is [Al/G/Al/G/Al], and finally [SS/G/SS/G/SS] is the fourth one. They distinguished that increasing of stainless-steel layers, progressed the mechanical properties. Tensile modulus, failure elongation, tensile toughness, flexural strength, percentage failure strain, flexural modulus, and Charpy impact energy increased by 79%, 92.5%, 92.4%, 60%, 60.34%, 94%, and 42.65% respectively, while the tensile strength decreased by 18.5% compared with glass fiber reinforced epoxy composite.

2.3.4 Carbon Fiber Composite/Aluminum base FML(Caral)

Many researchers have conducted studies on the mechanical properties of carbon fiber composite/aluminum (Caral). Tamilarasan, Karunamoorthy, and Palanikumar, (2015) considered the mechanical behavior of [C0/C90/C0/C90/C0/ AA 6061T3/ C0/C90/C0/C90/C0] fiber metal laminate that is composed of aluminum as a core and cross carbon laminate as a skin. To impede debonding between the composite and metal layer, an inverted root formed on the outer surface of aluminum. The tensile strength extended 283-324 MPa while the flexural load extended 1.79-2.52 KN due to the difference in the production methods. SEM identified fiber breakage, fiber pullout, fiber debonding, and pits faults. Dhaliwal and Newaz, (2016) discovered that Caral B [C/Al/C/Al/C] flexural strength and modulus are higher than that of Caral A [Al/C/Al/C/Al] by 6% and 3%, respectively. On the other hand, the failure strain of Caral A is higher than that of Caral B by 44.4%. The bending toughness of Caral A is higher than the bending toughness of Caral B because the amount of aluminum presence in Caral A is 65% and in Caral B is 50%. The delamination between fiber and metal occurred after fiber breakage and load drop in Caral A while delamination in Caral B occurred in the final failure stage. Bellini *et al.*, (2019a), (2019b), (2020) considered two arrangements of Caral, the first one is C/Al/C and the second one is C/Al/C/Al/C with and without adhesive films between carbon fabrics and metal sheets. They concluded that the highest flexural strength, flexural modulus, and flexural strain are for Caral C/Al/C without any adhesive films. Moreover, the highest interlaminar shear strength and flexural toughness are for Caral C/Al/C/Al/C with adhesive films. Bellini *et al.*, (2021) verified the experimental flexural behavior of long beam and short beam Caral [Al/C/Al] with the numerical one. The failure of the long beam Caral was due to fiber breakage in the middle part while the failure of the short beam Caral was due to fiber delamination of carbon fiber in the same part. Hynes *et al.*, (2022); Chen *et al.*, (2023); Gao *et*

al., (2023) validated the experimental mechanical properties with numerical or theoretical modeling for Caral FML. Gao *et al.*, (2023) took into account four stacking sequences of Caral. The first two are [Al/C0/C0/Al] and [C0/Al/C0], and the other two are [Al/C0/C0/Al/C0/C0/Al] and [C0/Al/C0/Al/C0/Al/C0]. The results indicate that the configuration [C0/Al/C0] possessed the highest bending strength and modulus because of the presence of carbon layers in the outer surfaces of FML. Also, both bending strength and modulus decreased with increasing the amount of metal in FML. Eventually, the experimental and modeling results are approximately coincided. Chen *et al.*, (2023) predicted theoretical flexural strength of 2/1, 3/2, and 4/3 Caral FML and experimentally validated. 3/2 Caral arrangement with three aluminum sheets and two carbon fibers has the highest flexural strength. The failure region is differentiated by fiber breakage and fiber/ metal border delamination. Hynes *et al.*, (2022) proposed two forms of Caral. Form one order is Al/C/Al/C/Al and form two is C/Al/C/Al/C where both of them are compared with the essential carbon/epoxy composite form. The maximum tensile strength, maximum tensile strain, maximum bending load, maximum bending displacement, and impact energy for form one is higher than carbon fiber/epoxy composite by 24.4%, 27.3%, 52%, 43.24%, and 80% respectively. The difference between the experimental and numerical results doesn't exceed 4%.

2.3.5 (Carbon Fiber Composite/ Titanium Base) Fiber Metal Laminate

[Titanium/ (carbon/epoxy) composite/ Titanium] fiber metal laminate utilized in high-temperature applications. Sun *et al.*, (2019) studied the influence of titanium sheet thickness, the number of carbon prepregs, and its direction, on the tensile properties of eight types of carbon laminated composite and eleven types of [Ti/C/Ti] fiber metal laminate. Laminate [C0/C0] and fiber metal laminate [Ti/C0/C0/Ti] owned the peak tensile strength and tensile modulus because of the presence of two unidirectional carbon fibers alone.

Minimum tensile properties have belonged to laminates [C90/C90] and [C-45/C45] as well as fiber metal laminates [Ti/C90/C90/Ti] and [Ti/C-45/C45/Ti] because of the presence of two successive 90° and 45° carbon fibers. The variance between estimated and experimental tensile properties doesn't exceed 10%.

2.3.6 Glass and Carbon Hybrid Fiber Composite/Aluminum FML

Many researchers studied the mechanical behavior of fiber metal laminate composed of glass and carbon fiber composite integrated with metal layers. Rajkumar *et al.*, (2014) found that the tensile strength increased while the bending strength and interlaminar shear strength decreased with increasing the strain rate. The highest tensile, flexural, and interlaminar shear strength is for Al3C6 FML while the lowest value of them is for AL3G6 FML. The other two stacking sequences Al3C2G4 and Al3C4G2 strengths lay between them. Nestler *et al.*, (2017) replaced steel by [Al/G(±45)-PA6/ C(0)-PA6/ C(0)-PA6/ C(0)-PA6/ G(±45)-PA6/Al] FML in automobile chassis. The new arrangement provided a 29% weight reduction. The two G (±45) beneath the metal layer declined the delamination and increased the torsion mechanical properties by 85%. On the other hand, the bending properties increased by 67% by introducing three unidirectional carbon layers in the center of the FML. Ostapiuk, Bieniaś, and Surowska, (2018) recognized the leverage of aluminum sheet thickness alongside the fiber orientation [0], [0, 90], [90, 0], [±45] on the flexural properties of [Al/G/Al] and [Al/C/Al] FMLs. They inferred that increasing aluminum sheet thickness leads to increase flexural strength and vice versa for flexural modulus. The angle of orientations [0,90] and [90,0] didn't influence the flexural strength. However, fiber metal laminates [Al/G0/G90/Al] and [Al/ C0/C90/Al] flexural modulus are higher than [Al/G90/G0/Al] and [Al/ C90/C0/Al] by 51% and 13%, respectively. Moreover, [±45] orientation reduced the flexural strength and raised the flexural modulus

by 3.36% and 6.52% for [Al/G/Al] as well as 24% and 14.7 for [Al/C/Al], respectively in comparison with [0] orientation for both FMLs. Smolnicki and Stabla, (2019) modeled [Al 2024 T3|0₂^{CFRP}]_s with 0.3mm and 0.5mm aluminum sheet thickness as well as [Al 2024 T3|45₂^{CFRP}]_s with 0.3mm aluminum thickness and compared with the bending experimental results of (Ostapiuk, Bieniaś and Surowska, 2018). If the layers of fiber metal laminate are deemed separately with their special properties then finite element modeling and experimental results are close to each other. Yang *et al.*, (2022) explored the tensile properties of steel and aluminum-based fiber metal laminate by using glass and carbon fibers as internal cores. The density of [Al/C/Al] and [Al/G/Al] are minimized by 15% and 12.5% respectively in comparison with aluminum sheet. The density of [S/C/S] and [S/G/S] are minimized by 27% and 28%, respectively in comparison with Steel alone. The tensile toughness of all FML is higher than that of metal and fiber laminate because of the addition of high ductility metal to high-strength fiber laminate composite. Trautmann *et al.*, (2020) pursued the mechanical properties for four types of FML arrangements that contained aluminum alloy AA6082-T4 as well as glass/polyamide 6 (G/PA6) and carbon/polyamide 6 (C/PA6) thermoplastic prepregs. The first and second arrangements are [Al/G0/C0]_s and [Al/(G0)₂/(C0)₂]_s, while the third and fourth arrangements are [Al/G±45/(C0)₂]_s and [Al/G0/(C0)₂/G0/Al]; respectively. The aluminum volume fractions are 61%, 44%, 44%, and 54% for the first, second, third, and fourth arrangements; respectively. The tensile strength for the second arrangement is higher than the first, third, and fourth arrangements by 28%, 50%, and 24%; respectively. The highest tensile strain for arrangement one because it contains the highest metal volume fraction. The flexural strength for the second arrangement is higher than the first, third, and fourth arrangements by 47%, 46%, and 17.4%; respectively. The highest flexural strain for arrangement three was because of

the presence of $G_{\pm 45}$ in the core which led to a decrease in the central deflection and hence increased the strain.

2.3.7 Comparison Between Aral, Caral, and Glare

Many researchers inserted aramid fiber into glass and carbon fibers in aluminum-based fiber metal laminates. Moussavi-Torshizi *et al.*, (2010) studied the tensile properties for nine different angles of orientation of [Al/G/K/G/Al] FML. The experimental results are validated with theoretical and finite element modeling. The higher tensile strength, yield strength, and tensile modulus for [Al/G₀/K₀/G₀/Al] FML is because of the presence of three unidirectional fibers in the core. Biliz and Çelik, (2022) assessed the impact of fiber type on the tensile strength and flexural strength for the following six patterns of FMLs: Aral, Glare, Caral, Ar-Caral, Ar-Glare, and Car-Glare. The tensile strength of Caral is higher than Aral and Glare by 50% and 65%, respectively. The flexural strength of Caral is higher than Aral and Glare by 35% and 37%, respectively. The presence of carbon fiber layer in Ar-Caral and Car-Glare FML progressed both strengths to be higher than Aral and Glare itself.

2.4 Free Vibration of Fiber Reinforce Polymer Composite

Multifunctional fiber-reinforced laminated polymer composites have been utilized in recent decades in structural applications, including automobiles, shafts, aircraft, bicycle frames, and tennis rackets, due to their superior properties, such as low density (low weight), high strength, high stiffness, and high damping capacity. The vibration energy dissipation of fiber-reinforced polymer composite (FRPC) can be achieved by increasing its viscoelastic behavior (Chung, 2003). FRPC damping capacity can be enhanced by increasing the number of interfacial regions, either by adding fibers or nano-fillers to its viscoelastic matrix, which then causes the vibrating energy to be dissipated by friction between the matrix and reinforcement. Hybridization is

one of the means to increase the damping capacity of FRPC by adding high elongation to low elongation fibers (Treviso *et al.*, 2015; Tang and Yan, 2020).

2.4.1 Dynamic Behavior of Glass and Carbon Fiber Reinforced Polymer Composite

Natural frequency and damping ratio represent the dynamic behavior of materials. Glass and carbon fibers are widely used in structural applications. Researchers (Erkliđ, Bulut and Yeter, 2015; Murugan, Ramesh and Padmanabhan, 2016; Suman, Murigendrappa and Kattimani, 2019; Aydin *et al.*, 2022; Pujar, Nanjundaradhya and Sharma, 2022) have illustrated that carbon fiber has a higher natural frequency than glass fiber due to the high flexural modulus value of carbon fiber in a polymer matrix. In contrast, glass fiber has a higher damping ratio than carbon fiber in a polymer matrix, as shown in Table (2.1). The mechanical and dynamic properties of materials are related to each other.

Table (2.1) Comparative dynamic behavior of glass and carbon fiber reinforced polymer composite (Erkliđ, Bulut and Yeter, 2015; Murugan, Ramesh and Padmanabhan, 2016; Suman, Murigendrappa and Kattimani, 2019; Aydin *et al.*, 2022; Pujar, Nanjundaradhya and Sharma, 2022)

FRPC	Natural Frequency [Hz]	Damping Ratio [%]
CFRPC	High	Low
GFRPC	Low	High

2.4.2 Relationship between Flexural Modulus, Natural Frequency, and Damping Ratio

Zhang *et al.*, (2012); and Swolfs *et al.*, (2015) illustrated that a laminated fiber composite with equal numbers of glass and carbon fibers gives the best flexural strength and modulus. The high flexural modulus and low strain to failure carbon fabric is added to the low flexural modulus and high strain to failure glass fabric to benefit from the advantages of each ingredient and exclude the disadvantages of them. The natural frequency is related to the

flexural modulus of the materials, increased with increasing flexural modulus, while the damping ratio is inversely related to the flexural modulus. To increase interfacial boundary regions, nano-filler is added to the epoxy matrix of inter-ply (G+C) hybrid fiber-reinforced composite so that more friction will occur when it vibrates; consequently, the damping ratio is increased.

2.4.3 Mechanical and Damping Characteristics of Glass Fiber Reinforced Composite

Zhang *et al.*, (2021) investigated the tensile properties and damping characteristics in both vacuum and air environments of nine conditions of E-glass/polyurethane laminate composites by changing glass volume fraction (V_f) 50 %, 55 %, 60 %, and angle of orientation 0° , 45° , and 90° . They deduced that the best damping capacity was for lower glass (V_f) with a greater angle of orientation, which leads to lower tensile strength. The damping capacity in the air is higher compared to that in a vacuum for the same laminate. (Navaneeth *et al.*, 2022) studied the tensile, flexural, and damping properties of woven glass/epoxy laminated composites with three different glass volume fractions: 50 %, 60 %, and 70 %. From collected experimental data, they found that the laminate with 60 % glass (V_f) obtained the best tensile and flexural properties (strength and stiffness), while the laminate with 70 % glass (V_f) obtained the highest natural frequency and lowest damping ratio.

2.4.4 Impact of Nano-Addition on the Dynamic Properties of Glass Fiber Composite

Pol *et al.*, (2013) researched the effect of adding 1 %, 2 %, 3 %, 5 %, and 7 % nano clay filler to 12-layer woven glass laminated epoxy composite and concluded that increasing the weight percentage of nano-filler to 5 % increased the natural frequency; after that, it decreased, but the damping ratio increased to 7 %. Khashaba, (2016) researched the impact of adding 1.5 % nano SiC and 1.5 % nano Al_2O_3 on the damping properties of quasi-isotropic laminates with

two stacking sequences $[0/\pm 45/90]$ and $[90/\pm 45/0]$. They proved that the highest damping capacity is obtained for the second stacking configuration with and without nano because the 90° first layer reduces the stiffness of the composites. Pujar, Nanjundaradhya, and Sharma, (2018) examined the effect of introducing 0.1 %, 0.5 %, and 1 % nano-graphene oxide (GO) on the damping properties of glass/epoxy composite by utilizing 0° and 45° fiber orientation and two boundary conditions (cantilever and free). They found that adding nano-GO improves damping capacity, whereas 0.5 % GO gives the highest damping ratio. Increasing the angle of fiber orientation between 0° and 45° leads to decrease natural frequency and increase damping ratio for cantilever boundary condition and vice versa for free condition.

2.4.5 Relationship Between Mechanical and Dynamic Properties of Fiber Reinforced Polymer Composite.

The mechanical and dynamic behavior of hybrid glass/carbon laminated composite studied by many researchers. Murugan, Ramesh, and Padmanabhan, (2016) concluded that the presence of carbon fiber in the middle of the laminated composite H1[GCCG] increases tensile strength, tensile modulus, and damping ratio, while the presence of carbon fiber in the outer surface of the laminated composite H2[CGGC] increases flexural strength, flexural modulus, and natural frequency for (50 % carbon: 50 % glass) fiber addition. Suman, Murigendrappa, and Kattimani, (2019) found that the inter-ply hybridization of equal numbers of glass and carbon fiber in laminated composite affects the dynamic properties. As a result, the arrangement GC1 [G/C/G/C/G/C/G/C]_s has a natural frequency of 46 Hz and a damping ratio of 0.095. In contrast, altering the arrangement by putting the carbon fiber on the external surface for the arrangement CC1[C/G/C/G/C/G/C/G]_s will slightly reduce both the natural frequency and damping ratio to 45 Hz and 0.088,

respectively. Pujar, Nanjundaradhya and Sharma, (2022) investigated the tensile and dynamic properties of laminated composite that is fabricated from 80 % glass and 20 % carbon. They found that H3[G/G/G/G/C]_s has maximum tensile strength and modulus because of the presence of one carbon ply in the middle of the laminate. The dynamic properties were accumulated for free FFFF and cantilever CFFF boundary conditions. In the FFFF condition, a higher natural frequency was found in H1[C/G/G/G/G]_s hybrid condition in the presence of one carbon fiber at the outer surface of the laminate. On the other hand, a higher damping ratio was found in the H3 hybrid condition in the presence of one carbon fiber in the middle of the laminate. In the CFFF condition, the natural frequency and damping ratio dropped in comparison with FFFF, with the higher natural frequency for the first hybrid condition H1, while the higher damping ratio for H2[G/G/C/G/G]_s condition in which one carbon fiber is present after two glass fibers from the outer surface. Aydin *et al.*, (2022) predicted the dynamic properties of non-hybrid, inter-layer, and intra-layer hybrid composites for carbon, glass, and aramid fiber reinforced in an epoxy matrix and taking the angle of orientation, stacking sequence, and number of plies into consideration. They found the best arrangement of fibers for higher dynamic properties by using the Taguchi program. Karthik *et al.*, (2016) investigated the damping properties of E-glass chopped mat/woven carbon hybrid with four different volume fractions in epoxy matrix and polyester matrix. They demonstrated that the damping capacity increased with increasing glass volume fraction for both matrices; furthermore, the addition of 5 % carbon fiber gave the best damping behavior and natural frequency for structural composite. Utomo, Susilo, and Raharja, (2017) studied the effect of increasing carbon layers and their position in an eight-layer hybrid glass/carbon laminated unsaturated polyester composite and concluded that with increasing numbers of carbon layers near the outer surface of the laminate, the natural frequency increased and damping capacity (ξ) decreased. In contrast, by

positioning carbon layers toward the center of the laminate, the natural frequency decreased while the damping capacity increased. Finally, the natural frequency and flexural stiffness are directly proportional to each other. Singh, Jain, and Bhaskar, (2020) studied the effect of stacking sequence and angle of orientations on the natural frequency and damping ratio of four-layer glass/carbon epoxy laminates and found that the laminate $[0C/90G]_s$ acquired the highest natural frequency, while $[90C/0G]_s$ obtained the lowest one. The highest damping ratio is attained for both laminates $[90G/90C]_s$ and $[90C/90G]_s$, while the laminate $[0C/0G]_s$ obtained the lowest damping ratio. Pingulkar and Suresha, (2016) utilized the ANSYS software package to evaluate the natural frequency and mode shapes of eight-layer glass/carbon hybrid laminated cantilever plates and concluded that important changes in natural frequency could be obtained by hybridization, change of angle of orientation, and stacking sequence more than the change in volume fraction.

2.4.6 Hybrid Composite

Fairlie and Njuguna, (2020) investigated the impact of stacking sequence and angle of orientation on the tensile and damping capacity of inter-ply hybrid carbon/flax epoxy laminated composite and attained that the outer layer in the laminate is the important layer to control the damping capacity of the laminate. By adding one flax layer at the exterior of the carbon/epoxy laminate, the damping ratio increased by 53.6 %, and by adding two flax layers, it increased by 94 %. Alexander, Kumar, and Augustine, (2015) studied the effect of boundary conditions, material properties, and laminate thickness on the natural frequency of glass/epoxy and basalt/epoxy laminated composite and concluded that the damping capacity of basalt/epoxy composite is higher than that for glass/epoxy composite. Erkljč, Bulut, and Yeter, (2015) inspected the dynamic behavior of inter-ply FRPC by using carbon, Kevlar, and glass fibers and determined that $[(0G/90G)3]_s$ and $[(0C/90C)3]_s$ had minimum and maximum natural frequencies, respectively. The laminates $[(0C/90C)3]_s$ and

[(0K/90K)₃]_s had the minimum and maximum damping capacity, respectively. To increase natural frequency, add higher stiffness fiber at the outer surface, like carbon; however, to increase the damping ratio of the structure, add higher viscoelastic fiber at the surface like Kevlar. Hybrid [(0C/90C)/(0K/90K)/(0G/90G)]_s had the maximum natural frequency compared to other hybrids, and the [(0/90)₃]_s fiber orientation had the maximum natural frequency compared to other orientations. Bulut *et al.*, (2019) investigated the influence of adding S-glass inter-ply to woven carbon-aramid intra-ply on the natural frequency and found that higher natural frequency can be obtained by positioning glass in the middle and (C+A) at the outer surface of the laminate, where the configuration [CA2G2]_s had the highest natural frequency. Senthamaraikannan and Ramesh, (2019) decided to increase the damping capacity of the woven carbon laminated structure by adding 11 % nano SiO₂ with 9 % micro CTBN rubber to the epoxy matrix, despite the slight drop in tensile and flexural modulus. Bulut, Erkliđ and Kanmaz, (2019) investigated the dynamic behavior of basalt/epoxy laminated composite by adding (0.1, 0.2, and 0.3) nano-graphene and determined that 0.1 % and 0.2 % of nano-pellets increased the natural frequency and damping ratio, but 0.3 % decreased both of them.

2.5 Free vibration of Fiber Metal Laminate

2.5.1 Glass Fiber Composite/Aluminum (Glare)

Many scholars investigated the dynamic characteristics of Glare. Botelho, Pardini, and Rezende,(2005) found that the natural frequency of Glare is higher than glass/epoxy composite by 20% and aluminum by 43% in dry status. The damping ratio of Glare is higher than glass/epoxy composite by 46% and aluminum by 94% in dry status. The damping ratio of glass/epoxy composite in wet condition is increased 2.25 times in dry condition because of epoxy plasticization (softening and increased flexibility of polymer). The main problem in FML is the bonding between metal and fiber layers. Zal *et al.*,

(2017) utilized various surface treatments and discovered that roughened aluminum surfaces led to the tear of fibers without delamination during the flexural loading test. They found that the ultimate damping value of glass/pvc composite is higher than [(glass/pvc)/Al] FML because of its lower flexural modulus. Cicco and Taheri, (2018) estimated the natural frequencies experimentally, numerically, and analytically of aluminum, [G0/G0/G90/G0/G90/G0]s composite, [Al/ G0/G0/G90/G0/G90/G0]s Glare and eventually 3D-FML. The structure of 3D-FML consists of 3D channels of glass fiber saturated with polyurethane foam arranged between two magnesium sheets. The highest natural frequency returned to 3D-FML because of its highest bending stiffness. In contrast, the lowest natural frequency belonged to Glare because of its lowest bending stiffness. Merzuki, *et al.*, (2019) determined the natural frequencies of 2/1 Glare and 3/2 Glare fabricated by two techniques. The compression molding technique raised the natural frequency of 3/2 Glare by 50.3% and 2/1 Glare by 16% in comparison with glass/epoxy composite. While the vacuum technique raised the natural frequency of 3/2 Glare by 54% and 2/1 Glare by 43% in comparison with glass/epoxy composite. Saini *et al.*, (2019) investigated the natural frequency of cracked and uncracked 3/2 Glare. The value of the natural frequency decreased with the presence and increment of crack length attributed to the decrease in beam stiffness. The natural frequency value decreased with increasing the fiber angle of orientation until 60°. Ciftci and Kadioglu, (2021) considered the impact of glass fiber orientation on the bending modulus and fundamental frequency of 3/2 Glare experimentally, analytically, and numerically. Unidirectional Glare [Al/G0/G0/Al/G0/G0/Al] has the highest flexural modulus and natural frequency. While 90° Glare [Al/G90/G90/Al/G90/G90/Al] has the lowest flexural modulus and natural frequency.

2.5.2 (Glass/Copper Base) Fiber Metal Laminate

Abdellah *et al.*, (2020) investigated the dynamic properties of glass/copper fiber metal laminate with various hole diameters (2mm, 4mm, 6mm, 8mm, 10mm, and 12mm). The natural frequency increased with increasing hole diameter and vice versa for the damping ratio.

2.5.3 Carbon Fiber Composite/Aluminum Base (Caral) FML

Maraş *et al.*, (2018) deemed four variables in the FML stacking sequence. The number of aluminum layers and the position of the individual layer were considered in categories A and B, respectively. While fiber direction and position of the 45° carbon layer were considered in categories C and D, respectively. The natural frequency increased by placing the aluminum layer toward the center of the laminate as well as by increasing the angle of fiber orientation to 45° as in conditions B and C, respectively. However, the natural frequency decreased by increasing the number of aluminum layers and positioning the 45° carbon prepreg toward the center of the laminate as in cases A and D, respectively. Ahmed and Meenakshisundaram, (2022) concluded that carbon/epoxy with nanographene bending strength and modulus are higher than carbon/epoxy composite by 17% and 26%, respectively. Also, they are higher than carbon/Al base fiber metal laminate by 57% and 85%, respectively. The natural frequency of carbon/epoxy is higher than carbon/epoxy with nanographene and carbon/Al FML by 2.55% and 10%, respectively. On the other hand, carbon/epoxy and carbon/epoxy with nanographene peak acceleration is lower than carbon/Al base FML by 56%, consequently, the damping of carbon/epoxy and carbon/epoxy with nanographene is higher than carbon/Al base FML.

2.5.4 (Glass and Carbon Hybrid Fiber Composite/Aluminum)

FML

Many researchers studied the free vibration response of fiber metal laminate contained glass and carbon fibers. Botelho *et al.*, (2005) found out that the natural frequency of [Al/C/Al/C/Al] 3/2 Caral is higher than glass/epoxy, carbon epoxy, aluminum, and [Al/G/Al/G/Al] 3/2 Glare by 37%, 8%, 55%, and 21%, respectively. The damping ratio of glass/epoxy is higher than carbon/epoxy, aluminum, Caral FML1, and Glare FML2 by 65%, 51%, 67%, and 33%, respectively. Merzuki, *et al.* (2019) validated numerically the experimental natural frequency for 2/1 and 3/2 Glare and Caral. [Al/G/Al] 2/1 Glare and [Al/C/Al] 2/1 Caral natural frequencies are higher than G/epoxy and C/epoxy composites by 31% and 46%, respectively. Moreover, 3/2 Glare and Caral natural frequencies are higher than G/epoxy and C/epoxy by 58% and 72%, respectively. Kali, Pathak, and Korla, (2020) figure out the influence of introducing bamboo natural fiber to the 3/2 Caral and Glare. The acceleration-time response and acceleration-frequency response were found in two situations. Positioning the accelerometer at the end of the FML cantilever beam is the first condition, but positioning it at the middle of the beam is the second condition. In general, replacing the middle aluminum layer of 3/2 Glare and Caral with a bamboo natural fiber layer reduces the acceleration amplitude which is an indication of the increase in damping ratio. The first condition acceleration response reduction is higher than the second condition. Merzuki *et al.*, (2022) verified numerically the experimental natural frequency for 2/1 as well as 3/2 Glare and Caral. The natural frequency of 3/2 Glare and Caral are higher than 2/1 Glare and Caral by 58% and 30%, respectively for cantilever status. For clamped-clamped status, 3/2 Glare and Caral natural frequencies are higher than 2/1 Glare and Caral by 46% and 16%, respectively. Fixed-fixed natural frequency is higher than fixed-free one. Ravishankar *et al.*, (2016) evaluated the fundamental natural frequency of hybrid composite and fiber

metal laminate beams numerically. Carbon-glass hybrid composite natural frequency is higher than aramid-glass or aramid-carbon because of its higher bending stiffness. Aluminum base followed by titanium base and finally magnesium base FML natural frequency descending order. Generally, with increasing the aspect ratio (L/H), the natural frequency decreased. Increasing the beam rotational speed led to an increase in the fundamental natural frequency because of the generating centrifugal force.

2.6 Deflection and Natural Frequency of Metal, FRPC, and FML Composites Plates

2.6.1 Isotropic Plate

Vanam, Rajyalakshmi, and Inala, (2012) found the deflection of 1×1 m aluminum isotropic plate theoretically and numerically at various boundary conditions. The deflection decreased with increasing plate thickness. The deflection minimized to zero for both clamped and simply supported boundary conditions under 500 Pa when the plate thickness was equal to 0.175 m and 0.165 m, respectively. While the deflection of the simply supported plate under 5000 N concentrated load minimized to zero at 0.08 m thickness. Generally, simply supported plate deflection under concentrated load is higher than under uniformly distributed load.

2.6.2 Factors Effectuated on the Deflection and Natural Frequency of FRPC Plate

Many scholars studied the influence of aspect ratio (length/width), modulus ratio (E_1/E_2), thickness ratio (length/ thickness), number of plies, the orientation of fibers, and boundary conditions on the deflection as well as normal stresses of laminated fiber composite plate under uniformly distributed load analytically and numerically. As the aspect ratio increased, the deflection as well as normal stresses decreased (El-Helloty and Salam, 2009; Reddy *et al.*, 2012). As the modulus ratio increased, the deflection decreased and normal

stresses increased (Reddy *et al.*, 2012). El-Helloty and Salam, (2009) discovered that the least deflection can be gained when the angle of fiber is 45° with an aspect ratio equal to 1 in angle ply laminate. Nevertheless, for aspect ratio > 1 , the least deflection can be gained when the fiber angle is 60° . Moreover, the maximum value of normal stresses can occur with a fiber angle equal to 30° . Saxena and Kirtania, (2016) found analytically and numerically, that the highest and lowest deflection are for laminate $[90/0/90]$ and laminate $[0/90/0]$, respectively at aspect ratio ≤ 1 . While the opposite is right for aspect ratio ≥ 1 . With increasing the number of 0° lamina in cross-laminate composite, the deflection increased for aspect ratio ≥ 1 and vice versa for aspect ratio ≤ 1 . Altunsaray and Bayer, (2013) examined the deflection and natural frequency of 24 different forms of quasi-isotropic carbon fiber/epoxy composite analytically and numerically. They explored that the maximum deflection and natural frequency of 12 laminates is similar to the other 12 laminates because the same element of stiffness matrix Q_{11} , Q_{12} , Q_{16} , Q_{22} , Q_{26} , and Q_{66} are utilized to evaluate the bending stiffness matrix $[D]$. (Beylergil, 2020) predicted numerically, the best (glass/carbon) hybrid composite with minimum cost and weight as well as superior stiffness and dynamic properties. Liu and Kam, (2023) evaluated the natural frequencies of thick cantilever carbon laminated composite plate analytically and experimentally. Laminate $[0]_8$, $[0/90_2/0]_s$ and $[45/-45_2/45]_s$ is the descending order of fundamental natural frequency. With an increasing thickness ratio, the natural frequency increased. Koppanati, Naga Rani, and Krishna Bhaskar, (2023) detected the effect of adding 1% wt. nanographene to the carbon /polyester plate in two boundary conditions. The first mode natural frequency of (simply- fixed- simply- fixed) SFSF boundary condition of (carbon/polyester) with 1% nanographene plate is higher than carbon/polyester and polyester with 1%wt nanographene by 3% and 52%, respectively.

2.6.3 Fiber Metal Laminate Plate

Many researchers questioned the free vibration response of fiber metal laminate. Ghasemi, Paknejad, and Fard, (2013) observed that increasing the number of external aluminum layers and the aspect ratio led to an increase in the natural frequency of Glare. Moreover, if the value of Θ in fiber arrangement $[0/\Theta/0/\Theta/0]$ s between $0^\circ - 45^\circ$ then the natural frequency of Glare increased, otherwise decreased. Prasad and Sahu, (2017) realized that the natural frequency of 3/2 Glare increased with increasing the aspect ratio of the plate. The highest natural frequency is achieved with clamped boundary condition. While the lowest natural frequency is achieved with cantilever boundary condition. Prasad and Sahu, (2018) recognized that the descending order of the internal fiber angle orientation from (0/90), (15, -15), (30, -30), and (45, -45) respectively decreased the natural frequency of the 3/2 Glare. Abdellah, Mohamed, and Hasan, (2019) figured out that the first mode natural frequency of aluminum is higher than steel, [glass/network steel] FML, and glass/epoxy by 57.7%, 40%, and 33%, respectively. On the other hand, the first mode damping ratio of steel is higher than glass/epoxy, [glass/network steel] FML, and aluminum by 13%, 17%, and 81%, respectively. Liu *et al.*, (2020) derived an analytical equation to evaluate the natural frequency of FML and validated it experimentally. The use of aluminum metal layer in FML reduced the natural frequency in comparison with titanium and stainless steel. Moreover, increasing the thickness of the metal sheet in FML minimized the natural frequency. Kallannavar and Kattimani, (2020) attained experimentally and numerically that the highest and lowest natural frequencies are for $[0_2/Al/0_2]$ and $[90_2/Al/90_2]$ Caral sandwich FML, respectively. Verma, Verma, and Kumhar, (2021) obtained that aluminum metal matrix with carbon nanotube addition has the highest fundamental natural frequency and is equal to 639 Hz followed by epoxy with carbon nanotube addition and equal to 600 Hz. Four-clamped square plate central deflection due to free vibration can be minimized

by using carbon/epoxy composite or epoxy with carbon nanotube. Rao *et al.*, (2023) proved analytically that aluminum-based fiber metal laminate's natural frequency is higher than magnesium-based FML. Moreover, the existence of a central aluminum layer in Glare [Al/G0/G90/Al/G90/G0/Al] led to an increase in the natural frequency in comparison with Glare without a central layer [Al/G0/G90/ G90/G0/Al].

2.7 Summary

The hybrid of glass with carbon fiber, a hybrid of polymer matrix with nanofiller addition, and a hybrid of fiber core with metal skins (FML) are three ways to increase the tensile, flexural, and free vibration properties of composite materials.

Based on the literature review, the best tensile, flexural, and vibration characteristics can be achieved at a hybrid ratio of G: C equal to 1:1; therefore, in this work, two groups of laminated epoxy composites were fabricated by vacuum-assisted resin infusion method, cross-laminate group and quasi-laminate group, in which both of them containing equal numbers of carbon and glass fiber layers with and without 2% nano Al₂O₃ but the stacking sequence changed which is not mentioned previously in the cited researches as well as for fiber metal laminate.

The maximum deflection and fundamental natural frequency of metal, FRPC, and FML are influenced by many factors, therefore it's necessary to determine these influences theoretically and compare them numerically (FEM, Ansys workbench 19.2). Maximum deflection and fundamental natural frequency of materials depend mainly on the bending stiffness coefficient d_{mn} . It is necessary to derive theoretically a new d_{mn} equation for quasi-isotropic laminate and quasi-fiber/stainless steel-based fiber metal laminate which is utilized to evaluate these properties for these types of selected FRPC and FML.

CHAPTER THREE

THEORETICAL AND NUMERICAL WORK

3.1 Introduction

This chapter depends on the classical lamination theory to estimate the deflection and natural frequency of isotropic and orthotropic materials, especially for thin plates where the effect of interlaminar shear stress can be ignored.

3.2 Classical Lamination Theory

It's utilized to provide the stress-strain relationship in a laminate that is subjected to tensile and shear loads as well as bending and torsion moments taking into consideration the following assumptions (Kaw, 2005):

- 1- Orthotropic and homogenous layers.
- 2- Shear strain components ($\gamma_{xz} = \gamma_{yz} = 0$).
- 3- Plane stress problem ($\sigma_z = \tau_{xz} = \tau_{yz} = 0$).
- 4- Elastic behavior of laminate layers.
- 5- Each layer is bonded to the adjacent one tightly.

Consider the xz view through plate thickness in Figure (3.1). Point A is a z distance away from the neutral midplane. The displacements of point A in the x and y direction after loading are

$$u = u_0 - z \frac{\partial w_0}{\partial x} \quad (3.1)$$

$$v = v_0 - z \frac{\partial w_0}{\partial y} \quad (3.2)$$

So, the strains in the xy area are

$$\varepsilon_x = \frac{\partial u_0}{\partial x} - z \frac{\partial^2 w_0}{\partial x^2} \quad (3.3)$$

$$\varepsilon_y = \frac{\partial v_0}{\partial y} - z \frac{\partial^2 w_0}{\partial y^2} \quad (3.4)$$

$$\gamma_{xy} = \frac{\partial u_0}{\partial y} + \frac{\partial v_0}{\partial x} - 2z \frac{\partial^2 w_0}{\partial x \partial y} \quad (3.5)$$

The laminate strains are

$$\begin{Bmatrix} \varepsilon_x \\ \varepsilon_y \\ \varepsilon_{xy} \end{Bmatrix} = \begin{Bmatrix} \varepsilon_x^0 \\ \varepsilon_y^0 \\ \varepsilon_{xy}^0 \end{Bmatrix} + z \begin{Bmatrix} K_x \\ K_y \\ K_{xy} \end{Bmatrix} \quad (3.6)$$

Where the midplane strains or membrane strains are

$$\begin{Bmatrix} \varepsilon_x^0 \\ \varepsilon_y^0 \\ \varepsilon_{xy}^0 \end{Bmatrix} = \begin{Bmatrix} \frac{\partial u_0}{\partial x} \\ \frac{\partial v_0}{\partial y} \\ \frac{\partial u_0}{\partial y} + \frac{\partial v_0}{\partial x} \end{Bmatrix} \quad (3.7)$$

And flexural strains or curvatures are

$$\begin{Bmatrix} K_x \\ K_y \\ K_{xy} \end{Bmatrix} = \begin{Bmatrix} -\frac{\partial^2 w_0}{\partial x^2} \\ -\frac{\partial^2 w_0}{\partial y^2} \\ -2\frac{\partial^2 w_0}{\partial x \partial y} \end{Bmatrix} \quad (3.8)$$

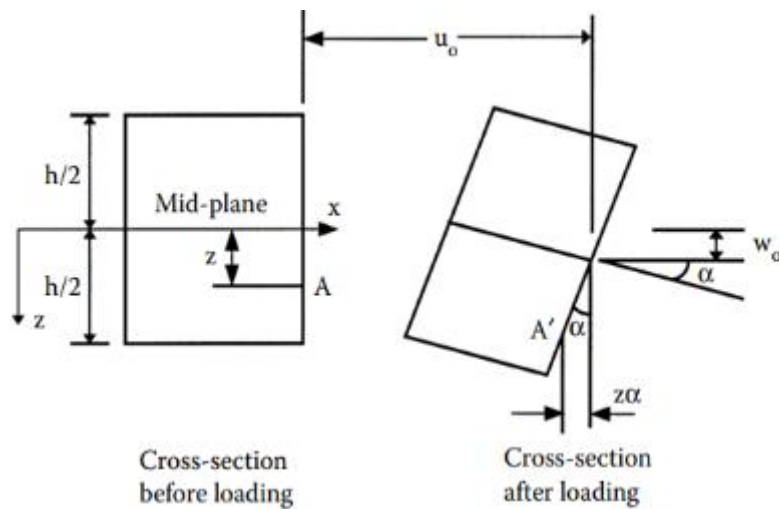


Figure (3.1) The displacement u and v relative to midplane displacement and slope (Kaw, 2005)

3.3 Orthotropic Stress-Strain Relationship

$$\begin{bmatrix} \sigma_x \\ \sigma_y \\ \tau_{xy} \end{bmatrix} = \begin{bmatrix} \bar{Q}_{11} & \bar{Q}_{12} & \bar{Q}_{16} \\ \bar{Q}_{12} & \bar{Q}_{22} & \bar{Q}_{26} \\ \bar{Q}_{16} & \bar{Q}_{26} & \bar{Q}_{66} \end{bmatrix} \begin{bmatrix} \varepsilon_x \\ \varepsilon_y \\ \gamma_{xy} \end{bmatrix} \quad (3.9)$$

Where, σ_x and σ_y are the normal stresses in the x and y direction as well as τ_{xy} is the shear stress in the xy plane.

Substituting equation (3.6) in (3.9) to get

$$\begin{bmatrix} \sigma_x \\ \sigma_y \\ \tau_{xy} \end{bmatrix} = \begin{bmatrix} \bar{Q}_{11} & \bar{Q}_{12} & \bar{Q}_{16} \\ \bar{Q}_{12} & \bar{Q}_{22} & \bar{Q}_{26} \\ \bar{Q}_{16} & \bar{Q}_{26} & \bar{Q}_{66} \end{bmatrix} \begin{bmatrix} \varepsilon_x^0 \\ \varepsilon_y^0 \\ \gamma_{xy}^0 \end{bmatrix} + z \begin{bmatrix} \bar{Q}_{11} & \bar{Q}_{12} & \bar{Q}_{16} \\ \bar{Q}_{12} & \bar{Q}_{22} & \bar{Q}_{26} \\ \bar{Q}_{16} & \bar{Q}_{26} & \bar{Q}_{66} \end{bmatrix} \begin{bmatrix} K_x \\ K_y \\ K_{xy} \end{bmatrix} \quad (3.10)$$

The components of the transformed reduced stiffness matrix $[\bar{Q}]$ can be evaluated from the following equations (Kaw, 2005)

$$\begin{aligned} \bar{Q}_{11} &= Q_{11}C^4 + Q_{22}S^4 + 2(Q_{12} + 2Q_{66})S^2C^2 \\ \bar{Q}_{12} &= (Q_{11} + Q_{22} - 4Q_{66})S^2C^2 + Q_{12}(C^4 + S^4) \\ \bar{Q}_{22} &= Q_{11}S^4 + Q_{22}C^4 + 2(Q_{12} + 2Q_{66})S^2C^2 \\ \bar{Q}_{16} &= (Q_{11} - Q_{12} - 2Q_{66})C^3S - (Q_{22} - Q_{12} - 2Q_{66})S^3C \\ \bar{Q}_{26} &= (Q_{11} - Q_{12} - 2Q_{66})CS^3 - (Q_{22} - Q_{12} - 2Q_{66})C^3S \\ \bar{Q}_{66} &= (Q_{11} + Q_{22} - 2Q_{12} - 2Q_{66})S^2C^2 + Q_{66}(S^4 + C^4) \end{aligned} \quad (3.11)$$

The elements of the plane stress-reduced stiffness matrix are

$$\begin{aligned} Q_{11} &= \frac{E_1}{1-\nu_{21}\nu_{12}} \\ Q_{12} &= \frac{\nu_{12}E_2}{1-\nu_{21}\nu_{12}} \\ Q_{22} &= \frac{E_2}{1-\nu_{21}\nu_{12}} \\ Q_{66} &= G_{12} \end{aligned} \quad (3.12)$$

Where

$C = \cos\theta$, $S = \sin\theta$, θ = fiber angle of orientation from reference global x-axis.

E_1, E_2 = longitudinal and transverse young modulus.

ν_{12}, ν_{21} = major and minor poisons ratio.

G_{12} = shear modulus.

The forces related to the midplane strains and curvatures (Kaw, 2005)

$$\begin{bmatrix} N_x \\ N_y \\ N_{xy} \end{bmatrix} = \begin{bmatrix} A_{11} & A_{12} & A_{16} \\ A_{12} & A_{22} & A_{26} \\ A_{16} & A_{26} & A_{66} \end{bmatrix} \begin{bmatrix} \varepsilon_x^0 \\ \varepsilon_y^0 \\ \gamma_{xy}^0 \end{bmatrix} + \begin{bmatrix} B_{11} & B_{12} & B_{16} \\ B_{12} & B_{22} & B_{26} \\ B_{16} & B_{26} & B_{66} \end{bmatrix} \begin{bmatrix} \kappa_x \\ \kappa_y \\ \kappa_{xy} \end{bmatrix} \quad (3.13)$$

The moments related to the midplane strains and curvatures

$$\begin{bmatrix} M_x \\ M_y \\ M_{xy} \end{bmatrix} = \begin{bmatrix} B_{11} & B_{12} & B_{16} \\ B_{12} & B_{22} & B_{26} \\ B_{16} & B_{26} & B_{66} \end{bmatrix} \begin{bmatrix} \varepsilon_x^0 \\ \varepsilon_y^0 \\ \gamma_{xy}^0 \end{bmatrix} + \begin{bmatrix} D_{11} & D_{12} & D_{16} \\ D_{12} & D_{22} & D_{26} \\ D_{16} & D_{26} & D_{66} \end{bmatrix} \begin{bmatrix} \kappa_x \\ \kappa_y \\ \kappa_{xy} \end{bmatrix} \quad (3.14)$$

Where, N_x, N_y are normal forces in x and y axis per unit length.

N_{xy} is the shear force in xy plane per unit length.

M_x, M_y , are bending moments about x and y per unit length.

M_{xy} is the twisting moment about xy plane per unit length.

$$A_{ij} = \sum_{K=1}^n [(\bar{Q}_{ij})]_k (h_k - h_{k-1}) \quad (3.15)$$

$$B_{ij} = \frac{1}{2} \sum_{K=1}^n [(\bar{Q}_{ij})]_k (h_k^2 - h_{k-1}^2) \quad (3.16)$$

$$D_{ij} = \frac{1}{3} \sum_{K=1}^n [(\bar{Q}_{ij})]_k (h_k^3 - h_{k-1}^3) \quad (3.17)$$

Where, A_{ij}, B_{ij}, D_{ij} are extensional, extensional-bending coupling, and bending stiffness matrices, respectively (Kaw, 2005).

3.4 Laminate Under Tensile and Shear Load

For symmetric laminated fiber composite $[B] = 0$, then equation (3.13) can be reduced into the following equation (Kaw, 2005)

$$\begin{bmatrix} \varepsilon_x^0 \\ \varepsilon_y^0 \\ \gamma_{xy}^0 \end{bmatrix} = \begin{bmatrix} A_{11}^* & A_{12}^* & A_{16}^* \\ A_{12}^* & A_{22}^* & A_{26}^* \\ A_{16}^* & A_{26}^* & A_{66}^* \end{bmatrix} \begin{bmatrix} N_x \\ N_y \\ N_{xy} \end{bmatrix} \quad (3.18)$$

For laminate subjected only to normal load N_x then the effective longitudinal young modulus E_x is

$$E_x = \frac{1}{hA_{11}^*} \quad (3.19)$$

The major effective Poisson's ratio is

$$\nu_{xy} = -\frac{A_{12}^*}{A_{11}^*} \quad (3.20)$$

For laminate subjected only to normal load N_y then the effective transverse young modulus E_y is (Kaw, 2005)

$$E_y = \frac{1}{hA_{22}^*} \quad (3.21)$$

The minor effective Poisson's ratio is

$$\nu_{yx} = -\frac{A_{12}^*}{A_{22}^*} \quad (3.22)$$

For laminate subjected only to shear load N_{xy} then the effective shear modulus G_{xy} is (Kaw, 2005)

$$G_{xy} = \frac{1}{hA_{66}^*} \quad (3.23)$$

3.5 Laminate under Bending Moment

For symmetric laminated fiber composite $[B] = 0$, then equation (3.14) can be reduced into the following equation

$$\begin{bmatrix} K_x \\ K_y \\ K_{xy} \end{bmatrix} = \begin{bmatrix} D_{11}^* & D_{12}^* & D_{16}^* \\ D_{12}^* & D_{22}^* & D_{26}^* \\ D_{16}^* & D_{26}^* & D_{66}^* \end{bmatrix} \begin{bmatrix} M_x \\ M_y \\ M_{xy} \end{bmatrix} \quad (3.24)$$

For laminate subjected only to bending moment M_x then the effective flexural longitudinal modulus E_x^f is (Kaw, 2005)

$$E_x^f = \frac{12}{h^3 D_{11}^*} \quad (3.25)$$

The effective flexural transverse modulus E_y^f is

$$E_y^f = \frac{12}{h^3 D_{22}^*} \quad (3.26)$$

The effective flexural shear modulus G_{xy}^f is

$$G_{xy}^f = \frac{12}{h^3 D_{66}^*} \quad (3.27)$$

The major effective flexural Poisson's ratio is

$$\nu_{xy}^f = -\frac{D_{12}^*}{D_{11}^*} \quad (3.28)$$

The minor effective flexural Poisson's ratio is

$$\nu_{yx}^f = -\frac{D_{12}^*}{D_{22}^*} \quad (3.29)$$

h = total laminate thickness.

3.6 Equation of Motions in Terms of Displacements

The linear equations of motion for homogenous orthotropic plate in terms of displacements (u_o, v_o, w_o) and rotations $(\frac{\partial w_o}{\partial x}, \frac{\partial w_o}{\partial y})$ (Reddy, 2003) are

$$\begin{aligned}
 & A_{11} \frac{\partial^2 u_o}{\partial x^2} + 2A_{16} \frac{\partial^2 u_o}{\partial x \partial y} + A_{66} \frac{\partial^2 u_o}{\partial y^2} + A_{16} \frac{\partial^2 v_o}{\partial x^2} + (A_{12} + A_{66}) \frac{\partial^2 v_o}{\partial x \partial y} + \\
 & A_{26} \frac{\partial^2 v_o}{\partial y^2} - [B_{11} \frac{\partial^3 w_o}{\partial x^3} + 3B_{16} \frac{\partial^3 w_o}{\partial x^2 \partial y} + (B_{12} + 2B_{66}) \frac{\partial^3 w_o}{\partial x \partial y^2} + B_{26} \frac{\partial^3 w_o}{\partial y^3}] = \\
 & I_0 \ddot{u}_o - I_1 \frac{\partial \ddot{w}_o}{\partial x} \tag{3.30}
 \end{aligned}$$

$$\begin{aligned}
 & A_{16} \frac{\partial^2 u_o}{\partial x^2} + (A_{12} + A_{66}) \frac{\partial^2 u_o}{\partial x \partial y} + A_{26} \frac{\partial^2 u_o}{\partial y^2} + A_{66} \frac{\partial^2 v_o}{\partial x^2} + 2A_{26} \frac{\partial^2 v_o}{\partial x \partial y} + \\
 & A_{22} \frac{\partial^2 v_o}{\partial y^2} - [B_{16} \frac{\partial^3 w_o}{\partial x^3} + (B_{12} + 2B_{66}) \frac{\partial^3 w_o}{\partial x^2 \partial y} + 3B_{26} \frac{\partial^3 w_o}{\partial x \partial y^2} + B_{22} \frac{\partial^3 w_o}{\partial y^3}] = \\
 & I_0 \ddot{v}_o - I_1 \frac{\partial \ddot{w}_o}{\partial x} \tag{3.31}
 \end{aligned}$$

$$\begin{aligned}
 & B_{11} \frac{\partial^3 u_o}{\partial x^3} + 3B_{16} \frac{\partial^3 u_o}{\partial x^2 \partial y} + (B_{12} + 2B_{66}) \frac{\partial^3 u_o}{\partial x \partial y^2} + B_{26} \frac{\partial^3 u_o}{\partial y^3} + B_{16} \frac{\partial^3 v_o}{\partial x^3} + \\
 & (B_{12} + 2B_{66}) \frac{\partial^3 v_o}{\partial x^2 \partial y} + 3B_{26} \frac{\partial^3 v_o}{\partial x \partial y^3} + B_{22} \frac{\partial^3 v_o}{\partial y^3} - [D_{11} \frac{\partial^4 w_o}{\partial x^4} + 4D_{16} \frac{\partial^4 w_o}{\partial x^3 \partial y} + \\
 & 2(D_{12} + 2D_{66}) \frac{\partial^4 w_o}{\partial x^2 \partial y^2} + 4D_{26} \frac{\partial^4 w_o}{\partial x \partial y^3} + D_{22} \frac{\partial^4 w_o}{\partial y^4}] + q = I_1 (\frac{\partial \ddot{u}_o}{\partial x} + \frac{\partial \ddot{v}_o}{\partial x}) + \\
 & I_0 \ddot{w}_o - I_2 (\frac{\partial^2 \ddot{w}_o}{\partial x^2} + \frac{\partial^2 \ddot{w}_o}{\partial y^2}) \tag{3.32}
 \end{aligned}$$

Equations (3.30) -(3.32) can be written in matrix form

$$\begin{bmatrix} C_{11} & C_{12} & C_{13} \\ C_{12} & C_{22} & C_{23} \\ C_{13} & C_{23} & C_{33} \end{bmatrix} \begin{Bmatrix} u_o \\ v_o \\ w_o \end{Bmatrix} + \begin{bmatrix} m_{11} & 0 & m_{13} \\ 0 & m_{22} & m_{23} \\ m_{13} & m_{23} & m_{33} \end{bmatrix} \begin{Bmatrix} \ddot{u}_o \\ \ddot{v}_o \\ \ddot{w}_o \end{Bmatrix} = \begin{Bmatrix} 0 \\ 0 \\ q \end{Bmatrix} \tag{3.33}$$

$$C_{11} = A_{11} d_x^2 + 2A_{16} d_x d_y + A_{66} d_y^2$$

$$C_{12} = A_{16} d_x^2 + (A_{12} + A_{66}) d_x d_y + A_{26} d_y^2$$

$$C_{13} = -[B_{11}d_x^3 + 3B_{16}d_x^2d_y + (B_{12} + 2B_{66})d_xd_y^2 + B_{26}d_y^3]$$

$$C_{22} = A_{66}d_x^2 + 2A_{26}d_xd_y + A_{22}d_y^2$$

$$C_{23} = -[B_{16}d_x^3 + (B_{12} + 2B_{66})d_x^2d_y + 3B_{26}d_xd_y^2 + B_{22}d_y^3]$$

$$C_{33} = D_{11}d_x^4 + 4D_{16}d_x^3d_y + 2(D_{12} + 2D_{66})d_x^2d_y^2 + 2D_{26}d_xd_y^3 + D_{22}d_y^4 \quad (3.34)$$

Coefficients m_{ij} are

$$m_{11} = -I_0, \quad m_{13} = I_1d_x, \quad m_{22} = -I_0$$

$$m_{23} = I_1d_y, \quad m_{33} = I_0 - I_2(d_x^2 + d_y^2) \quad (3.35)$$

The differential operators are

$$d_x^i = \frac{\partial^i}{\partial x^i}, \quad d_y^i = \frac{\partial^i}{\partial y^i}, \quad d_t^i = \frac{\partial^i}{\partial t^i} \quad (i=1, 2, 3) \quad (3.36)$$

3.7 Symmetrical Laminate

Layers of laminate above and below the midplane have the same material, thickness, and angle of orientation. For example, [G0/C30/C30/G0] is a symmetric laminate.

No warpage was produced after cooling the fabricated laminate in symmetric laminate. The extension-bending coupling matrix [B] in symmetric laminate is equal to zero (Kaw, 2005).

3.8 Cross Laminate

The laminate is cross if 0° and 90° plies are present in its stacking sequence, e.g., laminate [0/90/90/0] is cross-laminate. Elements $A_{16} = A_{26} = 0$, $B_{26} = 0$, and $D_{16} = D_{26} = 0$. Especially orthotropic laminate is a symmetric cross-laminate with coupling matrix [B]=0 (Kaw, 2005).

3.9 Quasi-Isotropic Laminate

The shear coupling element $A_{16} = A_{26} = 0$. Laminates [0/90/±45]_s and [0/±60]_s are examples of quasi-isotropic laminate (Kaw, 2005).

3.10 Bending of Simply Supported Rectangular Plates

By omitting the nonlinear and dynamic forms from equation (3.32), the following governing equation for static bending deflection of symmetric cross-laminated composite found (Reddy, 2003)

$$D_{11} \frac{\partial^4 w_0}{\partial x^4} + 2(D_{12} + 2D_{66}) \frac{\partial^4 w_0}{\partial x^2 \partial y^2} + D_{22} \frac{\partial^4 w_0}{\partial y^4} = q \quad (3.37)$$

The boundary conditions of the simply supported rectangular plate shown in Figure (3.2) are

$$w_0(x, 0) = 0, w_0(x, b) = 0, w_0(0, y) = 0, w_0(a, y) = 0 \quad (3.38)$$

$$M_{xx}(0, y) = 0, M_{xx}(a, y) = 0, M_{yy}(x, 0) = 0, M_{yy}(x, b) = 0 \quad (3.39)$$

The bending moments -transverse deflection relationships are

$$M_{xx} = -(D_{11} \frac{\partial^2 w_0}{\partial x^2} + D_{12} \frac{\partial^2 w_0}{\partial y^2})$$

$$M_{yy} = -(D_{12} \frac{\partial^2 w_0}{\partial x^2} + D_{22} \frac{\partial^2 w_0}{\partial y^2})$$

$$M_{xy} = -2D_{66} \frac{\partial^2 w_0}{\partial x \partial y} \tag{3.40}$$

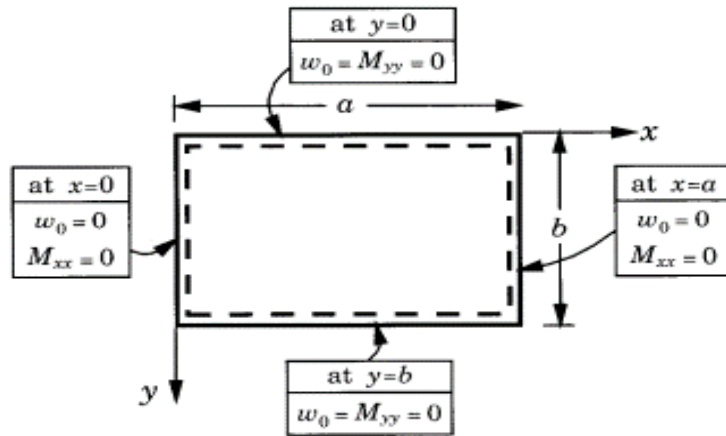


Figure (3.2) Simply Supported Plate boundary conditions (Reddy, 2003)

3.11 The Navier Solution for Symmetric Cross Laminate

The Navier solution is applied only to the simply supported boundary conditions. The lateral deflection $w_0(x, y)$ and lateral load $q(x, y)$ are expanded by double trigonometric (Fourier) series (Reddy, 2003).

$$w_0(x, y) = \sum_{n=1}^{\infty} \sum_{m=1}^{\infty} W_{mn} \sin \alpha x \sin \beta y \quad (3.41)$$

$$q(x, y) = \sum_{n=1}^{\infty} \sum_{m=1}^{\infty} Q_{mn} \sin \alpha x \sin \beta y \quad (3.42)$$

$$Q_{mn} = \frac{4}{ab} \int_0^b \int_0^a q(x, y) \sin \alpha x \sin \beta y \, dx \, dy \quad (3.43)$$

Where $\alpha = \frac{m\pi}{a}$, $\beta = \frac{n\pi}{b}$, W_{mn} and Q_{mn} are coefficients to be determined.

$$\frac{\partial^4 w_0}{\partial x^4} = \sum_{n=1}^{\infty} \sum_{m=1}^{\infty} \alpha^4 W_{mn} \sin \alpha x \sin \beta y$$

$$\frac{\partial^4 w_0}{\partial y^4} = \sum_{n=1}^{\infty} \sum_{m=1}^{\infty} \beta^4 W_{mn} \sin \alpha x \sin \beta y$$

$$\frac{\partial^2 w_0}{\partial x^2 \partial y^2} = \sum_{n=1}^{\infty} \sum_{m=1}^{\infty} \alpha^2 \beta^2 W_{mn} \sin \alpha x \sin \beta y$$

Substitute equation (3.41) and (3.42) into equation (3.37) to get

$$\sum_{n=1}^{\infty} \sum_{m=1}^{\infty} \{-W_{mn} [D_{11} \alpha^4 + 2(D_{12} + 2D_{66}) \alpha^2 \beta^2 + D_{22} \beta^4] + Q_{mn}\} \sin \alpha x \sin \beta y = 0 \quad (3.44)$$

$$W_{mn} = \frac{Q_{mn}}{d_{mn}} \quad (3.45)$$

$$d_{mn} = \frac{\pi^4}{b^4} [D_{11} m^4 s_1^4 + 2(D_{12} + 2D_{66}) m^2 n^2 s_1^2 + D_{22} n^4] \quad (3.46)$$

$$w_0(x, y) = \sum_{n=1}^{\infty} \sum_{m=1}^{\infty} \frac{Q_{mn}}{d_{mn}} \sin \alpha x \sin \beta y \quad (3.47)$$

$\alpha = \frac{m\pi}{a}$, $\beta = \frac{n\pi}{b}$, $s_1 = \frac{1}{s}$, W_{mn} and Q_{mn} are coefficients to be determined.

$s = \frac{a}{b}$ is the plate aspect ratio and a, and b are the plate length and width, respectively.

3.12 The Load Coefficient Q_{mn} for Uniform Load $q(x, y)$

If the plate is subject to uniform load $q = q_0$ as shown in Figure (3.3), then equation (3.43) (Reddy, 2003) will be

$$Q_{mn} = \frac{4}{ab} \int_0^b \int_0^a q_0 \sin \frac{m\pi}{a} x \sin \frac{n\pi}{b} y \, dx \, dy$$

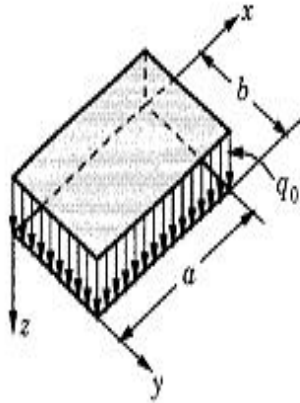
$$\frac{a}{m\pi} \int_0^a \frac{m\pi}{a} \sin \frac{m\pi}{a} x \, dx = \frac{a}{m\pi} [\cos m\pi - 1]$$

$$\frac{b}{n\pi} \int_0^b \frac{n\pi}{b} \sin \frac{n\pi}{b} y \, dy = \frac{b}{n\pi} [\cos n\pi - 1]$$

$$Q_{mn} = \frac{4q_0}{mn\pi^2} [\cos m\pi - 1][\cos n\pi - 1]$$

$$Q_{mn} = \frac{16q_0}{\pi^2 mn}, \quad (m, n = 1, 3, 5, \dots) \quad (3.48)$$

Uniform load,
 $q = q_0$



$$Q_{mn} = \frac{16q_0}{\pi^2 mn}$$

$$(m, n = 1, 3, 5, \dots)$$

Figure (3.3) Q_{mn} for uniform distributed load condition (Reddy, 2003).

3.13 The Navier Solution for symmetric Quasi-Isotropic laminate

By omitting the nonlinear and dynamic forms from equation (3.32), the following governing equation for static bending deflection of symmetric quasi-isotropic laminated composite found

$$D_{11} \frac{\partial^4 w_0}{\partial x^4} + 2(D_{12} + 2D_{66}) \frac{\partial^4 w_0}{\partial x^2 \partial y^2} + 4D_{16} \frac{\partial^4 w_0}{\partial x^3 \partial y} + 4D_{26} \frac{\partial^4 w_0}{\partial x \partial y^3} + D_{22} \frac{\partial^4 w_0}{\partial y^4} = q \quad (3.50)$$

The Navier solution is applied only to the simply supported boundary conditions. The lateral deflection $w_0(x, y)$ and lateral load $q(x, y)$ are expanded by double trigonometric (Fourier) series (Reddy, 2003).

By reusing equations (3.41) and (3.42), the following new equation can be obtained

$$W_{mn} [D_{11} \alpha^4 + 2(D_{11} + 2D_{66}) \alpha^2 \beta^2 - 4D_{16} (\alpha^3 \beta \cot \alpha x \cot \beta y) - 4D_{26} (\alpha \beta^3 \cot \alpha x \cot \beta y) + D_{22} \beta^4] - Q_{mn} = 0 \quad (3.51)$$

$$W_{mn} = \frac{Q_{mn}}{d_{mn}}$$

$$d_{mn} = \frac{\pi^4}{b^4} [D_{11} m^4 s_1^4 + 2(D_{12} + 2D_{66}) m^2 n^2 s_1^3 + D_{22} n^4 - 4D_{16} (m^3 n s_1^3) \cot \alpha x \cot \beta y - 4D_{26} (m n^3 s_1) \cot \alpha x \cot \beta y] \quad (3.52)$$

$\alpha = \frac{m\pi}{a}$, $\beta = \frac{n\pi}{b}$, $s_1 = \frac{1}{s}$, W_{mn} and Q_{mn} are coefficients to be determined.

$s = \frac{a}{b}$ is the plate aspect ratio and a, and b are the plate length and width, respectively.

3.14 Free Vibration of Symmetric Cross Simply Supported Plate

To evaluate the natural frequency of the symmetric cross plate, the equation of motion (3.32) is utilized, and the applied load is set to zero (Reddy, 2003).

$$D_{11} \frac{\partial^4 w_0}{\partial x^4} + 2(D_{12} + 2D_{66}) \frac{\partial^4 w_0}{\partial x^2 \partial y^2} + D_{22} \frac{\partial^4 w_0}{\partial y^4} = I_0 \ddot{w}_0 - I_2 \left(\frac{\partial \ddot{w}_0}{\partial x^2} + \frac{\partial \ddot{w}_0}{\partial y^2} \right) \quad (3.53a)$$

$$I_0 = \sum_{k=1}^L \rho_0^{(k)} (z_{k+1} - z_k), \quad I_2 = \frac{1}{3} \sum_{k=1}^L \rho_0^{(k)} (z_{k+1}^3 - z_k^3) \quad (3.53b)$$

Where, L= total number of plies, I_0, I_2 = mass moment of inertia.

Assume periodic solution

$$W_{mn}(t) = W_{mn}^0 e^{i\omega t} \quad (3.54)$$

$$\{D_{11}\alpha^4 + 2(D_{12} + 2D_{66})\alpha^2\beta^2 + D_{22}\beta^4 - w^2[I_0 + (\alpha^2 + \beta^2)I_2]\} \times W_{mn} \sin \alpha x \sin \beta y = 0 \quad (3.55)$$

$$w_{mn}^2 = \frac{\pi^4}{I_0 b^4} \left[D_{11} m^4 \left(\frac{b}{a}\right)^4 + 2(D_{12} + 2D_{66}) m^2 n^2 \left(\frac{b}{a}\right)^2 + D_{22} n^4 \right] \quad (3.56)$$

$$\tilde{I}_0 = I_0 + I_2 \left[\left(\frac{m\pi}{a}\right)^2 + \left(\frac{n\pi}{b}\right)^2 \right] \quad (3.57)$$

For various values of m and n, there corresponds a unique frequency w_{mn} and a corresponding mode shape

$$w_0(x, y) = W_{mn}^0 \sin \frac{m\pi x}{a} \sin \frac{n\pi y}{b} \quad (3.58)$$

Where W_{mn}^0 is the amplitude of the vibration mode (m, n).

For square laminate equation (3.56) simplified into

$$w_{mn}^2 = \left(\frac{\pi}{a}\right)^4 \frac{[D_{11}m^4 + 2(D_{12} + 2D_{66})m^2n^2 + D_{22}n^4]}{[I_0 + I_2\left(\frac{\pi}{a}\right)^2(m^2 + n^2)]} \quad (3.59)$$

When the rotary inertia I_2 is canceled, equation (3.56) reduces into

$$w_{mn}^2 = \frac{\pi^4}{I_0 b^4} \left[D_{11} m^4 \left(\frac{b}{a}\right)^4 + 2(D_{12} + 2D_{66}) m^2 n^2 \left(\frac{b}{a}\right)^2 + D_{22} n^4 \right] \quad (3.60)$$

For the square plate equation (3.60) become

$$w_{mn}^2 = \frac{\pi^4}{I_0 b^4} [D_{11} m^4 + 2(D_{12} + 2D_{66}) m^2 n^2 + D_{22} n^4] \quad (3.61)$$

The Fundamental natural frequency occurs at $m=n=1$, then equation (3.60) reduces into

$$w_{mn}^2 = \frac{\pi^4}{I_0 b^4} \left[D_{11} \left(\frac{b}{a}\right)^4 + 2(D_{12} + 2D_{66}) \left(\frac{b}{a}\right)^2 + D_{22} \right] \quad (3.62)$$

3.15 Free Vibration of Symmetric Quasi-Isotropic Simply Supported Plate

To evaluate the natural frequency of the symmetric quasi-isotropic plate, the equation of motion (3.32) is utilized, and the applied load is set to zero.

$$D_{11} \frac{\partial^4 w_0}{\partial x^4} + 4D_{16} \frac{\partial^4 w_0}{\partial x^3 \partial y} + 2(D_{12} + 2D_{66}) \frac{\partial^4 w_0}{\partial x^2 \partial y^2} + 4D_{26} \frac{\partial^4 w_0}{\partial x \partial y^3} + D_{22} \frac{\partial^4 w_0}{\partial y^4} = I_0 \ddot{w}_0 - I_2 \left(\frac{\partial^2 \ddot{w}_0}{\partial x^2} + \frac{\partial^2 \ddot{w}_0}{\partial y^2} \right) \quad (3.63a)$$

$$I_0 = \sum_{k=1}^L \rho_0^{(k)} (z_{k+1} - z_k), \quad I_2 = \frac{1}{3} \sum_{k=1}^L \rho_0^{(k)} (z_{k+1}^3 - z_k^3) \quad (3.63b)$$

Where, L = total number of plies, I_0, I_2 = mass moment of inertia.

Assume periodic solution

$$W_{mn}(t) = W_{mn}^0 e^{i\omega t} \quad (3.64)$$

$$\{D_{11} \alpha^4 + 2(D_{12} + 2D_{66}) \alpha^2 \beta^2 - 4D_{16} \alpha^3 \beta \cos \alpha x \cos \beta y - 4D_{26} \alpha \beta^3 \cos \alpha x \cos \beta y + D_{22} \beta^4 - w^2 [I_0 + (\alpha^2 + \beta^2) I_2]\} \times W_{mn} \sin \alpha x \sin \beta y = 0 \quad (3.65)$$

$$w_{mn}^2 = \frac{\pi^4}{I_0 b^4} \left[D_{11} m^4 \left(\frac{b}{a}\right)^4 + 2(D_{12} + 2D_{66}) m^2 n^2 \left(\frac{b}{a}\right)^2 - 4D_{16} \left(\frac{b}{a}\right)^3 \cot \frac{m\pi}{a} x \cot \frac{n\pi}{b} y - 4D_{26} \left(\frac{b}{a}\right) \cot \frac{m\pi}{a} x \cot \frac{n\pi}{b} y + D_{22} n^4 \right] \quad (3.66)$$

When the rotary inertia I_2 is neglected, then

$$w_{mn}^2 = \frac{\pi^4}{I_0 b^4} \left[D_{11} m^4 \left(\frac{b}{a}\right)^4 + 2(D_{12} + 2D_{66}) m^2 n^2 \left(\frac{b}{a}\right)^2 - 4D_{16} m^3 n \left(\frac{b}{a}\right)^3 \cot \frac{m\pi}{a} x \cot \frac{n\pi}{b} y - 4D_{26} m n^3 \left(\frac{b}{a}\right) \cot \frac{m\pi}{a} x \cot \frac{n\pi}{b} y + D_{22} n^4 \right] \quad (3.67)$$

For square plate

$$w_{mn}^2 = \frac{\pi^4}{I_0 b^4} \left[D_{11} m^4 + 2(D_{12} + 2D_{66}) m^2 n^2 - 4D_{16} m^3 n \cot \frac{m\pi}{a} x \cot \frac{n\pi}{b} y - 4D_{26} m n^3 \cot \frac{m\pi}{a} x \cot \frac{n\pi}{b} y + D_{22} n^4 \right] \quad (3.68)$$

The fundamental frequency occurs at $m=n=1$ then equation (3.67) reduces into

$$w_{mn}^2 = \frac{\pi^4}{I_0 b^4} \left[D_{11} \left(\frac{b}{a}\right)^4 + 2(D_{12} + 2D_{66}) \left(\frac{b}{a}\right)^2 - 4D_{16} \left(\frac{b}{a}\right)^3 \cot \frac{\pi}{a} x \cot \frac{\pi}{b} y - 4D_{26} \left(\frac{b}{a}\right) \cot \frac{\pi}{a} x \cot \frac{\pi}{b} y + D_{22} \right] \quad (3.69)$$

3.16 Static Deflection and Free Vibration of Isotropic Simply Supported Plate

For isotropic materials with constant E and ν where $G = \frac{E}{2(1+\nu)}$ and thickness h , the stiffnesses in the laminated composite will become (Reddy, 2003)

$$A_{11} = \frac{Eh}{1-\nu^2}, \quad A_{12} = \nu A_{11}, \quad A_{22} = A_{11}, \quad 2A_{66} = (1-\nu)A_{11}$$

$$D_{11} = \frac{Eh^3}{12(1-\nu^2)}, \quad D_{12} = \nu D_{11}, \quad D_{22} = D_{11}, \quad 2D_{66} = (1-\nu)D_{11} \quad (3.70)$$

Then equations (3.46), (3.47), and (3.52) become

$$w_0(x, y) = \frac{b^4}{\pi^4} \sum_{n=1}^{\infty} \sum_{m=1}^{\infty} \frac{Q_{mn}}{D[S^2 m^2 + n^2]^2} \sin \alpha x \sin \beta y \quad (3.71)$$

Where $w_0(x, y)$ represents the deflection of isotropic plate subjected to lateral load Q_{mn} .

On the other hand, the natural frequency of isotropic plate can be found by reducing equation (3.60) and (3.67) into

$$w_{mn}^2 = \frac{D\pi^4}{I_0 b^4} \left[m^4 \left(\frac{b}{a} \right)^4 + 2m^2 n^2 \left(\frac{b}{a} \right)^2 + n^4 \right]$$

$$w_{mn}^2 = \frac{D\pi^4}{I_0 b^4} \left[m^2 \left(\frac{b}{a} \right)^2 + n^4 \right]^2 \quad (3.72)$$

The fundamental natural frequency is given by (Reddy, 2003)

$$w_{11} = \frac{\pi^2}{b^2} \sqrt{\frac{D}{I_0}} \left[\left(\frac{b}{a} \right)^2 + 1 \right] \quad (3.73)$$

3.17 Bending of Beam

3.17.1 Bending of Isotropic Beam

The bending stress of the isotropic beam shown in Figure (3.4a and b) subjected to bending moment M (Kaw, 2005) is given by

$$\sigma = \frac{My}{I} \quad (3.74)$$

Where

y = distance from the neutral axis.

I = second moment of area.

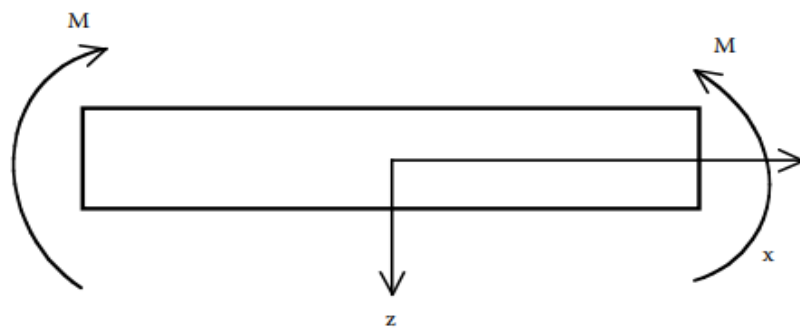
The bending deflection w can be found in the following differential equation

$$EI \frac{d^2 w}{dx^2} = M \quad (3.75)$$

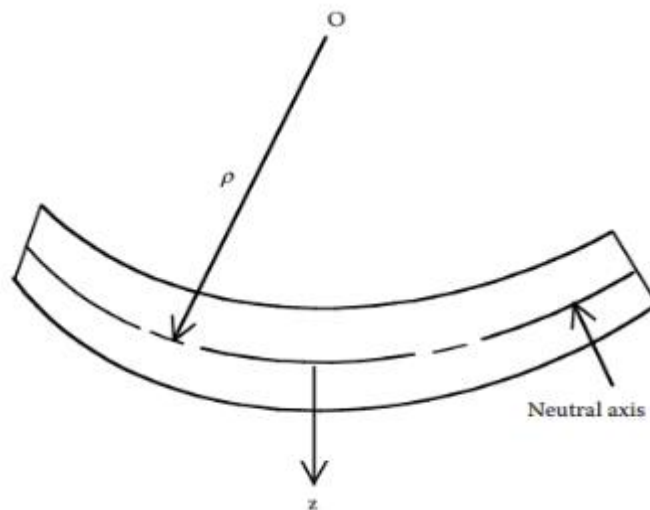
E = elastic tensile modulus of the beam.

$\frac{d^2 w}{dx^2} = \kappa_x$ = the curvature of the beam.

The equation (3.75) is used only for the isotropic beam because the elastic modulus is assumed to be constant.



(a)



(b)

Figure (3.4) The bending of isotropic beam: (a) before bending, (b) after bending (Kaw, 2005)

3.17.2 Bending of Orthotropic Symmetric Beam

Consider an orthotropic symmetric beam with a rectangular cross-section. Matrix $[B]$ is equaled to zero, then equation (3.14) reduces into equation (3.24) (Kaw, 2005) and

$$K_x = \frac{d^2 w_0}{dx^2} = D_{11}^* M_x \quad (3.76)$$

$$\frac{d^2 w}{dx^2} = \frac{M_x b}{E_x I} \quad (3.77)$$

Substitute equation (3.76) into equation (3.77) to get

$$E_x^f = \frac{12}{h^3 D_{11}^*} \quad (3.78)$$

Which is identical to equation (3.25) for the orthotropic plate.

E_x^f is the effective longitudinal bending modulus.

3.18 Transverse Free Vibration of Isotropic and Orthotropic Beams

When the length-to-depth ratio is greater than 10 and the deflection is small compared to thickness then thin beam theory is usable (Rao, 2019).

The equation of motion for the transverse vibration of the beam is

$$\frac{\partial^2}{\partial x^2} \left(EI \frac{\partial^2 y}{\partial x^2} \right) + \rho A \frac{\partial^2 w}{\partial t^2} = f(x, t) \quad (3.79)$$

For transverse free vibration, the external force is equal to zero then equation (3.79) reduces into

$$\frac{\partial^2}{\partial x^2} \left[EI(x) \frac{\partial^2 w(x,t)}{\partial x^2} \right] + \rho A(x) \frac{\partial^2 w(x,t)}{\partial t^2} = 0 \quad (3.80)$$

For uniform beam equation (3.80) reduces into equation (3.81)

$$c^2 \frac{\partial^2 w(x,t)}{\partial x^2} + \frac{\partial^2 w(x,t)}{\partial t^2} = 0 \quad (3.81)$$

$$\text{Where } c = \sqrt{\frac{EI}{\rho A}} \quad (3.82)$$

EI = beam stiffness.

ρ = beam density.

A = beam cross-sectional area.

By using the separation of variable method (Rao, 2019), the transverse natural frequency of the beam is

$$w_n = (\beta l)^2 \sqrt{\frac{EI}{\rho AL^4}} \quad (3.83)$$

βl is constant determined from the beam boundary condition.

Equation (3.83) used for isotropic beam. If the material changes to orthotropic then exchange E by E_x^f (Reddy, 2003).

The first four natural frequencies of the fixed-free beam and their corresponding mode shapes are shown in Figure (3.5).

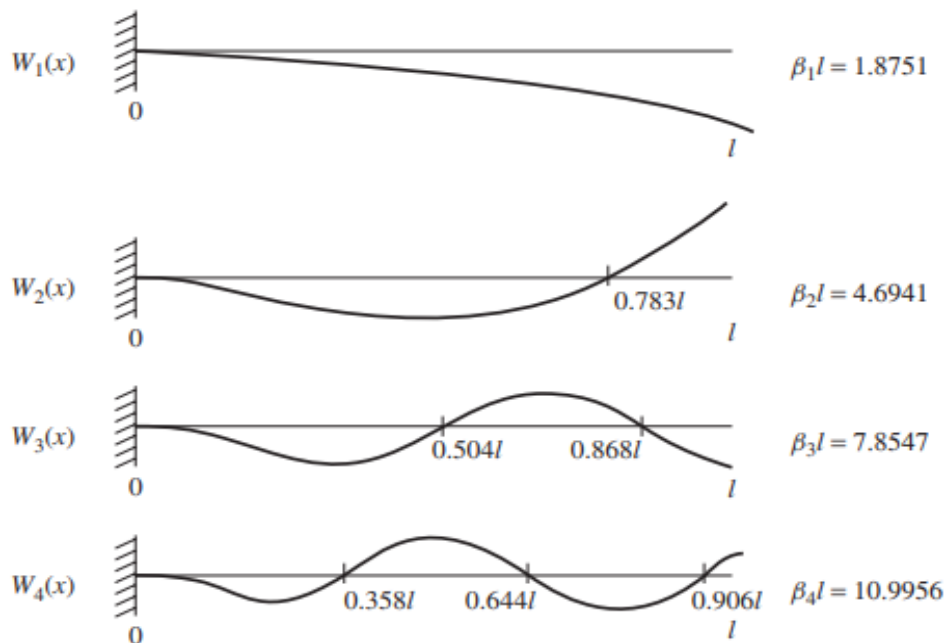


Figure (3.5) The first four natural frequencies and their mode shapes for cantilever beam (Rao, 2019)

3.19 Numerical Work (Finite Element Modeling)

Fiber-reinforced polymer composite and fiber metal laminate sandwich layers, beam, and plate, are discretized by utilizing three-dimensional solid element 185 with element size equal to 1mm in (ANSYS 19.2) workbench (finite element modeling software) as shown in Figure (3.6).

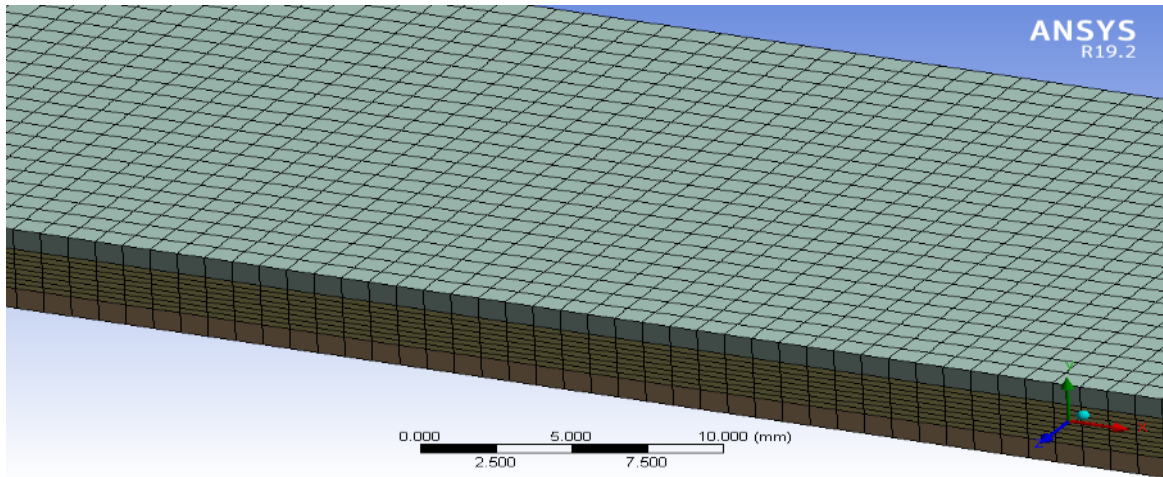


Figure (3.6) Finite element modeling of FML beam

Firstly, the mechanical properties like density, modulus of elasticity, and Poisson's ratio are entered into the engineering data section. Secondly, a design modeler is used to draw the structure with detailed dimensions. Thirdly, ACP(Pre) defines the fiber-reinforced polymer fabric layer which is drawn as a surface from a sketch and then transferred as a solid element to the static structural and modal modeling section. While the mechanical model is used to define the metal layer, supports, and pin load. Finally, finite element modeling is completed by applying the boundary conditions to the structural beam or plate. A bonded connection is used to connect metal skin to the FRPC core. A frictionless connection is used between FRPC, FML, and supports. A frictional connection is used to connect the pin load to FRPC or FML surfaces.

3.20 Beam Modeling

3.20.1 FRPC Modeling

3.20.1.1 Tensile Test Modeling

The practical maximum tensile load is validated numerically by using the ANSYS workbench simulation steps to model the test as shown in Figure (3.7). The FRPC tensile sample with tabs is shown in Figure (3.8).

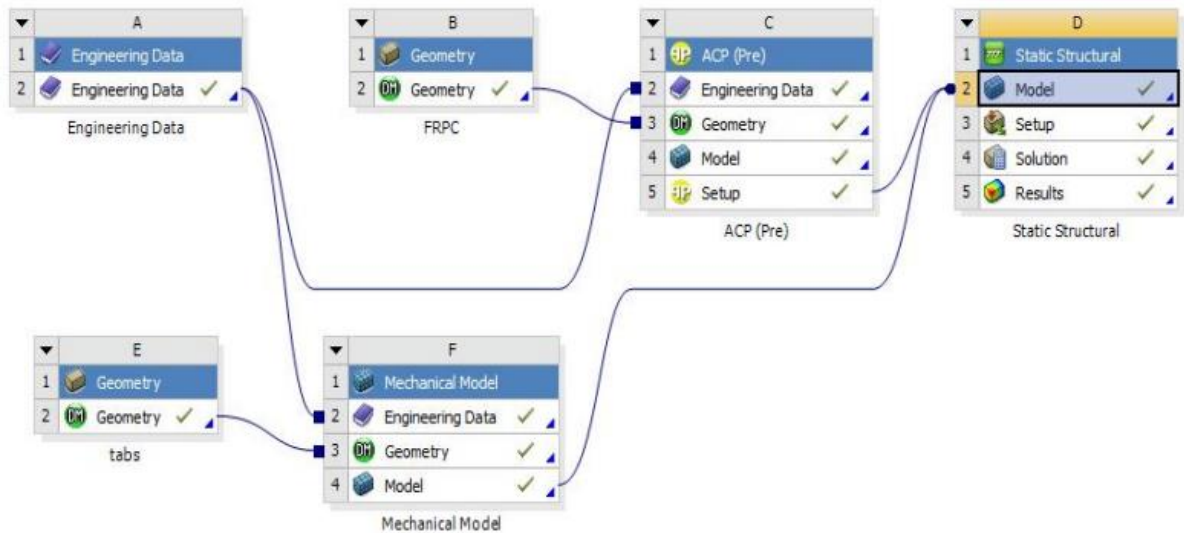


Figure (3.7) Steps of modeling tensile test for FRPC laminates in ANSYS workbench.

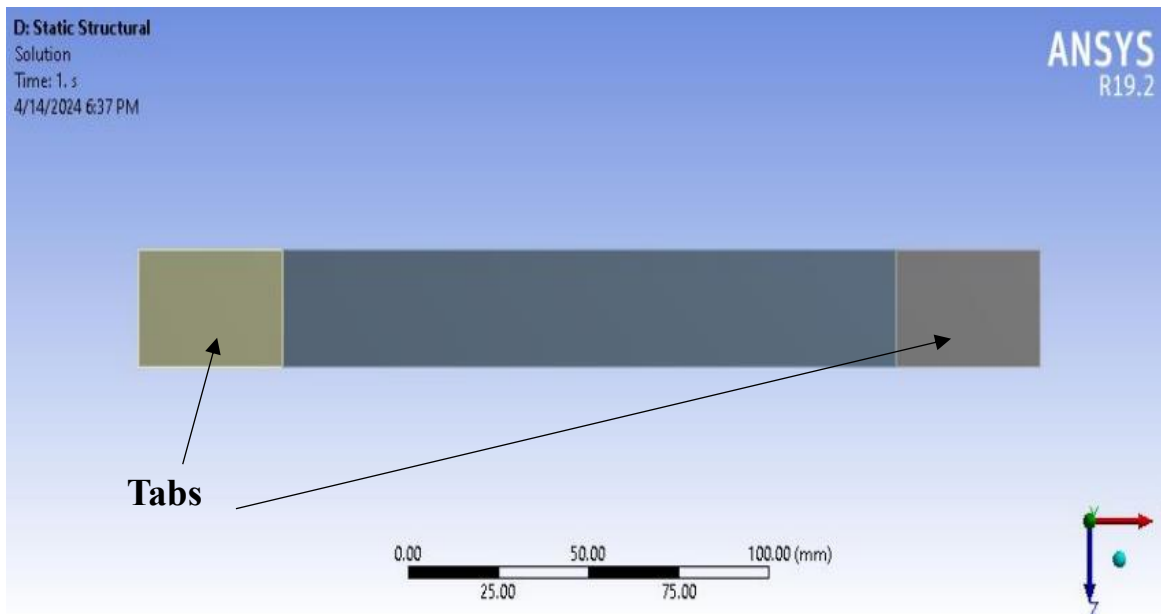


Figure (3.8) FRPC tensile sample with tabs.

3.20.1.2 Flexural Test Modeling

The practical maximum flexural load is validated numerically by using ANSYS workbench simulation steps to model the test as shown in Figure (3.9).

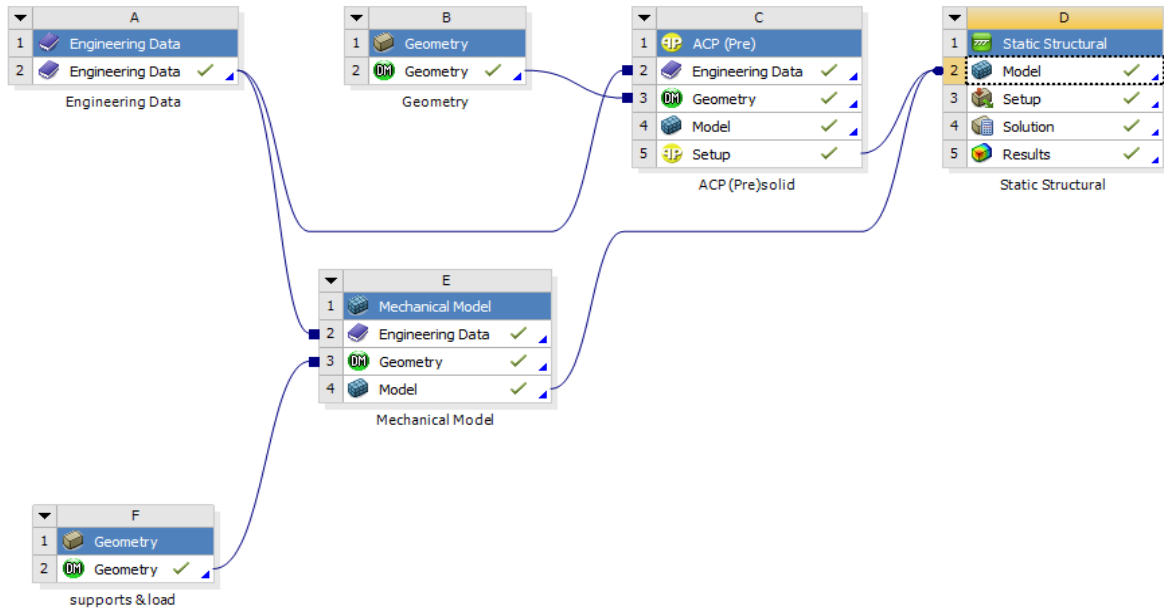


Figure (3.9) Steps of modeling flexural test for FRPC laminates in ANSYS workbench.

3.20.1.3 Free Vibration Test Modeling

ANSYS workbench simulation package was used to find the first six natural frequencies and their mode shape by using the steps shown in Figure (3.10).

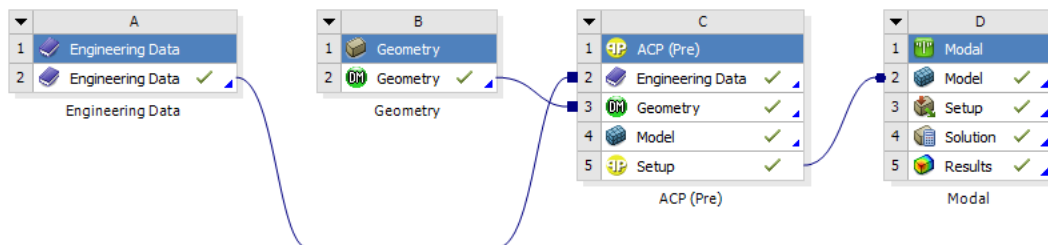


Figure (3.10) Steps of modeling laminates in ANSYS workbench.

3.20.2 FML Modeling

3.20.2.1 Tensile Test Modeling

Practical maximum tensile load is validated numerically by using ANSYS workbench simulation to model the test as shown in Figure (3.11). The FML sandwich tensile sample is shown in Figure (3.12).

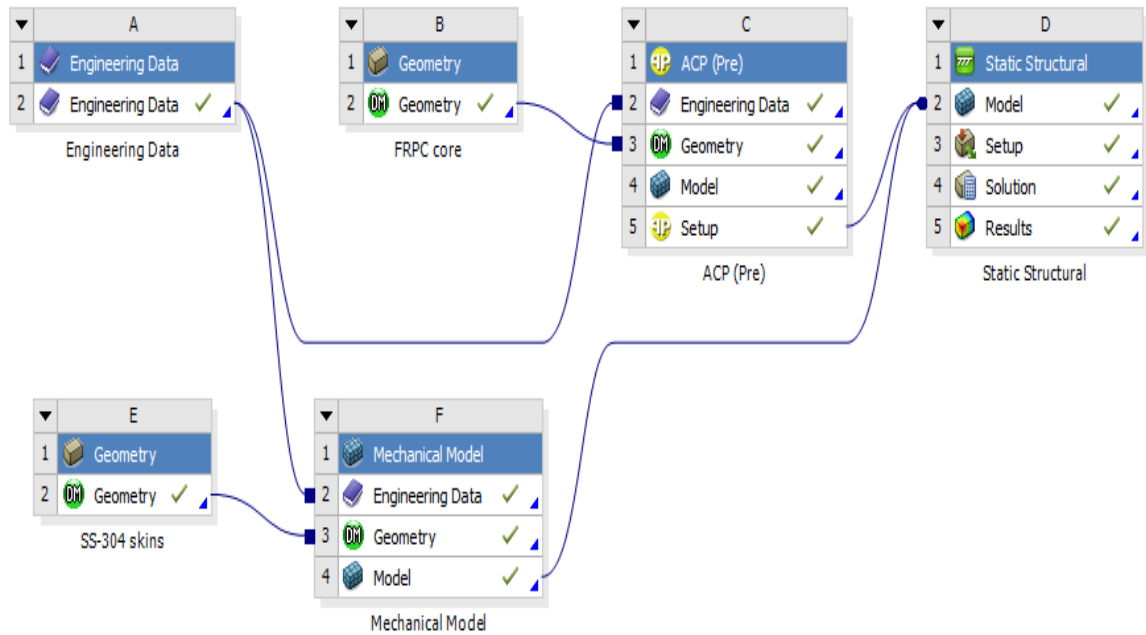


Figure (3.11) Steps of modeling tensile test for FML in ANSYS workbench.

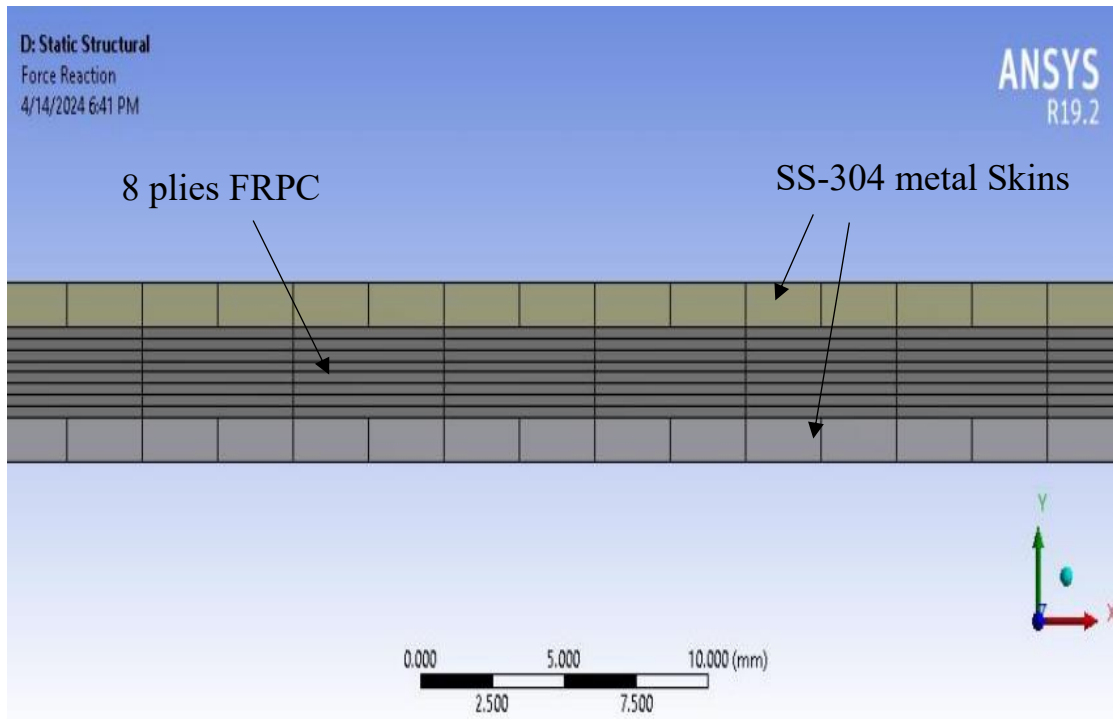


Figure (3.12) FML sandwich plies tensile sample.

3.20.2.2 Flexural Test Modeling

Practical maximum tensile load is validated numerically by using ANSYS workbench simulation to model the test as shown in Figure (3.13).

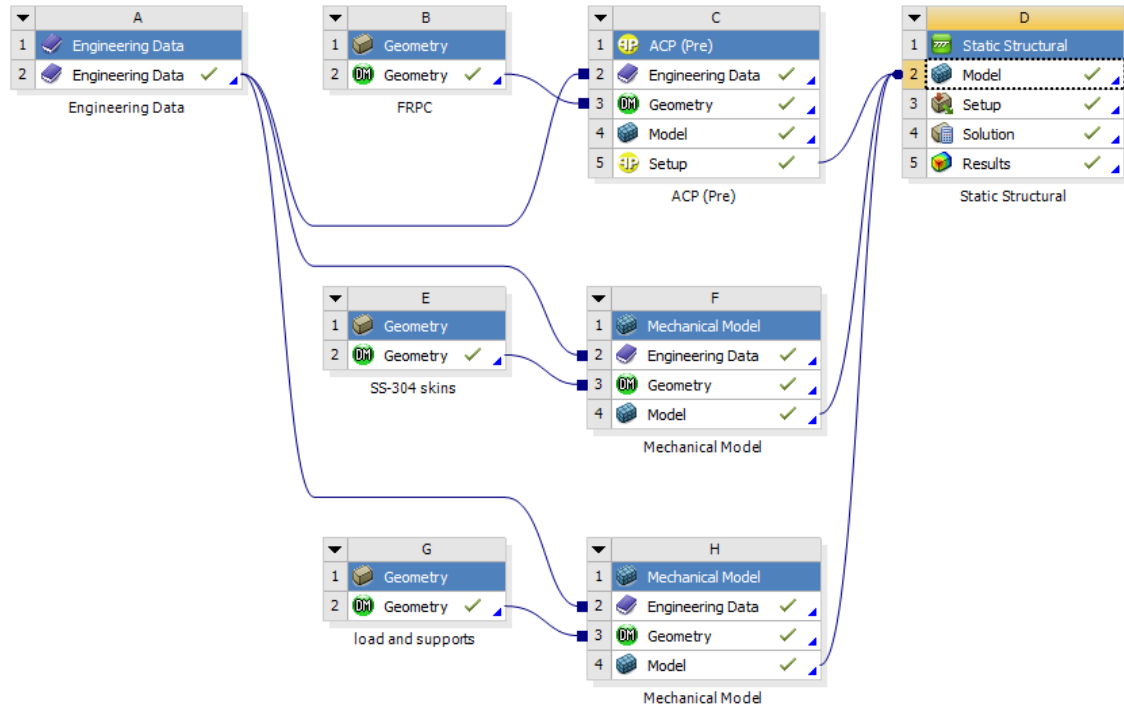


Figure (3.13) Steps of modeling flexural test for FML in ANSYS workbench.

3.20.2.3 Free Vibration Test Modeling

Figure (3.14) shows the free vibration steps modeling of fiber metal laminate in (ANSYS) workbench.

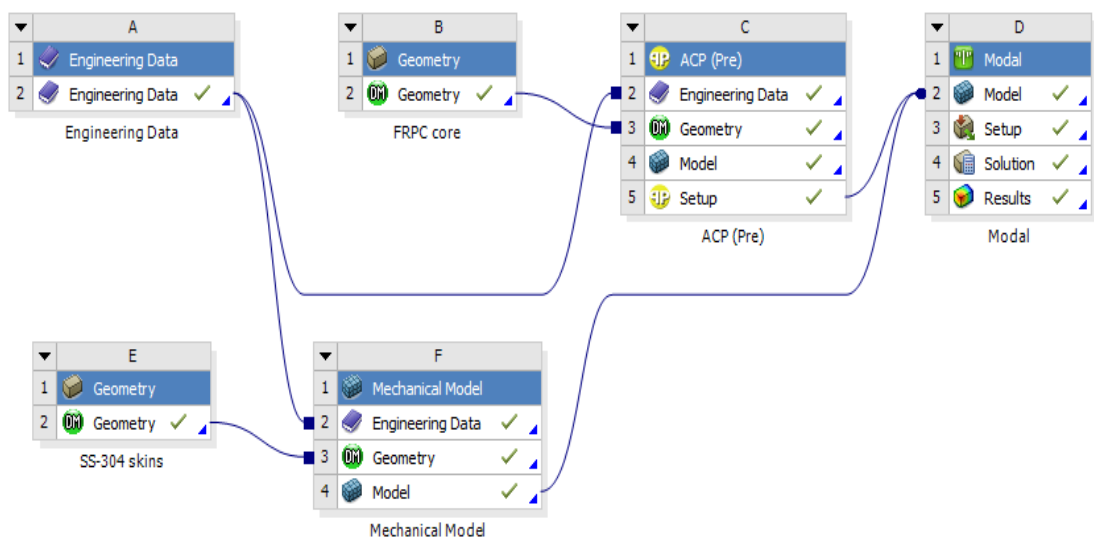


Figure (3.14) Fiber metal laminate modeling in (ANSYS) workbench.

3.21 Plate Bending Modeling

3.21.1 Metal Plate Modeling

3.21.1.1 Plate Thickness

Stainless steel 304 square plates with length (a) and width (b) of 300 mm, and different thicknesses (h) of (1, 2, 3, and 4 mm) are used. The maximum deflection of the simply supported plates due to uniformly distributed pressure (q_0), and the fundamental natural frequency due to its free vibration are determined analytically and verified through the use of FEM (ANSYS workbench 19.2) as shown in Figure (3.15).

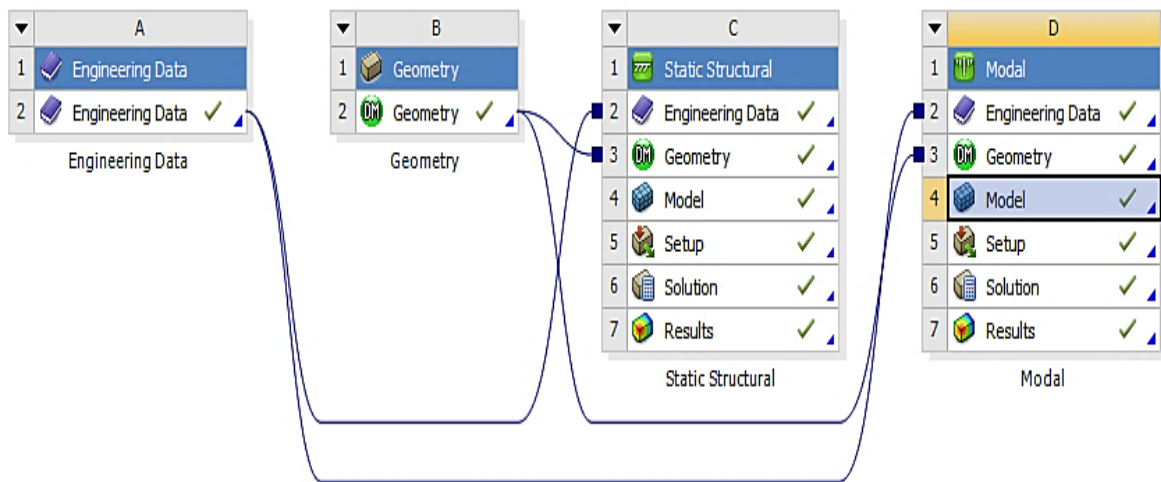


Figure (3.15) Steps of modeling isotropic plate in ANSYS workbench to evaluate deflection and natural frequencies.

3.21.1.2 Metal Type

Three types of metal are selected because of their many uses in structural applications which are stainless steel 304, aluminum 6061-T6, and Titanium alloy Ti-6Al-4V, where their mechanical properties are shown in Table (4.4) and Table (3.1), respectively (Hibbeler, 2012).

Table (3.1) Mechanical properties of aluminum 6061-T6 and Titanium alloy Ti-6AL-4V (Hibbeler, 2012)

Metal	Density (kg/m ³)	Young Modulus (GPa)	Poissons ratio
Aluminum 6061-T6	2710	69	0.35
Titanium Alloy Ti-6AL-4V	4430	120	0.36

The maximum deflection of the square simply supported metal plates ($a=b=300$ mm), and thickness $h=4$ mm, due to uniformly distributed pressure (q_0), and the fundamental natural frequency due to its free vibration are determined analytically and verified through the use of FEM (ANSYS workbench 19.2) as shown in Figure (3.15).

3.21.2 FRPC Plate Modeling

3.21.2.1 Stacking Sequence and Angle of Orientation

Four different stacking sequences and angle of orientations of (Carbon: Glass) /epoxy laminated composite simply supported square plate are selected as shown in Table (3.2). Both length (a) and width (b) are equal to 300 mm, with thickness (h) equal to 2 mm are used.

The maximum deflection of the plates due to uniformly distributed pressure (q_0), and the fundamental natural frequency due to its free vibration are calculated analytically and verified by using FEM (ANSYS workbench 19.2) as shown in Figure (3.16).

Table (3.2) C1, C2, Q1, and Q2 fiber-reinforced epoxy composite configuration plates.

Laminates	Configuration
C1	[G0/C90/C0/G90]s
C2	[G0/G90/C0/C90]s
Q1	[G0/C90/C45/G-45]s
Q2	[G0/G90/C45/C-45]s



Figure (3.16) Steps of modeling orthotropic plate in ANSYS workbench to evaluate deflection and natural frequencies.

3.21.2.2 Nano Al₂O₃ Addition

Two percent of nano Al₂O₃ is added to the epoxy matrix of C1, C2, Q1, and Q2 fiber laminated composite to construct C1WN, C2WN, Q1WN, and Q2WN fiber laminated composite.

The maximum deflection for the new four hybrid conditions of the square fiber laminated plates ($a = b = 300$ mm), and thickness $h = 2$ mm, due to uniformly distributed pressure (q_0), and the fundamental natural frequency due to its free vibration are calculated analytically and verified by using FEM (ANSYS workbench 19.2) as shown Figure (3.16).

3.21.2.3 Aspect Ratio

The ratio of plate length (a) to its width (b) is called aspect ratio. Five different aspect ratios (1, 1.5, 2, 2.5, and 3) are selected to clarify the effect of increasing the length versus decreasing the width of the plate on the deflection and natural frequency. The thickness of the laminated plate at all conditions is equal to 2 mm.

The maximum deflection of the fiber laminated composite plates C1, C2, Q1, and Q2 with aspect ratios equal to (1, 1.5, 2, 2.5, and 3) due to uniformly distributed pressure (q_0), and the fundamental natural frequency due to its free vibration are calculated analytically and verified by using FEM (ANSYS workbench 19.2) as shown in Figure (3.16).

3.21.2.4 Hybrid Ratio

Hybrid ratio change for C1, C2, Q1, and Q2 as well as the position of carbon ply in laminate as shown in Table (3.3) is affected on the deflection and natural frequency of laminated composite.

The maximum deflection of the square fiber laminated plates C1, C2, Q1, and Q2 ($a = b = 300$ mm), and thickness $h = 2$ mm, with hybrid ratios (G: C) equal to (4:4, 6:2 and 2:6) due to uniformly distributed pressure (q_0) and the fundamental natural frequency due to its free vibration are calculated

analytically and verified by using FEM (ANSYS workbench 19.2) as shown in Figure (3.16).

Table (3.3) Hybrid ratio and carbon ply position change in C1, C2, Q1, and Q2 FRPC configurations.

Group	Laminate	Hybrid Ratio G:C
C1	C1[G0/C90/C0/G90]s	4:4
	C1A[G0/C90/G0/G90]s	6:2
	C1B[G0/C90/C0/C90]s	2:6
C2	C2[G0/G90/C0/C90]s	4:4
	C2A[G0/G90/C0/G90]s	6:2
	C2B[G0/G90/G0/C90]s	6:2
Q1	Q1[G0/C90/C45/G-45]s	4:4
	Q1A[G0/C90/G45/G-45]s	6:2
	Q1B[G0/C90/C45/C-45]s	2:6
Q2	Q2[G0/G90/C45/C-45]s	4:4
	Q2A[G0/G90/C45/G-45]s	6:2
	Q2B[G0/G90/G45/C-45]s	6:2

3.21.3 Fiber Metal Laminate Sandwich

Due to the brittle property of fiber/epoxy composite and to reduce the harsh environmental effects, FRPC will be reinforced by metal layers as a skin to produce fiber metal laminate sandwich.

Three types of metal are selected because of their many uses in structural applications which are stainless steel 304, aluminum 6061-T6, and Titanium alloy Ti-6Al-4V, where their mechanical properties are shown in Table (4.4) (practical) and Table (3.1) (Hibbeler, 2012), respectively.

These skin metal plates ($a= 300$ mm, $b=300$, and $h=1$ mm) will be assumed to be bonded perfectly to C1, C2, Q1, and Q2 core composite plate ($a= 300$ mm, $b=300$, and $h=2$ mm) to produce fiber metal laminates sandwich as shown in Figure (3.16) and Table (3.4). The maximum deflection of the FML sandwich plates due to uniformly distributed pressure (q_o), and the fundamental natural frequency due to its free vibration are calculated analytically and validated by using FEM (ANSYS workbench 19.2) as shown in Figure (3.17).

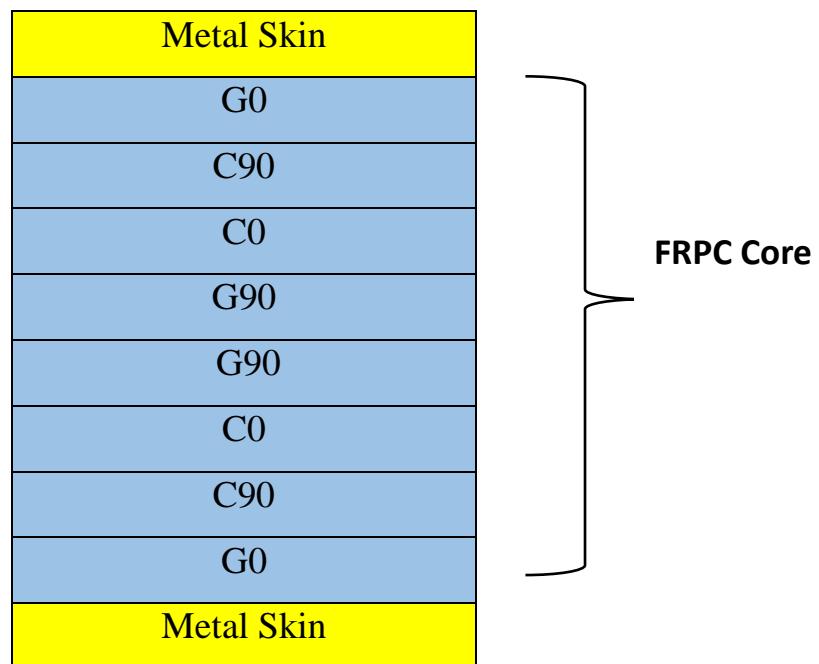


Figure (3.17) Schematic sketch of metal/C1 composite/metal FML sandwich.

Table (3.4) Fiber metal laminate sandwich plate configuration.

FML	Configuration
SS/C1/SS	[SS/G0/C90/C0/G90]s
SS/C2/SS	[SS/G0/G90/C0/C90]s
SS/Q1/SS	[SS/G0/C90/C45/G-45]s
SS/Q2/SS	[SS/G0/G90/C45/C-45]s
Al/C1/Al	[Al/G0/C90/C0/G90]s
Al/C2/Al	[Al/G0/G90/C0/C90]s
Al/Q1/Al	[Al/G0/C90/C45/G-45]s
Al/Q2/Al	[Al/G0/G90/C45/C-45]s
Ti/C1/Ti	[Ti/G0/C90/C0/G90]s
Ti/C2/Ti	[Ti/G0/G90/C0/C90]s
Ti/Q1/Ti	[Ti/G0/C90/C45/G-45]s
Ti/Q2/Ti	[Ti/G0/G90/C45/C-45]s

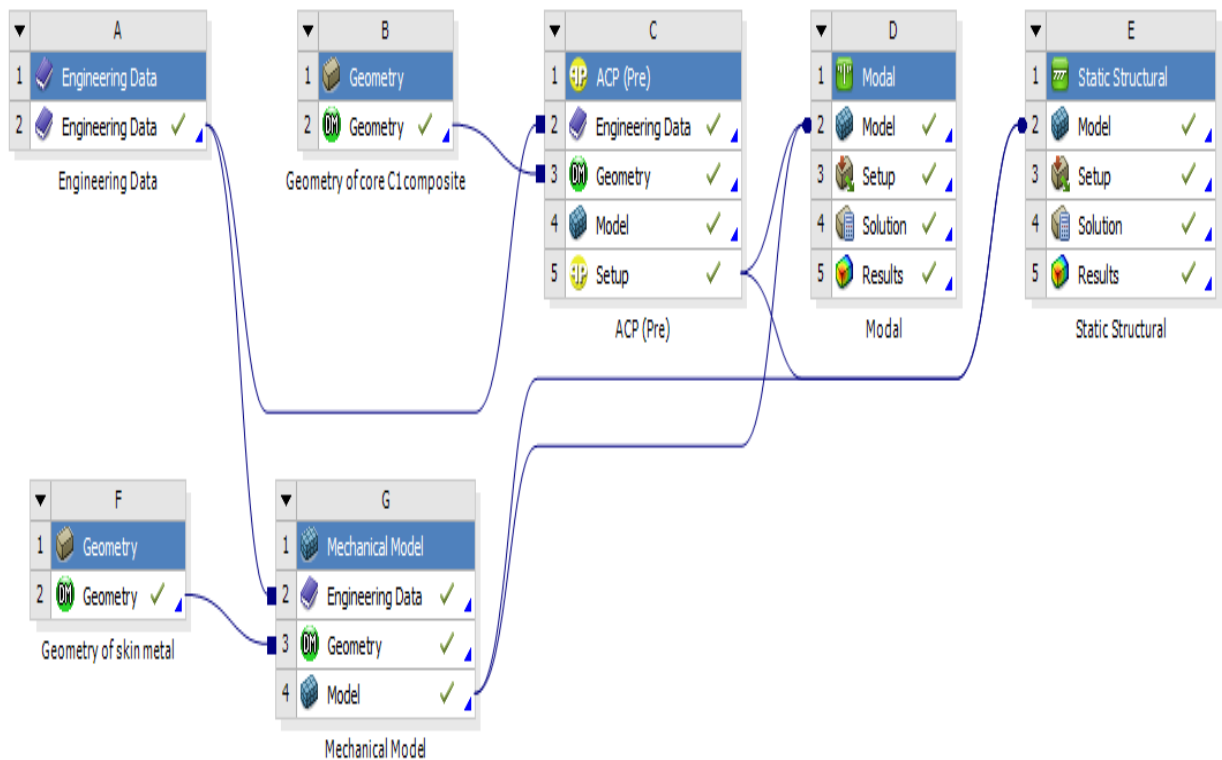


Figure (3.18) Steps of modeling FML sandwich plates in ANSYS workbench to evaluate deflection and natural frequency.

CHAPTER FOUR

EXPERIMENTAL WORK

4.1 Introduction

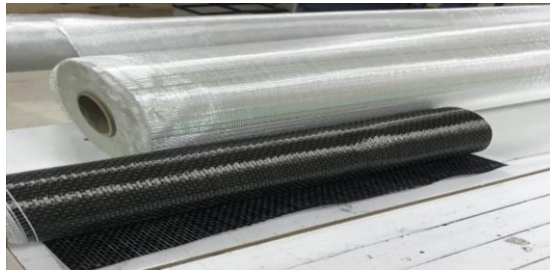
In this chapter, the fiber-reinforced polymer composite FRPC and fiber metal laminate FML ingredients, stacking sequence construction, and fabrication were discussed in detail. On the other hand, tensile, flexural, and free vibration tests have been done for both FRPC and FML to evaluate their mechanical and dynamic properties.

4.2 Materials

The matrix material used in this study is the laminating epoxy resin MGS L285 with hardener H285 in a 100:40 mixing ratio (resin: hardener). The density for resin and hardener is equal to 1.18 g/cm^3 - 1.23 g/cm^3 and 0.94 g/cm^3 - 0.97 g/cm^3 , respectively. While the viscosity for them is equal to 600 mPa.s-900 mPa.s and 50 mPa.s-100 mPa.s, respectively. Unidirectional carbon and E-glass fabric were used as fiber reinforcement with weights equal to 300 g/cm^2 and 330 g/cm^2 , respectively. Both the epoxy matrix and fibers were supplied by the DOST KIMYA Company, Turkey. Spherical aluminum oxide (Al_2O_3) nanopowder with a size of 48 nm was used as a filler reinforcement and supplied by Nanografi Nanotechnology Company, Turkey. On the other hand, FML sandwich composite is constructed by using FRPC, stainless steel 304 (SS 304), and Araldite 2011 structural adhesive. The Araldite 2011 A resin with Araldite 2011 B hardener mixed ratio is 100:80. The density of Araldite 2011 A and Araldite 2011 B are 1.15 g/cm^3 , and 0.96 g/cm^3 , respectively. While the viscosity for them is equal to 30000 mPa.s-50000 mPa.s and 20000 mPa.s-35000 mPa.s, respectively. Araldite 2011 is used to stick a laminated composite structure with a stainless steel 304 sheet from both sides tightly. All the utilized materials are shown in Figure (4.1)



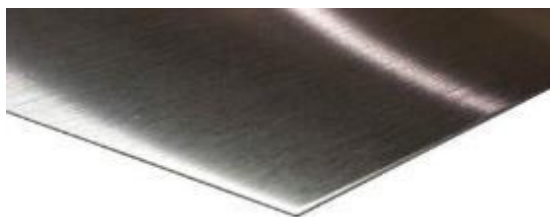
a- Laminating epoxy resin MGS L285 and hardener H285



b- Unidirectional carbon and E-glass fabric



c- Aluminium Oxide Nanopowder



d- Stainless Steel 304 (SS 304)



e- Araldite 2011 Structural Adhesive

Figure (4.1) The ingredients utilized to fabricate fiber-reinforced polymer laminate composite and fiber metal laminate sandwich

4.3 Fiber-Reinforced Epoxy Laminated Composite Manufacturing

4.3.1 Ultrasonic Dual Mixing Method (UDMM)

Aluminium Oxide (Al_2O_3) nanopowder with a weight fraction of 2% was added to 370 g MGS L285 epoxy base resin and premixed manually. The suspension (Al_2O_3 +resin) was subjected to an ultrasonic dual mixing method, ultrasonic pulsed vibration stirrer with an amplitude of 70% and pulsed time equal to 2 sec on and 3 sec off (VCX 500, Sonics, USA) simultaneously along with a magnetic stirrer bars 30×6 mm at 350 rpm and 22 °C (MR Hei-Tech, Heidolp, Germany) were used for 2 hours to obtain uniformly distributed nanoparticles in epoxy resin. To prevent too much temperature rise above 50 °C which leads to resin degradation during UDMM, an ice bath was provided around the suspension container, as shown in Figure (4.2 a). The vacuum process came after UDMM for about 15 min to remove air bubbles(voids), which were initiated during the mixing process as shown in Figure (4.2 b). Finally, the degassed suspension was mixed with 148 g hardener and then drawn to laminated fiber composite via vacuum-assisted resin infusion method.

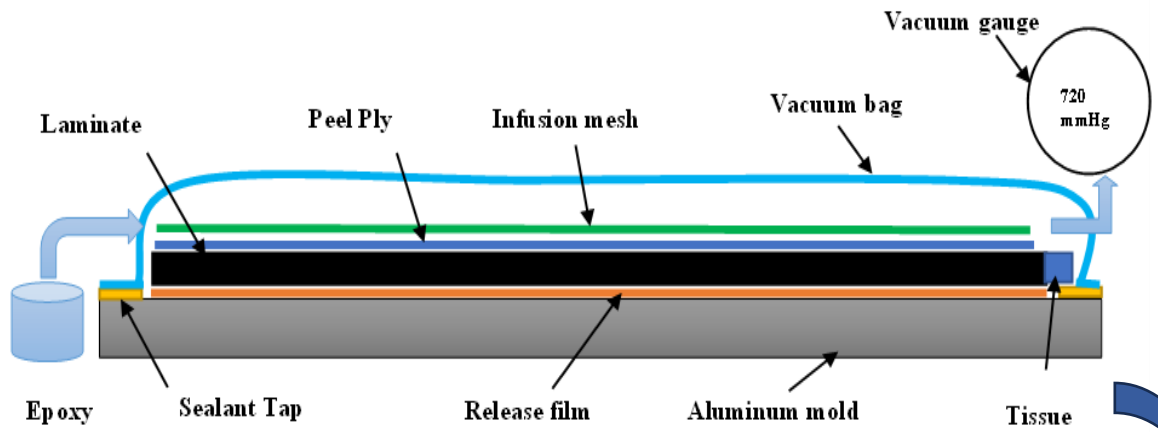


Figure (4.2) Aluminium Oxide Nanopowder (Al_2O_3) and epoxy resin suspension mixing process, (a) UDMM, (b) Vacuum chamber degassing process

4.3.2 Vacuum-Assisted Resin Infusion Molding Process

Hybrid G/C laminated nanocomposite plates 50×50 cm were prepared by vacuum-assisted resin infusion molding process (VARIM) as shown in Figure (4.3). Each laminated composites consist of eight layers of fibers, four layers of carbon, and four other layers of glass. The weight fraction of fibers was 53%, where the ratio of glass to carbon by weight is (56.2:43.8). Table (4.1) shows the stacking sequence configuration for symmetrical laminated epoxy composite.

All eight plies of dry fabric were cut off and positioned over release film that was fixed over an aluminum sandwich mold by using two-edged sealant tape. After that, peel ply was placed over them, where on its side, there were several tissues set in between to absorb excessive epoxy. The next layer was infusion mesh which was used to force the toughened epoxy to distribute uniformly through the surface. Finally, the system is enclosed by using a vacuum bag. Before toughened epoxy was withdrawn, the temperature of the aluminum mold increased steeply to 30 °C to remove voids from the closed system. The vacuum was started with pressure of 720 mmHg, and it should be constant. Otherwise, there would be a leakage in the system that must be solved. When the enclosed system with its connecting apparatus was satisfactory, the toughened epoxy was drawn by vacuum through an infusion hose to the laminated composite system, which was left at 80°C for 15 hours to cure by using automatic control of VARIM (Goren and Atas, 2008). The laminated composite plates of average thickness equal to 2 mm were cut according to the ASTM standard dimensions by using a water-jet cutting machine to prepare the tensile, flexural, and free vibration samples.



(a)



(b)

Figure (4.3) Laminated fiber epoxy composite fabrication: a) Schematic diagram of VARIM, (b) Practical producing FRP laminate

Table (4.1) Stacking Sequence G: C configuration of hybrid laminated epoxy composites.

Symbol	Laminates	Stacking sequence	Hybrid ratio G: C	Density (kg/m ³)	Thickness (mm)
C1	Cross no.1	[G0/C90/C0/G90]s	4:4	1651.3	2.07
C1WN	Cross no.1 with nano Al ₂ O ₃	[G0/C90/C0/G90]s	4:4	1686.0	2.07
C2	Cross no.2	[G0/G90/C0/C90]s	4:4	1653.5	1.9
C2WN	Cross no.2 with nano Al ₂ O ₃	[G0/G90/C0/C90]s	4:4	1676.2	2.00
Q1	Quasi no.1	[G0/C90/C45/G-45]s	4:4	1679.6	1.91
Q1WN	Quasi no.1 with nano Al ₂ O ₃	[G0/C90/C45/G-45]s	4:4	1681.0	1.95
Q2	Quasi no.2	[G0/G90/C45/C-45]s	4:4	1692.5	2.04
Q2WN	Quasi no.2 with nano Al ₂ O ₃	[G0/G90/C45/C-45]s	4:4	1702.7	2.05

4.4 Mechanical Properties Measurement of Unidirectional FRPC

The universal tensile test machine was used to measure the mechanical properties of unidirectional glass and carbon laminated composite with and without nano Al_2O_3 , providing validation data for the study.

The density of laminated composites is measured using RADWAG AS 220.R2, based on Archimedes' principle, as illustrated in Figure (4.4).

Poisson's ratio is the negative quotient of the lateral (transverse) strain to the longitudinal (axial) strain. Practically, Poisson's ratio can be evaluated by using 0-90 strain gauge that is formed from two parts. The first part is 0° strain gauge where its metal foil along with the fiber direction (i.e., with the direction of load) is used to measure axial strain. The second part is 90° strain gauge where its metal foil perpendicular to the fiber direction is used to measure lateral strain.

To prepare the laminated composite surface, use abrasive paper grade 400 and 600 to remove the epoxy matrix, clean the area with wet tissue and acidic liquid, and then attach the 0-90 strain gauge using glue as shown in Figure (4.5).

Data Collect Logger shown in Figure (4.6 a) connected to the strain gauge terminals as well as transfers the data of the longitudinal and lateral strains of the tensile sample at each time increments to the IPRTRONIR strain gauge program to calculate Poisson's ratio ν_{12} as shown in Figure (4.6 b).



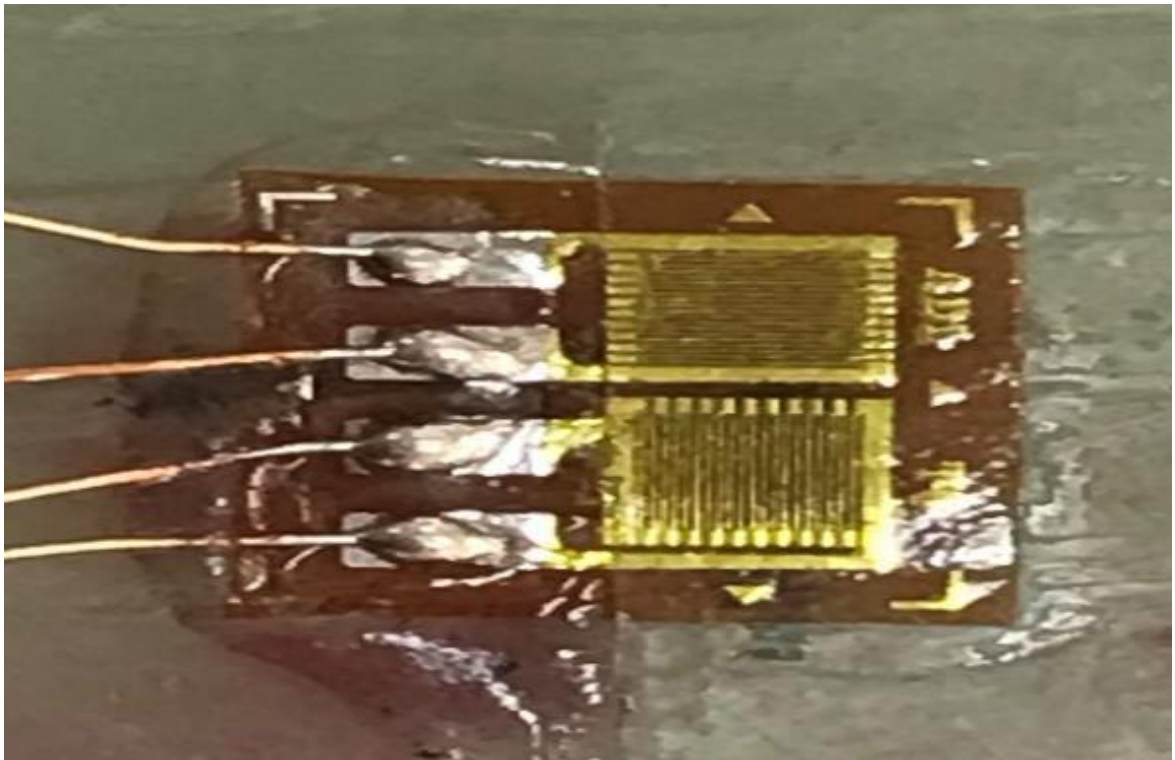
Figure (4.4) RADWAG AS 220.R2 Density Measurement Device



(a)

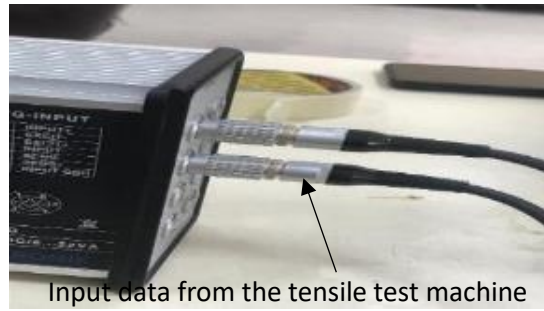


(b)



(c)

Figure (4.5) Strain gauge cleaning and sticking tools; (a) Acidic, (b) glue, (c) 0-90 strain gauge stuck to the sample surface



(a)



(b)

Figure (4.6) Poisson's ratio measurement apparatus: (a) Data Collect Logger and its different view, (b) the overall connection

The value ν_{12} is calculated in the elastic region of laminate tensile response that is noticed before the white spot appearance on the tensile sample surface which means before the first fiber breakage, it can be heard like guitar wire breakage.

Table (4.2) Mechanical properties of unidirectional glass and carbon fiber with and without nano Al_2O_3

Laminates	Density kg/m ³	E_1 MPa	E_2 MPa	ν_{12}	G_{12} MPa
UD glass/epoxy	1658	31802	12804	0.22	4271
UD carbon/epoxy	1484	99438	6273	0.25	4031
UD glass/epoxy with nano Al_2O_3	1883	33507	13344	0.27	4500
UD carbon/epoxy with nano Al_2O_3	1574	105044	6626	0.3	4260

4.5 Fiber Metal Laminate SS 304/ FRPC / SS 304 Manufacturing

Sandwich fiber metal laminate was innovated to utilize in structural applications to reduce internal FRPC degradation due to environmental conditions. On the other hand, the brittle performance of FRPC needs some ductility by adjoining metal sheet layers. The properties of FML depend on the bonding between the FRPC layer and the metal layer. Strong bonding leads to maximize the properties of FML, while weak bonding leads to minimize the properties of FML.

The eight FRPCs fabricated in Table (4.1) were utilized to join with 304 stainless steel metal sheets by using Araldite 2011 structural adhesive.

The stainless steel 304 chemical composition shown in Table (4.3) is inspected by using the OXFORD instrument, X-MET 7500 as shown in Figure

(4.7). The mechanical properties of 304 stainless steel are shown in Table (4.4) found from the simple tensile test.

Table (4.3) Chemical composition of 304 stainless steel by using material analysis instrument.

%Element	Si%	S%	V%	Cr%	Mn%	Fe%	Co%	Ni%	Cu%
	0.69	0.05	0.05	17.77	1.2	71.97	0.02	8.65	0.36
%Element	Mo%	W%							
	0.19	0.04							

Table (4.4) The mechanical properties of 304 stainless steel.

Density (Kg/m ³)	Ultimate Tensile Strength (MPa)	Yield strength MPa	Young Modulus GPa	Poissons ratio ν_{12}
8519	571	380	38	0.27

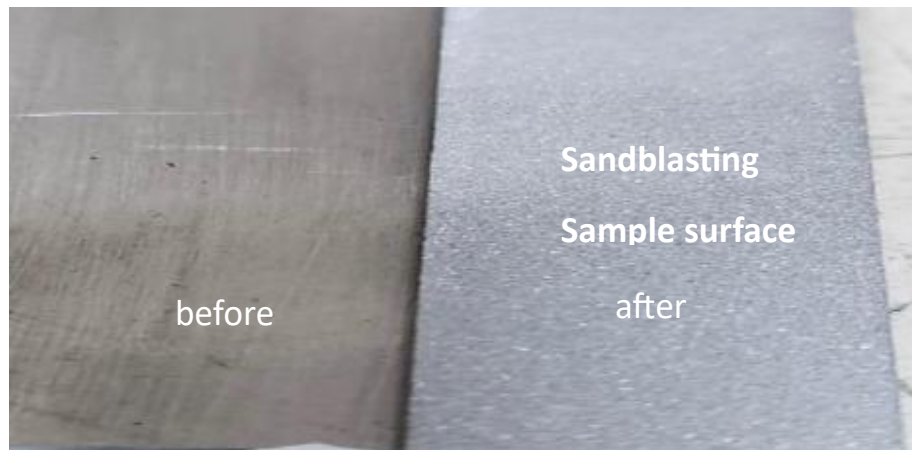


Figure (4.7) Material analysis OXFORD instrument, X-MET 7500.

A pneumatic sandblasting gun (PARKSIDE PISTOLA NEUMATICA) is used to eliminate rust, and difficult dirt from the metal surface by flowing adjustable abrasive sands (silica or silicon dioxide) with grain sizes 0.2-0.8mm, and 320 L/min air flow rate and 0.63 MPa working pressure from nozzle ends as shown in Figure (4.8).



(a)



(b)

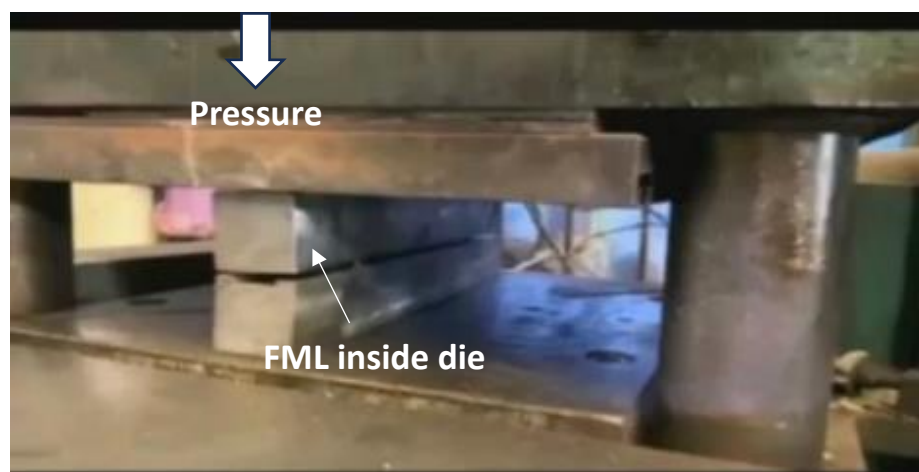
Figure (4.8) Pneumatic sandblasting gun: (a) PARKSIDE PISTOLA NEUMATICA, (b) sandblasting sample surface (before and after)

Steps to bond stainless steel 304 metal sheet with fiber-reinforced polymer composite to form SS304/FRPC/SS304 sandwich FML:

- 1- The surface of the metal sheet is cleaned and roughened by using a sandblasting process.
- 2- The treated metal surface is washed with dishwashing liquid and dried in a furnace for 1 hour at 50 °C.
- 3- Araldite 2011 A and B components mixed and distributed on the surface wanted to bond.
- 4- The layer sequence SS/FRPC/SS is arranged in the groove of the mold shown in Figure (4.9 a) and compressed as shown in Figure (4.9 b).
- 5- The mold remained closed for 1 day after that the sample was removed from the die to repeat the above steps and reproduce another sandwich FML. Table (4.5) shows the produced sandwich fiber metal laminate.



(a)



(b)

Figure (4.9) FML manufacturing: (a) layers sequence arrangement in mold, (b) compression machine

Table (4.5) Stacking sequence arrangement of sandwich [SS/FRPC/SS] FML

Symbol	Laminates	Stacking sequence	Density (kg/m ³)	Thickness (mm)
SS/C1/SS	Cross no.1 FML	[SS/G0/C90/C0/G90]s	5085	4.07
SS/C1WN/SS	Cross no.1 with nano Al ₂ O ₃ FML	[SS/G0/C90/C0/G90]s	5102.3	4.07
SS/C2/SS	Cross no.2 FML	[SS/G0/G90/C0/C90]s	5086	3.9
SS/C2WN/SS	Cross no.2 with nano Al ₂ O ₃ FML	[SS/G0/G90/C0/C90]s	5097.4	4.00
SS/Q1/SS	Quasi no.1 FML	[SS/G0/C90/C45/G-45]s	5099	3.91
SS/Q1WN/SS	Quasi no.1 with nano Al ₂ O ₃ FML	[SS/G0/C90/C45/G-45]s	5099.8	3.95
SS/Q2/SS	Quasi no.2 FML	[SS/G0/G90/C45/C-45]s	5105.5	4.04
SS/Q2WN/SS	Quasi no.2 with nano Al ₂ O ₃ FML	[SS/G0/G90/C45/C-45]s	5110.6	4.05

4.6 Mechanical Tests

The mechanical behavior of the produced laminated composites was evaluated on five samples for each tensile and flexural test. The prepared tensile sample dimensions were 250 × 25 × 2 mm according to ASTM D3039 (International, 2007). Four glass/epoxy tabs were added to the ends of the tension sample to prevent stress concentration at the fixture position and sample slip. The prepared flexural sample dimensions were 100 × 12.7 × 2 mm according to ASTM D 790 I (ASTM, 2007). The three-point flexural test was arranged by positioning the standard rectangular flexural sample between two roller supports of 30 mm diameter with 60 mm span length, while the nose load point diameter was equal to 10 mm at the mid-point of the sample. The experimental flexural strength and strain were evaluated according to the following equations (ASTM, 2007).

$$\sigma_f = \frac{3Pl}{2bd^2} \quad (4.1)$$

$$\varepsilon_f = \frac{6Dd}{L^2} \quad (4.2)$$

Where σ_f is flexural strength in MPa, ε_f is flexural strain (mm/mm), P is load in N, and D is the central deflection of the beam in mm. The tensile and flexural tests were carried out using the Shimadzu AGS-X Plus Universal Testing Machine (100 KN load Cell) with loading rates equal to 2mm/min for the tension test and 1 mm/min for the flexural test as shown in Figure (4.10). A digital video extensometer with high accuracy that is non-contact was used to measure the strain values. It offered extremely accurate measurements of elongation by JIS B 7741 Class 0.5 and ISO 9513 Class 0.5.

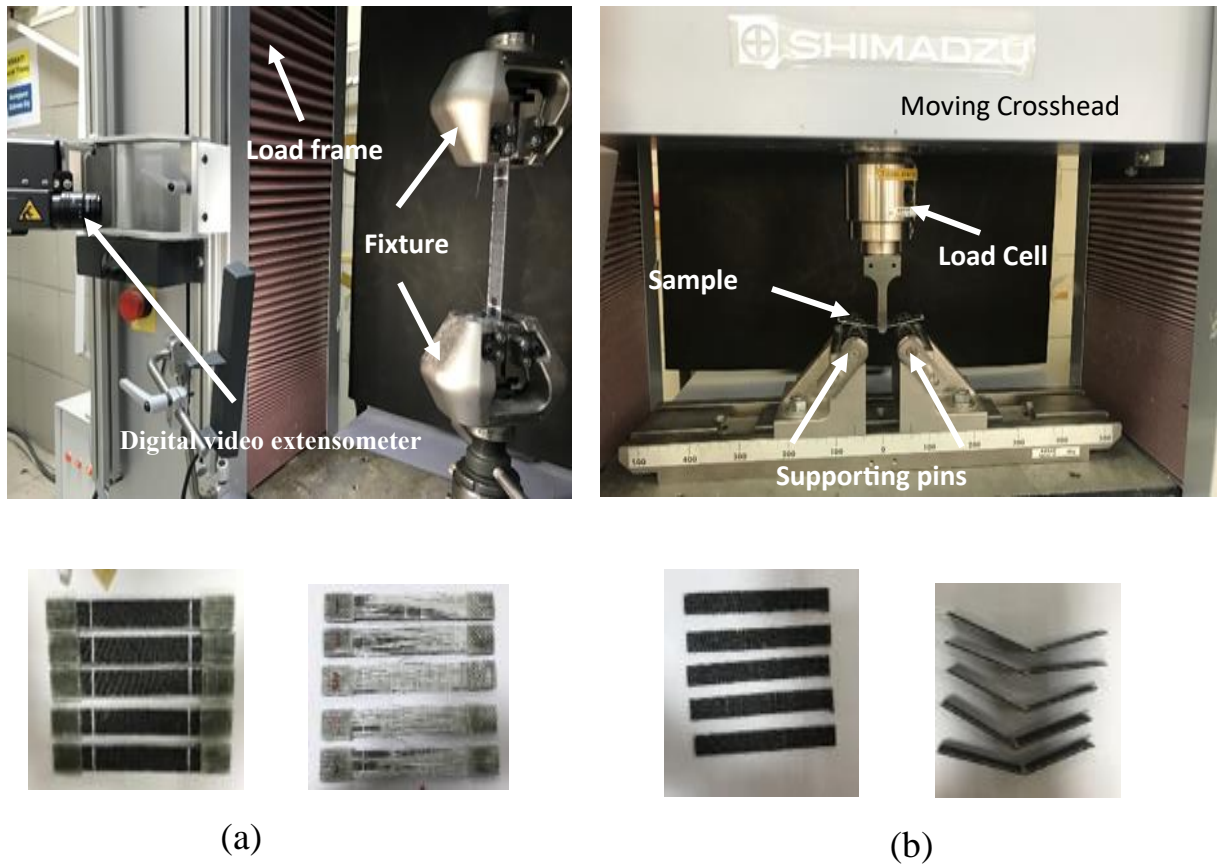
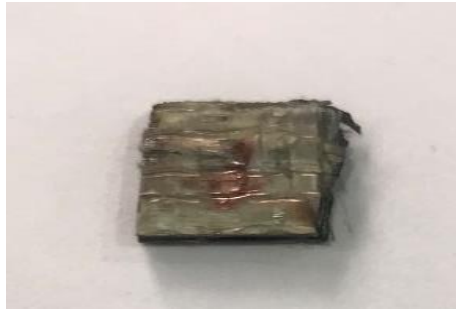


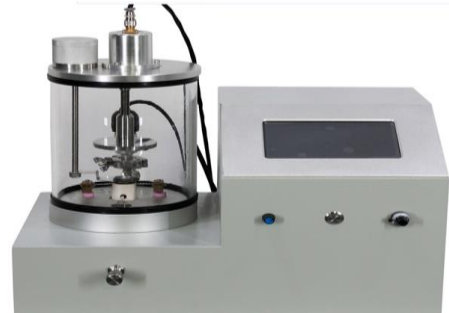
Figure (4.10) Universal tester and samples of (a) tensile test and (b) Three-point flexural test.

4.7 Scanning Electron Microscope Sample Preparation Technique and Devices

Samples of dimensions 10×10 mm as shown in Figure (4.11a) were cut from the flat fractured area of Q2, Q2WN tensile samples and C1, C1WN flexural samples, and their sides were polished via sand papers to achieve flat smooth sides, which were then coated with gold by spraying coater machine as shown in Figure (4.11b) and finally scanned by using Zeiss EVo 50 scanning electron microscope operating at 25 kV as shown in Figure (4.11c) that produces images of a sample by scanning the surface with a focused beam of high- energy electrons.



(a)



(b)



(c)

Figure (4.11) Scanning electron microscope (SEM) sequence: (a) Prepared sample, (b) gold spraying coater machine, (c) Zeiss EVO 50 scanning electron microscope.

4.8 Free Vibration Test

The dynamic properties of the FRPC beam with dimensions are 250 mm length \times 25 mm width and 2 mm thickness; they were measured by using the experimental setup shown in Figure (4.12), which consists of the following apparatuses. Firstly, an impact hammer transducer was used to excite an impulsive force and measure it at the midpoint of the beam (Brüel & Kjær, type 8206). Secondly, a piezoelectric accelerometer was used to measure the vibration response of the excited beam (Brüel & Kjær, type 4507 B30515) positioned at the free end of the beam. Finally, the both hammer and accelerometer were connected to the Brüel & Kjær controller modules type 7539A, 5-channels, to analyze the collected data by using Fast Fourier

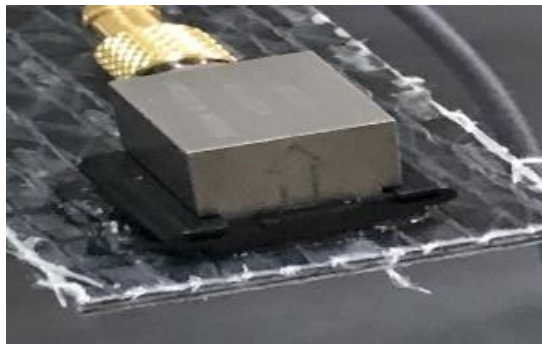
Transform (FFT) Analyzer to obtain the dynamic response of the free vibration test, in terms of time domain and frequency domain.



Free vibration setup



Impact hammer



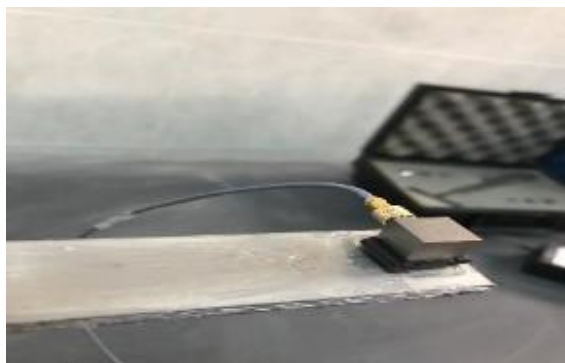
Accelerometer sensor



Blank module`

Figure (4.12) Free vibration test setup and its parts.

The free vibration response of sandwich SS/FRPC/SS FML is measured by the same device but the aluminum impact hammer is exchanged for a rubber impact hammer as shown in Figure (4.13).



(a)



(b)

Figure (4.13) Free vibration Test of FML: (a) accelerometer sensor, (b) rubber impact hammer.

CHAPTER FIVE

RESULTS AND DISCUSSION

5.1 Introduction

In this chapter, the mechanical and dynamic behavior of fiber-reinforced polymer composite and sandwich SS- 304/FRPC/SS- 304, fiber metal laminate will be presented with FEM validation. Firstly, the tensile and flexural behavior is displayed with maximum stress, strain, and toughness. Secondly, the free vibration response is presented with their natural frequency and damping ratio.

5.2 Tensile Behavior of Fiber-Reinforced Polymer Composite

Tensile stress-strain curves for the eight laminated glass/carbon epoxy (cross and quasi) composites are shown in Figure 5.1 (a, and b), respectively. All laminated epoxy composites behaved linearly in the elastic region until the ultimate point. Debonding between fibers and matrix occurred in both cross and quasi-laminated composites before burst load drop (delamination). Little debonding occurred in cross compared with quasi-laminated composites, which were backed to the presence of two layers of 0° carbon fabric in the first one and two layers of carbon fabric with either 90° or ±45° in the other.

Therefore, ultimate tensile strength and tension toughness, alongside burst load drop of quasi-laminated composites, were lower than that of cross one because debonding decreases the slope of the stress-strain curve and leads to more separation between fiber and matrix (Abd Ghani and Mahmud, 2020). Figure (5.2) demonstrates the tensile properties of all laminated epoxy composites. To increase load carrying capacity, nano-Al₂O₃ was added to both stacking sequences [G/C/C/G/G/C/C/G], [G/G/C/C/C/C/G/G] of the cross (C1, C2) and quasi (Q1, Q2) laminates via increasing the adhesion between fibers and epoxy matrix; therefore, samples C1WN, C2WN, Q1WN, and Q2WN are more deformable with higher ultimate tensile strength, ultimate tensile strain, and tensile toughness than C1, C2, Q1, and Q2 respectively as shown in Figure

(5.2). It was obvious that C2WN has a maximum tensile strength 628 MPa, maximum tensile strain 1.74%, and maximum tensile toughness $5.46 \times 10^6 \text{ J/m}^3$ because of the presence of four carbon plies in the middle of the laminate in the cross-laminated group. Both C1WN and C2WN are characterized by high glass fiber pullout at the outer surface after carbon fiber underneath breakage represented as a white spot with internal delamination. The quasi-laminated group is characterized by high off-axis shear stress at $\pm 45^\circ$ which led to internal severe delamination with little glass fiber pullout and little carbon fiber breakage, similar to the results of (Abd Ghani and Mahmud, 2020) as shown in Figure (5.3). Q2WN has the maximum tensile properties (strength, strain, and toughness) which are equal to 294 MPa, 1.98%, and $2.91 \times 10^6 \text{ J/m}^3$; respectively, in the quasi-group laminate because of the presence of four carbon layers in the middle of the laminate with $\pm 45^\circ$ angle of orientation.

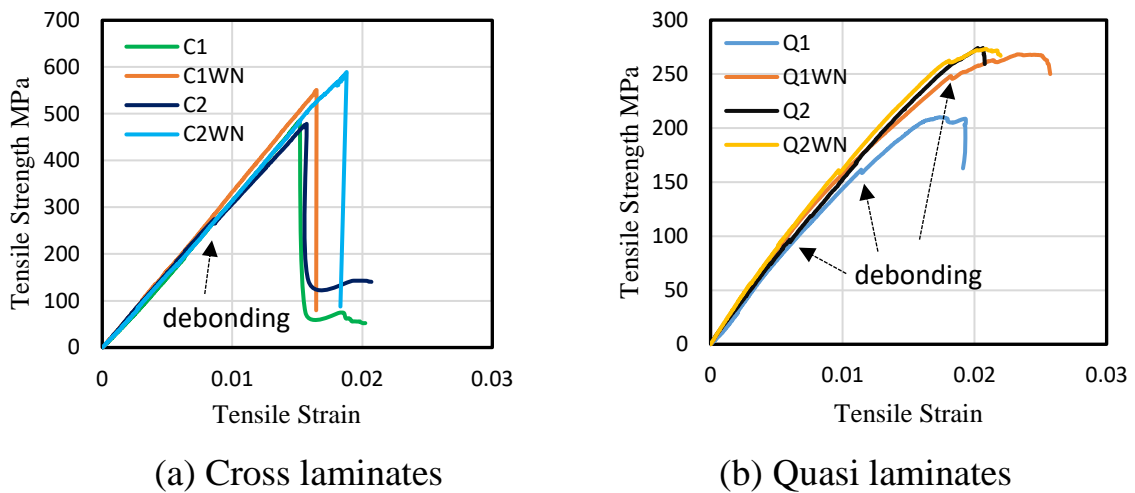


Figure (5.1) Tensile stress-strain curves for symmetrical hybrid cross and quasi-laminated epoxy composite with and without nano- Al_2O_3 .

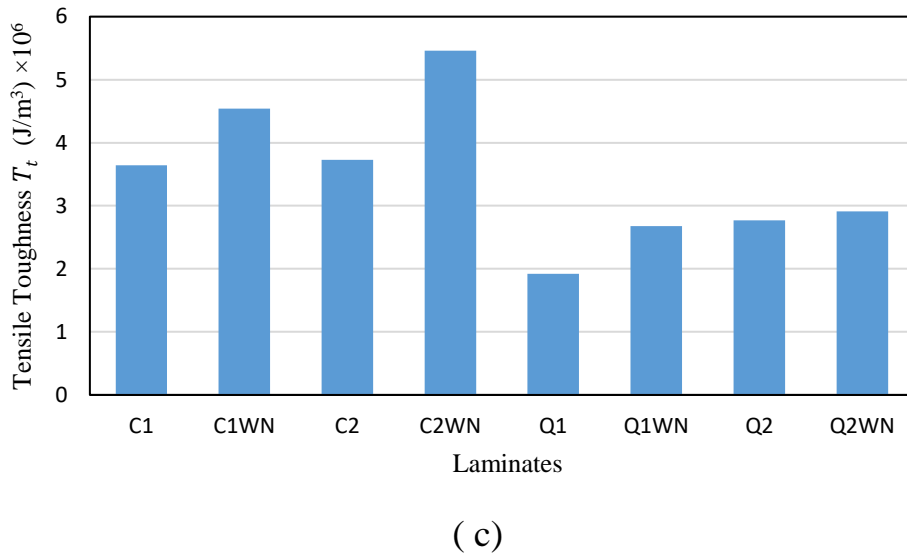
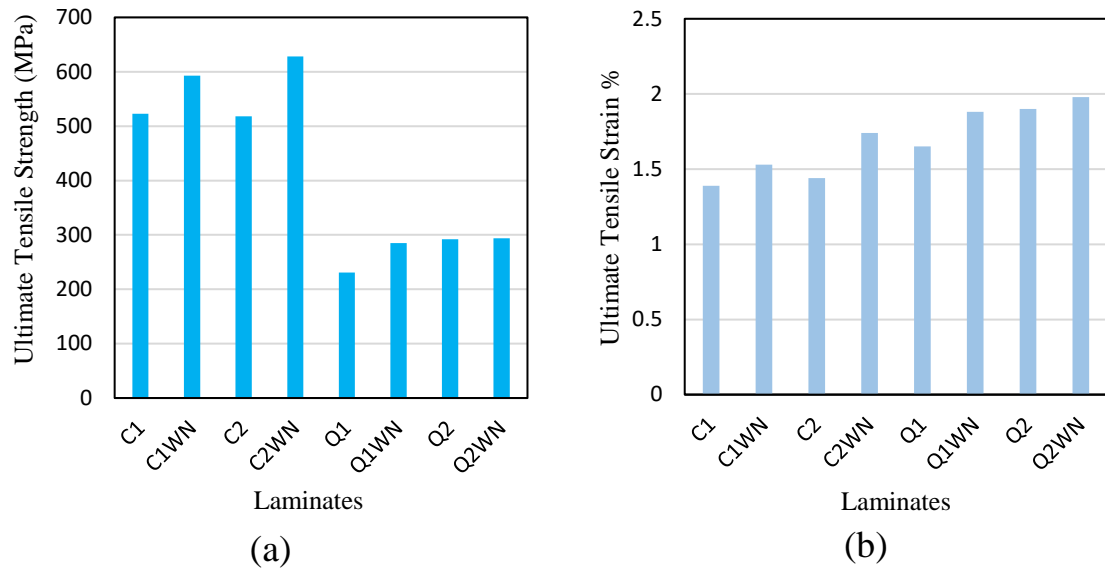
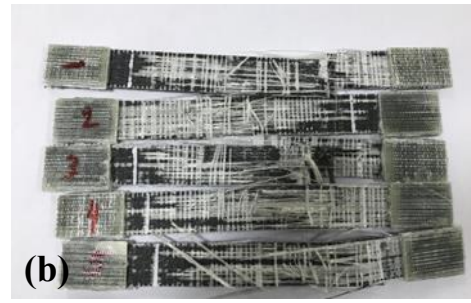


Figure (5.2) Tensile properties for cross and quasi-laminated epoxy composite with and without nano- Al_2O_3 : (a) Ultimate tensile strength, (b) Ultimate tensile strain %, and (c) Tensile toughness.



C1



C1WN



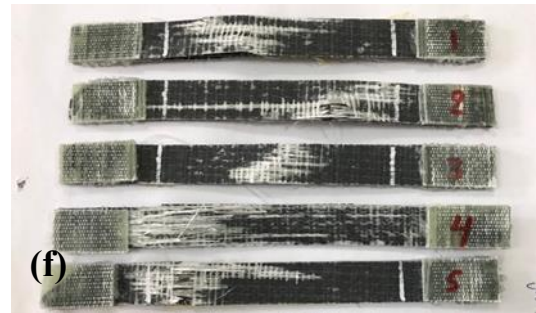
C2



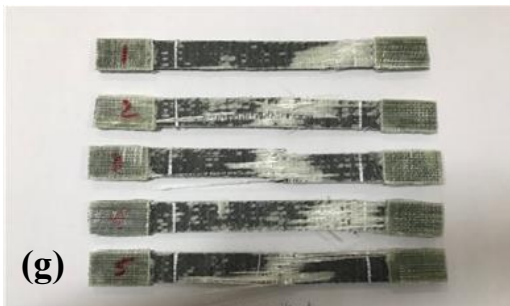
C2WN



Q1



Q1WN



Q2



Q2WN

Figure (5.3) Tensile failure modes for cross and quasi-laminated epoxy composite with and without nano- Al_2O_3 .

Practical and FEM maximum tensile load difference of FRPC is shown in Figure (5.4). The maximum practical tensile load of FRPC is 2%-15% higher than FEM.

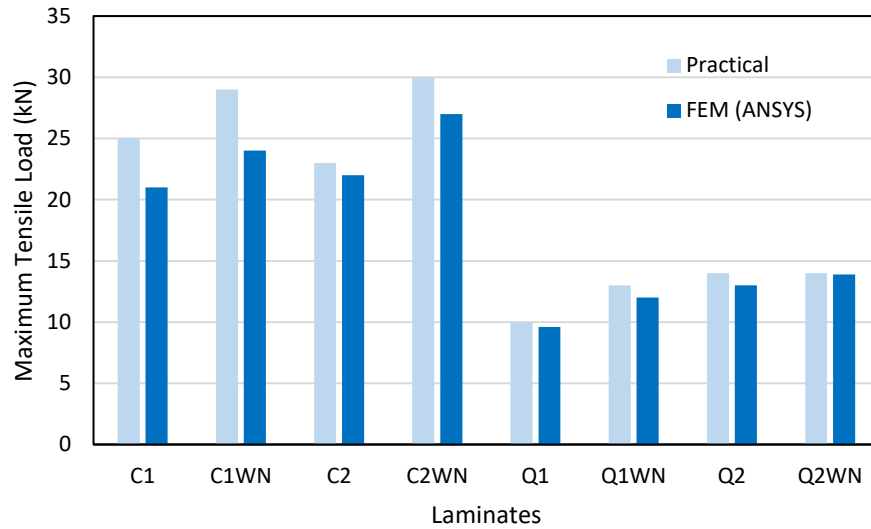


Figure (5.4) Practical and FEM maximum tensile load difference of FRPC.

5.3 Tensile Behavior of Sandwich SS304/FRPC/SS304 FML

Tensile load-displacement behavior curves of the cross and quasi-reinforced polymer composite compared with cross and quasi fiber /stainless steel -304 base fiber metal laminate are shown in Figure (5.5) and Figure (5.6), respectively.

The brittle behavior is obvious for cross and quasi-FRPC. The purpose of adding 304- stainless steel metal skins to the FRPC core is to delay failure occurrence. Also, to decline or omit the brittle behavior of FRPC.

As the load is applied, the core and skins elastically deformed until the yield point. After that, the slope of the tensile load-extension curves declines because the metal began to deform plastically while the fiber layers still deformed elastically. Interlaminar shear stress is present in the interface between fiber and metal due to metal plastic deformation. FRPC tried to bring back the lost stiffness. As the load increased, fiber breakage, fiber pullout, and

delamination occurred before the burst load dropped due to fiber metal debonding similar to the results (Megahed *et al.*, 2019; Sun *et al.*, 2019; Dahshan *et al.*, 2020; El-baky and Attia, 2022).

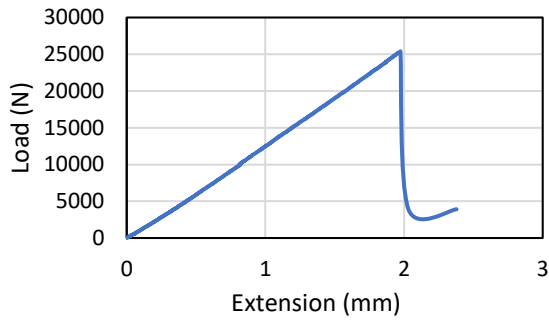
The maximum tensile load of SS/C1/SS, SS/C1WN/SS, SS/C2/SS, SS/C2WN/SS, SS/Q1/SS, SS/Q1WN/SS, SS/Q2/SS, SS/Q2WN/SS increased by 50%, 40%, 53%, 42%, 72%, 64%, 66%, and 66% in comparison with C1, C1WN, C2, C2WN, Q1, Q1WN, Q2, and Q2WN, respectively.

Extension at maximum load of SS/C1/SS, SS/C1WN/SS, SS/C2/SS, SS/C2WN/SS, SS/Q1/SS, SS/Q1WN/SS, SS/Q2/SS, SS/Q2WN/SS increased by 71%, 65%, 70%, 68%, 57%, 70%, 68%, and 65% in comparison with C1, C1WN, C2, C2WN, Q1, Q1WN, Q2, and Q2WN, respectively.

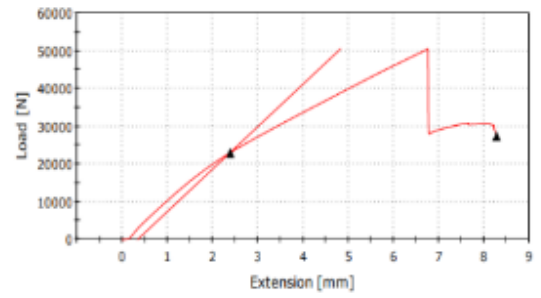
Tensile toughness represents the energy absorbed during the tension test until the maximum burst load (debonding). Tensile toughness can be found by evaluating the area under the curves. The perfect bonding of two metal skins to the outer surfaces of FRPC increased the tensile toughness of the FML sandwich. Tensile toughness of SS/C1/SS, SS/C1WN/SS, SS/C2/SS, SS/C2WN/SS, SS/Q1/SS, SS/Q1WN/SS, SS/Q2/SS, SS/Q2WN/SS increased by 74%, 70%, 74%, 67%, 87%, 80%, 83%, and 82% in comparison with C1, C1WN, C2, C2WN, Q1, Q1WN, Q2, and Q2WN, respectively as shown in Figure (5.7).

Fiber metal laminate tensile failure modes are characterized by fiber breakage, fiber pullout, delamination, and finally severe debonding between metal skin surfaces and fiber composite surfaces as shown in Figure (5.8).

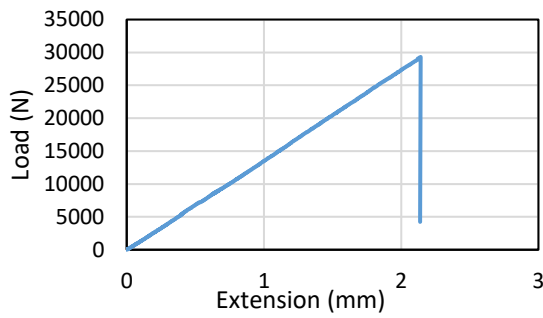
The practical and FEM maximum tensile load difference of FRPC and FML is shown in Figure (5.9). The FEM maximum tensile load of FML is twice the practical one. As a result, the Araldite 2011 can be replaced with another that has twice the shear strength.



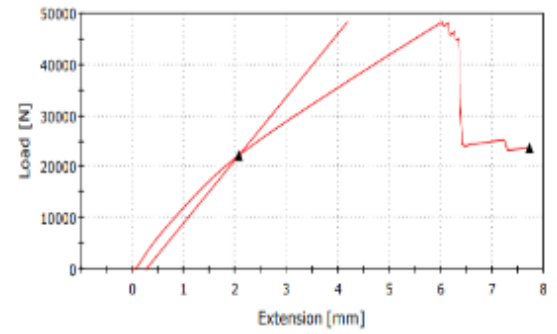
(a) C1



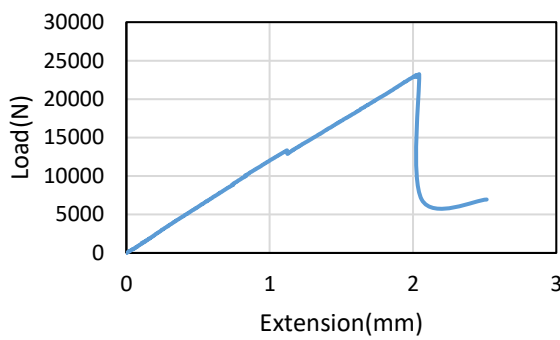
(b) SS/C1/SS



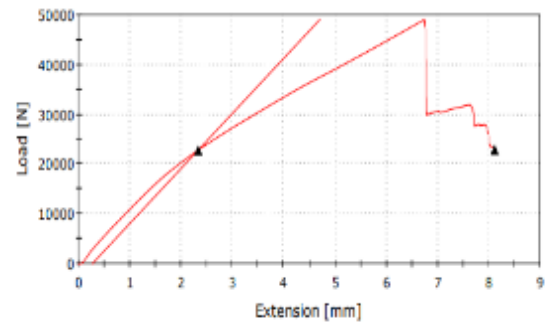
(c) C1WN



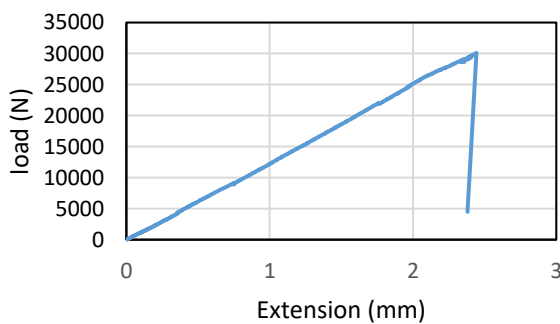
(d) SS/C1WN/SS



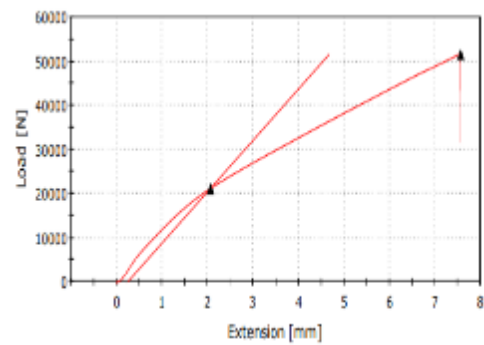
(e) C2



(f) SS/C2/SS

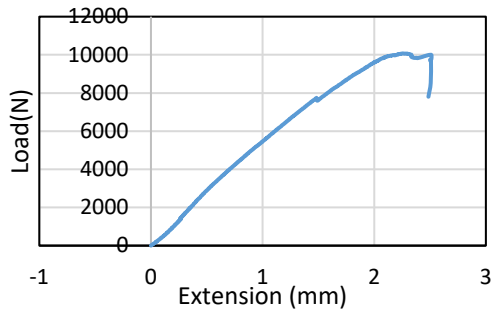


(g) C2WN

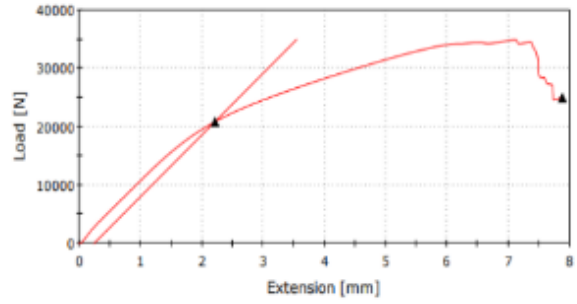


(h) SS/C2WN/SS

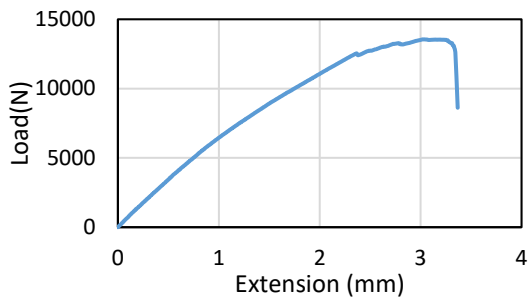
Figure (5.5) Comparison between tensile load-extension of Cross FRPC and FML.



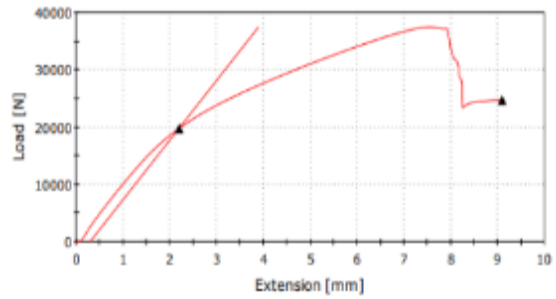
(a) Q1



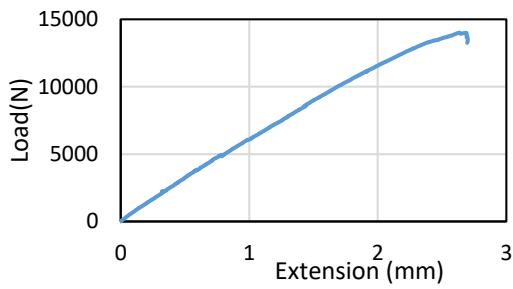
(b) SS/Q1/SS



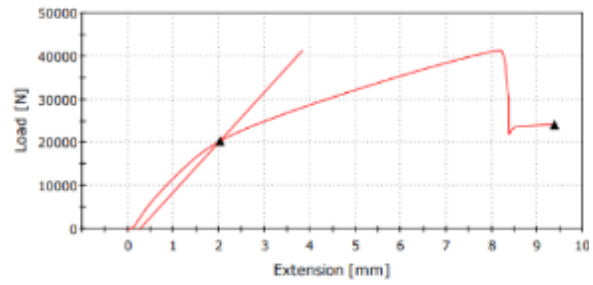
(c) Q1WN



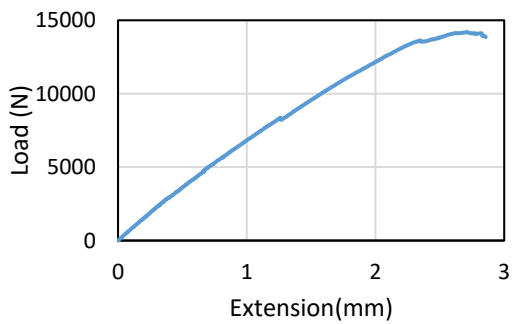
(d) SS/Q1WN/SS



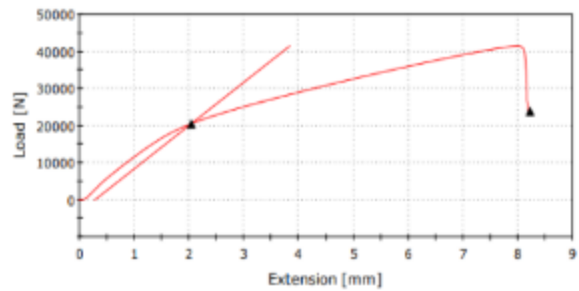
(e) Q2



(f) SS/Q2/SS

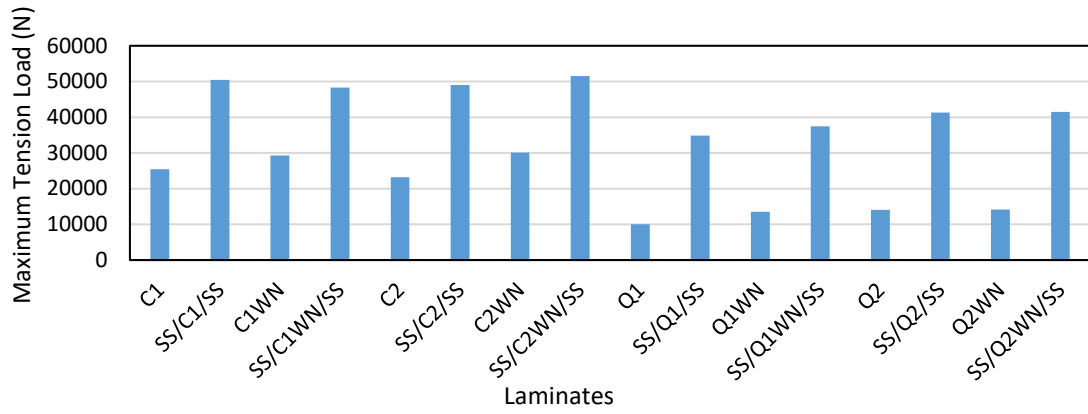


(g) Q2WN

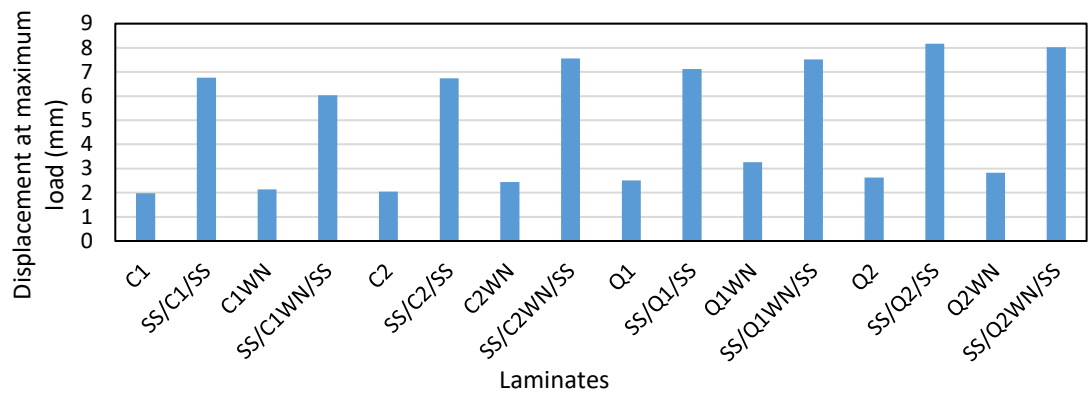


(h) SS/Q2WN/SS

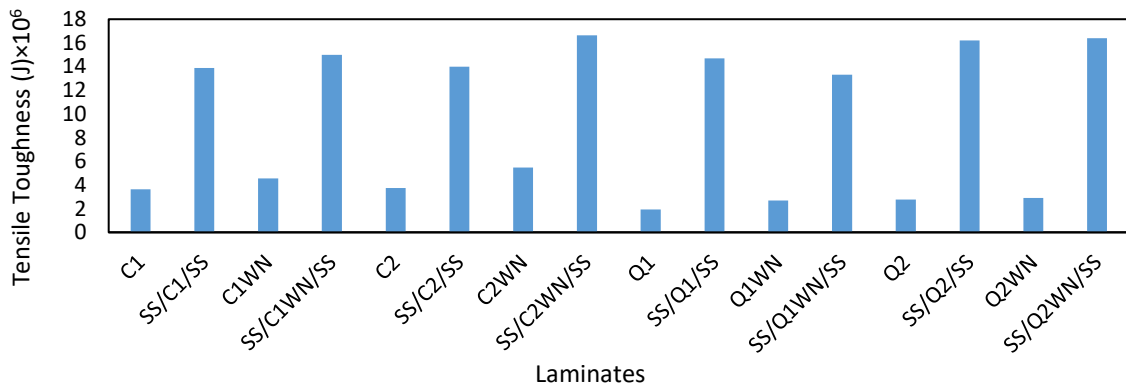
Figure (5.6) Comparison between tensile load-extension of quasi FRPC and FML.



(a)

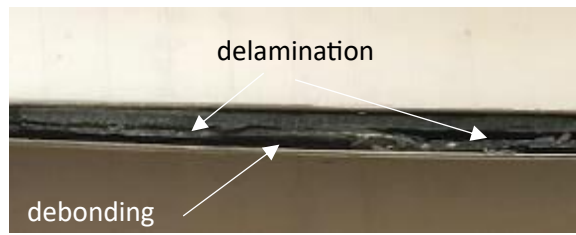


(b)

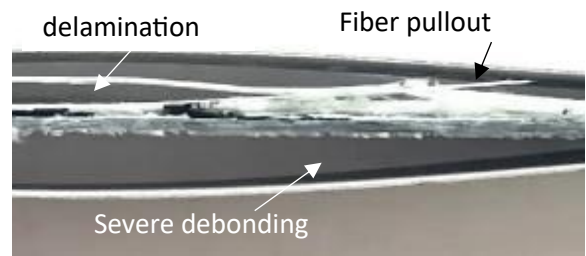


(c)

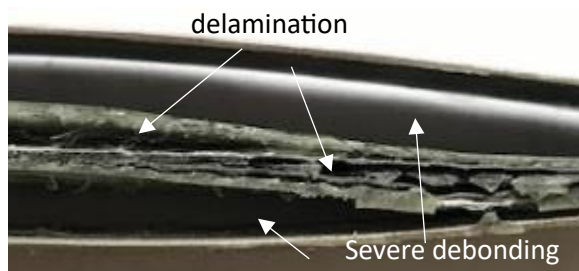
Figure (5.7) Tensile properties for FRPC and FML with and without nano- Al_2O_3 : (a) Maximum tensile load, (b) Displacement at maximum load, and (c) Tensile toughness.



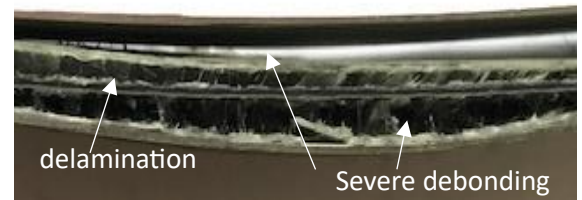
(a) SS/C1/SS



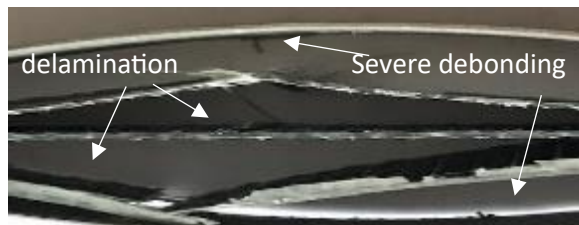
(b) SS/C1WN/SS



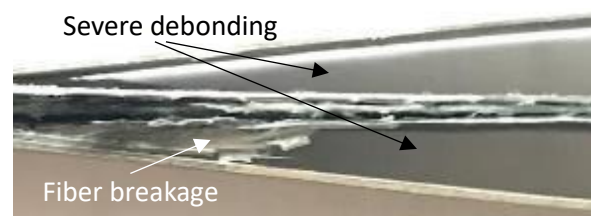
(c) SS/C2/SS



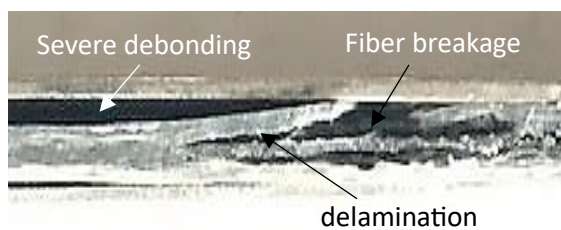
(d) SS/C2WN/SS



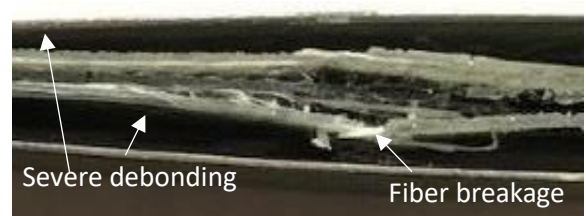
(e) SS/Q1/SS



(f) SS/Q1WN/SS



(g) SS/Q2/SS



(h) SS/Q2WN/SS

Figure (5.8) Tensile failure modes for cross and quasi-laminated epoxy composite /stainless steel 304 base with and without nano- Al_2O_3 .

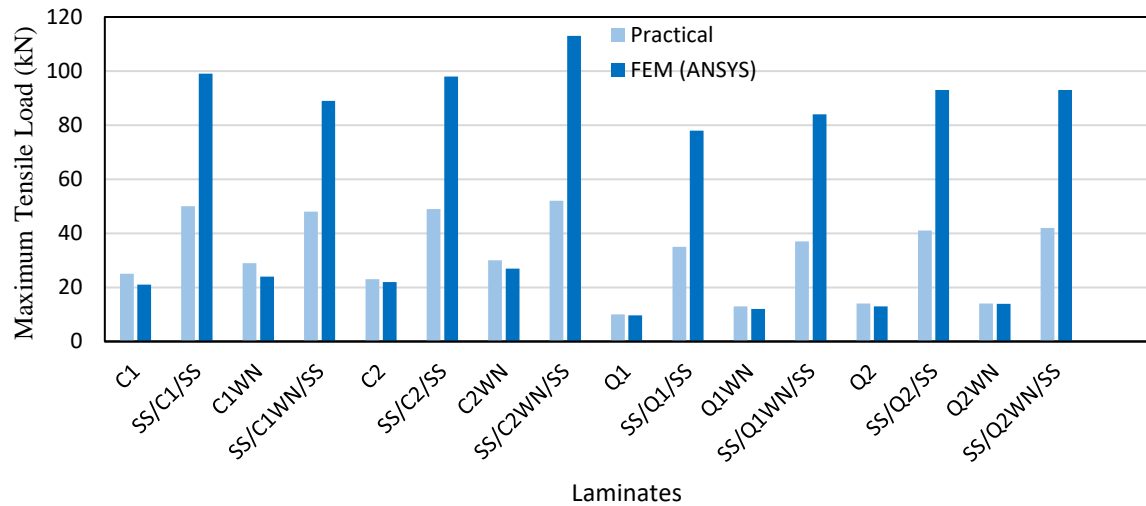
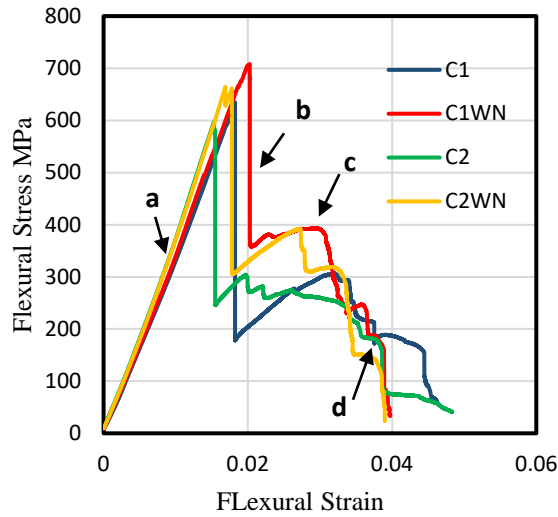


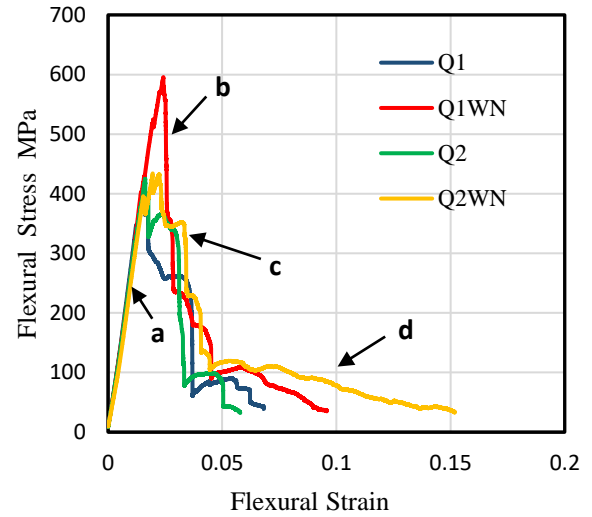
Figure (5.9) Practical and FEM maximum tensile load difference of FRPC and FML sandwiches.

5.4 Flexural Behavior of Fiber-Reinforced Polymer Composite

Flexural stress-strain curves for the eight laminated glass/carbon epoxy (cross and quasi) composites were passed through four stages (a) elastic stage, (b) compressive failure stage, (c) hill failure stage (plateau), and (d) tensile failure stage are shown in Figure (5.10) (a, and b), respectively similar to the results of researches (Abd Ghani and Mahmud, 2020; Alcludia-Zacarias *et al.*, 2020). All laminated epoxy composites behaved linearly in the elastic region until the ultimate point, along with the occurrence of a small amount of debonding in the quasi group. Laminates were subjected to flexural load in the compressive region which then shifted through it to the tensile region. As the compressive layers failed, then the load carrying capacity transferred to the tension layers through stage c was characterized by load rising before tensile layer failure similar to research (Alcludia-Zacarias *et al.*, 2020). The plateau stage for quasi laminate group is little or absent, but the tension failure stage is longer in comparison with cross laminate group.



(a) Cross Laminates



(b) Quasi Laminates

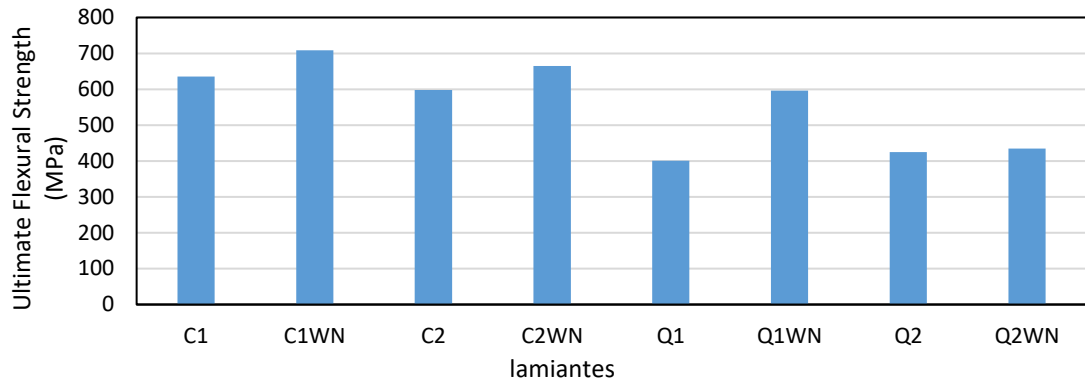
Figure (5.10) Flexural stress-strain curves for symmetrical hybrid cross and quasi-laminated epoxy composite with and without nano- Al_2O_3

Figure (5.11) demonstrates the flexural properties of all laminated epoxy composites. To increase load carrying capacity, nano- Al_2O_3 was added to both stacking sequence $[G/C/C/G/G/C/C/G]$, $[G/G/C/C/C/C/G/G]$ of cross (C1, C2) and quasi (Q1, Q2) laminates via increasing the adhesion between fibers and epoxy matrix; therefore, samples C1WN, C2WN, Q1WN, and Q2WN are more deformable with higher ultimate flexural strength, ultimate flexural strain and flexural toughness than C1, C2, Q1, and Q2 respectively similar to the results of researches (Matykiewicz, 2020; Mohanty and Srivastava, 2015; Kaybal *et al.*, 2018). It was obvious that the stacking sequence $G/C/C/G/G/C/C/G$ with nano- Al_2O_3 for both cross and quasi groups have the best flexural properties than $G/G/C/C/C/C/G/G$ because of the presence of carbon layer near the outer surfaces of the laminates far from the neutral axis. Generally, the cross-laminate C1WN has two 0° carbon fiber layers so the flexural properties were the best among the other laminates. In the cross-laminate group, C1WN had the maximum flexural properties (strength, strain, and toughness) which are equal to 708.2 MPa, 2.027%, and 7.36×10^6 J/m³, respectively. In the quasi group,

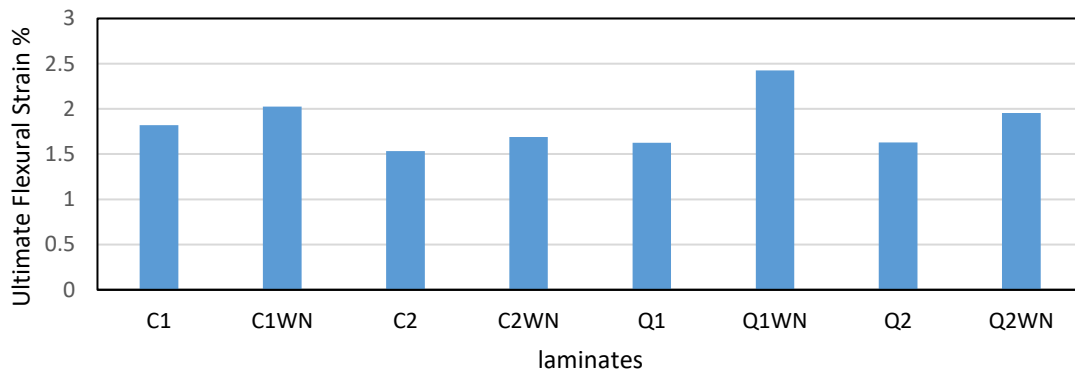
Q1WN had the maximum flexural properties (strength, strain, and toughness) which are equal to 596 MPa, 2.424%, and 7.22×10^6 J/m³, respectively.

In general, the flexural failure modes are characterized by fiber buckling at the compression side and fiber breakage or fiber pullout in the tension side with little internal delamination and transverse crack propagation as shown in Figure (5.16) similar to the results of research (Dong and Davies, 2013; Abd Ghani and Mahmud, 2020; Alcludia-Zacarías *et al.*, 2020).

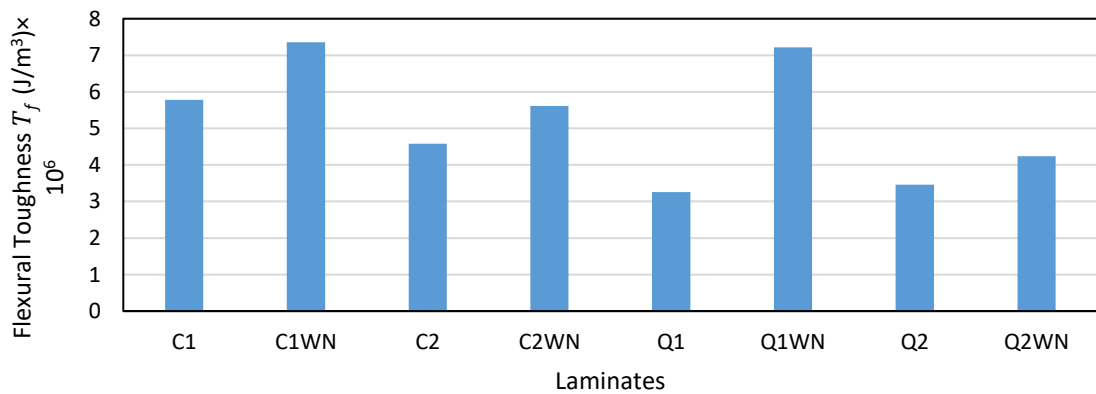
The FRPC Flexural sample with supports and load is shown in Figure (5.13). Practical and FEM maximum flexural load difference FRPC is shown in Figure (5.14). C2, Q1, and Q2WN FEM maximum flexural load is higher than the practical one because the sample thickness is lower than 2 mm.



(a)



(b)



(c)

Figure (5.11) Flexural properties for cross and quasi laminated epoxy composite with and without nano- Al_2O_3 : (a) Ultimate Flexural strength, (b) Ultimate Flexural strain, and (c) Flexural toughness.

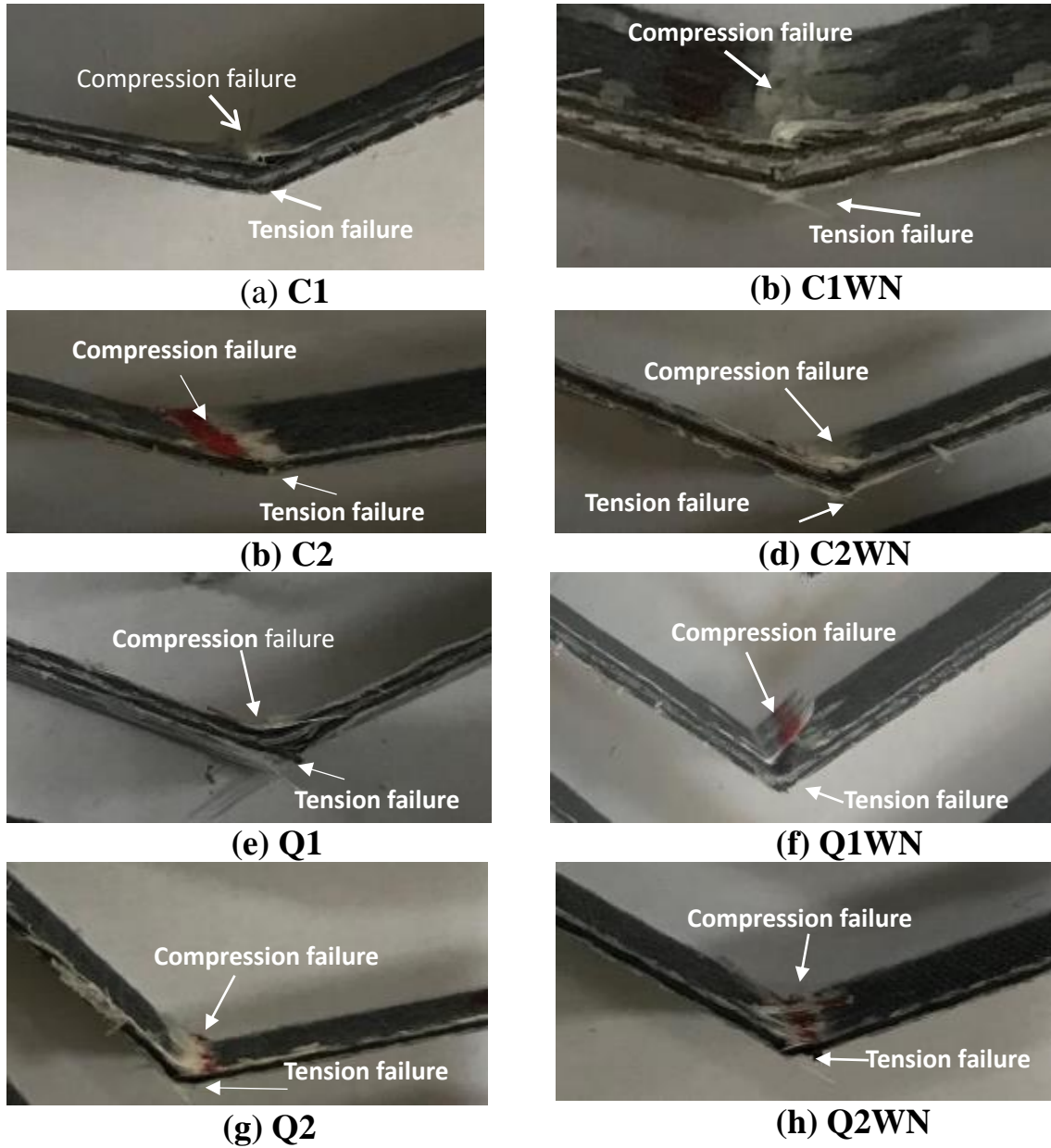


Figure (5.12) Flexural failure modes for cross and quasi-laminated epoxy composite with and without nano- Al_2O_3 .

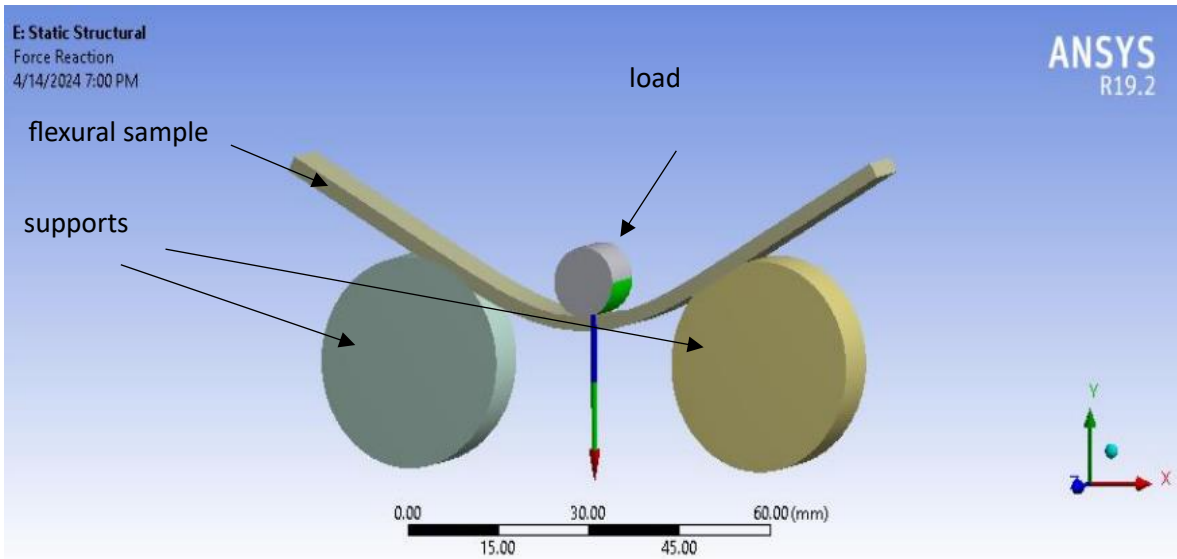


Figure (5.13) FRPC flexural sample with supports and load.

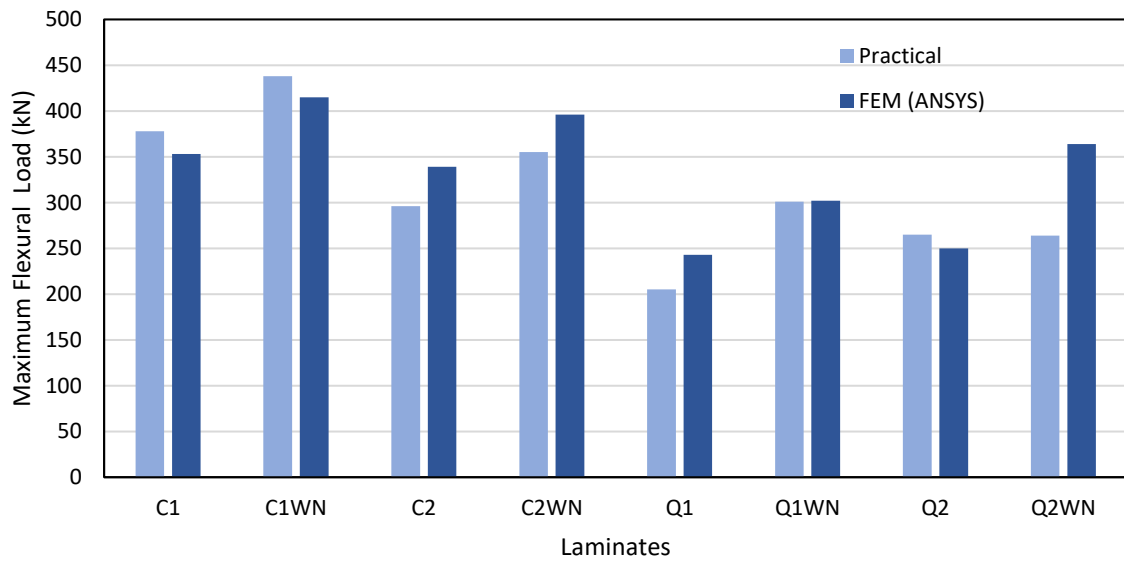


Figure (5.14) Practical and FEM maximum flexural load difference of FRPC.

5.5 Flexural Behavior of Sandwich SS304/FRPC/SS304 FML

Flexural load-displacement behavior curves of cross and quasi-reinforced polymer composite compared with cross and quasi fiber /stainless steel -304 base fiber metal laminate are shown in Figure (5.15) and Figure (5.16), respectively.

The brittle behavior is obvious for cross and quasi-FRPC. The purpose of adding 304- stainless steel metal skins to the FRPC core is to decrease deflection occurrence. Also, to decline or omit the brittle behavior of FRPC.

As the load is applied, the core and skins elastically deformed until the yield point. After that, the slope of the flexural load-extension curves declines progressively because the metal began to deform plastically while the fiber layers still deformed elastically. The weak bonding between metal and fibers led to little change in the slope. While the load transferred from the compression side to the tension side, and the load reached its ultimate value, the first sudden load dropped due to fiber breakage at the tension side. The load is redistributed between fibers to increase load carrying capacity until the second drop occurs due to debonding between fiber and metal either in compression or in tension sides similar to the results of (Dhaliwal and Newaz, 2016; S Singh and Angra, 2018; Sun *et al.*, 2019; Chen *et al.*, 2023; Gao *et al.*, 2023).

The maximum flexural load of SS/C1/SS, SS/C1WN/SS, SS/C2/SS, SS/C2WN/SS, SS/Q1/SS, SS/Q1WN/SS, SS/Q2/SS, and SS/Q2WNSS increased by 70%, 69%, 72%, 65%, 74%, 79%, 75%, and 73% in comparison with C1, C1WN, C2, C2WN, Q1, Q1WN, Q2, and Q2WN, respectively.

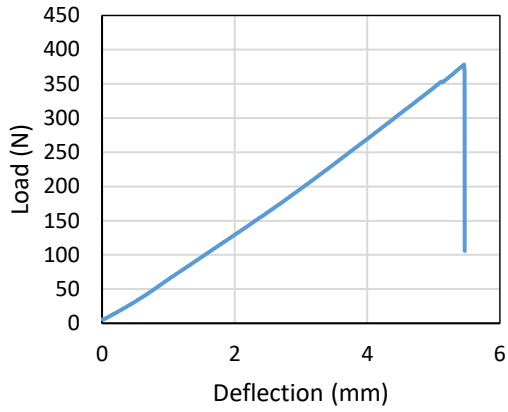
Deflection at maximum load of SS/C1/SS, SS/C1WN/SS, SS/C2/SS, SS/C2WN/SS, SS/Q1/SS, SS/Q1WN/SS, SS/Q2/SS, and SS/Q2WNSS

decreased by 45%, 42%, 55%, 66%, 67%, 22%, 56%, and 66% in comparison with C1, C1WN, C2, C2WN, Q1, Q1WN, Q2, and Q2WN, respectively.

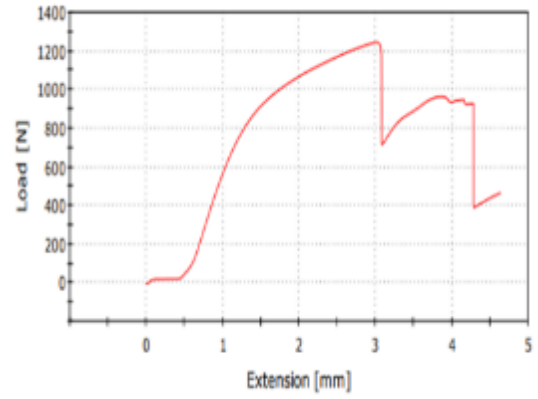
Flexural toughness represents the energy absorbed during the bending test until the maximum burst load (debonding). Flexural toughness can be found by evaluating the area under the curves. The perfect bonding of two metal skins to the outer surfaces of the FRPC core increased the flexural toughness of the FML sandwich (Megahed *et al.*, 2019; El-baky and Attia, 2022; Khalili, Mittal, and Kalibar, 2005). Flexural toughness of SS/C1/SS, SS/C1WN/SS, and SS/Q1WN/SS increased by 21%, 21%, and 40% in comparison with C1, C1WN, and Q1WN, respectively as shown in Figure (5.17). Flexural toughness of SS/C2/SS, SS/C2WN/SS, SS/Q1WN/SS, SS/Q2/SS, and SS/Q2WNSS decreased by 35%, 55%, 56%, 23%, and 46% in comparison with C2, C2WN, Q1, Q2, and Q2WN, respectively as shown in Figure (5.17) because of low bonding between fiber and metal.

Fiber metal laminate flexural failure modes are characterized by fiber breakage, delamination, and finally severe debonding between metal skin surfaces and fiber composite surfaces as shown in Figure (5.18).

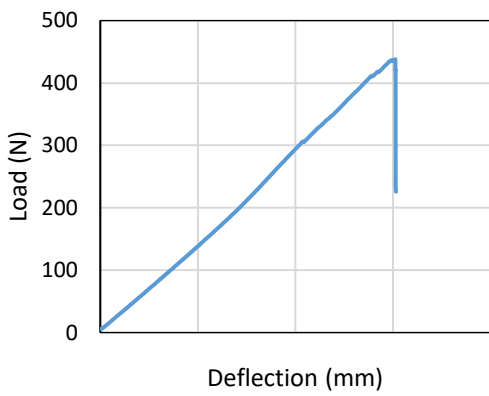
The FML Flexural sample with supports and load is shown in Figure (5.19). Practical and FEM maximum flexural load difference of FML is shown in Figure (5.20). The FEM maximum flexural load for SS/C1WN/SS is higher than the practical one because of the weak bonding between fiber and metal due to low surface roughness despite an increase in its toughness value in comparison with C1WN FRPC.



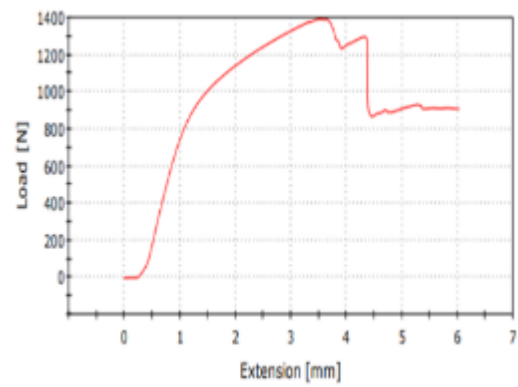
(a) C1



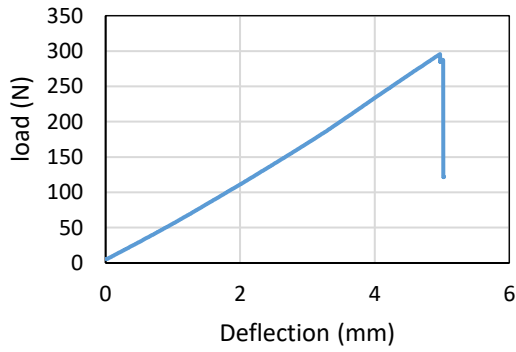
(b) SS/C1/SS



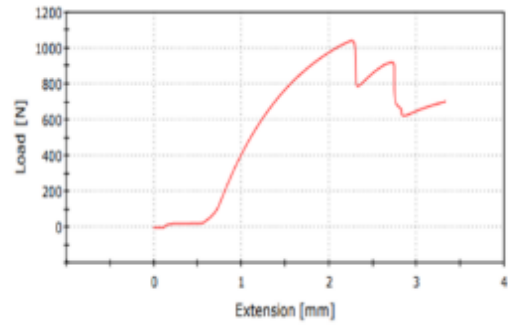
(c) C1WN



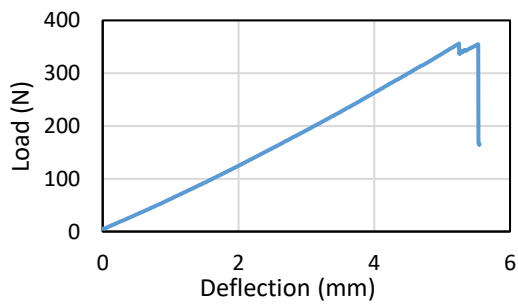
(d) SS/C1WN/SS



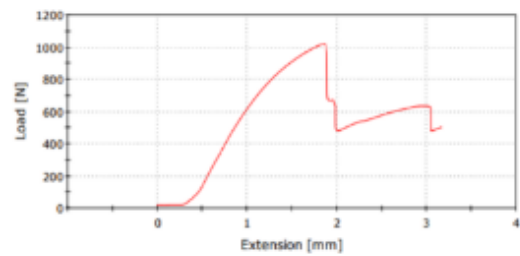
(e) C2



(f) SS/C2/SS

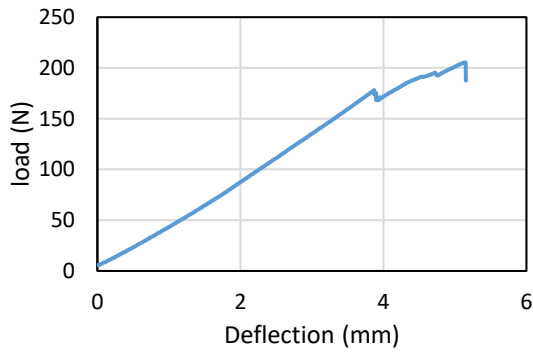


(g) C2WN

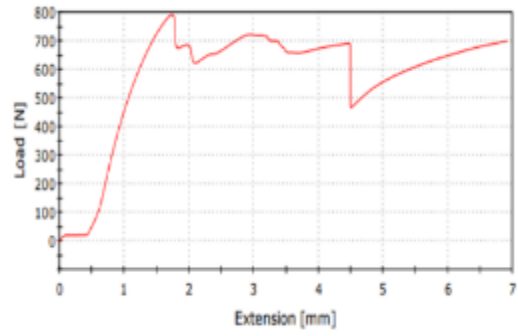


(h) SS/C2WN/SS

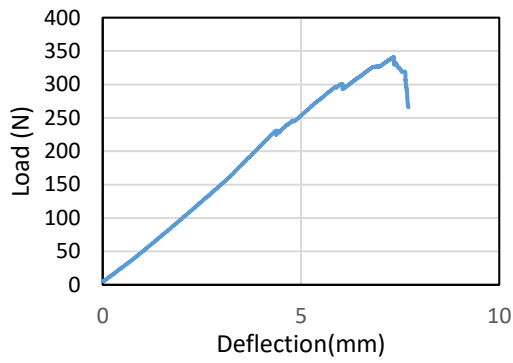
Figure (5.15) Comparison between flexural load-extension of Cross FRPC and FML.



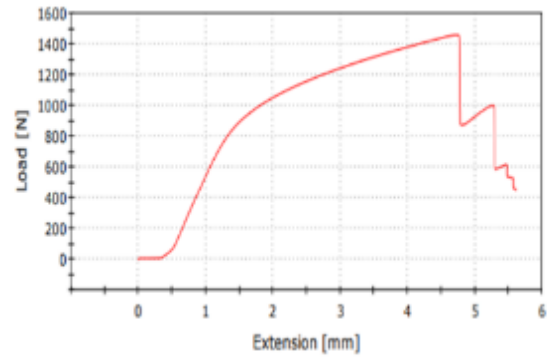
(a) Q1



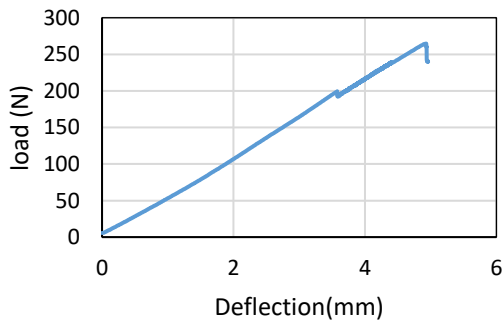
(b) SS/Q1/SS



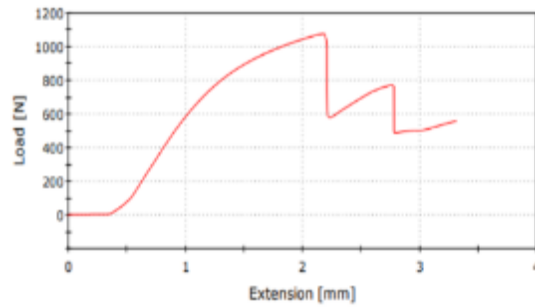
(c) Q1WN



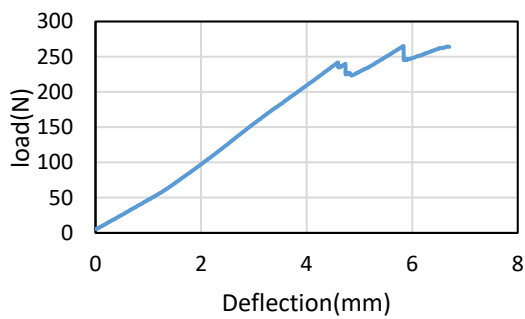
(d) SS/Q1WN/SS



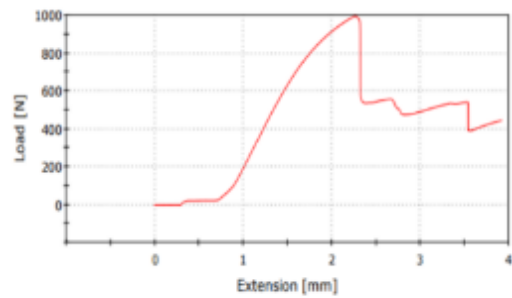
(e) Q2



(f) SS/Q2/SS

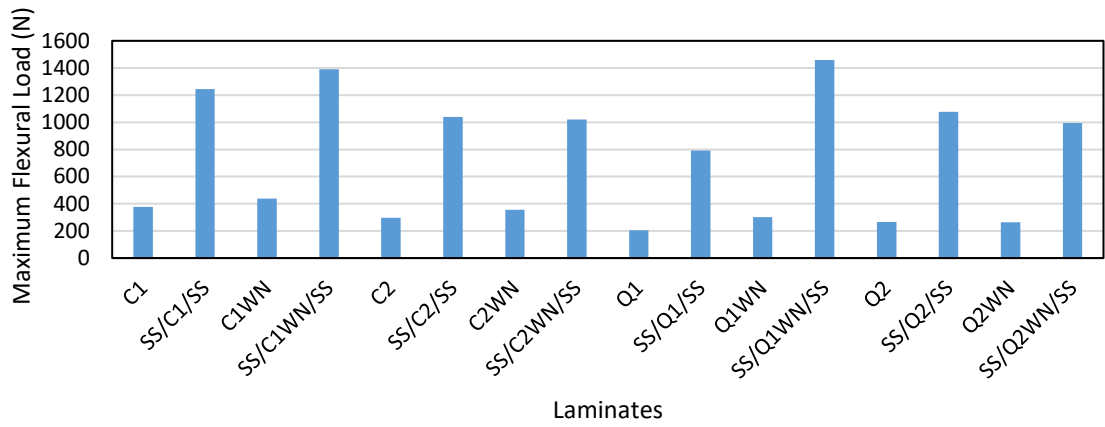


(g) Q2WN

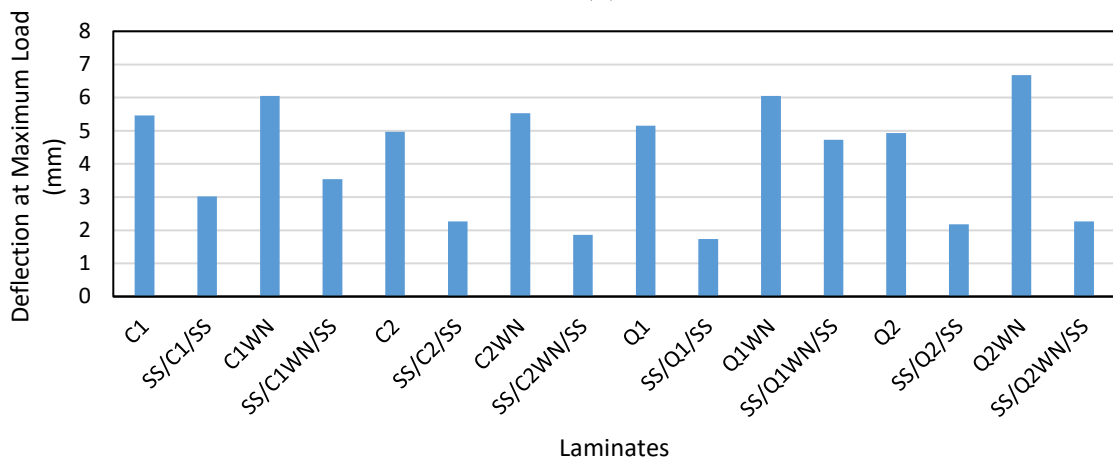


(h) SS/Q2WN/SS

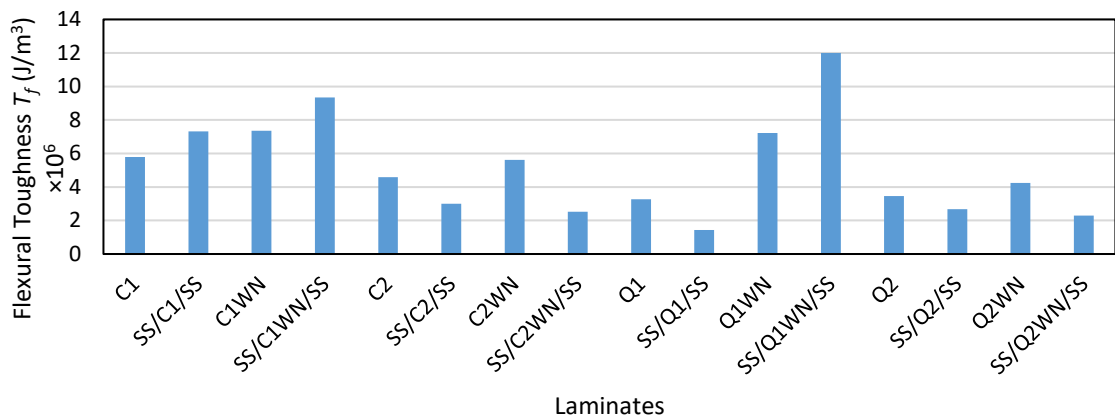
Figure (5.16) Comparison between flexural load-extension of quasi-FRPC and FML.



(a)



(b)



(c)

Figure (5.17) Flexural properties for FRPC and FML with and without nano- Al_2O_3 : (a) maximum tensile load, (b) Deflection at maximum load, and (c) Flexural toughness.

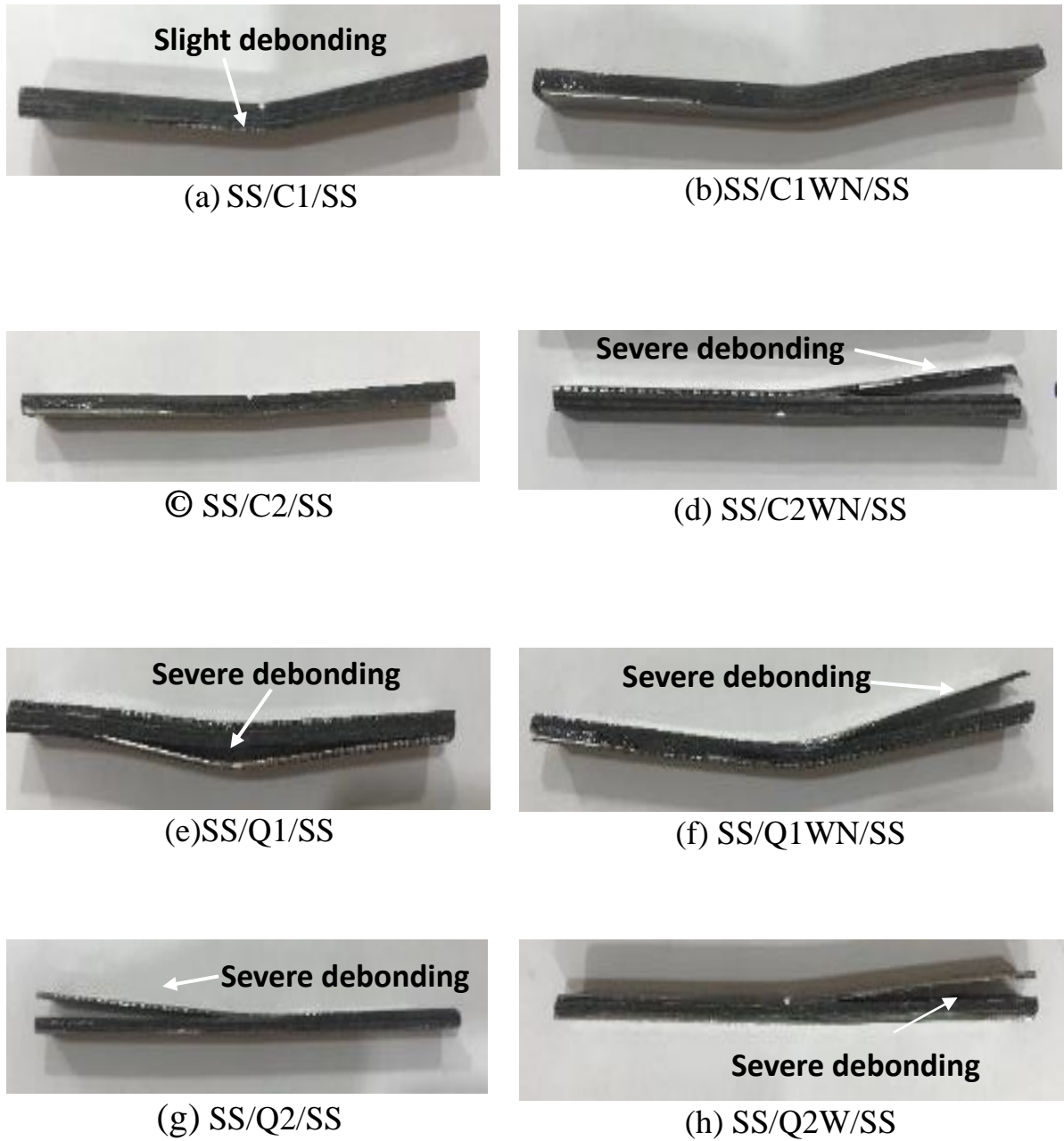


Figure (5.18) Flexural failure modes for cross and quasi-laminated epoxy composite /stainless steel 304 base with and without nano- Al_2O_3 .

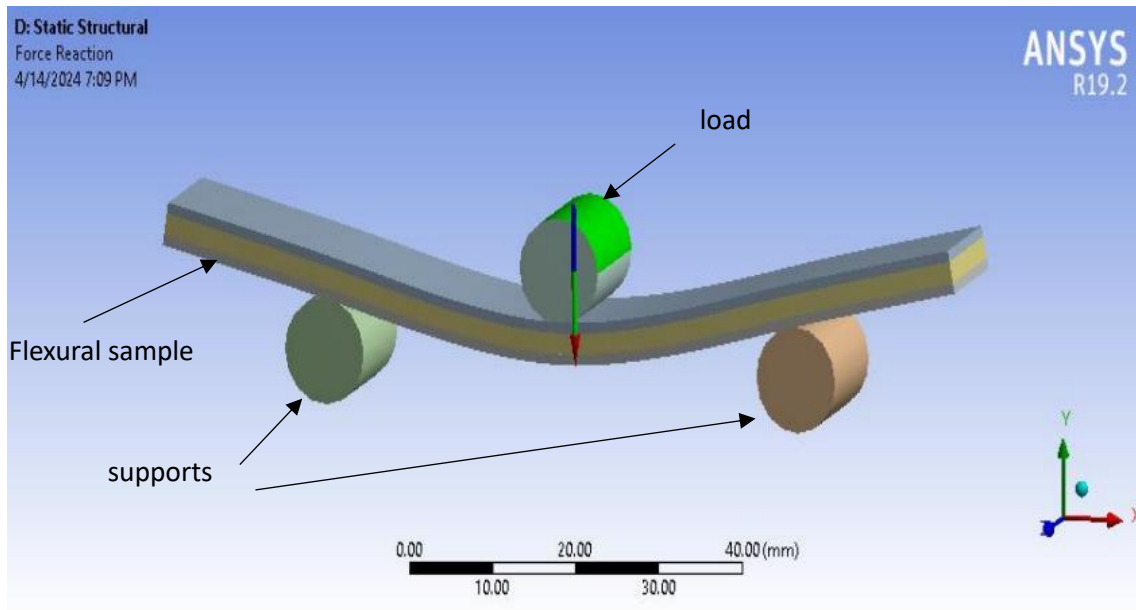


Figure (5.19) FML flexural sample with supports and load.

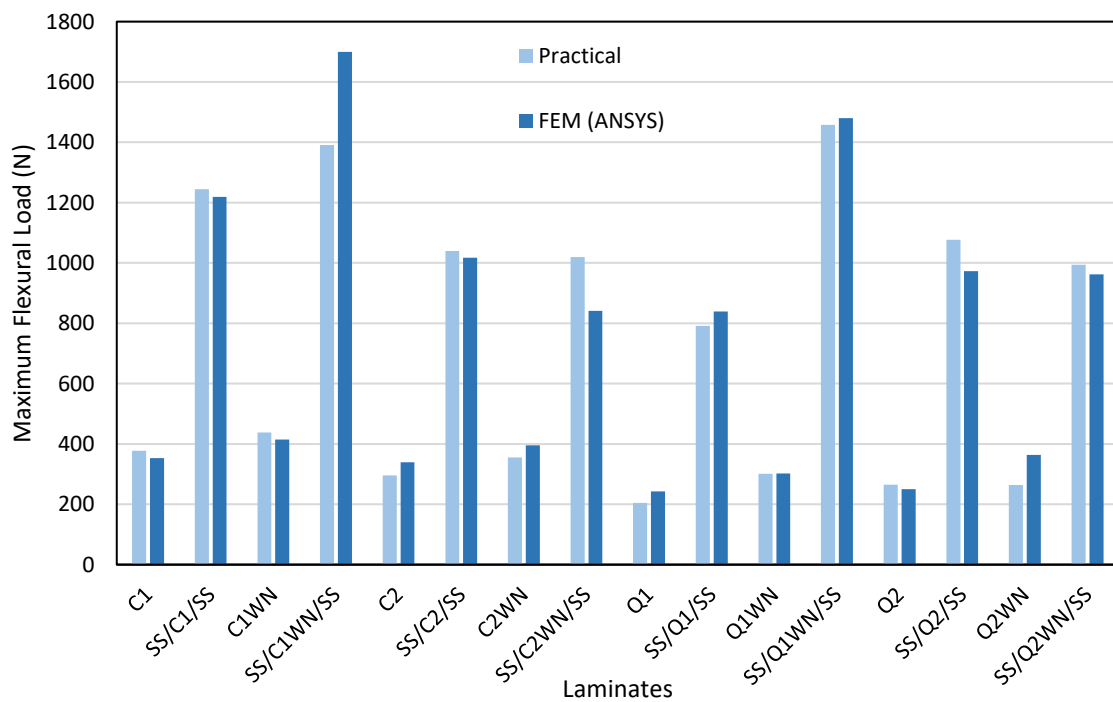


Figure (5.20) Practical and FEM maximum flexural load difference of FML sandwiches.

5.6 Morphology (Scanning Electron Microscopy) Images

The scanning electronic microscopy SEM was to oversight and observe the morphology of the internal structure of the laminates through the adhesion between fibers and matrix and notice the failure modes, which affect totally on the mechanical properties of the laminated epoxy composites (Khan *et al.*, 2021).

Q2 and Q2WN tensile samples as well as C1 and C1WN flexural samples were scanned as shown in Figures (5.21-5.24) with a magnification of 1000. SEM gave us a clear picture of the types of failure in both tensile and flexural samples like transverse matrix crack propagation, delamination, fiber pullout and fiber breakage, matrix fragmentation, and fiber imprints. Delamination may either occur between glass and carbon layers or between carbon and carbon layers.

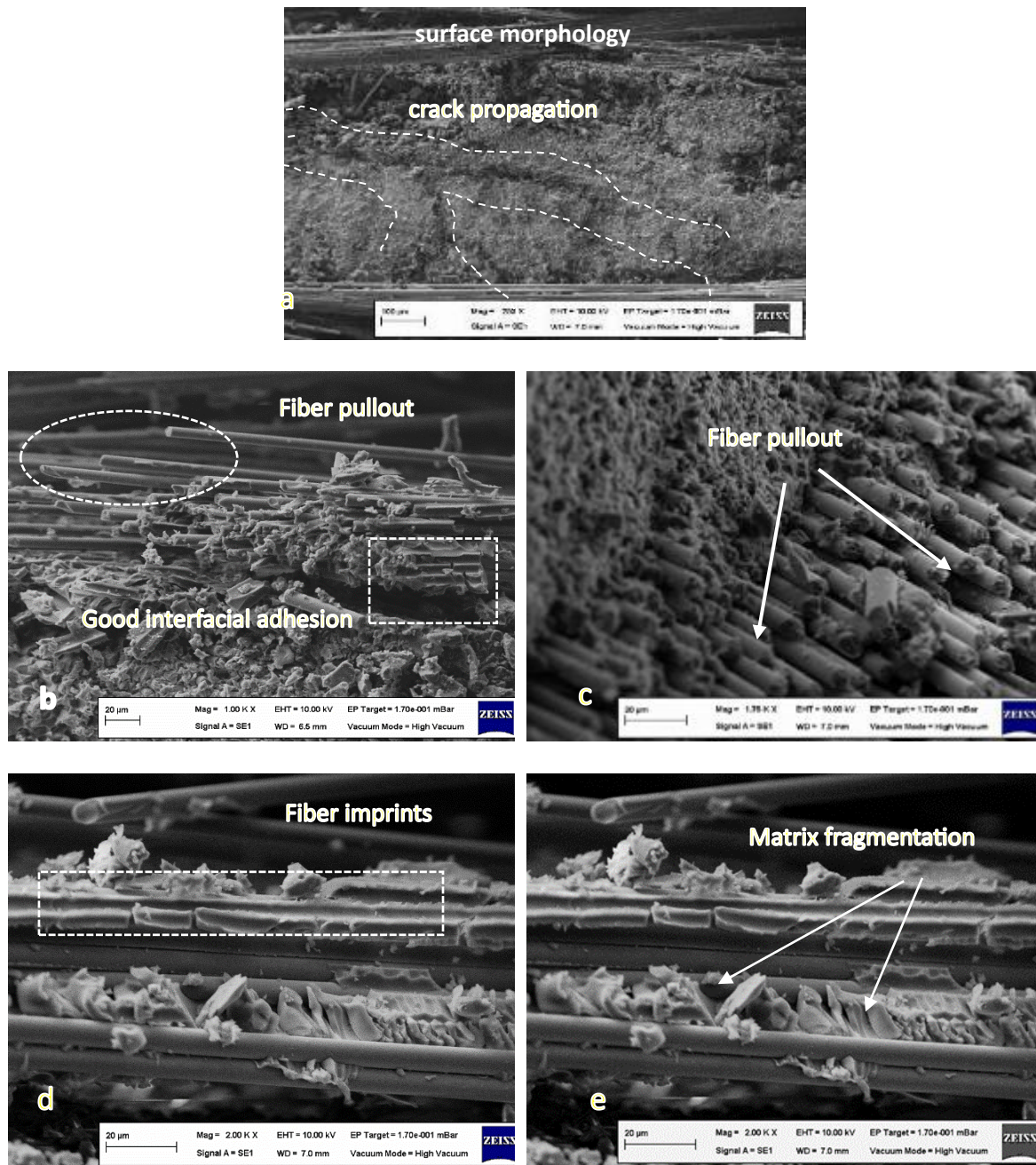


Figure (5.21) SEM of Q2 quasi laminate tensile sample: (a) crack propagation, (b) good interfacial adhesion, (c) fiber pull-out, (d) fiber imprints, (e) matrix fragmentation

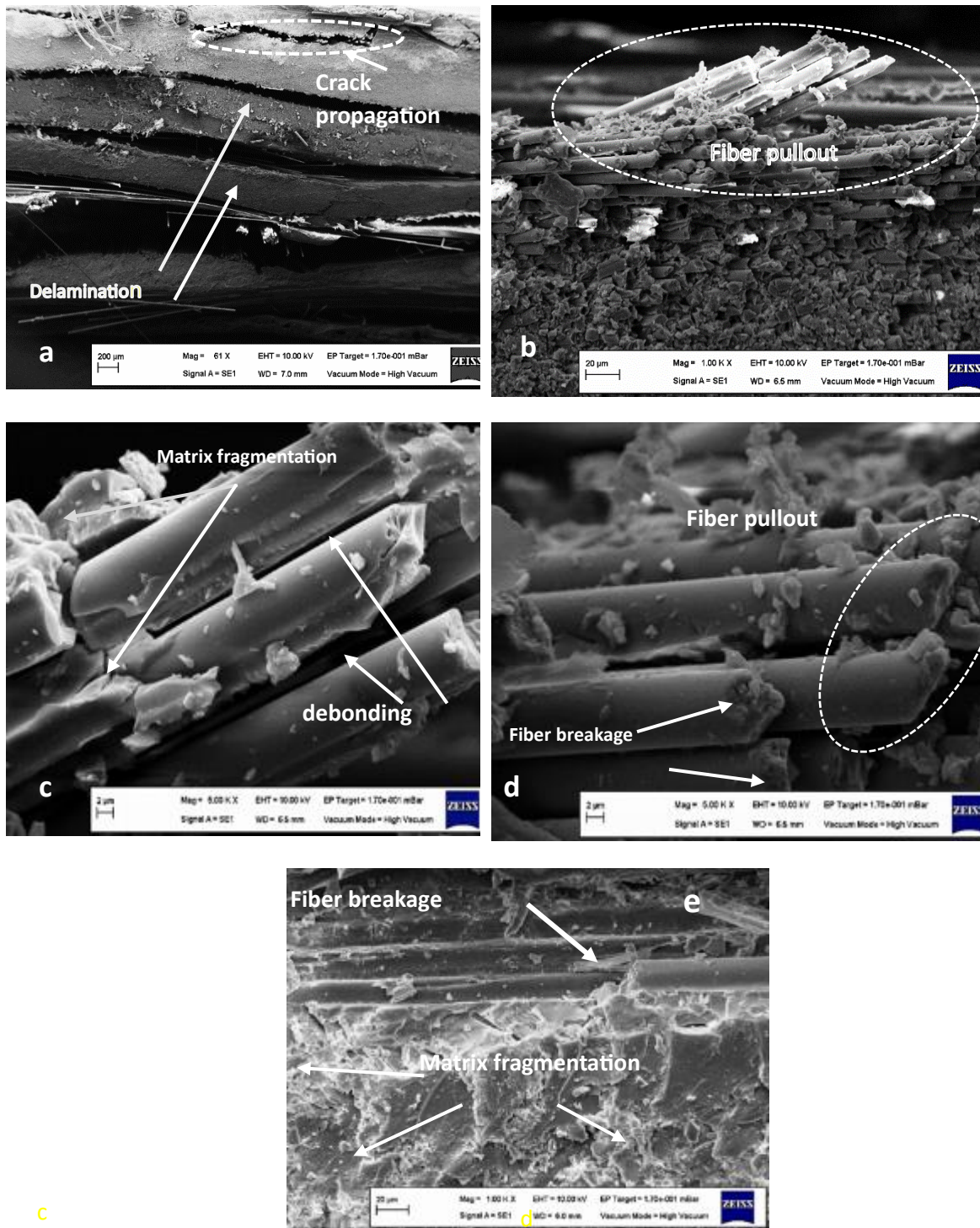


Figure (5.22) SEM of Q2WN quasi laminate tensile sample: (a) crack propagation, (b) Fiber pull out, (c) debonding, (d) fiber breakage, (e) matrix fragmentation

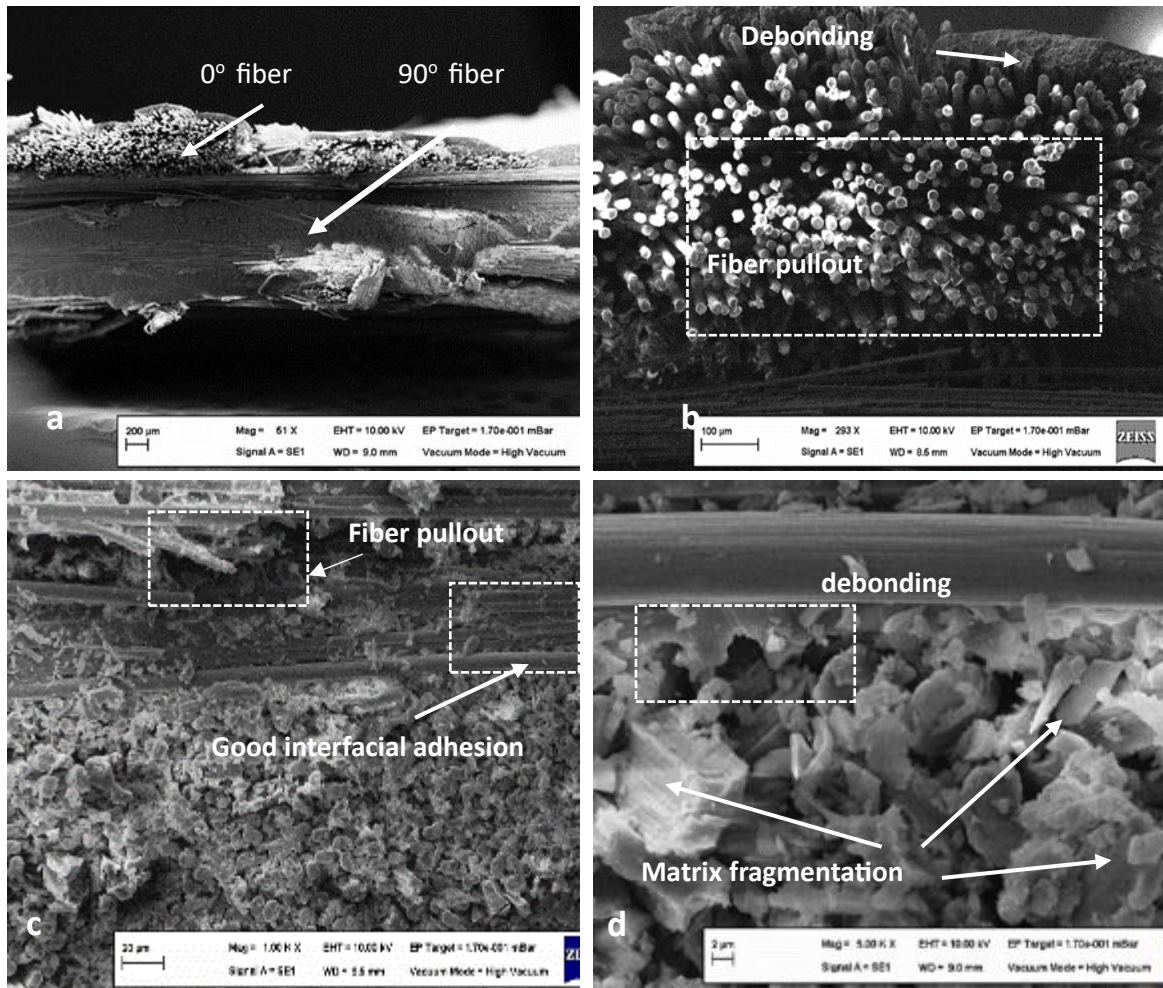


Figure (5.23) SEM of C1 cross-laminate flexural sample: (a) 0° fiber and 90° fiber at failed region, (b) fiber pull-out, (c) good interfacial adhesion, (d) matrix fragmentation

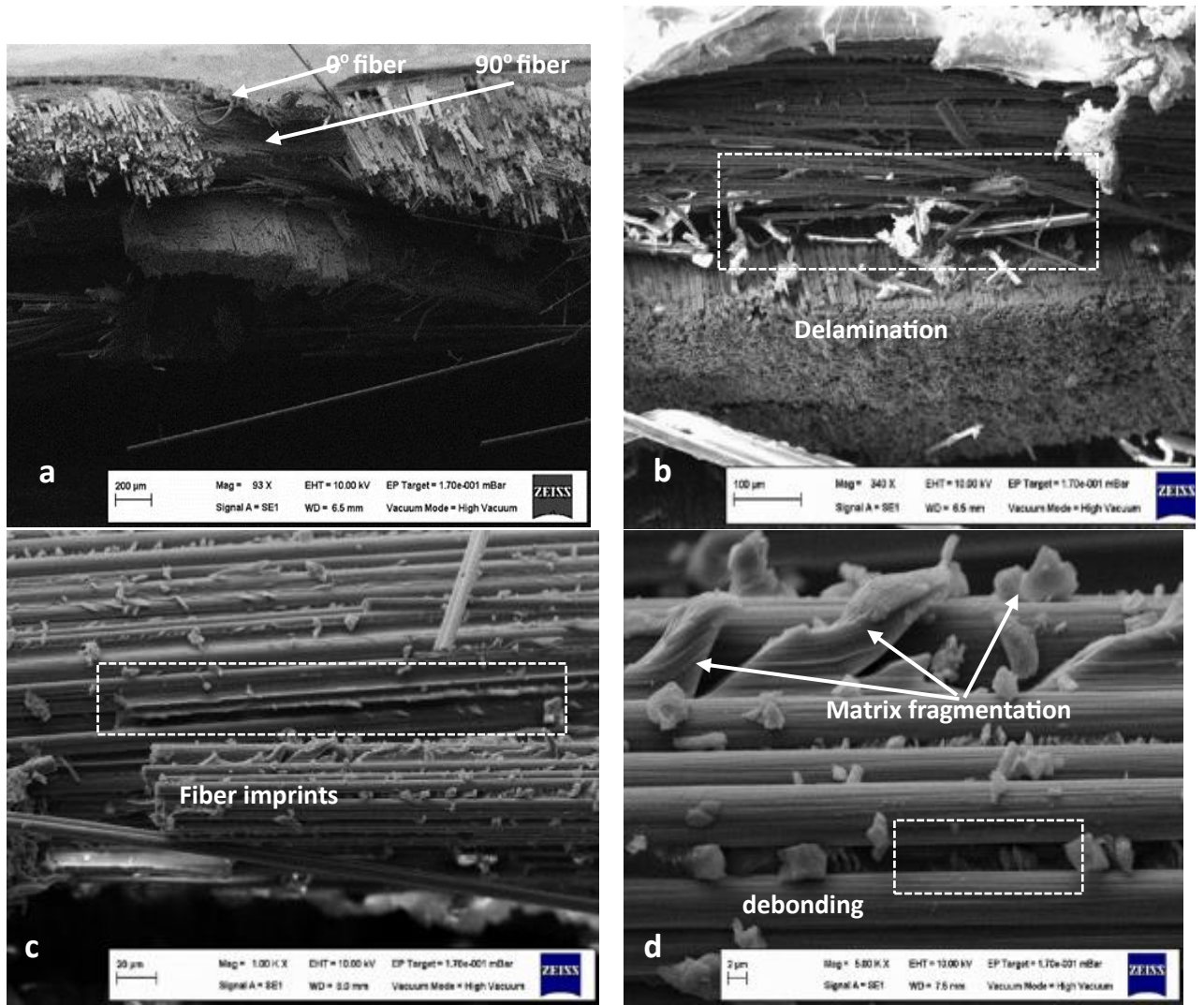


Figure (5.24) SEM of C1WN cross laminate flexural sample: (a) 0° fiber and 90° fiber at the failed region, (b) Delamination, (c) fiber imprints, (d) matrix fragmentation

5.7 Free Vibration Response of Fiber-Reinforced Polymer Composite

Knowledge of the dynamic properties of FRPC is just as important as that of the static ones. It is suitable to utilize static stiffness to estimate the natural frequency of laminated composite (Treviso *et al.*, 2015). Classical laminate plate theory (CLPT) was used to evaluate the theoretical flexural modulus and fundamental natural frequency for all laminates as shown in Table (5.1) by using the mechanical properties for unidirectional glass and carbon fibers with and without nano- Al_2O_3 .

The flexural stiffness matrix and theoretical flexural modulus for each laminate can be calculated by using Eqs. (3.17) and (3.25) (Kaw, 2005).

Table (5.1) demonstrates the $[\mathbf{D}]$ matrix, theoretical flexural modulus E_b , and fundamental natural frequency ω_n for all laminated epoxy composites. The fundamental frequency is the smallest frequency for the structure; for the case of a cantilever beam, ω_n can be calculated from Eq. (3.83) (Reddy, 2003).

The results in Table (5.1) show that cross-laminate has a higher flexural modulus than quasi-laminate, similar to the results of (Utomo, Susilo and Raharja, 2017; Aydin *et al.*, 2022). C2WN and Q2WN laminates have maximum flexural modulus E_b in the cross and quasi groups, respectively. Despite the presence of two glass layers on the exterior of both laminates, it is in contrast with the results (Karthik *et al.*, 2016) because of the effect of elements Q11, Q12, and Q66 in the $[\mathbf{Q}_{ij}]$ matrix of the 90° glass layer. By adding 2 % nano Al_2O_3 , the natural frequency for all laminates slightly dropped despite the increase in flexural modulus, similar to the results of the research (Khashaba, 2016). The density of the composite increases with the addition of nano powder to its matrix. The maximum natural frequency had been obtained for C2 in the cross-group, while in the quasi-group, Q2 had the maximum natural frequency.

Table (5.1) Flexural stiffness matrix, theoretical flexural modulus E_b , and fundamental natural frequency ω_n .

Laminates	Flexural stiffness matrix [D] [Pa·m ³]	Theoretical flexural modulus, E_b [GPa]	Fundamental natural frequency, ω_n [Hz]
C1	$\begin{bmatrix} 21.2 & 1.56 & 0 \\ 1.56 & 25.6 & 0 \\ 0 & 0 & 2.78 \end{bmatrix}$	31.6	23.254
C1WN	$\begin{bmatrix} 22.46 & 2.01 & 0 \\ 2.01 & 27.05 & 0 \\ 0 & 0 & 2.94 \end{bmatrix}$	33.5	22.75
C2	$\begin{bmatrix} 22.43 & 1.81 & 0 \\ 1.81 & 12.95 & 0 \\ 0 & 0 & 2.83 \end{bmatrix}$	33.3	23.78
C2WN	$\begin{bmatrix} 23.79 & 2.33 & 0 \\ 2.33 & 13.71 & 0 \\ 0 & 0 & 2.98 \end{bmatrix}$	35.1	23.29
Q1	$\begin{bmatrix} 16.21 & 3.21 & 1.65 \\ 3.21 & 27.26 & 1.65 \\ 1.65 & 1.65 & 4.43 \end{bmatrix}$	23.0	19.78
Q1WN	$\begin{bmatrix} 17.24 & 3.74 & 1.75 \\ 3.74 & 28.83 & 1.75 \\ 1.75 & 1.75 & 4.66 \end{bmatrix}$	24.4	19.42
Q2	$\begin{bmatrix} 17.7 & 3.62 & 1.46 \\ 3.62 & 14.07 & 1.46 \\ 1.46 & 1.46 & 4.64 \end{bmatrix}$	24.75	20.52
Q2WN	$\begin{bmatrix} 18.8 & 4.23 & 1.55 \\ 4.23 & 14.91 & 1.55 \\ 1.55 & 1.55 & 4.88 \end{bmatrix}$	26.0	20.05

Due to FRPC beam free vibration, the dynamic behavior of the glass/carbon epoxy laminated composite can be found in terms of the time domain (displacement-time envelope) and frequency domain (acceleration-frequency envelope). The original aspect is that the frequency response is neither represented in terms of input impulsive force with respect to frequency nor within output acceleration with respect to frequency; the new representation

was in terms of output over input (acceleration/impulsive force) in the y-axis against the frequency in the x-axis, as shown in Figure (5.25). The red cursor position in Figure (5.25) represents the resonant frequency, for the range of frequency is between 0 Hz and 30 Hz, as represented by the critical frequency for the laminates and not necessarily the maximum frequency. If the laminate is subjected to force with an excited frequency equal to this resonance frequency, then the amplitude of the vibration pulse will be magnified and cause failure and the presence of a crack in the same laminate. The dynamic responses of all laminates are illustrated in Figure (5.26) in terms of the time domain. The number of peaks for cross- and quasi-group vibration response to a 400 ms time are 5 and 4 peaks respectively; this is due to the increase of natural frequency of cross-group in comparison with quasi-group as shown in Tables (5.1) and Figure (5.33), similar to the results of studies (Singh, Jain and Bhaskar, 2020; Aydin *et al.*, 2022). The maximum natural frequency for the laminate C2 is equal to 23.5 Hz in the cross group. On the other hand, the maximum one in the quasi group is for the laminate Q2 and equal to 20.25 Hz as shown in Figure (5.33a) because the flexural modulus of the arrangement of GGCCCCGG organized by two glass plies at the outer surface is higher than that of the arrangement GCCGGCCG as shown in Table (5.1) which is different from the results of studies (Utomo, Susilo and Raharja, 2017; Pujar, Nanjundaradhya and Sharma, 2022). The elements Q11, Q12, and Q66 of $[Q_{ij}]$ matrix for 90° glass fiber are higher than that for 90° carbon. Therefore, the presence of 90° glass as a second layer in the laminate leads to an increase in the first element of $[D]$ matrix and then the flexural modulus. By adding 2% nano Al₂O₃ to all laminated composites, the amplitude of the vibration response decreased in comparison with the original state as shown in Figure (5.26). This is due to the increase of the damping ratio for the nanoparticle addition case in comparison with the non-addition case, similar to the results of researches (Pol *et al.*, 2013; Karthik *et al.*, 2016; Khashaba, 2016; Utomo, Susilo and Raharja,

2017; Pujar, Nanjundaradhya and Sharma, 2018; Bulut, Erkliđ and Kanmaz, 2019; SenthamaraiKannan and Ramesh, 2019; Zhang *et al.*, 2021) as shown in Figure (5.27 b). This occurs because of the increase of the interfacial regions in the composite leading to more energy dissipation by friction (heat) (Treviso *et al.*, 2015; Tang and Yan, 2020). Despite the amplitude of the dynamic response for C2, C2WN, Q2, and Q2WN being lower than the amplitude for C1, C1WN, Q1, and Q1WN, respectively, as shown in Figure (5.26), the damping ratio of C2 is lower than the damping ratio of C1 by 24.2 %, and the damping ratio of C2WN is lower than the damping ratio of C1WN by 8 %. Its behavior is because the ratio of the maximum peak amplitude to the minimum peak amplitude is higher for C1 and C1WN than that for C2 and C2WN, respectively as shown in Figure (5.26). The reverse situation for the quasi group, where the damping ratio for Q2 is higher than the damping ratio of Q1 by 5.62 % and the damping ratio for Q2WN is higher than the damping ratio of Q1WN by 6.64 % is because the ratio of the maximum peak amplitude to the minimum peak amplitude is higher for Q2 and Q2WN than Q1 and Q1WN, respectively, as shown in Figure (5.26). The stacking sequence and angle of orientation have a major effect on the value of the bending modulus, natural frequency, and damping ratio. For a structural material system, it is necessary to make a balance between these properties alongside its strength. The configuration Q2 and Q2WN [G0/G90/C45/C-45]_s is specialized by increasing flexural modulus, natural frequency, and damping ratio simultaneously, in comparison with Q1 and Q1WN [G0/C90/C45/G-45]_s, respectively, as shown in Tables (5.1) and Figure (5.27).

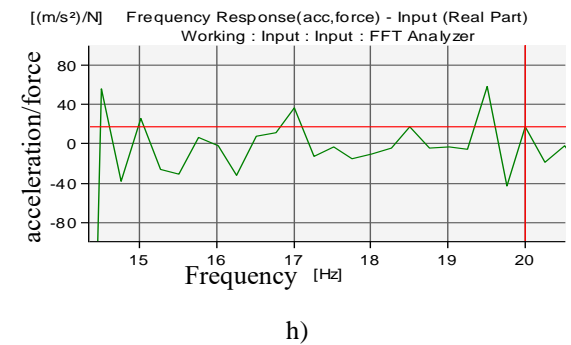
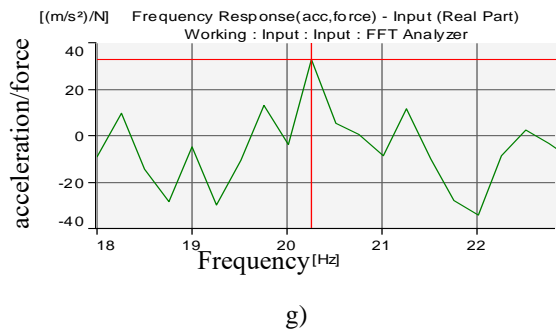
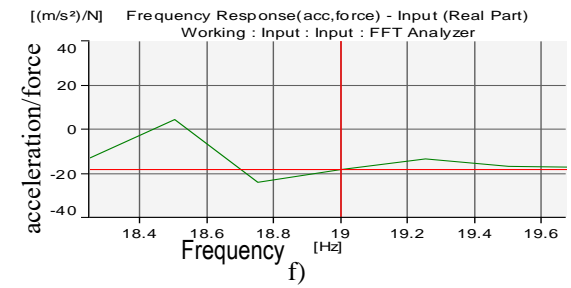
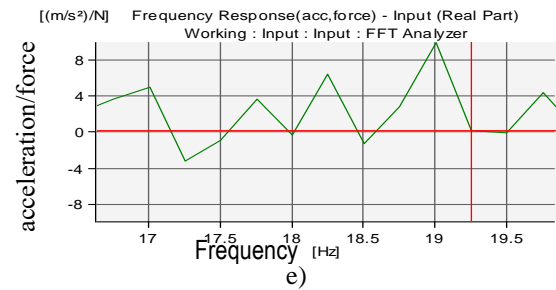
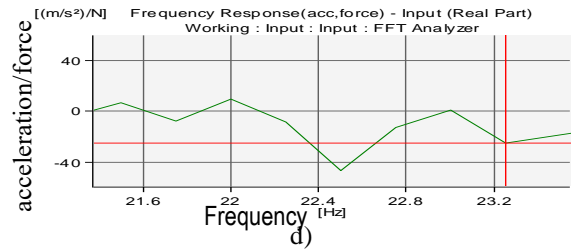
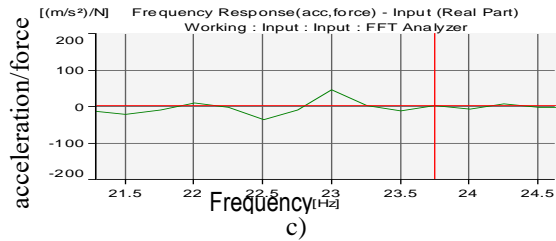
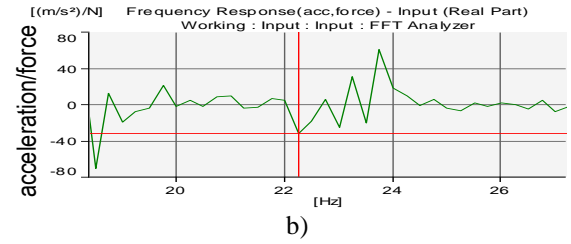
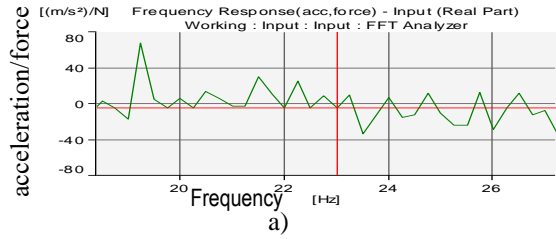


Figure (5.25) Frequency responses of laminated epoxy composites with and without nano Al_2O_3 : a) C1, b) C1WN, c) C2, d) C2WN, e) Q1, f) Q1WN, g) Q2, and h) Q2WN

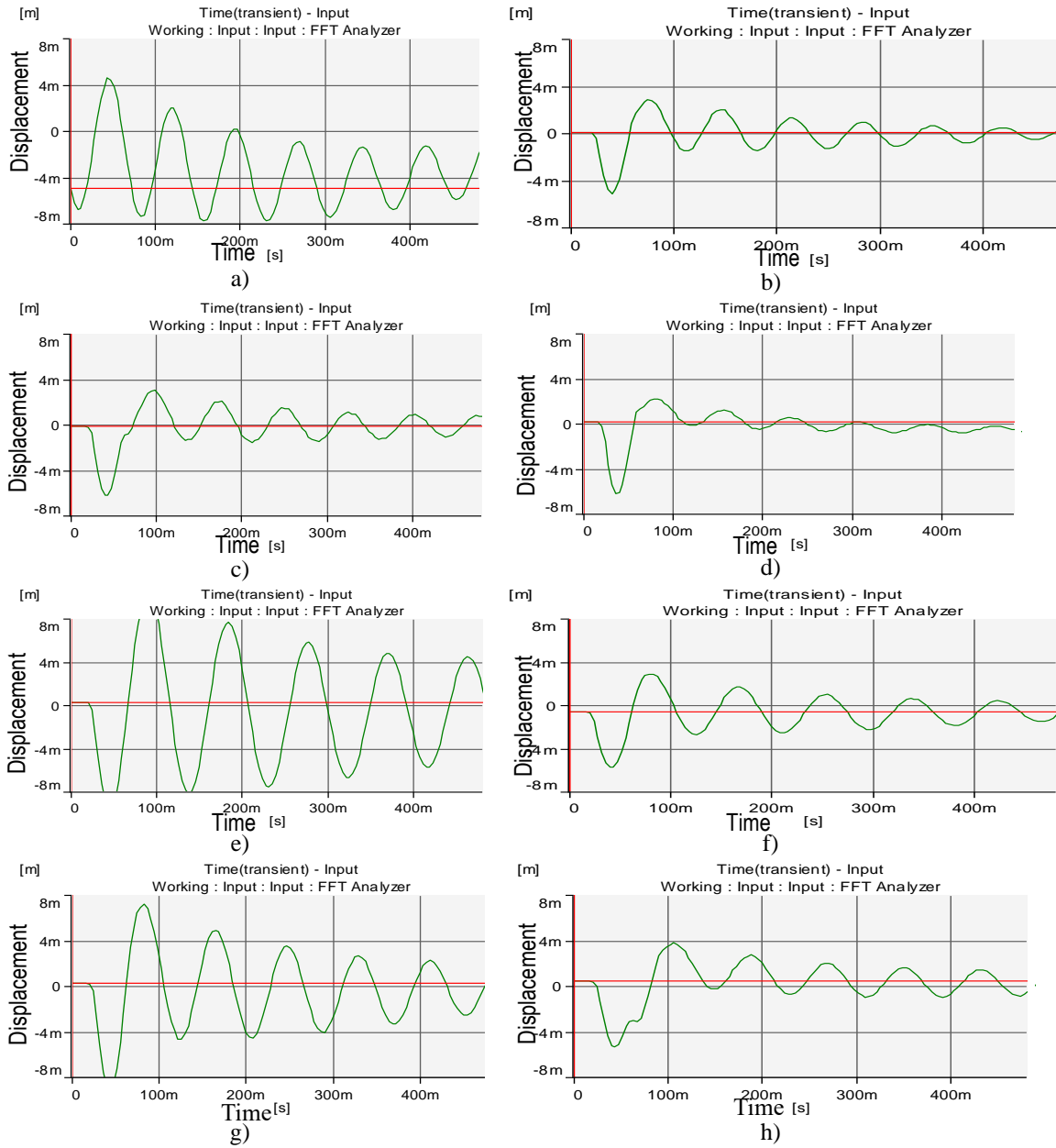


Figure (5.26) Vibration responses of laminated epoxy composites with and without nano Al_2O_3 : a) C1, b) C1WN, c) C2, d) C2WN, e) Q1, f) Q1WN, g) Q2, and h) Q2WN.

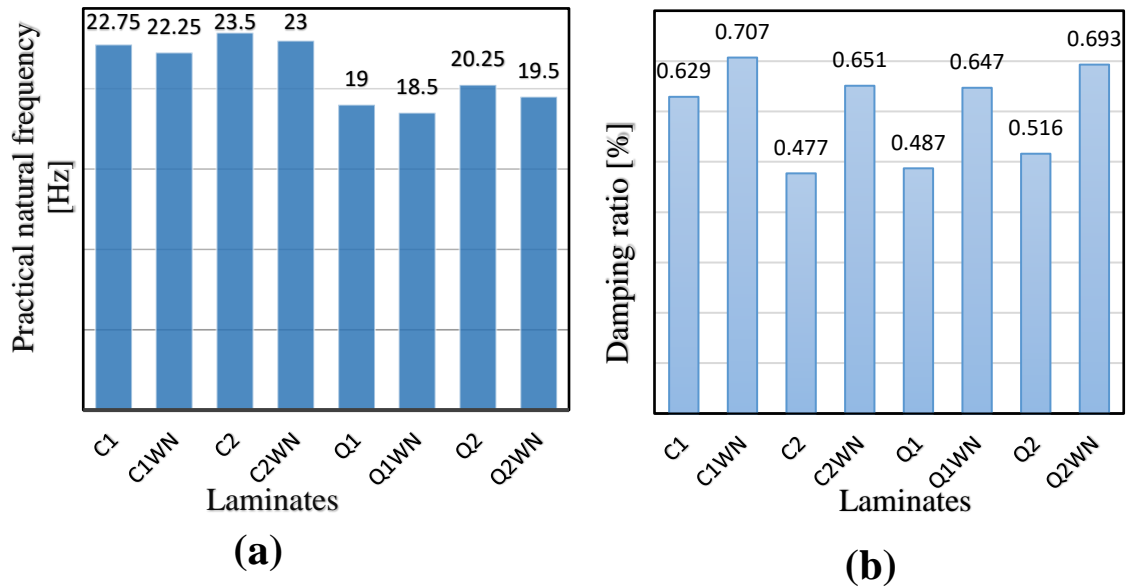
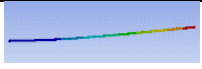
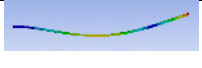

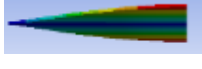
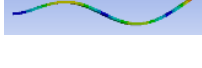



Figure (5.27) Dynamic Characteristics of FRPC with and without nano Al_2O_3 : (a) Natural Frequency, (b) Damping Ratio.

The first six natural frequencies with their mode's shapes are given in Table (5.2). It is obvious that all modes are bending modes, except mode 4 is torsional mode. Moreover, the maximum natural frequency for the 1st, 2nd, 3rd, 5th, and 6th modes existed in C2 laminate, while for the 4th mode, the maximum natural frequency existed in Q2, where in the laminates C2 and Q2 stacking sequence of G/G/C/C/C/C/G/G was utilized.

Finally, it is found that the analytical, practical, and numerical natural frequencies are very close to each other, as shown in Figure (5.28).

Table (5.2) The first six natural frequencies and their mode shapes for all laminates.

No	Mode shape	Natural frequency [Hz]							
		C1	C1WN	C2	C2WN	Q1	Q1WN	Q2	Q2WN
1		23.185	22.752	23.8	23.313	19.821	19.452	20.59	20.138
2		145.16	142.45	148.98	145.94	124.08	121.77	128.9	126.07
3		263.89	258.42	265.8	260.2	218.92	214.86	231.4	225.78
4		309.84	303.71	309.75	303.59	320.66	313.71	326	318.95
5		405.87	398.29	416.45	407.94	347.04	340.58	360.5	352.71
6		793.69	778.86	808.91	791.91	679.17	666.55	705.7	690.54

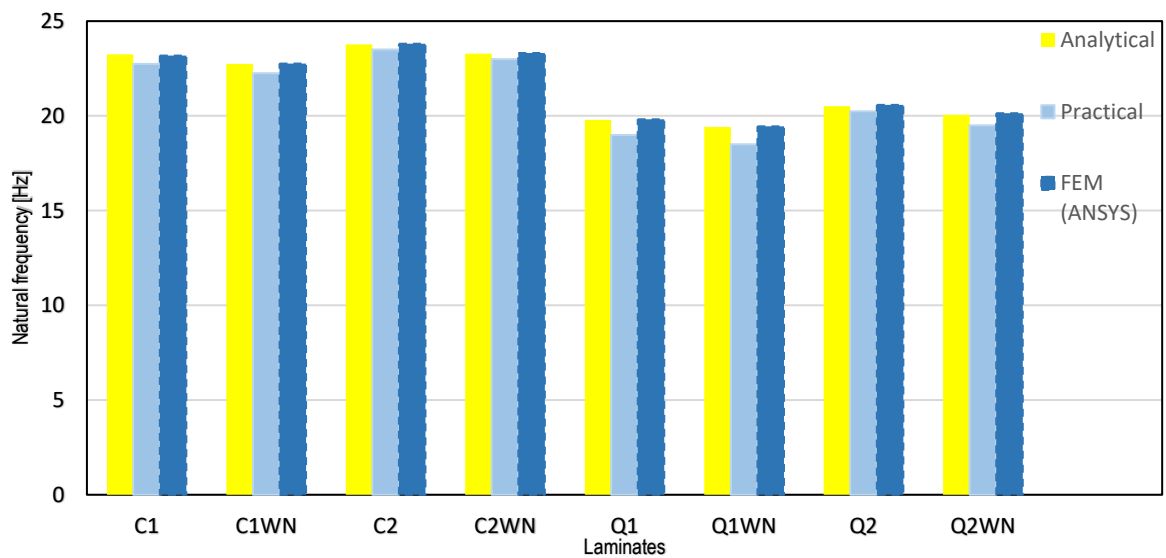


Figure (5.28) Natural frequencies comparison in analytical, practical, and numerical methods

5.8 Free vibration response of Sandwich SS304/FRPC/SS304

The flexural stiffness matrix and theoretical flexural modulus for each laminate can be calculated by using Eqs. (3.17), (3.25), and (3.70) (Kaw, 2005). Table (5.3) demonstrates the $[D]$ matrix, theoretical flexural modulus E_b , and fundamental natural frequency ω_n for all fiber metal laminates. The fundamental frequency is the smallest frequency for the structure; for the case of a cantilever beam, ω_n can be calculated from Eq. (3.83) (Reddy, 2003).

(Quasi/stainless steel 304 base) FML theoretical flexural modulus and fundamental natural frequency are lower than (Cross/stainless steel 304 base) FML one by 3%, and 1.4%, respectively. Because of the presence $\pm 45^\circ$ angles fiber plies in the first type of fiber metal laminate. The contribution of the two stainless steel metal skins (1mm thickness) in the flexural stiffness matrix $[D]$ is between 90%-97%. Theoretical Flexural modulus and natural frequency of all fiber metal laminates are not influenced by fiber stacking sequence. Theoretical flexural modulus of SS/C1/SS, SS/C1WN/SS, SS/C2/SS, SS/C2WN/SS, SS/Q1/SS, SS/Q1WN/SS, SS/Q2/SS, and SS/Q2WN/SS are higher than C1, C1WN, C2, C2WN, Q1, Q1WN, Q2 and Q2WN by 16%, 11%, 11%, 7%, 37%, 33%, 32%, and 29%, respectively. Because the elements of the flexural stiffness matrix are growing with the bonding of metal skins to the fiber-reinforced polymer composite core. Consequently, theoretical natural frequency of SS/C1/SS, SS/C1WN/SS, SS/C2/SS, SS/C2WN/SS, SS/Q1/SS, SS/Q1WN/SS, SS/Q2/SS, and SS/Q2WN/SS are higher than C1, C1WN, C2, C2WN, Q1, Q1WN, and Q2WN by 17.4%, 19%, 16%, 17%, 29%, 30%, 26%, and 27.4%, respectively.

The dynamic response of all (SS/FRPC/SS) fiber metal laminate in terms of frequency domain is shown in Figure (5.29). The y-axis represents the acceleration over impulsive force, while the x-axis represents the frequency. Time domain- dynamic response of all (SS/FRPC/SS) fiber metal laminate are

shown in Figure (5.30). The number of peaks for (Cross/stainless steel 304 base) FML and (Quasi/stainless steel 304 base) FML to a 400 ms time is between 18-19 peaks. The dynamic response amplitude of all fiber metal laminate decreased by adding 2% nano Al_2O_3 to all fiber reinforced polymer composite. Practical natural frequency of SS/C1/SS, SS/C1WN/SS, SS/C2/SS, SS/C2WN/SS, SS/Q1/SS, SS/Q1WN/SS, SS/Q2/SS, and SS/Q2WN/SS are lower than the theoretical by 13.2%, 14.2%, 11.2%, 12.5%, 23.5%, 24.3%, 21.1%, and 22.2%, respectively. This is due to the weak bonding between metal skin and fiber core and low stiffness.

Table (5.3) Flexural stiffness matrix, theoretical flexural modulus E_b , and fundamental natural frequency ω_n for all fiber metal laminate sandwich.

FML sandwich	Flexural stiffness matrix $[D]$ [Pa·m ³]	Theoretical flexural modulus, E_b [GPa]	Fundamental natural frequency, ω_n [Hz]
SS/C1/SS	$\begin{bmatrix} 212.4 & 53.2 & 0 \\ 53.2 & 217 & 0 \\ 0 & 0 & 72.6 \end{bmatrix}$	37.4	28.15
SS/C1WN/SS	$\begin{bmatrix} 214 & 54 & 0 \\ 54 & 218 & 0 \\ 0 & 0 & 73 \end{bmatrix}$	37.61	28
SS/C2/SS	$\begin{bmatrix} 214 & 53.5 & 0 \\ 53.5 & 204 & 0 \\ 0 & 0 & 72.6 \end{bmatrix}$	37.45	28.17
SS/C2WN/SS	$\begin{bmatrix} 215 & 54 & 0 \\ 54 & 205 & 0 \\ 0 & 0 & 72.8 \end{bmatrix}$	37.66	28.03
SS/Q1/SS	$\begin{bmatrix} 208 & 55 & 1.65 \\ 55 & 219 & 1.65 \\ 1.65 & 1.65 & 74.24 \end{bmatrix}$	36.32	27.74
SS/Q1WN/SS	$\begin{bmatrix} 209 & 55.4 & 1.75 \\ 55.4 & 220 & 1.75 \\ 1.75 & 1.75 & 74.5 \end{bmatrix}$	36.48	27.58
SS/Q2/SS	$\begin{bmatrix} 209 & 55.3 & 1.46 \\ 55.3 & 205 & 1.46 \\ 1.46 & 1.46 & 74.5 \end{bmatrix}$	36.39	27.77
SS/Q2WN/SS	$\begin{bmatrix} 210 & 56 & 1.55 \\ 56 & 206 & 1.55 \\ 1.55 & 1.55 & 75 \end{bmatrix}$	36.55	27.61

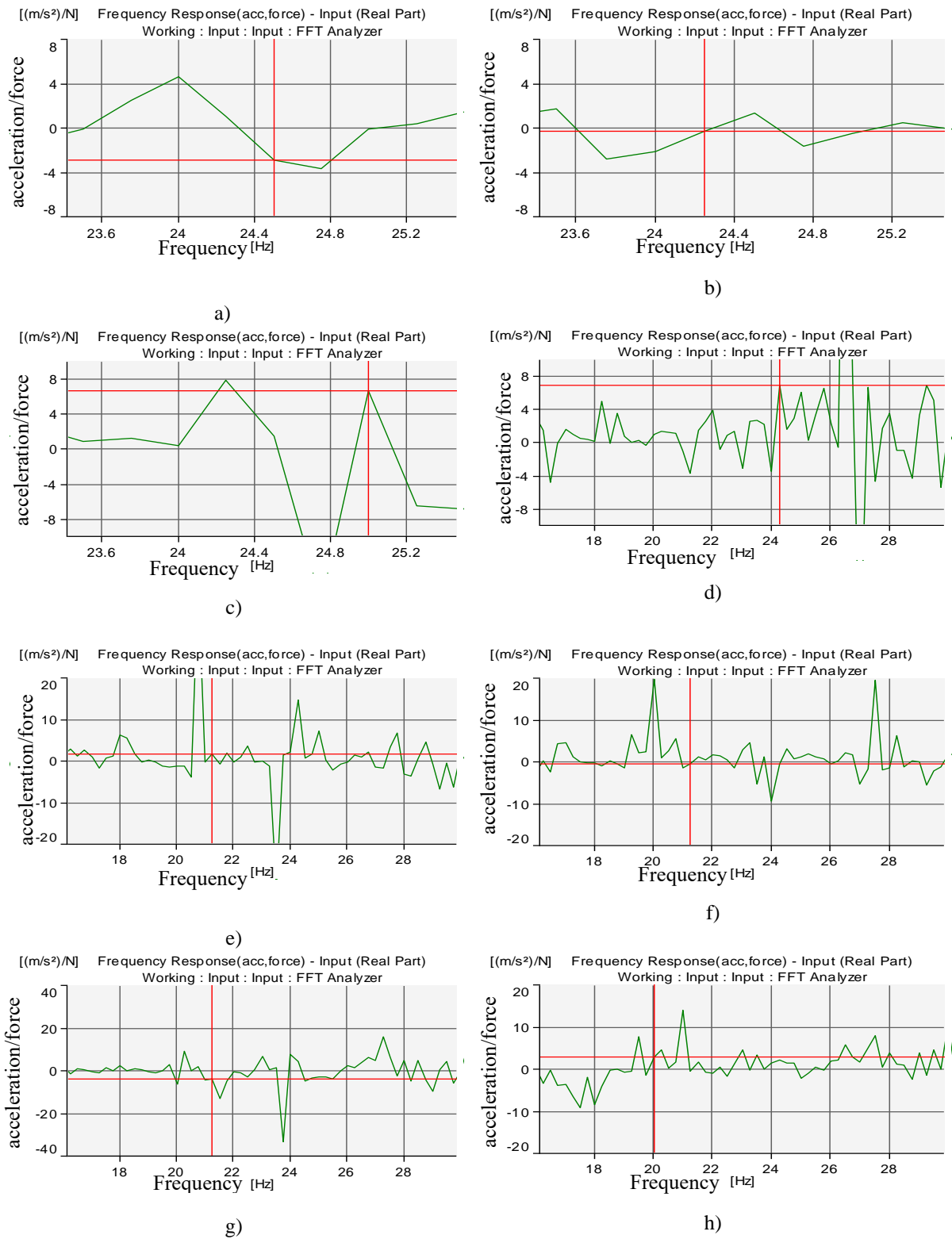


Figure (5.29) Frequency responses of fiber metal laminate sandwiches with and without nano Al_2O_3 : a) SS/C1/SS, b) SS/C1WN/SS, c) SS/C2/SS, d) SS/C2WN/SS, e) SS/Q1/SS, f) SS/Q1WN/SS, g) SS/Q2/SS, and h) SS/Q2WN/SS.

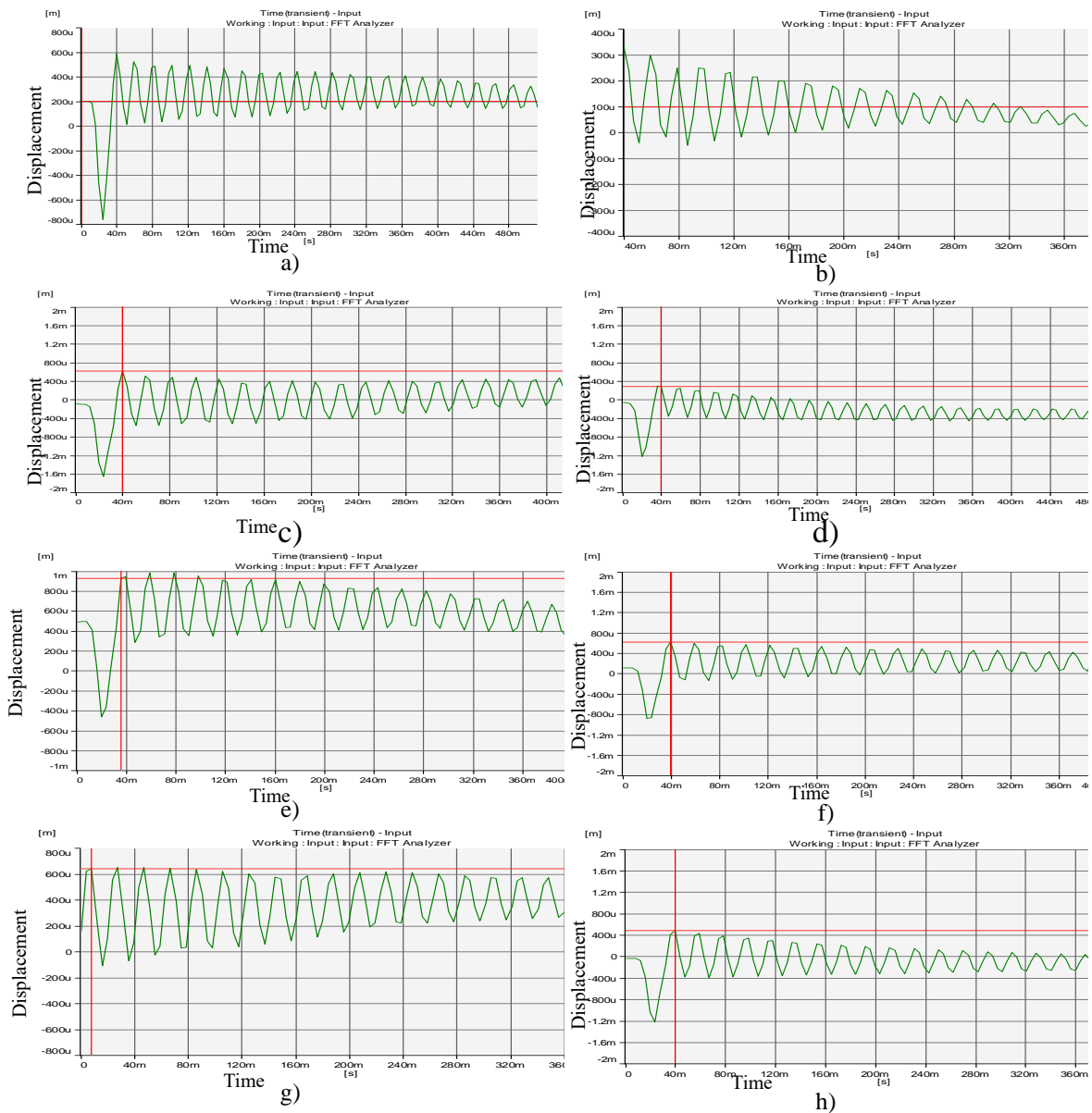
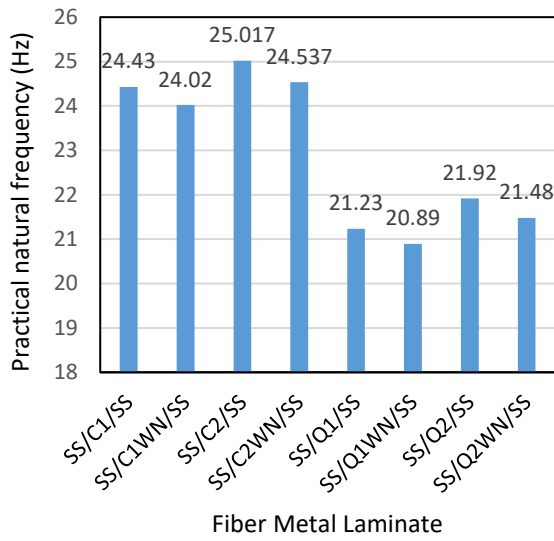
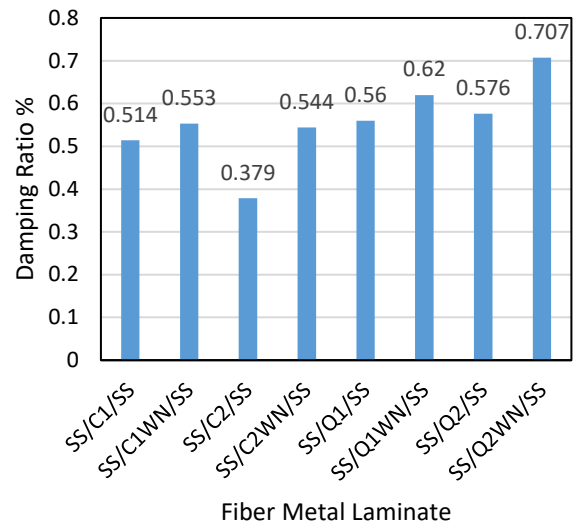


Figure (5.30) Vibration responses of Fiber metal laminate with and without nano Al_2O_3 : a) SS/C1/SS, b) SS/C1WN/SS, c) SS/C2/SS, d) SS/C2WN/SS, e) SS/Q1/SS, f) SS/Q1WN/SS, g) SS/Q2/SS, and h) SS/Q2WN/SS.

The damping ratio of SS/C2/SS and SS/C2WN/SS is lower than the damping ratio of SS/C1/SS and SS/C1WN/SS by 26% and 2%, respectively as shown in Figure (5.31b). The ratio of the maximum peak amplitude to the minimum peak amplitude is higher for SS/C1/SS and SS/C1WN/SS than that for SS/C2/SS and SS/C2WN/SS, respectively as shown in Figure (5.30). Opposite status for (quasi/stainless steel 304 base) fiber metal laminate, where the damping ratio of SS/Q2/SS and SS/Q2WN/SS is higher than the damping ratio of SS/Q1/SS and SS/Q1WN/SS by 3% and 12.3%, respectively as shown in Figure (5.31b). The ratio of the maximum peak amplitude to the minimum peak amplitude is higher for SS/Q2/SS and SS/Q2WN/SS than that for SS/Q1/SS and SS/Q1WN/SS, respectively as shown in Figure (5.30). The first six natural frequency and their mode shapes are shown in Table (5.4). All the first six natural frequencies for all fiber metal laminate are approximately equal because the contribution of metal layer skin in FML is higher than 90% in comparison with FRPC core. Analytical and FEM (ANSYS) natural frequencies are equaled and higher than the experimental natural frequency of all fiber metal laminate as shown in Figure (5.32) because weak bonding between the FRPC core and metal layer skin leads to lower stiffness of the FML sandwich.



(a)



(b)

Figure (5.31) Dynamic Characteristics of FML with and without nano Al_2O_3 :
(a) Natural Frequency, (b) Damping Ratio.

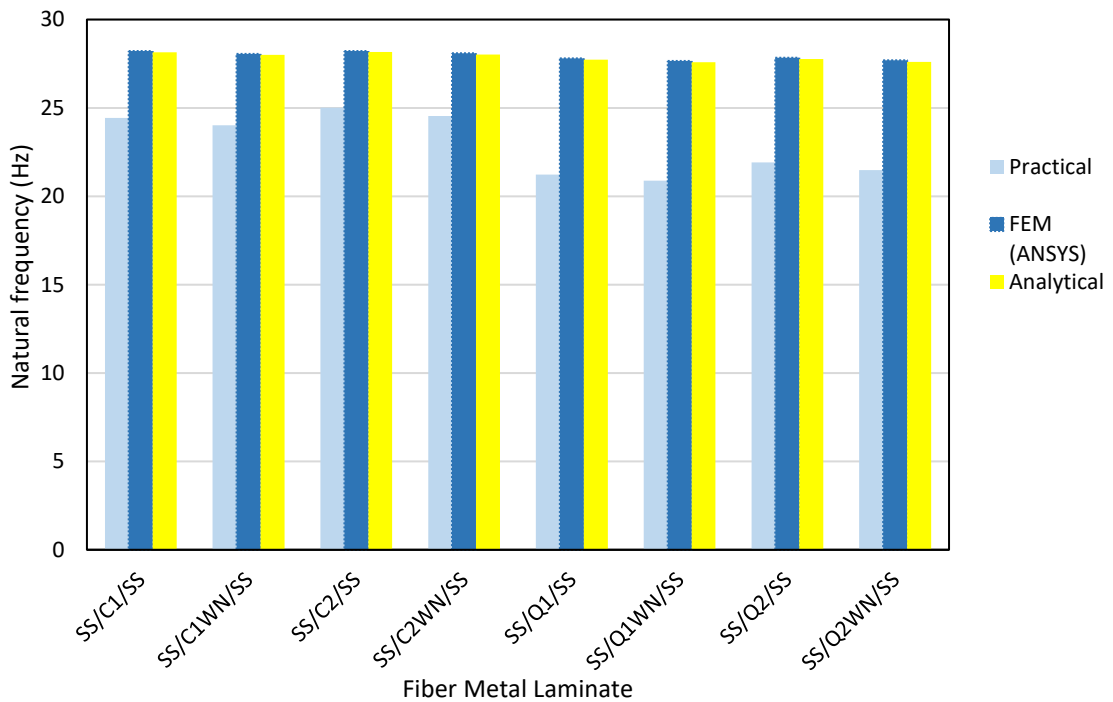
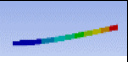
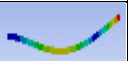
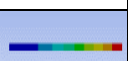
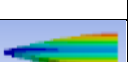

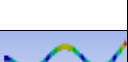


Figure (5.32) Analytical, practical, and numerical natural frequencies comparison.

Table (5.4) The first six natural frequencies and their mode shapes.

No	Mode shape	Natural frequency [Hz]							
		SS/C1/SS	SS/C1WN/SS	SS/C2/SS	SS/C2WN/SS	SS/Q1/SS	SS/Q1WN/SS	SS/Q2/SS	SS/Q2WN/SS
1		28.214	28.06	28.225	28.09	27.801	27.65	27.84	27.69
2		176.17	175.21	176.24	175.41	174	173	174	173
3		175.85	175.07	174.1	175.04	152	152	154	154
4		476.88	475.02	477	475	480	479	481	480
5		490.6	488.09	490.81	488.6	484	481	484.4	482
6		954	949	954	950	941	936	942.3	938

5.9 Factors Affecting the Maximum Deflection and Fundamental Natural Frequency of Metal, FRPC, and FML Sandwich Plates.

Many factors impact the deflection and natural frequency of isotropic and laminated simply supported plates. Material stiffness is inversely proportional to deflection and directly proportional to natural frequency.

5.9.1 Metal

5.9.1.1 Plate Thickness

Stainless steel 304 square plate with length (a) and width (b) of 300 mm, and different thicknesses (h) of 1 mm, 2 mm, 3 mm, and 4 mm are used. The maximum deflection of the simply supported plates due to uniformly distributed pressure (q_0) equal to 2.222×10^{-4} MPa, and the fundamental natural frequency due to its free vibration are shown in Figure (5.33).

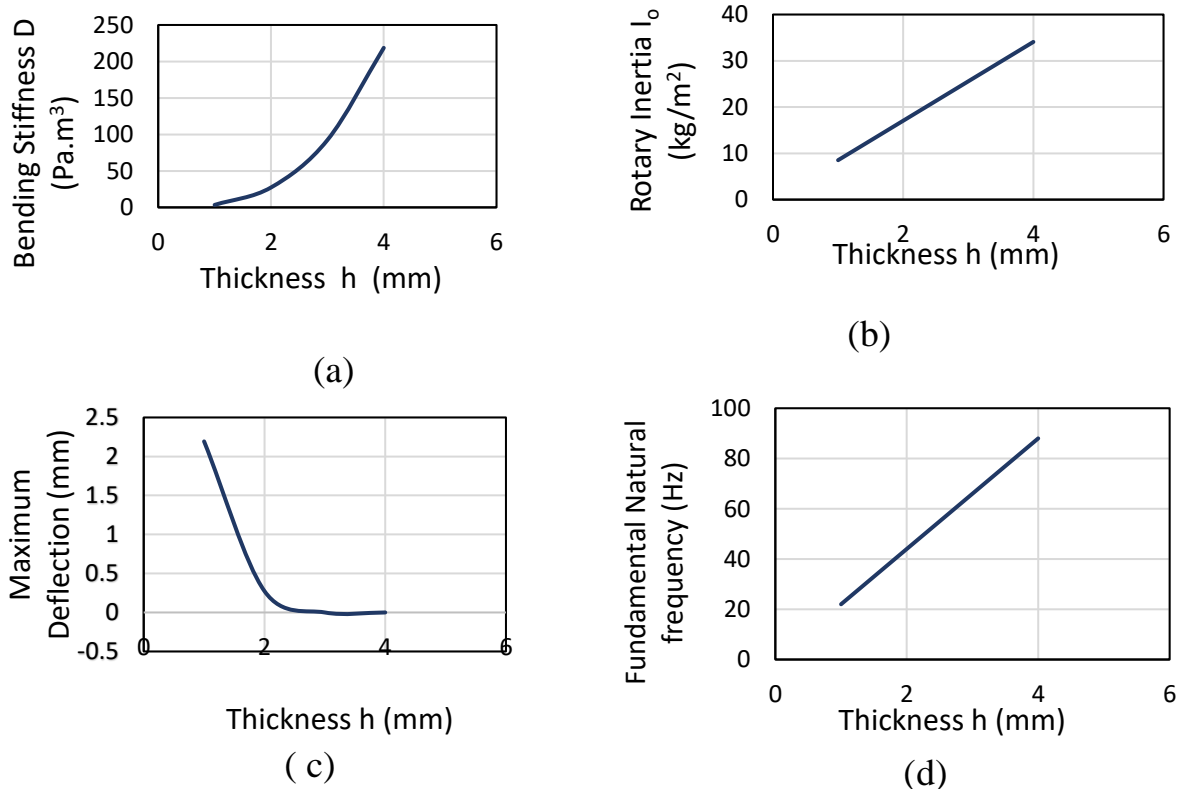


Figure (5.33) Effect of stainless steel 304 plate thickness change on the (a) bending stiffness, (b) rotary inertia, (c) maximum deflection, and (d) fundamental natural frequency.

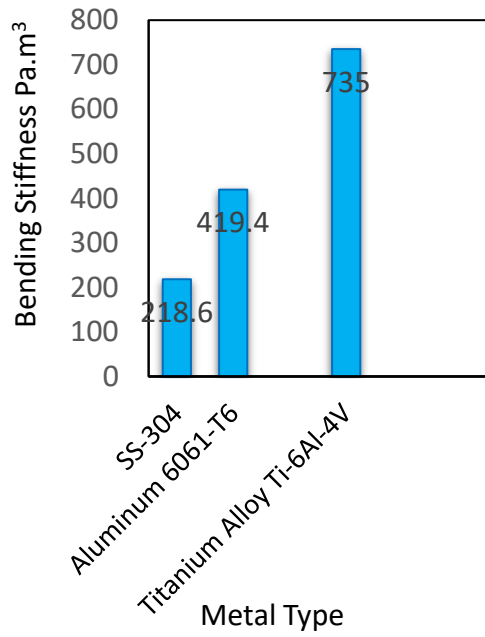
Bending stiffness D and rotary inertia I_o are related directly to the plate thickness as shown in Figure (5.33-a) and Figure (5.33-b), respectively. The ratio of bending stiffness to the rotary inertia is also increased with increasing plate thickness.

As a result, the deflection is decreased with increasing plate thickness similar to Vanam, Rajyalakshmi and Inala, (2012) as shown in Figure (5.33-c), since it has an inverse relationship with both the increased moment of inertia and the bending stiffness. On the other hand, the fundamental natural frequency is increased with increasing plate thickness as shown in Figure (5.33-d). Since the moment of inertia increased and it is directly correlated with the ratio of bending stiffness to rotary inertia.

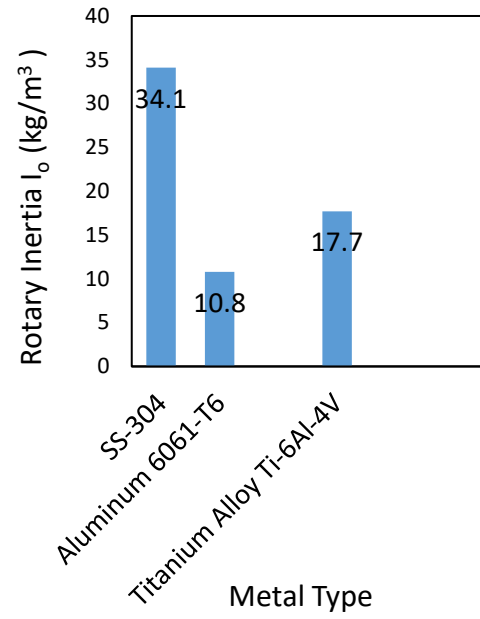
5.9.1.2 Metal Type

Three types of metal are selected because of their many uses in structural applications which are stainless steel 304, aluminum 6061-T6, and Titanium alloy Ti-6Al-4V, where their mechanical properties are shown in Table (4.4) and Table (3.1), respectively (Hibbeler, 2012).

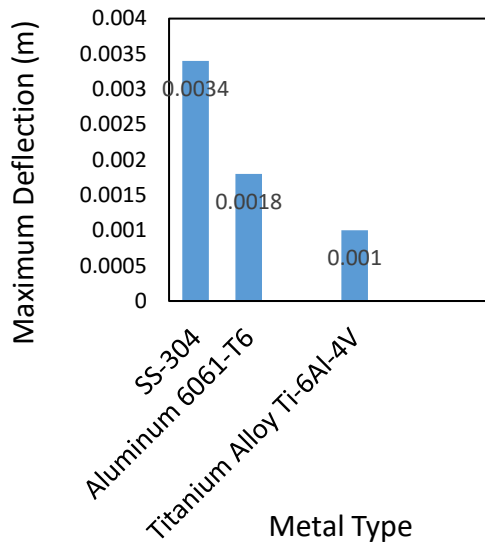
The maximum deflection of the square metal plates ($a= b=300$ mm), and thickness $h=4$ mm, due to uniform distributed pressure (q_o) equal to 2.222×10^{-4} MPa, and the fundamental natural frequency due to its free vibration are shown in Figure (5.34).



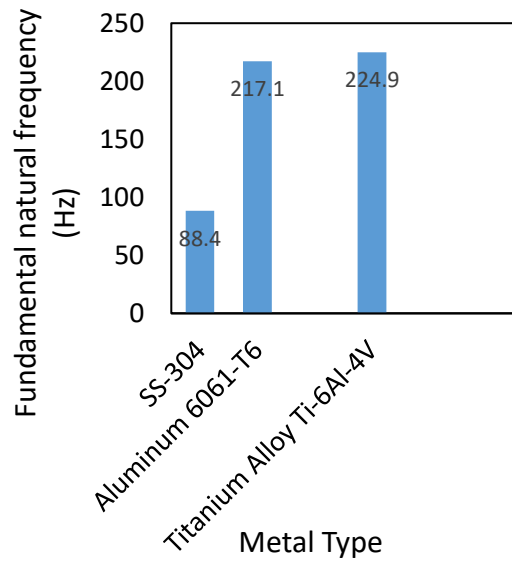
(a)



(b)



(c)



(d)

Figure (5.34) Effect of metal type on the (a) bending stiffness, (b) rotary inertia, (c) maximum deflection, and (d) fundamental natural frequency.

It is obvious from Figure (5.34-a) that the bending stiffness of titanium alloy is higher than stainless steel and aluminum by 70% and 43%, respectively. since it has a higher young modulus than stainless steel and aluminum, which indicates that it is more resistant to elastic deformation.

Consequently, the maximum deflection of titanium alloy is lower than stainless steel and aluminum by 70% and 44% respectively, as shown in Figure (5.34-c).

It is clear from Figure (5.34-b) that the rotary inertia of stainless steel is higher than that of aluminum and titanium by 68% and 48% respectively due to its highest density among the two others. However, the fundamental natural frequency of titanium is higher than that of stainless steel and aluminum by 61% and 4%, respectively as shown in Figure (5.34-d). Despite having a lower mass than aluminum and stainless steel, it has a higher young modulus.

5.9.2 Fiber Reinforced Polymer Composite

Many factors influence the deflection and natural frequency of simply supported fiber-reinforced polymer laminated composite plate.

5.9.2.1 Stacking Sequence and Angle of Orientation

Four different stacking sequences and angle of orientations of (Carbon: Glass) /epoxy laminated composite simply supported square plate are selected. Both length (a) and width (b) are equal to 300 mm, with thickness (h) equal to 2 mm, as shown in Table (3.2).

The maximum deflection of the plates due to uniform distributed pressure (q_0) equal to 2.222×10^{-4} MPa, and the fundamental natural frequency due to its free vibration are shown in Figure (5.35).

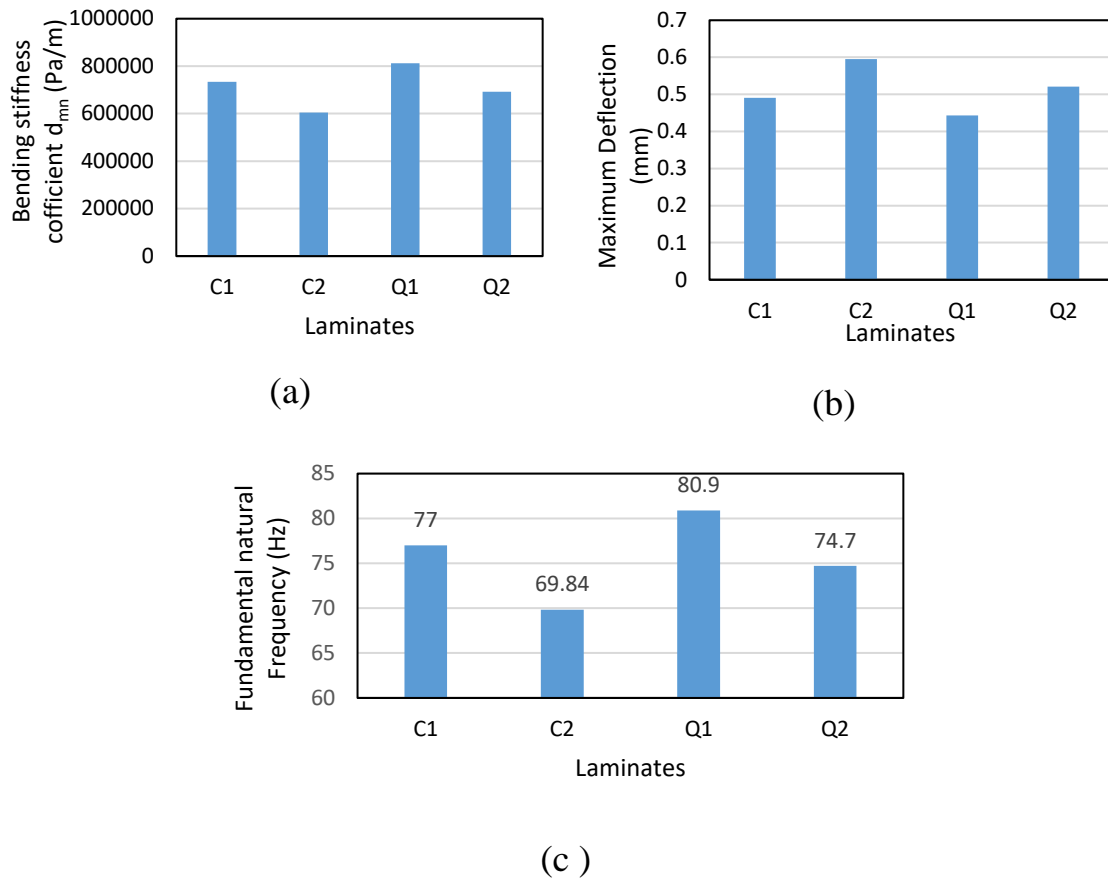


Figure (5.35) Effect of stacking sequence and angle of orientation on the (a) bending stiffness coefficient, (b) maximum deflection, and (c) fundamental natural frequency of FRPC plate.

It is conspicuous from Figure (5.35-a) that the bending stiffness coefficient d_{mn} for Q1 laminate is higher than C1, C2, and Q2 laminates by 10%, 26%, and 15%, respectively because Q1 laminate has a higher bending stiffness element D22 value than C1, C2, and Q2, respectively. Consequently, the maximum deflection of Q1 laminate is lower than C1, C2, and Q2 laminates by 10%, 26%, and 15% respectively, as shown in Figure (5.35-b) since the young modulus in the y-direction determine the D22 value. Also, the fundamental natural frequency of Q1 laminate is higher than C1, C2, and Q2 laminates by 5%, 14%, and 8%, respectively, as shown in Figure (5.35-c), because Q1 laminate has a higher young modulus in the y-direction than the other laminate. Rotary inertia is constant for all laminates because they include 4 plies of glass and 4 plies of carbon simultaneously.

5.9.2.2 Nano Al₂O₃ Addition

Two percent of nano Al₂O₃ is added to the epoxy matrix of C1, C2, Q1, and Q2 fiber laminated composite to construct C1WN, C2WN, Q1WN, and Q2WN fiber laminated composite.

The maximum deflection for the new four hybrid conditions of the square fiber laminated plates ($a = b = 300$ mm), and thickness $h = 2$ mm, due to uniform distributed pressure (q_0) equal to 2.222×10^{-4} MPa, and the fundamental natural frequency are Figure (5.36).

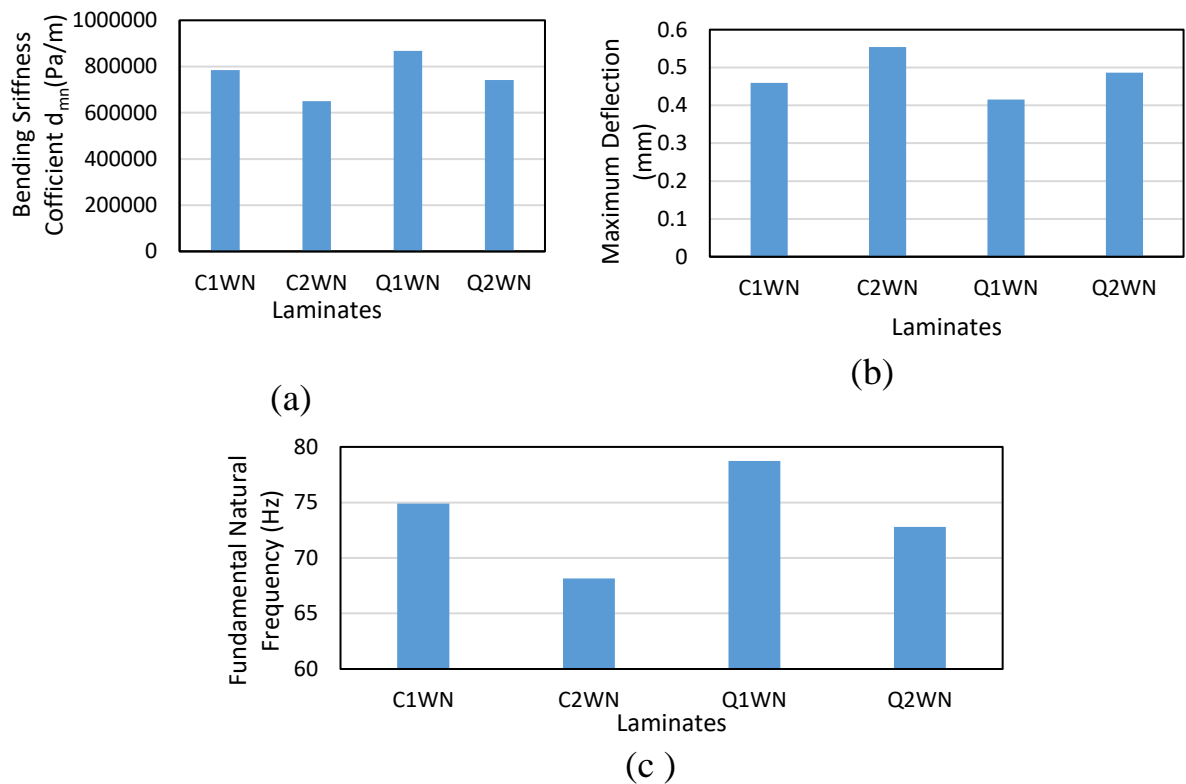


Figure (5.36) Effect of nano Al₂O₃ addition on the (a) bending stiffness coefficient, (b) maximum deflection, and (c) fundamental natural frequency of FRPNC plate.

It is evident from Figure (5.36-a) that the bending stiffness coefficient d_{mn} for Q1WN laminate is higher than C1WN, C2WN, and Q2WN laminates by 10%, 25%, and 15%, respectively because Q1 laminate has a higher bending

stiffness element D22 value than C1, C2, and Q2, respectively. Consequently, the maximum deflection of Q1WN laminate is lower than C1WN, C2WN, and Q2WN laminates by 10%, 25%, and 15% respectively, as shown in Figure (5.36-b) since the young modulus in the y-direction determines the D22 value. Also, the fundamental natural frequency of Q1WN laminate is higher than C1WN, C2WN, and Q2WN laminates by 5%, 14%, and 8%, respectively, as shown in Figure (5.36-c), because the young modulus of the materials with 2% nano Al_2O_3 in the y-direction for Q1 laminate is higher than the other laminate.

The maximum deflection and fundamental natural frequency for C1WN, C2WN, Q1WN, and Q2WN laminated composite is reduced by 7% and 3% in comparison with C1, C2, Q1, and Q2. For the nano-addition laminates, the bending stiffness coefficient d_{mn} is 7% higher than in the case of the non-addition laminates. Since the non-addition case has a lower young modulus than the nano-addition case in the y-direction. The resistance of the material to deformation increased. Rotary inertia for C1WN, C2WN, Q1WN, and Q2WN is increased by 12% compared with C1, C2, Q1, and Q2 because the density of the material matrix increased.

5.9.2.3 Aspect Ratio

The ratio of plate length (a) to its width (b) is called aspect ratio. Five different aspect ratios (1, 1.5, 2, 2.5, and 3) are selected to clarify the effect of increasing the length versus decreasing the width of the plate on the deflection and natural frequency. The thickness of the laminated plate at all conditions is equal to 2 mm.

The maximum deflection of the fiber laminated composite plates C1, C2, Q1, and Q2 with aspect ratios equal to (1, 1.5, 2, 2.5, and 3) due to uniform distributed pressure (q_0) equal to 2.222×10^{-4} MPa, 3.333×10^{-4} MPa, 4.444×10^{-4} MPa, 5.556×10^{-4} MPa, and 6.667×10^{-4} MPa respectively, and the fundamental natural frequency due to its free vibration are shown in Figure (5.37).

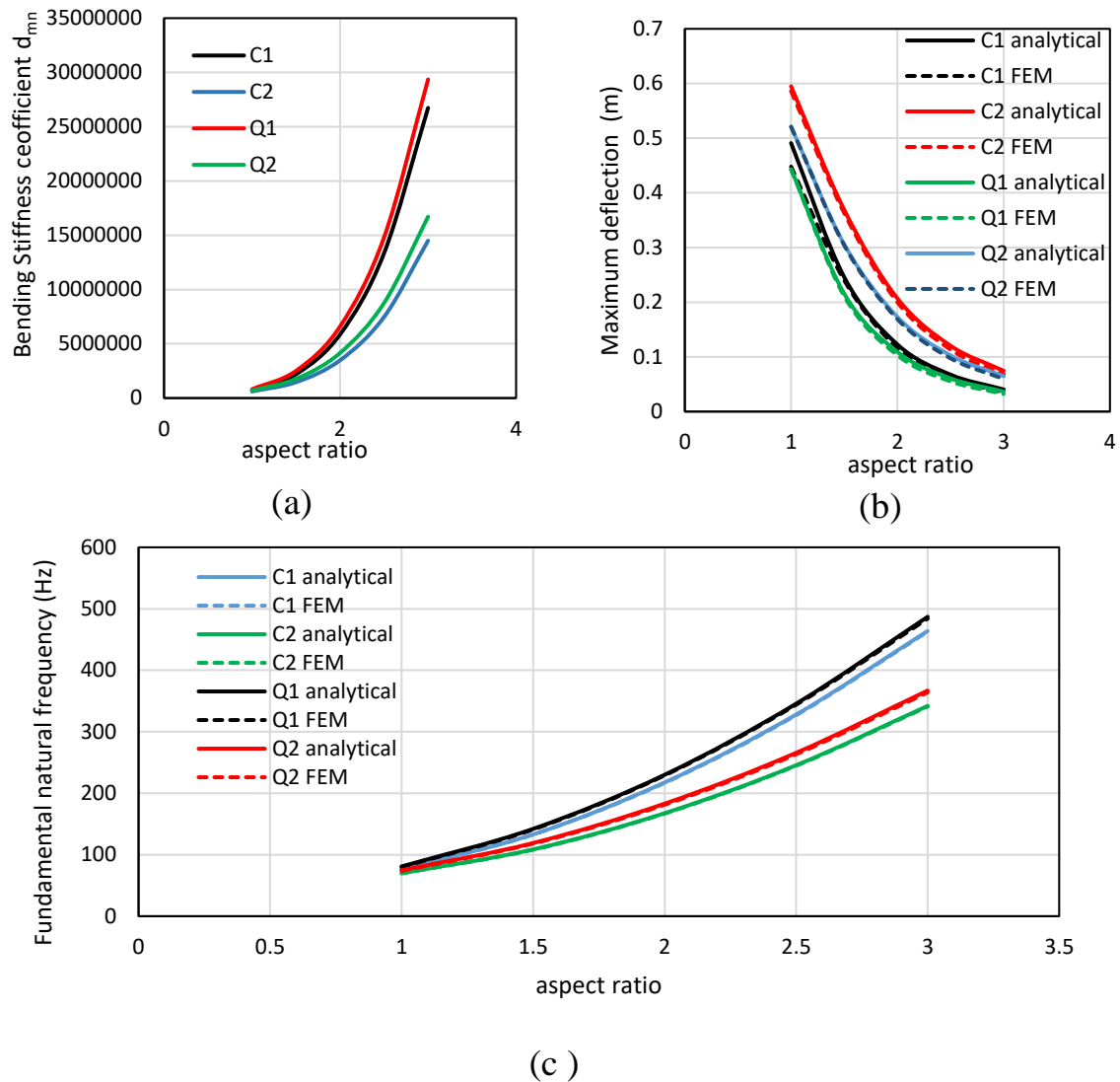


Figure (5.37) Effect of aspect ratio on (a) the bending stiffness coefficient, (b) the maximum deflection, and (c) the fundamental natural frequency of C1, C2, Q1, and Q2 fiber reinforced epoxy composite plates.

It is obvious from Figure (5.37-a) that for an aspect ratio equal to 1, the bending stiffness coefficient d_{mn} of Q1 laminate is higher than C1, C2, and Q2 laminates by 10%, 26%, and 15%, respectively. For an aspect ratio equal to 1.5, the bending stiffness coefficient d_{mn} of Q1 laminate is higher than C1, C2, and Q2 laminates by 12%, 42%, and 30%, respectively. For an aspect ratio equal to 2, the bending stiffness coefficient d_{mn} of Q1 laminate is higher than C1, C2,

and Q2 laminates by 11%, 47%, and 37%, respectively. For an aspect ratio equal to 2.5, the bending stiffness coefficient d_{mn} for Q1 laminate is higher than C1, C2, and Q2 laminates by 10%, 50%, and 41%, respectively. For an aspect ratio equal to 3, the bending stiffness coefficient d_{mn} for Q1 laminate is higher than C1, C2, and Q2 laminates by 9%, 51%, and 43%, respectively. Considering that the Q1 laminate composite has a higher D22 bending stiffness element value than the other laminates. Also, as the aspect ratio increased, D22's contribution increased as well, increasing the modulus of elasticity in the y-direction. Consequently, for an aspect ratio equal to 1, the maximum deflection of Q1 laminate is lower than C1, C2, and Q2 laminates by 10%, 26%, and 15% respectively. For an aspect ratio equal to 1.5, the maximum deflection of Q1 laminate is lower than C1, C2, and Q2 laminates by 12%, 42%, and 30%, respectively. For an aspect ratio equal to 2, the maximum deflection of Q1 laminate is lower than C1, C2, and Q2 laminates by 11%, 47%, and 37% respectively. For an aspect ratio equal to 2.5, the maximum deflection of Q1 laminate is lower than C1, C2, and Q2 laminates by 10%, 50%, and 41% respectively. For an aspect ratio equal to 3, the maximum deflection of Q1 laminate is lower than C1, C2, and Q2 laminates by 9%, 51%, and 43% respectively as shown in Figure (5.37-b). The modulus of elasticity in the y-direction increased as the contribution of D22 increased with increasing aspect ratio similar to (El-Helloty and Salam, 2009; Reddy *et al.*, 2012).

For an aspect ratio equal to 1, the fundamental natural frequency of Q1 laminate is higher than C1, C2, and Q2 laminates by 5%, 14%, and 8%, respectively. For aspect ratio equal to 1.5, the fundamental natural frequency of Q1 laminate is higher than C1, C2, and Q2 laminates by 6%, 23%, and 16%, respectively. For aspect ratio equal to 2, the fundamental natural frequency of Q1 laminate is higher than C1, C2, and Q2 laminates by 5%, 27%, and 21%, respectively. For aspect ratio equal to 2.5, the fundamental natural frequency of Q1 laminate is higher than C1, C2, and Q2 laminates by 5%, 30%, and 23%,

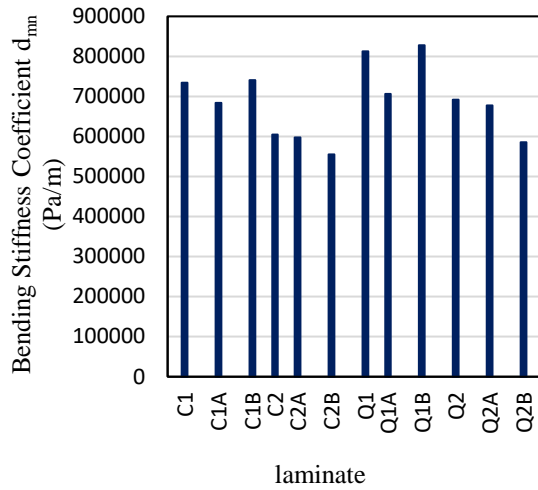
respectively. For aspect ratio equal to 3, the fundamental natural frequency of Q1 laminate is higher than C1, C2, and Q2 laminates by 5%, 30%, and 25%, respectively as shown in and Figure (5.37-c). The mass of the plate reduced as the aspect ratio rose because the surface area shrank.

5.9.2.4 Hybrid Ratio

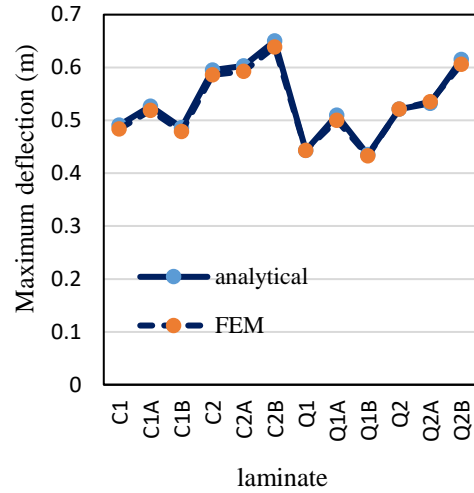
Hybrid ratio change for C1, C2, Q1, and Q2 as well as the position of carbon ply in laminate as shown in Table (3.3) is affected on the deflection and fundamental natural frequency of laminated composite.

The maximum deflection of the square fiber laminated plates C1, C2, Q1, and Q2 ($a = b = 300$ mm), and thickness $h = 2$ mm, with hybrid ratios (G: C) equal to (4:4, 6:2 and 2:6) due to uniform distributed pressure (q_0) equal to 2.222×10^{-4} MPa and the fundamental natural frequency due to its free vibration are shown in Figure (5.38).

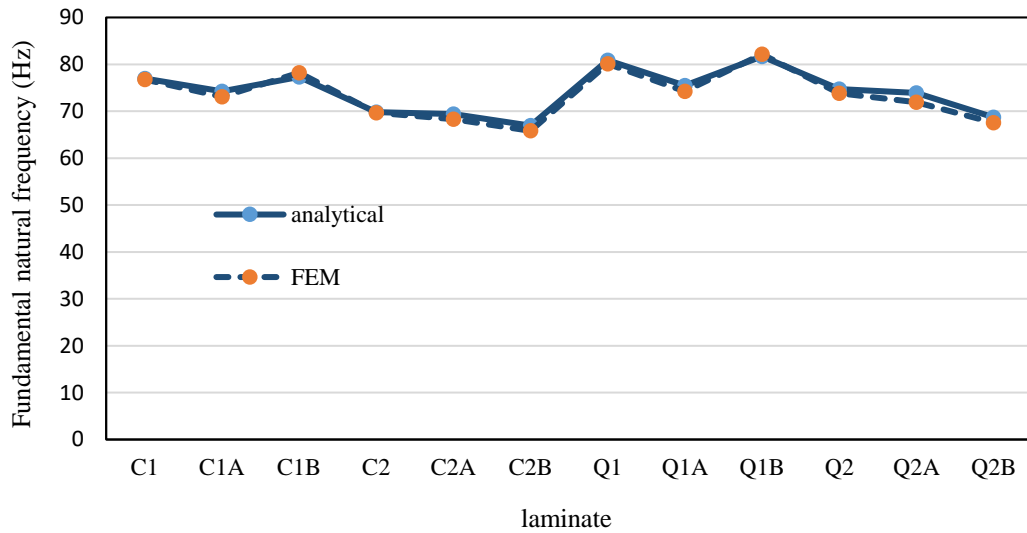
C1B (2G: 6C), C2 (4G: 4C), Q1B (2G: 6C), and Q2 (4G: 4C) laminates in C1, C2, Q1, and Q2 groups are the best sequence laminate. Their bending stiffness coefficient d_{mn} are the highest in their groups as shown in Figure (5.38-a). Consequently, the deflections of them are lower than the other sequences in the same group and vice versa for fundamental natural frequency as shown in Figure (5.38-b and c). As the number of carbon plies increased, the D22 element's contribution increased as well, increasing the material's young modulus and resistance to elastic deformation. Furthermore, because of its increased modulus, the material's resistance to elastic deformation increased as the carbon ply position got closer to the exterior surface.



(a)



(b)



(c)

Figure (5.38) Effect of hybrid ratio on (a) the bending stiffness coefficient, (b) the maximum deflection, and (c) the fundamental natural frequency of C1, C1A, C1B, C2, C2A, C2B, Q1, Q1A, Q1B, Q2, Q2A, and Q2B fiber reinforced epoxy composite plates.

5.9.3 Fiber Metal Laminate Sandwich

Due to the brittle property of fiber/epoxy composite and to reduce the harsh environmental effects, FRPC will be reinforced by metal layers as a skin to produce fiber metal laminate sandwich.

Three types of metal are selected because of their many uses in structural applications which are stainless steel 304, aluminum 6061-T6, and Titanium alloy Ti-6Al-4V, where their mechanical properties are shown in Table (4.4) and Table (3.1) (Hibbeler, 2012), respectively.

These skin metal plates ($a= 300$ mm, $b=300$ mm, and $h=1$ mm) will be assumed to be bonded perfectly to C1, C2, Q1, and Q2 core composite plate ($a= 300$ mm, $b=300$ mm, and $h=2$ mm) to produce fiber metal laminates sandwich shown in Table (3.4).

The maximum deflection of the FML sandwich plates due to uniform distributed pressure (q_0) equal to 2.222×10^{-4} MPa, and the fundamental natural frequency due to its free vibration are shown in Figure (5.39).

In general, adding stainless steel 304, aluminum 6061-T6, and Titanium alloy Ti-6Al-4V to the fiber-reinforced polymer composite core C1, C2, Q1, and Q2 leads to an increase in the bending stiffness coefficient d_{mn} of the FML structure in comparison with the neat FRPC C1, C2, Q1, and Q2 structure. FML is better able to withstand elastic deformation and support load than FRPC because its bending stiffness elements (D_{11} , D_{12} , D_{22} , and D_{66}) are greater than those of FRPC. The contribution of metal skin is higher than fiber-reinforced polymer core in fiber metal laminate sandwich.

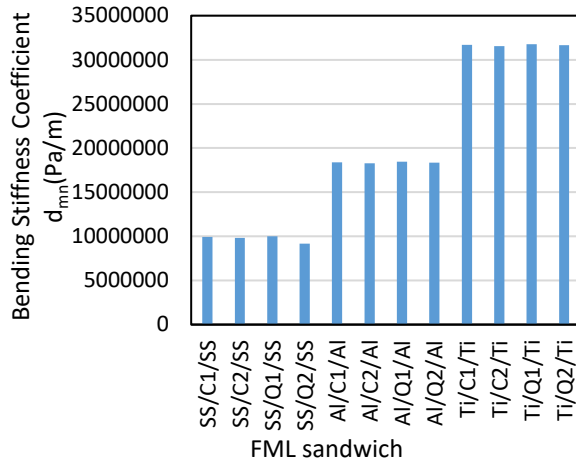
The bending stiffness coefficient d_{mn} of Ti/C1/Ti, Ti/C2/Ti, Ti/Q1/Ti, and Ti/Q2/Ti is higher than SS/C1/SS, SS/C2/SS, SS/Q1/SS, SS/Q2/SS, and Al/C1/Al, Al/C2/Al, Al/Q1/Al, Al/Q2/Al by 70% and 42%, respectively as shown in Figure (5.39-a). Consequently, the maximum deflection of Ti/C1/Ti, Ti/C2/Ti, Ti/Q1/Ti, and Ti/Q2/Ti is lower than SS/C1/SS, SS/C2/SS, SS/Q1/SS, SS/Q2/SS, and Al/C1/Al, Al/C2/Al, Al/Q1/Al, Al/Q2/Al by 70%

and 42%, respectively as shown in Figure (5.39-c). The ability of Ti-base FML to maintain its shape is greater than SS-304-base and Al-base FML because its bending stiffness elements (D11, D12, D22, and D66) are higher.

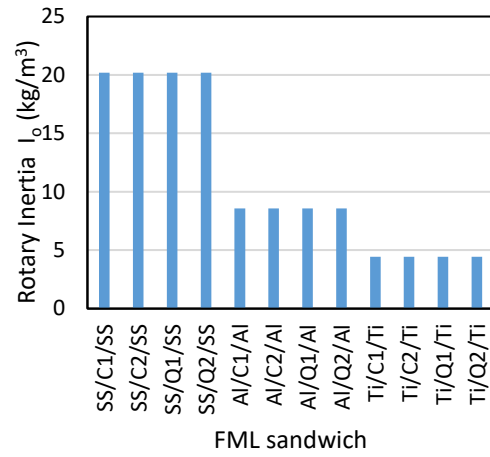
Rotary inertia I_o of stainless-steel 304 base fiber metal laminate is higher than aluminum 6061-T6, and Titanium alloy Ti-6Al-4V base FML by 58%, and 78%, respectively as shown in Figure (5.39-b) because the density of stainless steel 304 is higher than aluminum, and titanium alloy base FML. As a result, the fundamental natural frequency of Titanium alloy Ti-6Al-4V base FML is higher than stainless steel base FML and aluminum 6061-T6 base FML by 57% and 10%, respectively as shown in Figure (5.39-d).

The first six natural frequencies and their mode shapes for all SS/FRPC/SS, Al/FRPC/Al, and Ti/FRPC/Ti simply supported plates are shown in Tables (5.5), (5.6), and (5.7), respectively.

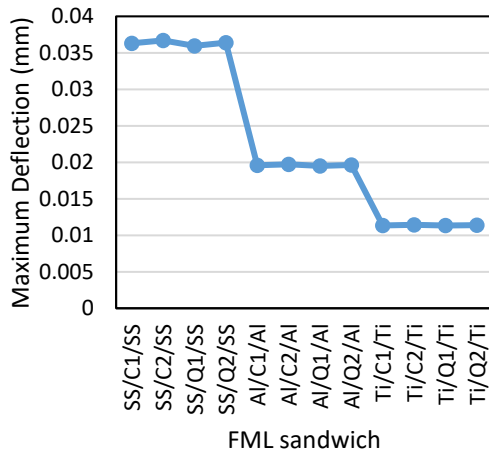
The first, third, fourth, and sixth mode shapes of SS/FRPC/SS, Al/FRPC/Al and Ti/FRPC/Ti are bending modes. While the second and fifth mode shapes are torsion modes. SS/Q1/SS, Al/Q1/Al, and Ti/Q1/Ti have the highest first, fourth, fifth, and sixth natural frequencies. But SS/C1/SS, Al/C1/Al, and Ti/C1/Ti have the highest second and third natural frequencies. The difference between the natural frequencies of fiber metal laminate sandwiches for the same metal base is very little because the contribution of the metal base is higher than fiber reinforced polymer composite core Contribution as shown in Figure (5.40).



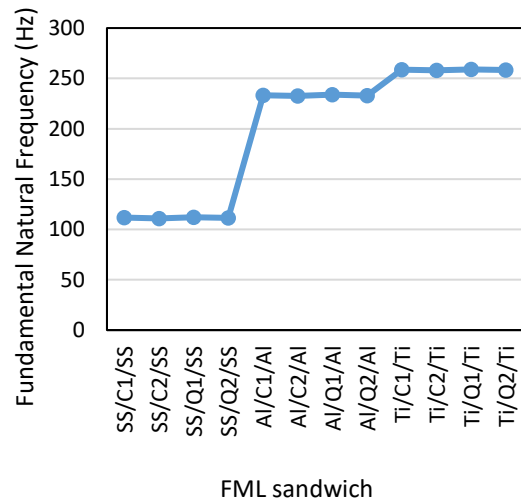
(a)



(b)



(c)



(d)

Figure (5.39) Effect of metal skin type on the (a) bending stiffness coefficient, (b) rotary inertia, (c) maximum deflection, and (d) fundamental natural frequency of FML plates.

Tabel (5.5) The first six natural frequencies and its mode shapes for all SS/FRPC/SS

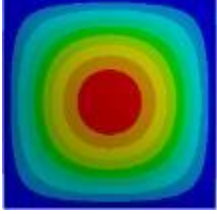

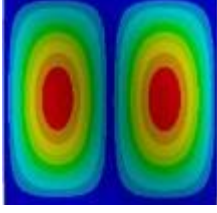
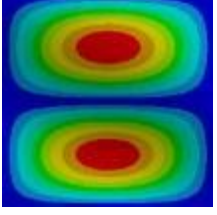

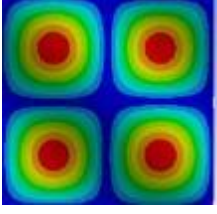
No.	Mode shape	Natural Frequencies (Hz)			
		SS/C1/SS	SS/C2/SS	SS/Q1/SS	SS/Q2/SS
1		110.7	109.93	111.1	110.36
2		241.8	241.57	240.92	239.73
3		280	276.1	278.7	277.3
4		281.3	280.2	283	279.4
5		395	393.66	400.5	391.4
6		442	439.3	443.61	441

Table (5.6) The first six natural frequencies and its mode shapes for all Al/FRPC/Al.

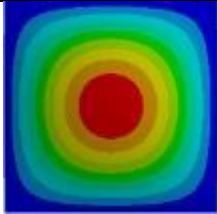

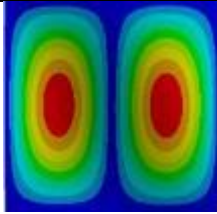
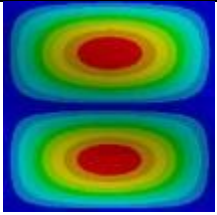
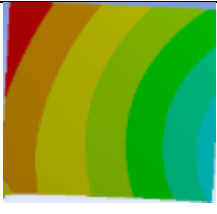
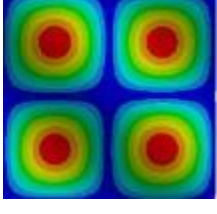
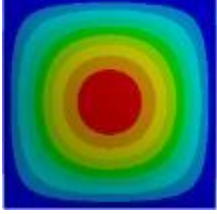

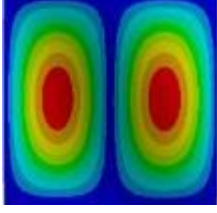
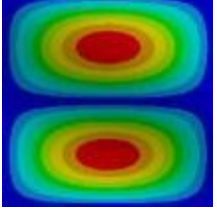

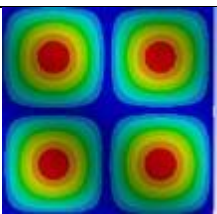
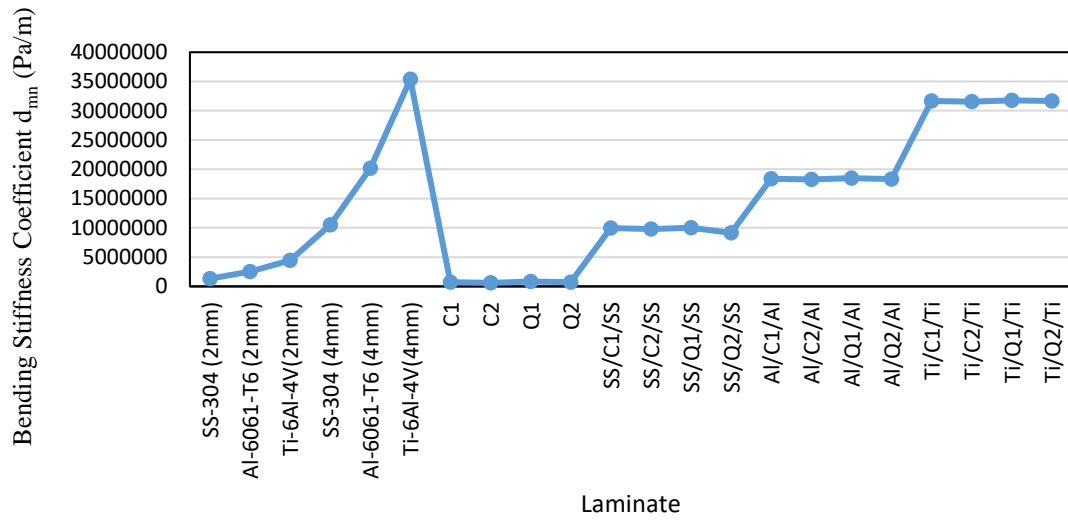
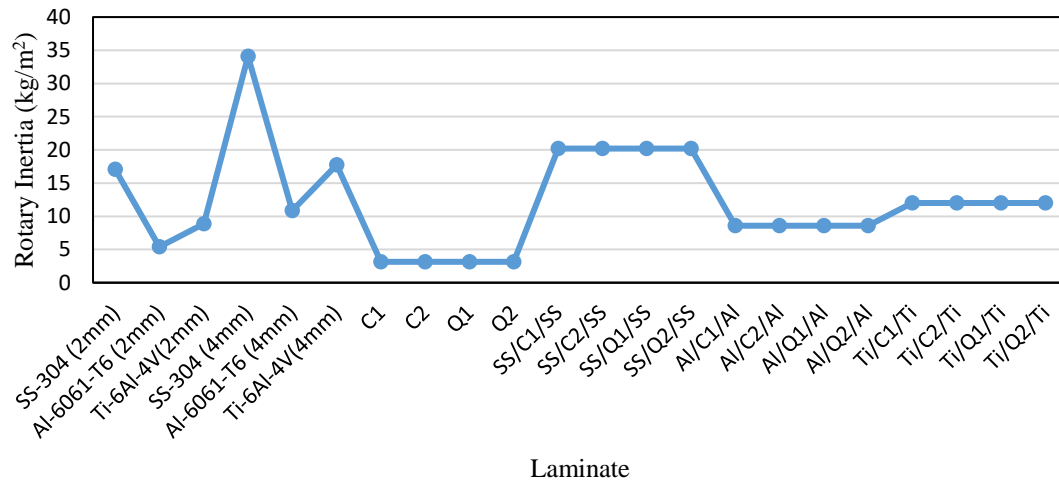
No.	Mode shape	Natural Frequencies (Hz)			
		Al/C1/Al	Al/C2/Al	Al/Q1/Al	Al/Q2/Al
1		230.3	229.5	230.69	229.9
2		473.8	473.5	472.2	470.4
3		579.6	575.2	578.1	576.6
4		581.1	579.8	582.9	578.9
5		774.6	773	783.3	769.9
6		915.7	912.6	917.4	914.3

Table (5.7) The first six natural frequencies and its mode shapes for all Ti/FRPC/Ti.

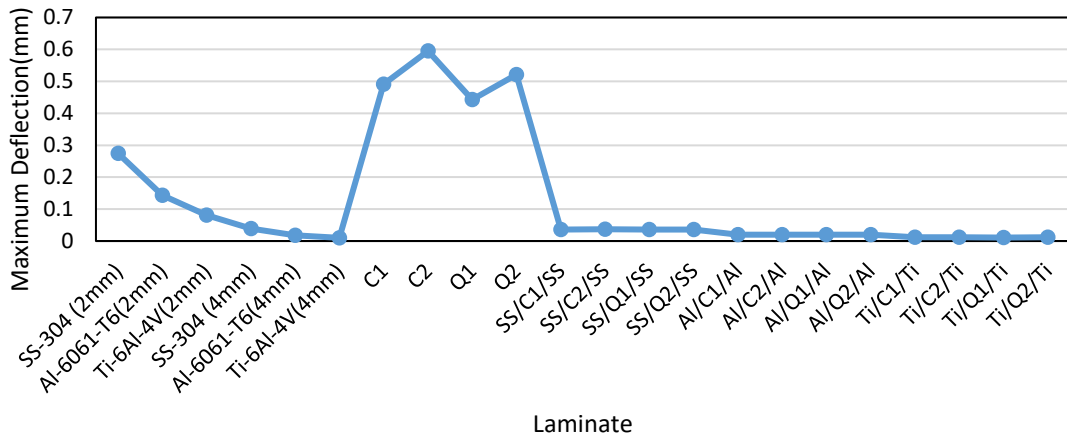
No.	Mode shape	Natural Frequencies (Hz)			
		Ti/C1/Ti	Ti/C2/Ti	Ti/Q1/Ti	Ti/Q2/Al
1		253.9	253.3	254.11	253.6
2		507.2	506.97	505.83	504.5
3		636.54	633.74	635.52	634.6
4		637.43	636.7	638.71	636.11
5		830.2	828.91	836.77	836.6
6		1003	1001	1004	1002



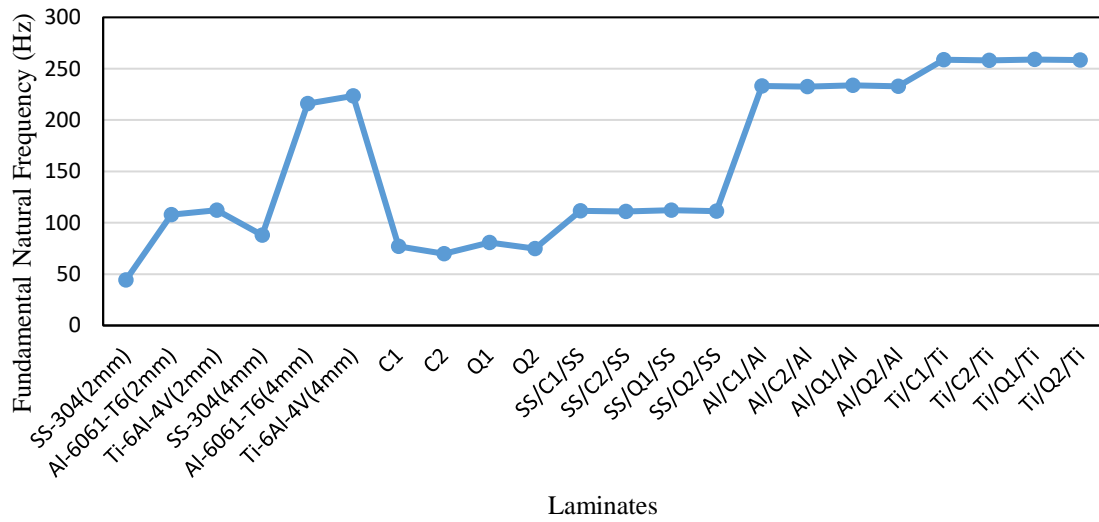
(a)



(b)



(c)



(d)

Figure (5.40) Comparison between (a) bending stiffness coefficient, (b) rotary inertia, (c) maximum deflection, and (d) fundamental natural frequency of metal, FRPC, and FML simply supported plates.

It is evident from Figure (5.54-a) that SS-304, Al-6061-T6, and Ti-6Al-4V metal plate (thickness $h=4$ mm) bending stiffness coefficient d_{mn} is higher than SS/Q1/SS, Al/Q1/Al, and Ti/Q1/Ti (thickness $h=4$ mm) by 5%, 8.5%, and 10%, respectively. On the other hand, SS-304, Al-6061-T6, and Ti-6Al-4V metal plate (thickness $h=2$ mm) bending stiffness coefficient d_{mn} is higher than Q1 FRPC ((thickness $h=2$ mm) by 38%, 68%, and 82%, respectively. Consequently, the maximum deflection of SS-304, Al-6061-T6, and Ti-6Al-4V metal plate (thickness $h=4$ mm) is lower than SS/Q1/SS, Al/Q1/Al, and Ti/Q1/Ti (thickness $h=4$ mm) by 5%, 8.5%, and 12%, respectively. On the other hand, the maximum deflection of SS-304, Al-6061-T6, and Ti-6Al-4V metal plate (thickness $h=2$ mm) is lower than Q1 FRPC (thickness $h=2$ mm) by 38%, 68%, and 82%, respectively as shown Figure (5.54-c).

It is evident from Figure(5.54-b) that SS-304, Al-6061-T6, and Ti-6Al-4V metal plate (thickness $h=4$ mm) rotary inertia I_o is higher than SS/Q1/SS, Al/Q1/Al, and Ti/Q1/Ti (thickness $h=4$ mm) by 41%, 21%, and 32%, respectively, because the density of SS-304, Al-6061-T6, and Ti-6Al-4V is higher than SS/Q1/SS, Al/Q1/Al, and Ti/Q1/Ti by 40%, 30%, and 31%, respectively. Therefore, the fundamental natural frequency of SS/Q1/SS, Al/Q1/Al, and Ti/Q1/Ti is higher than SS-304, Al-6061-T6, and Ti-6Al-4V metal plate (thickness $h=4$ mm) by 22%, 8%, and 14%, respectively, as shown in Figure (5.54-d).

CHAPTER SIX

CONCLUSIONS AND RECOMMENDATIONS

This study investigated the tensile, flexural, and free vibration characteristics of three distinct types of hybrid composites. The first type is the G: C inter-ply fiber-reinforced polymer composite (FRPC). The second type, known as Nano-FRPC, incorporates a 2% Al_2O_3 nano-addition into the epoxy matrix of the FRPC. The third type is a sandwich fiber metal laminate, featuring titanium, aluminum, and stainless steel 304 as the metal skin and a fiber core.

This chapter contains a set of conclusions obtained from this research. It also, supplies admonishing suggestions, that may be utilized in future work.

6.1 Conclusions

The following conclusions are deduced

1. Derive a new equation for the bending stiffness coefficient factor d_{mn} characterized for quasi-isotropic simply supported plate by using Navier solution, equation (3.52), that is not previously mentioned in the cited research. The factor d_{mn} is useful to calculate the deflection and fundamental natural frequency for a simply supported plate.
2. Quasi-laminated FRPC has lower tensile and flexural properties than cross-laminated FRPC.
3. Stacking sequence [GGCC]s has better tensile properties, while [GCCG]s has better flexural properties.
4. Tensile and flexural properties of FML are higher than FRPC except for deflection.
5. Tensile and flexural properties of FRPC and FML increased with adding 2% nano Al_2O_3 .
6. The theoretical flexural modulus of stacking sequence [GGCC]s is higher than [GCCG]s.

7. By adding 2% nano Al_2O_3 to FRPC, the natural frequency decreased and the damping ratio increased.
8. Theoretical flexural modulus and fundamental natural frequency of FML are not influenced by fiber orientation or stacking sequence.
9. The flexural modulus and damping ratio are inversely related to each other. However, adding two glass plies at the outer surface of the quasi-group laminate leads to increase flexural modulus, natural frequency, and damping ratio simultaneously as in configurations Q2 and Q2WN in comparison with Q1 and Q1WN.
10. Maximum deflection due to uniformly distributed load for metal and FML decreased and natural frequency increased with increasing metal plate thickness and metal Young's modulus.
11. The Quasi-FRPC (Q1) plate has a lower maximum deflection due to uniformly distributed load, while the Cross-FRPC (C2) plate has a higher maximum deflection and vice versa for natural frequency.
12. With increasing aspect ratio ($S = a/b$), deflection decreased, and fundamental natural frequency increased.
13. With increasing number of glass plies in FRPC, maximum deflection increased, and fundamental natural frequency decreased, and vice versa for increasing carbon plies.

6.2 Recommendation for future work

1. Replace the glass fiber plies with carbon fiber plies and the carbon fiber plies with glass for the same hybrid ratio and re-evaluation of mechanical and dynamic behavior for all eight laminated FRPC configurations.
2. Insert Kevlar as the third fiber layer with glass and carbon fiber plies.
3. Using intra-ply hybrid in combination with inter-ply hybridization.
4. Fabricate FML by using aluminum and titanium metal layers as skin.

REFERENCES

- Daniel, I.M. & Ori Ishai (2006) *Engineering mechanics of composite materials*, Oxford University Press, inc.
- Rajak, D.K. *et al.* (2019) ‘Recent progress of reinforcement materials: A comprehensive overview of composite materials’, *Journal of Materials Research and Technology*, 8(6), pp. 6354–6374. DOI: 10.1016/j.jmrt.2019.09.068.
- Barros, M.A.S., Fujiyama, R.T. and Leite, J.C. (2015) ‘Advantages of applying composite material to replace metal alloys in aviation’, *ITEGAM-JETIA*, 1(3). DOI: 10.5935/2447-0228.20150023.
- Akay, M. (2015) ‘An introduction to polymer matrix composites’, *Irelandia: Ventus Publishing APs*.
- Kaw, A.K. (2005) *Mechanics of composite materials*. CRC press.
- Kar, K.K. (2016) *Composite materials: processing, applications, characterizations*. Springer.
- Barbero, E.J. (2010) *Introduction to composite materials design*. CRC press.
- Campbell, F.C. (2010) *Structural composite materials*. ASM international.
- Chawla, K.K. (2012) *Composite materials: science and engineering*. Springer Science & Business Media.
- Harris, B. (1999) ‘Engineering composite materials’. The Institute of Materials, London.a
- Thakur, V.K., Thakur, M.K. and Gupta, R.K. (2017) *Hybrid polymer composite materials: processing*. Woodhead Publishing.
- Ding, Z. *et al.* (2021) ‘A review on forming technologies of fibre metal laminates’, *International Journal of Lightweight Materials and Manufacture*, 4(1), pp. 110–126. DOI:10.1016/j.ijlmm.2020.06.006.
- Logesh, K. *et al.* (2017) ‘Review on manufacturing of fibre metal laminates and its characterization techniques’, *Int J Mech Eng Technol*, 8(10), pp. 561–578.

- Ikbal, M.H., Wang, Q.T. and Li, W. (2016) ‘Effect of glass/carbon ratios and laminate geometry on flexural properties of glass/carbon fiber hybrid composites’, in *International Conference on Materials Chemistry and Environmental Protection 2015*. Atlantis Press, pp. 114–118. DOI: 10.2991/meep-15.2016.31.
- Swolfs, Y., Gorbatiikh, L. and Verpoest, I. (2014) ‘Fibre hybridisation in polymer composites: A review’, *Composites Part A: Applied Science and Manufacturing*, 67, pp. 181–200. DOI:10.1016/j.compositesa.2014.08.027.
- Kretsis, G. (1987) ‘A review of the tensile, compressive, flexural and shear properties of hybrid fibre-reinforced plastics’, *Composites*, 18(1), pp. 13–23. DOI:10.1016/0010-4361(87)90003-6.
- Zhang, J. *et al.* (2012) ‘Hybrid composite laminates reinforced with glass/carbon woven fabrics for lightweight load bearing structures’, *Materials & Design (1980-2015)*, 36, pp. 75–80. DOI: 10.1016/j.matdes.2011.11.006.
- Jesthi, D.K., *et al.* (2018 a) ‘Evaluation of mechanical properties of hybrid composite laminates reinforced with glass/carbon woven fabrics’, *IOP Conference Series: Materials Science and Engineering*, 377(1). DOI:10.1088/1757-899X/377/1/012157.
- Jesthi, D.K., *et al.* (2018 b) ‘Improvement of mechanical properties of carbon/glass fiber reinforced polymer composites through inter-ply arrangement’, in *IOP Conference Series: Materials Science and Engineering*. IOP Publishing, p. 12182. DOI:10.1088/1757-899X/377/1/012182.
- Jesthi, D.K., *et al.* (2018 c) ‘Effect of carbon/glass fiber symmetric inter-ply sequence on mechanical properties of polymer matrix composites’, *Procedia Manufacturing*, 20, pp. 530–535. DOI: 10.1016/j.promfg.2018.02.079.
- Dong, C. and Davies, I.J. (2013) ‘Flexural properties of glass and carbon fiber reinforced epoxy hybrid composites’, *Proceedings of the Institution of Mechanical Engineers, Part L: Journal of Materials: Design and Applications*, 227(4), pp. 308–317. DOI: 10.1177/1464420712459396.
- Khan, T. *et al.* (2020) ‘The effect of hybridization on microstructure and thermo-mechanical properties of composites reinforced with different weaves of glass and carbon fabrics’, *Journal of Composite Materials*, 55(12), pp. 1635–1651. DOI: 10.1177/0021998320974728.

- Alcudia-Zacarías, E. *et al.* (2020) ‘Experimental assessment of residual integrity and balanced mechanical properties of GFRP/CFRP hybrid laminates under tensile and flexural conditions’, *Applied Composite Materials*, 27(6), pp. 895–914. DOI:10.1007/s10443-020-09839-x.
- Ikbal, M.H. *et al.* (2017) ‘Hybrid composites made of unidirectional T600S carbon and E-glass fabrics under quasi-static loading’, *Journal of Industrial Textiles*, 46(7), pp. 1511–1535. DOI: 10.1177/1528083715624259.
- Wu, W. *et al.* (2018) ‘The effects of hybridization on the flexural performances of carbon/glass interlayer and intralayer composites’, *Polymers*, 10(5), p. 549. DOI: 10.3390/polym10050549.
- Wu, W., Wang, Q. and Li, W. (2018) ‘Comparison of tensile and compressive properties of carbon/glass interlayer and intralayer hybrid composites’, *Materials*, 11(7), p. 1105. DOI: 10.3390/ma11071105.
- Guo, R. *et al.* (2022) ‘Effect of fiber hybridization types on the mechanical properties of carbon/glass fiber reinforced polymer composite rod’, *Mechanics of Advanced Materials and Structures*, 29(27), pp. 6288–6300. DOI:10.1080/15376494.2021.1974620.
- Agarwal, G., Patnaik, A. and Agarwal, J. (2014) ‘Effect of stacking sequence on physical, mechanical and tribological properties of glass-carbon hybrid composites’, *Friction*, 2(4), pp. 354–364. DOI: 10.1007/s40544-014-0068-9.
- Pujar, N. V, Nanjundaradhya, N. V and Sharma, R.S. (2019) ‘Experimental studies on the tensile and flexural properties of epoxy based unidirectional glass/carbon interlayer hybrid composites’, in *AIP Conference Proceedings*. AIP Publishing LLC, p. 20041. DOI:10.1063/1.5085612.
- Abd Ghani, A.F. and Mahmud, J. (2020) ‘Characterisation of hybrid carbon glass fiber reinforced polymer (C/GFRP) of balanced cross ply and quasi isotropic under tensile and flexural loading’, *International Journal of Automotive and Mechanical Engineering*, 17(1), pp. 7792–7804. DOI: 10.15282/ijame.17.1.2020.25.0580.
- Matykiewicz, D. (2020) ‘Hybrid epoxy composites with both powder and fiber filler: a review of mechanical and thermomechanical properties’, *Materials*, 13(8), p. 1802. DOI: 10.3390/ma13081802.
- Halder, S. *et al.* (2013) ‘Ultrasonic dual mode mixing and its effect on tensile properties of SiO₂-epoxy nanocomposite’, *Journal of Adhesion Science and Technology*, 27(2), pp. 111–124. DOI: 10.1080/01694243.2012.701510.

- Ghosh, P.K., Kumar, K. and Chaudhary, N. (2015) 'Influence of ultrasonic dual mixing on thermal and tensile properties of MWCNTs-epoxy composite', *Composites Part B: Engineering*, 77, pp. 139–144. DOI: 10.1016/j.compositesb.2015.03.028
- Mohanty, A. and Srivastava, V.K. (2015) 'Effect of alumina nanoparticles on the enhancement of impact and flexural properties of the short glass/carbon fiber reinforced epoxy based composites', *Fibers and Polymers*, 16(1), pp. 188–195. DOI: 10.1007/s12221-015-0188-5.
- Afrouzian, A. *et al.* (2017) 'Effect of nano-particles on the tensile, flexural and perforation properties of the glass/epoxy composites', *Journal of Reinforced Plastics and Composites*, 36(12), pp. 900–916. DOI: 10.1177/0731684417694753.
- Kaybal, H.B. *et al.* (2018) 'Effects of alumina nanoparticles on dynamic impact responses of carbon fiber reinforced epoxy matrix nanocomposites', *Engineering Science and Technology, an International Journal*, 21(3), pp. 399–407. DOI: 10.1016/j.jestch.2018.03.011.
- Abu-Okail, M. *et al.* (2021) 'Effect of dispersion of alumina nanoparticles and graphene nanoplatelets on microstructural and mechanical characteristics of hybrid carbon/glass fibers reinforced polymer composite', *Journal of Materials Research and Technology*, 14, pp. 2624–2637. DOI: 10.1016/j.jmrt.2021.07.158.
- Hassan, M.K. *et al.* (2015) 'Investigation of the mechanical behavior of novel fiber metal laminates', *International Journal of Mechanical & Mechatronics Engineering IJMME-IJENS*, 15(3), pp. 112–118. DOI: 157103-8282-IJMME-IJENS © June 2015 IJENS.
- Merzuki, M.N.M. *et al.* (2018) 'Finite element simulation of aluminium/GFRP fibre metal laminate under tensile loading', in *IOP Conference Series: Materials Science and Engineering*. IOP Publishing, p. 12072. DOI: 10.1088/1757-899X/318/1/012072.
- Dahshan, B. *et al.* (2020) 'Experimental and numerical study on the tensile, three-point-bending, and interlaminar fracture toughness of GLARE', *Journal of Mechanical Science and Technology*, 34, pp. 3273–3281. DOI: 10.1007/s12206-020-0719-x.

- Ammar, M.M. *et al.* (2019) ‘A tensile characterization of random glass fiber/metal laminates composites’, *Materials Research Express*, 6(8), p. 85349. DOI: 10.1088/2053-1591/ab2994.
- Annamalai, I. *et al.* (2021) ‘Experimental investigation of mechanical properties of GLARE composite with different layup sequences’, *Materials Today: Proceedings*, 46, pp. 1371–1375. DOI: 10.1016/j.matpr.2021.02.487.
- Megahed, M. *et al.* (2019) ‘An experimental investigation on the effect of incorporation of different nanofillers on the mechanical characterization of fiber metal laminate’, *Composites Part B: Engineering*, 176, art. ID 107277, 12 pages. DOI: 10.1016/j.compositesb.2019.107277.
- Keshavarz, R., Aghamohammadi, H. and Eslami-Farsani, R. (2020) ‘The effect of graphene nanoplatelets on the flexural properties of fiber metal laminates under marine environmental conditions’, *International Journal of Adhesion and Adhesives*, 103, art ID 102709, 10 pages. DOI: 10.1016/j.ijadhadh.2020.102709.
- El-baky, M.A.A. and Attia, M.A. (2022) ‘The mechanical performance of the laminated aluminum-epoxy/glass fiber composites containing halloysite nanotubes: An experimental investigation’, *Journal of Industrial Textiles*, 51(5_suppl), pp. 8690S-8737S. DOI:10.1177/1528083720960735.
- Khalili, S.M.R., Mittal, R.K. and Kalibar, S.G. (2005) ‘A study of the mechanical properties of steel/aluminium/GRP laminates’, *Materials Science and Engineering: A*, 412(1–2), pp. 137–140. DOI: 10.1016/j.msea.2005.08.016.
- Tamilarasan, U., Karunamoorthy, L. and Palanikumar, K. (2015) ‘Mechanical properties evaluation of the carbon fibre reinforced aluminium sandwich composites’, *Materials Research*, 18, pp. 1029–1037. DOI: 10.1590/1516-1439.017215.
- Dhaliwal, G.S. and Newaz, G.M. (2016) ‘Experimental and numerical investigation of flexural behavior of carbon fiber reinforced aluminum laminates’, *Journal of Reinforced Plastics and Composites*, 35(12), pp. 945–956. DOI: 10.1177/0731684416632606.
- Bellini, C. *et al.* (2019a) ‘Analysis of CFRP/Al hybrid laminates flexural strength’, *Procedia Structural Integrity*, 18, pp. 368–372. DOI:10.1016/j.prostr.2019.08.176.

- Bellini, C. *et al.* (2019b) ‘Performance evaluation of CFRP/Al fibre metal laminates with different structural characteristics’, *Composite Structures*, 225, p. 111117. DOI: 10.1016/j.compstruct.2019.111117.
- Bellini, C. *et al.* (2020) ‘Failure energy and strength of Al/CFRP hybrid laminates under flexural load’, *Material Design & Processing Communications*, 2(5), p. e109. DOI:10.1002/mdp2.109.
- Bellini, C. *et al.* (2021) ‘CFRP/aluminum fibre metal laminates: numerical model for mechanical properties simulation’, *Procedia Structural Integrity*, 33, pp. 824–831. DOI: 10.1016/j.prostr.2021.10.092.
- Gao, S. *et al.* (2023) ‘Numerical and experimental investigation of flexural properties and damage behavior of CFRTP/Al laminates with different stacking sequence’, *Applied Sciences*, 13(3), p. 1667. DOI: 10.3390/app13031667
- Chen, Y. *et al.* (2023) ‘Theoretical modeling and experimental verification of the bending deformation of fiber metal laminates’, *Materials*, 16(9), p. 3486. DOI:10.3390/ma16093486.
- Hynes, N.R.J. *et al.* (2022) ‘Effect of stacking sequence of fibre metal laminates with carbon fibre reinforced composites on mechanical attributes: Numerical simulations and experimental validation’, *Composites Science and Technology*, 221, p. 109303. DOI:10.1016/j.compscitech.2022.109303.
- Sun, J. *et al.* (2019) ‘Tensile failure of fibre-metal-laminates made of titanium and carbon-fibre/epoxy laminates’, *Materials & Design*, 183, p. 108139. DOI: 10.1016/j.matdes.2019.108139.
- Rajkumar, G.R. *et al.* (2014) ‘Investigation of tensile and bending behavior of aluminum-based hybrid fiber metal laminates’, *Procedia Materials Science*, 5, pp. 60–68. DOI:10.1016/j.mspro.2014.07.242
- Nestler, D. *et al.* (2017) ‘Continuous film stacking and thermoforming process for hybrid CFRP/aluminum laminates’, *Procedia Cirp*, 66, pp. 107–112. DOI:10.1016/j.procir.2017.03.221.
- Ostapiuk, M., Bienias, J. and Surowska, B. (2018) ‘Analysis of the bending and failure of fiber metal laminates based on glass and carbon fibers’, *Science and Engineering of Composite Materials*, 25(6), pp. 1095–1106. DOI: 10.1515/secm-2017-0180.

Smolnicki, M. and Stabla, P. (2019) ‘Finite element method analysis of fibre-metal laminates considering different approaches to material model’, *SN Applied Sciences*, 1(5), p. 467. DOI: 10.1007/s42452-019-0496-2.

Yang, H. *et al.* (2022) ‘Mechanical properties study on sandwich hybrid metal/(carbon, glass) fiber reinforcement plastic composite sheet’, *Advanced Composites and Hybrid Materials*, 5(1):3, pp. 1–8. DOI:10.1007/s42114-021-00213-4.

Trautmann, M. *et al.* (2020) ‘Mechanical properties of thermoplastic-based hybrid laminates with regard to layer structure and metal volume content’, *Metals*, 10(11), p. 1430. DOI: 10.3390/met10111430.

Moussavi-Torshizi, S.E. *et al.* (2010) ‘A study on tensile properties of a novel fiber/metal laminates’, *Materials Science and Engineering: A*, 527(18–19), pp. 4920–4925. DOI: 10.1016/j.msea.2010.04.028.

Biliz, İ. and Çelik, Y.H. (2022) ‘Investigation of mechanical properties of layered composites formed from glass, carbon and Aramid fibers and aluminum Plates’, *European Journal of Technique (EJT)*, 12(2), pp. 117–122. DOI: 10.36222/ejt.1122360.

Chung, D.D.L. (2003) *Composite materials: functional materials for modern technologies*. Springer Science & Business Media.

Treviso, A. *et al.* (2015) ‘Damping in composite materials: Properties and models’, *Composites Part B: Engineering*, 78, pp. 144–152. DOI: 10.1016/j.compositesb.2015.03.081.

Tang, X. and Yan, X. (2020) ‘A review on the damping properties of fiber reinforced polymer composites’, *Journal of Industrial Textiles*, 49(6), pp. 693–721. DOI: 10.1177/1528083718795914.

Murugan, R., Ramesh, R. and Padmanabhan, K. (2016) ‘Investigation of the mechanical behavior and vibration characteristics of thin-walled glass/carbon hybrid composite beams under a fixed-free boundary condition’, *Mechanics of Advanced Materials and Structures*, 23(8), pp. 909–916. DOI: 10.1080/15376494.2015.1056394

Suman, M.L.J., Murigendrappa, S.M. and Kattimani, S. (2019) ‘Experimental investigation on modal characteristics of plain woven glass/carbon hybrid composite beams with fixed-free end condition’, in *AIP Conference Proceedings*. AIP Publishing 2057(1):020011. DOI: 10.1063/1.5085582.

Pujar, N. V, Nanjundaradhya, N. V and Sharma, R.S. (2022) ‘Experimental investigation of the tensile and modal properties of epoxy-based symmetric interlayer glass/carbon hybrid composites’, *Materials Research Express*, 9(2), p. 25304. DOI:10.1088/2053-1591/ac4f88.

Aydin, M.R. *et al.* (2022) ‘Comparative dynamic analysis of carbon, aramid and glass fiber reinforced interply and intraply hybrid composites’, *Composite Structures*, 291, p. 115595. DOI: 10.1016/j.compstruct.2022.115595.

Erkliđ, A., Bulut, M. and Yeter, E. (2015) ‘The effect of hybridization and boundary conditions on damping and free vibration of composite plates’, *Science and Engineering of Composite Materials*, 22(5), pp. 565–571. DOI: 10.1515/secm-2014-0070.

Swolfs, Y. *et al.* (2015) ‘The effect of fibre dispersion on initial failure strain and cluster development in unidirectional carbon/glass hybrid composites’, *Composites Part A: Applied Science and Manufacturing*, 69, pp. 279–287. DOI: 10.1016/j.compositesa.2014.12.001.

Zhang, B. *et al.* (2021) ‘Research on damping performance and strength of the composite laminate’, *Scientific Reports*, 11(1), p. 18281. DOI: 10.1038/s41598-021-97933-w.

Navaneeth, I.M. *et al.* (2022) ‘Damped free vibration analysis of woven glass fiber-reinforced epoxy composite laminates’, *Advances in Materials Science and Engineering*, Volume 2022, Article ID 6980996, 13 pages. DOI: 10.1155/2022/6980996.

Pol, M.H. *et al.* (2013) ‘Effects Of nano-particles concentration on dynamic response of laminated nano-composite beam’, *Mechanika* 19(1), pp. 53–57. DOI: 10.5755/j01.mech.19.1.3617.

Khashaba, U.A. (2016) ‘Nanoparticle type effects on flexural, interfacial and vibration properties of GFRE composites’, *Chinese journal of Aeronautics*, 29(2), pp. 520–533. DOI: 10.1016/j.cja.2015.09.001.

Pujar, N. V, Nanjundaradhya, N. V and Sharma, R.S. (2018) ‘Effect of graphene oxide nanofiller on dynamic behaviour of GFRP composites’, in *AIP conference proceedings*. volume (1943), Issue (1), pp. 020107. AIP Publishing. DOI:10.1063/1.5029683.

Karthik, K. *et al.* (2016) ‘Free vibration test for damping characteristics of hybrid polyester matrix composite with carbon particles’, *Nano Hybrids and Composites*, 11, pp. 1–6. DOI: 10.4028/www.scientific.net/NHC.11.1.

Utomo, J.T., Susilo, D.D. and Raharja, W.W. (2017) ‘The influence of the number and position of the carbon fiber lamina on the natural frequency and damping ratio of the carbon-glass hybrid composite’, in *AIP Conference Proceedings*. volume 1788, art. ID 030046, 6 pages, AIP Publishing. DOI:10.1063/1.4968299.

Singh, K., Jain, N. and Bhaskar, J. (2020) ‘Vibrational analysis of glass/carbon fiber reinforced hybrid laminate composites’ *Journal of Theoretical and Applied Mechanics*, vol.50, p. 259-277. DOI: 10.7546/JTAM.50.20.03.04.

Pingulkar, P. and Suresha, B. (2016) ‘Free vibration analysis of laminated composite plates using finite element method’, *Polymers and Polymer Composites*, 24(7), pp. 529–538. DOI: 10.1177/096739111602400712.

Fairlie, G. and Njuguna, J. (2020) ‘Damping properties of flax/carbon hybrid epoxy/fibre-reinforced composites for automotive semi-structural applications’, *Fibers*, 8(10), p. 64. DOI: 10.3390/fib8100064.

Bulut, M. *et al.* (2019) ‘The effects of S-glass fiber hybridization on vibration-damping behavior of intraply woven carbon/aramid hybrid composites for different lay-up configurations’, *Proceedings of the Institution of Mechanical Engineers, Part C: Journal of Mechanical Engineering Science*, 233(9), pp. 3220–3231. DOI: 10.1177/0954406218813188.

Senthamaraiannan, C. and Ramesh, R. (2019) ‘Evaluation of mechanical and vibration behavior of hybrid epoxy carbon composite beam carrying micron-sized CTBN rubber and nanosilica particles’, *Proceedings of the Institution of Mechanical Engineers, Part L: Journal of Materials: Design and Applications*, 233(9), pp. 1738–1752. DOI: 10.1177/1464420718784315.

Bulut, M., Erkliğ, A. and Kanmaz, P. (2019) ‘Vibration-damping characterization of the basalt/epoxy composite laminates containing graphene nanopellets’, *Science and Engineering of Composite Materials*, 26(1), pp. 147–153. DOI: 10.1515/secm-2017-0380.

Botelho, E.C., Pardini, L.C. and Rezende, M.C. (2005) ‘Hygrothermal effects on damping behavior of metal/glass fiber/epoxy hybrid composites’, *Materials Science and Engineering: A*, 399(1–2), pp. 190–198. DOI: 10.1016/j.msea.2005.02.093.

Zal, V. *et al.* (2017) ‘Evaluation of the effect of aluminum surface treatment on mechanical and dynamic properties of PVC/aluminum/fiber glass fiber metal laminates’, *Proceedings of the Institution of Mechanical Engineers, Part E:*

Journal of Process Mechanical Engineering, 231(6), pp. 1197–1205. DOI: 10.1177/0954408916657371.

Cicco, D. De and Taheri, F. (2018) ‘Use of a simple non-destructive technique for evaluation of the elastic and vibration properties of fiber-reinforced and 3D fiber-metal laminate composites’, *Fibers*, 6(1), p. 14. DOI: 10.3390/fib6010014.

Merzuki, M.N.M. *et al.* (2019 a) ‘Investigation of modal analysis on glass fiber laminate aluminum reinforced polymer: An experimental study’, in *IOP conference series: materials science and engineering*. IOP Publishing, p. 12065. DOI: 10.1088/1757-899X/469/1/012065.

Saini, N.K. *et al.* (2019) ‘Vibration analysis of fiber metal laminate beam in ANSYS parametric design language’, *International Journal of Applied Engineering Research*, 14, pp. 149–155.

Ciftci, U. and Kadioglu, F. (2021) ‘Effects of different fiber orientations on the dynamic response of the GLARE FML beams’, *SAMPE neXus 2021*.

Abdellah, M.Y. *et al.* (2020) ‘Effect of specimen size on natural vibration of open hole copper/glass-reinforced epoxy laminate composites.’, *AIMS Materials Science*, 7(4).

Maraş, S. *et al.* (2018) ‘Free vibration analysis of fiber metal laminated straight beam’, *Open Chemistry*, 16(1), pp. 944–948. DOI: 10.1515/chem-2018-0101.

Ahmed, J.P.S. and Meenakshisundaram, O. (2022) ‘Flexural and dynamic response of carbon/epoxy laminates with graphene nanofillers and Al6061 alloy’, *Engineering Research Express*, 4(2), p. 25021. DOI: 10.1088/2631-8695/ac6e30.

Botelho, E.C. *et al.* (2005) ‘Damping behavior of continuous fiber/metal composite materials by the free vibration method’, *composites part B: Engineering*, 37(2–3), pp. 255–263. DOI: 10.1016/j.compositesb.2005.04.003.

Merzuki, M.N.M. *et al.* (2019 b) ‘Experimental investigation of free vibration analysis on fibre metal composite laminates’, *Journal of Mechanical Engineering and Sciences*, 13(4), pp. 5753–5763. DOI: 10.15282/jmes.13.4.2019.03.0459.

Kali, N., Pathak, S. and Korla, S. (2020) ‘Effect on vibration characteristics of fiber metal laminates sandwiched with natural fibers’, *Materials Today: Proceedings*, 28, pp. 1092–1096. DOI: 10.1016/j.matpr.2020.01.088.

Merzuki, M.N.M. *et al.* (2022) ‘Experimental and numerical investigation of fibre-metal-laminates (FMLs) under free vibration analysis’, *Materials Today: Proceedings*, 48, pp. 854–860. DOI: 10.1016/j.matpr.2021.02.409.

Ravishankar, H. *et al.* (2016) ‘Free vibration behaviour of fiber metal laminates, hybrid composites, and functionally graded beams using finite element analysis’, *International Journal of Acoustics and Vibration*, 21(4), pp. 418–428. DOI: 10.20855/ijav.2016.21.4436.

Vanam, B.C.L., Rajyalakshmi, M. and Inala, R. (2012) ‘Static analysis of an isotropic rectangular plate using finite element analysis (FEA)’, *Journal of Mechanical Engineering Research*, 4(4), pp. 148–162. DOI: 10.5897/JMER11.088.

Reddy, B.S. *et al.* (2012) ‘Bending analysis of laminated composite plates using finite element method’, *International journal of engineering, science and technology*, 4(2), pp. 177–190. DOI: 10.4314/ijest.v4i2.14.

El-Helloty, A. and Salam, O. (2009) ‘Stress analysis of laminated composite plates using the finite element method’, *Civil Engineering Research Magazine (CERM)*, 31(4), pp. 1377–1401.

Saxena, M. and Kirtania, S. (2016) ‘Stiffness analysis of symmetric cross-ply laminated composite plates’, *ADBU Journal of Engineering Technology*, Volume 4(1), p.76.

Altunsaray, E. and Bayer, İ. (2013) ‘Deflection and free vibration of symmetrically laminated quasi-isotropic thin rectangular plates for different boundary conditions’, *Ocean Engineering*, 57, pp. 197–222. DOI:10.1016/j.oceaneng.2012.09.009.

Beylergil, B. (2020) ‘Multi-objective optimal design of hybrid composite laminates under eccentric loading’, *Alexandria Engineering Journal*, 59(6), pp. 4969–4983. DOI: 10.1016/j.aej.2020.09.015.

Liu, C.W. and Kam, T.Y. (2023) ‘Free vibration of rectangular composite cantilever plate and Its application in material degradation assessment’, *Applied Sciences*, 13(8), p. 5101. DOI: 10.3390/app13085101.

Koppanati, M.S., Naga Rani, M. and Krishna Bhaskar, K. (2023) ‘Free Vibration Analysis of Graphene Reinforced Laminated Composite Plates using Experimental Modal Testing’, *Mechanics Of Advanced Composite Structures*, 10(2), pp. 363–374. DOI:10.22075/mac.2023.28869.1448.

Ghasemi, F.A., Paknejad, R. and Fard, K.M. (2013) ‘Effects of geometrical and material parameters on free vibration analysis of fiber metal laminated plates’, *Mechanics & Industry*, 14(4), pp. 229–238. DOI: 10.1051/meca/2013062.

Prasad, E. V and Sahu, S.K. (2017) ‘Free vibration analysis of fiber metal laminated plates’. Proceedings of ICTACEM 2017 International Conference on Theoretical, Applied, Computational and Experimental Mechanics December 28-30, IIT Kharagpur, India

Prasad, E. V and Sahu, S.K. (2018) ‘Vibration analysis of woven fiber metal laminated plates—experimental and numerical studies’, *International journal of structural stability and dynamics*, 18(11), p. 1850144. DOI: 10.1142/S0219455418501444.

Abdellah, M.Y., Mohamed, A.F. and Hasan, M.K. (2019) ‘Characteristic analysis: Vibration behaviour of composite laminated structures compared to monotonic materials’, *Int. J. Mech. Mechatron. Eng. IJMME-IJENS*, 19, pp. 57–69.

Liu, Y. *et al.* (2020) ‘Study on natural characteristics of fiber metal laminates thin plates under cantilever boundary’, *Journal of Vibroengineering*, 22(4), pp. 909–922. DOI: 10.21595/jve.2020.21383.

Kallannavar, V. and Kattimani, S. (2020) ‘Modal analysis of laminated composite and sandwich plates using finite element method’, in *AIP Conference Proceedings*. AIP Publishing. DOI:10.1063/5.0004159.

Verma, M., Verma, A.K. and Kumhar, V. (2021) ‘Evaluation of ultimate strength and fundamental frequency of fiber/epoxy and fiber/Al6061 composite plate’, *Biointerface Research in Applied Chemistry*, pp. 12–13. DOI: 10.33263/BRIAC123.33903406.

Rao, N.N. *et al.* (2023) ‘Effect of boundary conditions and metal alloy layer on natural frequencies of fibre metal laminates’, *Composites Theory and Practice*, 23(2), pp.97-103.

Reddy, J.N. (2003) *Mechanics of laminated composite plates and shells: theory and analysis*. CRC press

Rao, S.S. (2019) *Vibration of continuous systems*. John Wiley & Sons.

Goren, A. and Atas, C. (2008) 'Manufacturing of polymer matrix composites using vacuum assisted resin infusion molding', *Archives of materials Science and Engineering*, 34(2), pp. 117–120.

International, A. (2007) *Standard test method for tensile properties of polymer matrix composite materials*. ASTM international.

ASTM, I. (2007) 'Standard test methods for flexural properties of unreinforced and reinforced plastics and electrical insulating materials', *ASTM D790-07*.

Hibbeler, R.C. (2012) *Mechanical of materials*. Published by Pearson Prentice Hall.

LIST OF PUBLICATIONS

International journals (Published)

1. Mohammed, A.A., Hassan, G.I. and Khdir, Y.K., 2023. The Dynamic Behaviour of Symmetrical Laminated Nano-composite Containing Equal Numbers of Glass and Carbon Fibre Layers. *Strojniški vestnik- Journal of Mechanical Engineering*, 69(5-6), pp.224-234. DOI: 10.5545/sv-jme.2022.403.
2. Mohammed, A., Hassan, G.I. and Khdir, Y.K., 2023. Mechanical Behavior of Hybrid Laminated Nano Composite Containing Equal Numbers of Glass and Carbon Fiber Plies. *International Journal of Automotive and Mechanical Engineering*, 20(2), pp.10335-10350. DOI: 10.15282/ijame.20.2.2023.01.0799.

The Dynamic Behaviour of Symmetrical Laminated Nano-composite Containing Equal Numbers of Glass and Carbon Fibre Layers

Ava A.K. Mohammed* - Gailan Ismail Hassan - Younis Khalid Khdir

Erbil Polytechnic University, Erbil Technical Engineering College,
Department of Technical Mechanical and Energy Engineering, Erbil 44001, Iraq

Fibre-reinforced polymer composite has many uses in structural components that required high strength, stiffness, and damping capacity. Cross and quasi-laminated epoxy composites with and without nano Al_2O_3 were used in this investigation to determine flexural modulus, natural frequency, damping ratio, and mode shapes by using analytical, experimental, and numerical (ANSYS) methods. It was demonstrated that adding 2 % nano Al_2O_3 improved the flexural modulus and the damping ratio while decreased the natural frequency. Cross number 2 and quasi number 2 had the highest natural frequency for cross and quasi laminate groups which are equal to 23.5 Hz and 20.25 Hz experimentally, respectively. On the other hand, the higher damping ratio was achieved for cross number 1 with nano Al_2O_3 and quasi number 2 with nano Al_2O_3 for both cross and quasi laminates, which are equal to 0.707 % and 0.693 %, respectively. The flexural modulus and damping ratio are inversely related to each other. However, the novelty in this article is that by adding two glass plies at the outer surface of quasi group laminate the flexural modulus, natural frequency, and damping ratio are increased simultaneously, as in the configurations quasi number 2 and quasi number 2 with nano Al_2O_3 in comparison with quasi number 1 and quasi number 1 with nano Al_2O_3 .

Key words: cross laminate, quasi laminate, natural frequency, damping ratio, nano Al_2O_3

Highlights

- Adding 2 % nano Al_2O_3 decreases natural frequency and increases damping capacity and flexural modulus.
- Adding two glass plies at the outer surface of all laminated composite increases flexural modulus and natural frequency, but the damping ratio is also increased jointly in the quasi-laminated group.
- Comparison between analytical, experimental, and numerical natural frequency for eight configurations of laminated composites.

0 INTRODUCTION

Multifunctional fibre-reinforced laminated polymer composites have been utilized in recent decades in structural applications, including automobiles, shafts, aircraft, bicycle frames, and tennis rackets,

due to the high bending modulus value of carbon fibre in a polymer matrix. In contrast, glass fibre has a higher damping ratio than carbon fibre in a polymer matrix, as shown in Table 1. The mechanical and dynamic properties of materials are related to each other. Zhang et al. [9] and Swolfs et al. [10] illustrated

RESEARCH ARTICLE

Mechanical Behavior of Hybrid Laminated Nano Composite Containing Equal Numbers of Glass and Carbon Fiber Plies

Ava A.K. Mohammed¹, Gailan Ismail Hassan and Younis Khalid Khdir

Department of Technical Mechanical and Energy Engineering, Erbil Technical Engineering College, Erbil Polytechnic University, 44001 Erbil, Iraq

ABSTRACT - Hybrid fiber reinforced polymer with nanofiller composite was introduced into a lot of industries due to its extreme mechanical properties in comparison with non-hybrid material. In this investigation, cross and quasi-fiber laminated epoxy composites with and without nano Al₂O₃ were fabricated using Vacuum Assisted Resine Infusion Method and Ultrasonic Dual Mixing Method. In general, the results of mechanical properties indicated that the addition of 2% nano Al₂O₃ enhances the tensile and flexural properties. Cross number 2 with nano Al₂O₃ laminate had the maximum tensile strength 628 MPa and maximum tensile strain of 1.74%, while cross number 1 with nano Al₂O₃ laminate had the maximum tensile modulus of 37.756 GPa in the cross group. In the quasi group, quasi number 2 with nano Al₂O₃ had the maximum tensile strength, maximum tensile strain, and maximum tensile modulus, equal to 294 MPa, 1.98%, and 16.409 GPa, respectively. Regarding the flexural properties, cross number 1 with nano Al₂O₃ laminate had a maximum flexural strength of 708.2 MPa and maximum flexural strain of 2.027%, while cross number 2 with nano Al₂O₃ laminate had a maximum flexural modulus of 38.73 GPa in the cross group. On the other hand, quasi number 1 with nano Al₂O₃ laminate had the maximum flexural strength, maximum flexural strain, and maximum flexural modulus equal to 596 MPa, 2.424%, and 29.2 GPa, respectively in the quasi group. The internal structures of the failure laminated composites through scanning electronic microscopy confirm that the adhesion between fibers and matrix is good.

ARTICLE HISTORY

Received : 18th July 2022
Revised : 24th Nov 2022
Accepted : 20th March 2023
Published : 30th June 2023

KEYWORDS

Glass/carbon hybrid;
Nano-Al₂O₃;
VARIM;
Cross laminates;
Quasi laminates

1.0 INTRODUCTION

High specific strength (strength to density ratio) and high specific stiffness (modulus to density ratio) connected with lightweight and enhancement in corrosion, wear and fatigue resistance are the essential reason to replace the conventional metal by fiber reinforced polymer laminated composite (FRP) in structural applications like aerospace, automobile and marine [1]. The most common fibers used in hybrid applications are carbon and glass. The use of carbon fiber

پوخته

لهم کاره‌دا دوو جور ماده بپیکهاته‌یی لامینیت‌ه‌کراو به‌کارده‌هینریت، ساندویچی بپیکهاته‌یی پۆلیمربه‌هیزکراوی ریشال (FRPC) و ساندویچی لامینیاتی کانزای ریشالی (FML) به نانو Al_2O_3 و به‌بی نانو.

تایبتمه‌ندی راکیشان و چرچوونیان لیکولینه‌وی له‌سەر ده‌کریت به شیوه‌یه‌کی پراکتیکی لیکولینه وه یان له سه ر ده کریت وبه به‌کارهینانی شیوازی توخمه سنوورداره‌کان (شیکاری ژماره‌یه وه پشتراست ده‌کریته وه (ANSYS workbench 19.2). ئەنجامه‌کان ئەوه نیشان ده‌دهن که تایبتمه‌ندی‌ه‌کانی راکیشانی FRPC زیاد بوو له‌گه‌ل زیادبوونی ژماره‌ی چینه کاربوئییه‌کان که له ناوه‌راستی لامینیاته‌که‌دا هه‌ن. ئەگه‌ر چینه کاربوئه‌که له رووی FRPC نزیک بیته‌وه، ئەوا تایبتمه‌ندییه‌ چه مانه وه ی زیاد ده‌بن. سه‌ره‌رای ئەومش، هه‌ردوو تایبتمه‌ندی راکیشانی و چه مانه وه‌ی FML به شیوه‌یه‌کی سه‌ره‌کی په‌یوه‌سته به په‌یوه‌ندی نیوان چینه‌کانی ریشال و کانزاکان. زیادکردنی 2٪ نانو Al_2O_3 بو FRPC و FML تایبتمه‌ندییه‌ میکانیکیه‌کانی زیاد کرد.

به زیادکردنی دوو چینی گلاس بو رووی دهره‌وه‌ی FRPC، مۆدیولی چه مانه وه ، فریکوینسی سروشتی و ریزه‌ی دامپین له هه‌مان کاتدا زیاد ده‌کریت به به‌راورد له‌گه‌ل 1 چینی گلاس بو رووی دهره‌وه‌ی FRPC. به زیادکردنی 2٪ نانو Al_2O_3 بو FRPC، مۆدیولی چه مانه وه و دامپین زیاد بوو له کاتیکدا فریکوینسی سروشتی که‌میک که‌میکرد به به‌راورد له‌گه‌ل که‌یسی به بی نانو. له ره له ری نازاد FML کاریگه‌ری نییه به‌هۆی ریککه‌وتی کۆکردنه‌وه و ناراسته‌ی ریشالی ناوه‌کی FRPC. زۆرتترین باری راکیشن پراکتیکی 15%-2% FRPC زیاتره له FEM، له کاتیکدا بو FML نیوه‌ی باری FEM ه. زۆرتترین باری پراکتیکی چه‌مانه‌وه‌ی 6%-5% FRPC زیاتره له FEM جگه له 3 پیکهاته‌ی نمونه، له کاتیکدا بو FML یه‌ک 2%-15% که‌متره له FEM جگه له 1 پیکهاته‌ی نمونه.

زۆرتترین لادان به‌هۆی باری دابه‌شکراوی یه‌کسان و فریکوینسی سروشتی بنه‌ره‌تی بو کانزا، FRPC و FML به شیوه‌یه‌کی سه‌ره‌کی په‌یوه‌سته به ریزه‌ی ره‌قبوونی چه‌مانه‌وه‌ی dmn. توخمه D22 له ماتریکسی ره‌قبوونی چه‌مانه‌وه‌ی و لیزه‌وه مۆدیولی یونگ له ناراسته‌ی y کاریگه‌ری سه‌ره‌کی له‌سه‌ر به‌های dmn هه‌یه که ده‌بیته هۆی ئەوه‌ی ماده‌که به‌رگری زیاتری هه‌بیت به‌رامبه‌ر به شیواندنی لاستیکی. به‌شداری پستی کانزا زیاتره له ناوه‌کی پۆلیمربه‌هیزکراوی ریشال له ساندویچی FML.



پشکنین له سه‌ر هه‌لسوکه‌وتی راکیشان، چه‌مانه‌وه وله‌ره‌له‌ری پیکهاته‌ی لامیناتی هایبرد کۆمبوزت

تیزیکه

پیشکه‌شی نه‌نجومه‌نی کۆلیژی ته‌کنیکی نه‌ندازیاری هه‌ولیر کراوه‌له
زانکۆی پۆلیتەکنیکی هه‌ولیر وه‌کو به‌شیک له‌پیداویستیه‌کانی به‌ده‌ست
هینانی پله‌ی دکتۆرای فه‌لسفه‌له‌زانستی نه‌ندازیاری میکانیک ووزه

له‌لایه‌ن

ناقا علی کمال محمد

به‌کالۆریۆس له‌نه‌ندازیاری میکانیک، ۱۹۹۶

ماسته‌ر له‌نه‌ندازیاری میکانیکی کرداره‌کی، ۱۹۹۹

به‌سه‌ریه‌رشتیاری

پ.ی.د. گیلان اسماعیل حسن

پ.ی.د. یونس خالد خدر

عێراق-کوردستان-هه‌ولیر

۲۰۲۴